Narrow band digital modulation for land mobile radio.

Bennouna, A.

Award date:
1984

Awarding institution:
University of Bath

NARROW BAND DIGITAL MODULATION FOR LAND MOBILE RADIO

submitted by

A Bennouna, BSc, MSc

for the degree of PhD

of the University of Bath,

1984

---oo0oo---

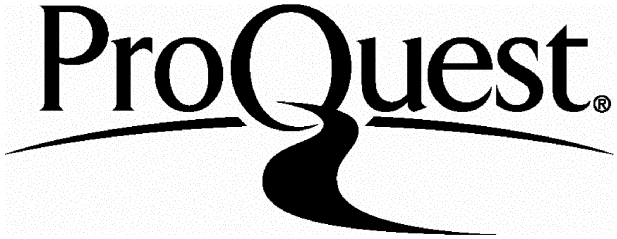

ACKNOWLEDGEMENTS

The author would like to express his deep gratitude to Dr G Allen for his constant and helpful advice throughout the various stages of this research. Thanks are also due to him for his patience and understanding during the writing up of this thesis.

The author is also indebted to Dr J P McGeehan for his provision of the fading simulator, as well as for his useful discussions.

A particular vote of thanks to Mr V Petrovic for providing the polar loop transmitter.

Many thanks to the staff of the Communication Research Laboratory for their co-operation.

Last, but not least, the author would like to extend his gratitude to the Government of the Kingdom of Morocco for their continuous financial support during the period of this research.

SUMMARY

Digital transmission of information is finding an ever-increasing number of applications in the land-mobile radio service. There is a possibility that in the long term, due to the increasing demand for mobile radio channels, their bandwidths will be reduced to 5kHz.

A digital minimum shift keying (MSK) modulation scheme is proposed in this work for narrow band digital mobile radio transmission. The design and implementation of an MSK modulator and coherent and noncoherent demodulators are given. Their structure is highly flexible and can accommodate a wide range of medium digital transmission rates. The demodulators were tested for the transmission of 2.4kbit/sec in simulated typical land-mobile radio transmission conditions. The results of these tests favoured the use of the noncoherent demodulator for this type of application.

Achieving spectrum efficiency in this proposed scheme relies on postmodulation filtering of the MSK signal. A polar loop VHF transmitter was tested for high efficiency linear power amplification of the MSK signal. It proved its validity for this type of application.

A digital clock recovery circuit suitable for use in mobile radio conditions has also been built and tested. The principles of the circuit operation and its implementation are discussed.

NARROW BAND DIGITAL MODULATION FOR LAND MOBILE RADIO

C O N T E N T S

CHAPTER 1

INTRODUCTION

It cannot be over-stated that mobility is the life-blood of modern civilisation. Therefore, there has been an ever increasing need for quick and reliable mobile communication to provide transfer of information and co-ordination between closely related activities being performed at widely separated and for most of the time non-stationary locations.

The most widespread requirements for mobile communication result from land mobile users. Examples of land mobile users' activities for which the importance of communications is becoming paramount are: public safety and emergency use by police, firemen and ambulances, land transportation by taxis, buses and trucks, dispatching and reporting of commercial vehicles and mobile telephony for government executives, doctors and businessmen.

The increase in demand in the past for mobile radio channels in the United Kingdom and throughout the industrialised world, coupled with the advance in communications technology, has led to a steady decrease in the channels bandwidth from 100kHz in the 1950s to the present day situation. In the UK, channels bandwidth at the present time is 12.5kHz in the VHF band (68-174MHz) and 25kHz in the UHF band (425-470MHz), with 12.5kHz channels spacing being gradually introduced to the UHF band.

The average annual growth in the use of land mobile radio in the

UK has been projected to be 10% per annum until the year 2000[1]. This is a conservative estimate and the growth is likely to be higher, especially when new services, like data transmission, become available thus attracting new users.

A short term strategy to meet this predicted increase in demand is to provide the users with means for a more efficient and versatile exploitation of existing channels. In the long term, the problem should be addressed by increasing the number of mobile radio channels. This will be accomplished either by vastly icreasing the bands of the frequency spectrum assigned for land mobile radio applications, or by reducing the channel bandwidth thus accommodating far more users in the same allocated bands. The latter is the most likely approach, as demand on the frequency spectrum is increasing by all radio communication users. Research is currently being carried out to reduce channel bandwidth to 6.25-5kHz while still using analogue modulation techniques (eg. single side-band, SSB, and narrow band frequency modulation, FM).

At the present time land mobile radio users rely mainly on voice communication. Digital transmission of information can provide possible means to meet short as well as long term objectives.

Many routine messages, like vehicle location, identification and status, can be transmitted in less time when using a digital format. Furthermore, these messages can be stored and transmitted automatically when the channel is clear, thus allowing greater utilisation of the mobile radio channel and thereby reducing the demand for additional frequency allocation. In addition, digital

transmission provides mobile radio users with services which otherwise could not be made available. Examples of these are: availability of permanent records when printers are used, display of maps and still pictures, and direct access at terminals mounted in vehicles for data stored in computer banks. Finally, transmitting speech in digital form offers an excellent opportunity for implementing different levels of voice security. This is of a great importance for some groups of users, eg. police, government executives, security agencies, ... , etc.

As a result of the versatility offered by adopting data transmission in mobile radio communication, a fleet operator may find that he needs only one channel to accommodate the same number of mobile units that required two voice channels.

In the long term, transmission of speech in digital form can offer an alternative for mobile radio voice communication in reduced channel spacing. In recent years considerable progress has been made in eliminating redundancy in speech so that it can be transmitted at reduced bit rates. Speech coding research in topics like linear predictive coding[2] have achieved bit rates of 4.8kbit/sec while maintaining intelligibility and a reasonable quality of speech. Bit rates of 2.4kbit/sec have also been considered[2] and results regarding voice quality and intelligibility are promising.

Given that the current trend in speech coding research and advances in integrated circuit fabrication technology will continue, it is reasonable to predict that in the next decade 2.4kbit/sec speech processors may become available. This will ultimately allow

establishing voice communications in much reduced land mobile radio channel spacings, depending on the technique adopted to digitally modulate the transmitted carrier frequency.

The obvious short and long term gains generated by introducing digital transmission in land mobile radio channels have prompted the search for suitable digital modulation techniques.

Until now analogue frequency modulation (FM) has been the standard modulation technique used in mobile radio voice communication at frequencies above 30MHz. Therefore, until recently research has focussed on digital modulation techniques which can be integrated in existing FM radio equipments. Consequently, subcarrier digital modulation, where the digital information modulates an audio tone termed a sub-carrier which is subsequently treated as an analogue signal at the transmitter, has been considered. At the receiver the signal is processed for digital information (ie. data) recovery at the output of the FM demodulator. Although this approach is attractive because it offers compatibility with existing equipments, it uses the available frequency spectrum inefficiently. The standard bit rate recently adopted in the UK for the transmission of data using subcarrier digital modulation of mobile FM radio equipments is 1.2kbit/sec in the 12.5kHz channels[3]. This represents a digital transmission efficiency - defined here as the ratio of the transmitted bit rate to the mobile radio channel bandwidth - of 0.1. In this research work it is demonstrated that by using a direct digital modulation scheme the transmission efficiency can be increased to more than 0.48 while still meeting the regulations laid down for analogue transmission with regard to

out-of-band radiation (-70dB) and maintaining a guard-band of 3.5kHz at 12.5kHz channel spacing and 7kHz at 25kHz.

Keeping in mind the possible reduction in land mobile radio channels bandwidth to 5kHz and the bit rate needed for satisfactory digital speech transmission to 2.4kbit/sec in the coming decade, it was decided to search for a spectrally efficient digital modulation scheme suitable for operation in the land mobile radio channel environment which meets the above objectives. However, as these can be considered as long term objectives it was also decided that the chosen scheme should also be capable of operating in the existing channels in parallel with analogue techniques. This will provide today's mobile radio users with alternative digital channels operating at medium speeds (6kbit/sec in 12.5kHz channels) to meet the short term ends offered by the user of data transmission.

Any data transmission scheme in land mobile radio will have to operate under extremely hostile conditions, suffering from the combined impairments of signal fading due to multipath propagation and shadowing, ignition noise interference and co-channel interference resulting from frequency re-use schemes. The characteristics of typical land-mobile radio channels are discussed in Chapter 2. Different narrow band digital modulation systems are studied in Chapter 3 and their performances in typical channel conditions are analysed and compared.

Based on this comparison it will be shown that direct (ie. the data signal directly modulates an RF carrier) minimum shift keying (MSK) is the most suitable candidate for digital transmission in land

mobile radio. The practical implementation of an MSK modulator and a coherent and noncoherent demodulators will be explained in Chapter 4. The modulator and demodulator were implemented bearing in mind they should work on bit rates higher than 2.4kbit/sec if required. Because of the analogue and digital signal processing needed to recover the reference signals from the received modulated signal and to perform the data recovery operation, the coherent demodulator has a considerably more complicated structure than the noncoherent demodulator.

The results of a wide range of measurements carried out to study the performance of both demodulators in simulated land mobile radio typical transmission conditions will be analysed in Chapter 5. Although the coherent demodulator performs better than the noncoherent in static (ie. non-fading conditions), it does not do so when the transmitted signal is subjected to mobile radio transmission conditions. Therefore, because of this and its simplicity, the noncoherent demodulator will be recommended for mobile radio applications. Furthermore, the noncoherent demodulator can double as an analogue FM detector.

Highly efficient class C power amplifiers are used in mobile radio analogue FM transmitters because the resultant FM signal has a constant envelope. To keep the high power efficiency advantage, recent research on digital modulation techniques for land mobile radio applications have focussed on those which have minimum out-of-band radiation, while maintaining the constant envelope property. These techniques exclude the use of post modulation filtering because it leads to the generation of amplitude

fluctuations in the originally constant envelope signal. If the filtered signal is passed through a nonlinear device (eg. Class C power amplifier) its spectrum side bands which have been removed by the filter will be reintroduced, thus causing out-of-band radiation. Therefore, research has concentrated on precise forms of premodulation filtering[4] or the use of partial response signalling[5,6]. Both cases lead to a much more complicated modulator structure as compared to the MSK one discussed here, and only relatively complicated coherent demodulators can be used to detect the signal at the receiving end with an acceptable error rate versus signal to noise ratio performance.

Fortunately a new technique of power amplification, named the polar loop transmitter, has been developed at the University of Bath which achieves extremely linear performance while maintaining the same efficiency of Class C amplifier[7]. This transmitter was originally designed for use with analogue single side band (SSB) modulated signals and involves adding an integrated IF signal processing circuit to a standard Class C VHF or UHF power amplifier.

Therefore, it was decided to use post modulation filtering as a simple way of achieving spectrum efficiency and the polar loop transmitter to accomplish highly efficient linear power amplification. The results of tests have shown that the transmitter is suitable for this type (MSK) of digital modulation.

In any data communication system, correct timing (ie. clock) signal is a prerequisite for successful operation. The timing signal serves two functions: controlling the integrate and dump (if used)

and sampling operations performed on the demodulated base band signal to recover the data and maintain synchronisation (ie. bit integrity) between the transmitted and received data for correct decoding.

The clock recovery process is complicated in the land mobile radio transmission because of fading which leads to the total loss of the received signal from time to time. The bit integrity may be achieved in this type of environment by the repeated transmission of a synchronisation word. However, the word itself can be lost during a deep fade which results in a corrupt reception of data even when the signal has recovered from the fade, until another synchronisation word is received. Hence, this word should be repeated over short intervals and consequently the data throughput will become very low. Therefore, the clock recovery circuit must be able to maintain bit integrity when the received signal is lost for as long as the transmitter and receiver clock oscillator's stabilities can possibly offer, ie. it should have as small as practically possible locking bandwidth. On the other hand, in order to accomplish rapid phase locking after a deep fade, the circuit locking bandwidth should be large.

A digital clock recovery circuit which can achieve these opposing requirements has been implemented and tested for a transmission rate of 2.4kbit/sec. The analysis of its operation and the practical realisation will be explained in Chapter 4. This recovery circuit is capable of maintaining bit integrity during deep fade intervals equal to or smaller than 20 seconds, given a total oscillators stabilities of ±10 parts per million (ppm). The circuit can easily be programmed to work over higher bit rates.

CHAPTER 1: REFERENCES

[1] Pannell, W M: "A study of the future frequency spectrum requirements for private mobile radio in the United Kingdom", Pye Telecommunications Ltd, Cambridge, England, 1976.

[2] Holmes, J N: "A survey of methods for digitally encoding speech signals", The Radio & Electronic Engineer, Vol.52, No.6, June 1982.

[3] "EEA preferred data transmission system for land mobile radio using a binary data format", Electronic Engineering Association, London, June 1982.

[4] Murota, K, Hirade, K: "GMSK modulation for digital mobile radio telephony", IEEE, Vol.COM-29, July 1981.

[5] de Jager, F and Dekker, C B: "Tamed frequency modulation. A novel method to achieve spectrum economy in digital transmission", IEEE, Vol. COM-26, No.5, 1978.

[6] Noordanus, J: "New digital phase modulation methods to establish digital voice transmission in mobile radio networks with optimum spectral efficiency", Proc. 3rd World Telecommunication Forum, Geneva, Switzerland.

[7] Petrovic, V and Gosling, W: "A radically new approach to SSB transmitter design", Conf. on Radio Transmitters and Modulation Techniques, London, England, 24-25 March 1980, IEE, 1980.

CHAPTER 2

THE LAND MOBILE RADIO CHANNEL ENVIRONMENT

2.1 Introduction

In any radio communication system the physical environment defines propagation and interference characteristics and hence the channel impairments. In a typical land mobile radio application one terminal of the communication system, the base station, is stationary with its antenna positioned high above the average surrounding terrain, on top of a building or a hill, with as few obstructions close to it as physically possible. The other terminal, at the vehicle, is mobile with its antenna usually about 1.5 - 2 metres above the local ground and with all sorts of close surrounding obstructions. These can be buildings of different heights and sizes, or other vehicles all in the vicinity of the mobile terminal.

The transmission path between the base station and the mobile terminal is rarely ever line-of-sight, especially in urban environments, and usually is a composite of many scattering and reflected paths. The random phase and amplitude of each scatter path wave contributes to the composite wave, thus creating a standing wave pattern through which the vehicle moves. This standing wave pattern, apart from the influence of other (especially large) vehicles within the immediate vicinity, can be considered as quasi-stationary over short travelled distances.

If the received signal strength is monitored, the most noticeable effect of multipath propagation is the rapid fluctuation

of the received signal level as the vehicle moves through the standing wave pattern. Fig 2.1(c) shows a typical record in an urban environment of the signal level at the input to a mobile receiver over a short distance in the order of tens of the carrier wave length. The fluctuations are rapid and occasionally deep around an almost constant local mean. This is known as short-term fading. This short-term rapid fading can also occur in suburban and rural areas[1]. In suburban environments conditions can change rapidly from virtually constant signal conditions on streets that are radial to the transmitter, to fast deep fading on streets that are perpendicular to it. Patches of short term rapid fading also occur in rural areas, where the local obstructions are isolated farm buildings, high hedgerows, trees and telegraph poles, etc. [1].

When the signal is observed over much further distances, in the order of hundreds of carrier wavelength, it can be seen from Figs 2.1(a) and (b) that superimposed over the rapid fading the local mean signal level exhibits relatively slow and shallow variations. This long-term fading is created by the presence of tall buildings and hills which cause shadowing and diffraction of the radiated signal. Furthermore, as the vehicle travels away from the base station, the mean received signal strength was shown[2,3] to approximately follow an inverse fourth power depending on distance.

In addition to impairments due to propagation characteristics, there are others caused by interference. The major source of interference in the mobile-radio environment is radio emission from sparks in vehicles' ignition systems. Other, and usually more controllable, forms of interference are co-channel and adjacent

channel interference. The first is caused by an interfering waveform appearing within the signal bandwidth. The latter refers to interference in one channel arising from spillover from an adjacent channel.

The combined effects of the above environmental conditions will govern the performance of any digital modulation system. They are discussed in detail and their influence on digital transmission is evaluated in the remainder of this chapter.

2.2 Multipath Fading

Fig 2.2 illustrates a typical arrangement for the signal arriving at the mobile receiver. This model and the subsequent analysis assume that the transmitter and receiver antennas are vertically polarised and omnidirectional, ie. they have uniform gain in all directions. In most situations, especially in urban environments, the line of sight component is small or non-existent. The received signal is composed of the summation of a large nummber of reflected and scattered horizontal plane waves arriving at the mobile antenna with random amplitudes and arrival angles. The statistics of the signal level arising from this situation were initially studied by Ossana[4]. His study was confined to a reflection model. Later Gilbert[5] studied some special cases of a more general scattering model. Finally Clarke[6] proposed the most widely accepted model, which is discussed in detail here.

The starting assumption in Clarke's model is that the total field at the mobile receiver at any location is made up of the summation of an infinite number of horizontally travelling plane

waves having random amplitudes and angles of arrival, and that their phases are uniformly distributed over 0 to 2π. The amplitude and phase of each wave are statistically independent. This assumption largely agrees with the physical situation shown in Fig 2.2.

Fig 2.3 shows the nth component received at the vehicle antenna. The XY plane is assumed horizontal and the vehicle is moving with uniform velocity v in the X direction. The doppler frequency shift in the nth wave introduced by the vehicle motion can be expressed as:

$$2\pi f_n = 2\pi f_c \frac{v}{c} \cos\alpha_n \qquad \ldots (2.1)$$

where f_c is the carrier frequency, α_n is the angle between the received wave and the direction of motion and C is the free space propagation constant (3×10^8 metre/sec). The maximum doppler shift, f_D, is $\pm f_c (v/c)$, which is very much less than the carrier frequency.

The field component, E_Z, arriving at the mobile antenna, can be written as:

$$E_Z(t) = E_o \sum_{n=1}^{\infty} C_n \cos(\omega_c t + \omega_n t + \phi_n) \qquad \ldots (2.2)$$

where ϕ_n is the phase angle of nth wave and can have a value between 0 and 2π with equal probability. The amplitude of the nth field wave is given by $E_o C_n$, where E_o is the mean amplitude and C_n is a random coefficient smaller than unity. The amplitude coefficients are normalised so that their ensemble average is equal to unity, ie:

$$\left\langle \sum_{n=1}^{\infty} C_n^2 \right\rangle = 1$$

Finally, the frequency of nth component is given by ($f_c + f_n$).

The field component E_Z may thus be described as a narrow band Gaussian process, in agreement with the central limit theory.

Recalling the assumption made at the beginning of the analysis on the receiver antenna and the travelling wave, the signal strength at the receiver input is directly proportional to the field strength. Hence it can be expressed as:

$$V(t) = V_o \sum_{n=1}^{\infty} C_n \cos(\omega_c t + \omega_n t + \phi_n)$$

and will have the same statistical properties as $E_Z(t)$. Following Rice[7] in his analysis of narrow band random Gaussian process, V(t) can be rewritten as:

$$V(t) = x(t)\cos\omega_c t - y(t)\sin\omega_c t$$

where

$$x(t) = V_o \sum_{n=1}^{\infty} C_n \cos(\omega_n t + \phi_n)$$

$$y(t) = V_o \sum_{n=1}^{\infty} C_n \sin(\omega_n t + \phi_n)$$

x(t) and y(t) are uncorrelated zero mean random Gaussian processes corresponding to the in-phase and quadrature components of V(t). X and Y are their respective values at a fixed time instant t. They have equal variance given by:

$$R_o^2 = \langle X^2 \rangle = \langle Y^2 \rangle = \frac{V_o^2}{2}$$

where R_o^2 is the mean signal power. Since X and Y are independent,

their joint expectation ‹XY› is equal to zero.

Given that X and Y are Gaussian, they have a probability density function (PDF) of the form:

$$P(m) = \frac{1}{\sqrt{2\pi R_o^2}} \; e^{-\frac{m^2}{2R_o^2}} \qquad \ldots (2.3)$$

where m = X or Y.

The envelope of the received signal, r, is given by:

$$r = \sqrt{X^2 + Y^2}$$

Rice[7] has shown that the PDF of the signal envelope, r, is expressed as:

$$P(r) = \frac{r}{R_o^2} \; e^{-r^2/2R_o^2} \qquad r \geq 0$$

$$= 0 \qquad r < 0 \qquad \ldots (2.4)$$

Equation 2.4 is the well known Rayleigh PDF, hence the short-term fading is named Rayleigh fading. P(r) is illustrated in Fig 2.4.

The cumulative distribution defined as the probability that the received signal envelope is less than a certain level, R, is given by:

$$P(r \leq R) = \int_{-\infty}^{R} P(r)\, dr$$

$$= \int_0^R \frac{r}{R_o^2} e^{-r^2/2R_o^2} \, dr$$

$$= 1 - e^{-R^2/2R_o^2} \qquad \ldots (2.5)$$

Eqn (2.5) is illustrated in Fig 2.5.

Further analysis carried out by Jakes[8] and Gans[9], based on the calculation of the frequency power spectra of the fading signal has led to important expressions, which will be used later to study the effect of short term fading on digital modulation systems. The first expression gives the level crossing rate, N_R, defined as the expected rate at which the received signal envelope crosses a specified signal level R in the positive direction, and is given by:

$$N_R = \sqrt{2\pi} \, f_D \frac{R}{R_o} e^{-(R/R_o)^2} \quad \text{crossing/second} \qquad \ldots (2.6)$$

The second equation gives the average duration, $\bar{\tau}_R$, the envelope spends below a specific level R:

$$\bar{\tau}_R = \frac{e^{(R/R_o)^2} - 1}{\frac{R}{R_o} f_D \sqrt{2\pi}} \quad \text{seconds} \qquad \ldots (2.7)$$

Eqns (2.6) and (2.7) are illustrated in Figs 2.6 and 2.7 for different values of f_D. In both figures the horizontal axis gives the signal level in dB relative to its mean value.

An examination of eqns (2.6) and (2.7) reveals that N_R is directly proportional to f_D, while $\bar{\tau}_R$ is inversely proportional to it. Thus, during an average transmission period $\bar{T}$, the average time

the envelope spends below certain level R, given by $N_R\bar{\tau}_R\bar{T}$ is independent of f_D and consequently the carrier frequency and the vehicle speed.

In most situations of mobile radio transmission, the Rayleigh model will give the best approximation for the received signal level statistics. Although it was assumed at the start of the analysis that the number of close scatterers is very large, it has been shown[10] that as few as six sinusoidal waves with independently varying random phase will give a resultant whose envelope closely follows Rayleigh statistics and whose phase is uniformly distributed.

The agreement between the Rayleigh fading model and field measurement of short-term signal strength in suburban areas[8] is shown in Fig 2.8. The horizontal axis is scaled so that the Rayleigh cumulative distribution appears as a straight line.

In some physical situations the short-term signal level statistics frequently deviate from the Rayleigh model. If a line-of-sight path exists between the two transmission terminals, the received signal will be composed of a steady component plus a Rayleigh fading signal. In this case the signal level statistics will follow the Rice fading model[11], which depends on the ratio between the mean square value of the steady component and fading signal. The extreme limits of Rice statistics occurs on one hand when the line-of-sight component becomes predominant and on the other hand when it becomes very small or nonexistent. The latter will lead to Rayleigh fading statistics, which represent the worst case situation.

2.3 Random FM Noise

Because of multipath propagation as the vehicle moves through the fading pattern, the phase of frequency components in the signal change with time in a random manner. Thus, the instantaneous frequency of each component exhibits a random frequency modulation. This appears in the form of random noise at the output of an FM demodulator, hence the process is termed random FM noise.

The received signal can be expressed as

$$S(t) = v(t)e^{j\psi(t)}$$

where $v(t)$ represents the signal envelope and $\psi(t)$ its phase. The instantaneous frequency is given by the time derivative of $\psi(t)$, $\dot{\psi}(t)$. $\dot{\psi}(t)$ is the term responsible for the random FM noise. The statistical properties of $\dot{\psi}(t)$ have been studied by Jakes[8]. The probability density function was found to be:

$$P(\dot{\psi}) = \frac{1}{\sqrt{2}} \frac{1}{2\pi f_D} \left[1 + 2 \left[\frac{\dot{\psi}}{2\pi f_D} \right]^2 \right]^{-\frac{3}{2}} \quad \ldots (2.8)$$

And its cumulative distribution function:

$$P(\dot{\psi} \leq \dot{\Psi}) = \frac{1}{2} \left[1 + \sqrt{2} \frac{\dot{\Psi}}{2\pi f_D} \left[1 + 2 \left[\frac{\dot{\Psi}}{2\pi f_D} \right]^2 \right]^{-\frac{1}{2}} \right]$$

$$\ldots (2.9)$$

Eqns (2.8) and (2.9) are plotted in Figs 2.9(a) and (b).

The one-sided baseband frequency power spectrum of random FM noise is shown in Fig 2.10[8]. It is a monotonically decreasing function of frequency.

2.4 Frequency Selective Fading

So far the effect of multipath propagation on the level and phase of a single carrier frequency has been considered. When the carrier is modulated by a baseband signal it occupies a frequency band of width depending on the frequency spectrum of the modulating signal and the technique of modulation used. The transmission path lengths of the constituent waves which compose the resultant modulated message and whose wavelengths are unequal, will be different. The different path lengths give rise to different propagation time delays. An impulse transmitted under such condition becomes a stretched pulse of width depending on the delay spread. This stretching of impulses will cause intersymbol interference in digital modulation systems if the bit period approaches the time delay spread.

The spread in time delays range from a fraction of microseconds to a few microseconds, depending on the type of environment. Longer delays spread are usually found in heavily build-up areas[8]. Lee[12] has concluded that for frequencies above 30MHz the delay spread is independent of the frequency. Typical measured values of time delays spread range from 0.2μsec to 2μsec in suburban areas and from 1μsec to 3μsec in urban areas[12].

The existence of the different time delays in the various component paths that constitute the modulated signal causes the

statistical properties of two components of different frequencies to become independent, ie. the fading phenomenon becomes frequency selective, if the frequency separation is large enough. The maximum frequency difference for which the signal envelope and phase statistics are still strongly correlated is called the coherence bandwidth of the radio transmission path. Fig 2.11 illustrates level and phase statistics correlation coefficients versus the product of the frequency difference and the time delay spread[12].

One common measure of coherence bandwidth corresponds to the frequency separation when the signal level or phase correlation is 0.5[9,12]. It is obvious from Fig 2.11 that the coherence bandwidth based on phase statistics correlation is smaller than that based on level statistics. Thus, in urban environments the minimum coherence bandwidth that satisfies 0.5 phase statistics correlation is approximately 26.5kHz, assuming a time delay spread of 3μsec.

2.5 Long-Term Fading

The slow and shallow variations of the mean short-term signal level, known as long-term fading, are illustrated in Fig 1(b). These are caused by reflection from and diffraction around distant scatterers and by shadowing, the obstacles being tall buildings and hills. Reudink[13] has studied the behaviour of the short-term mean received signal level averaged over travelled distances of 10 to 20 metres, ie. the long-term mean signal level. His study was based upon experimental data collected by various workers in both Japan and USA. He concluded that the probability density function of the long-term mean signal level, $\overline{R}_o$, follows a log-normal distribution. Thus, $P(\overline{R}_o)$ can be expressed as:

$$P(\bar{R}_o) = \frac{\log_{10}e}{\sqrt{2\pi}\ \sigma\ \bar{R}_o} e^{(\log\bar{R}_o - \log R_o)^2/2\sigma^2} \quad \bar{R}_o \geq 0$$

$$= 0 \qquad \bar{R}_o < 0 \qquad \ldots (2.10)$$

where

R_o = short-term mean signal level

$\bar{R}_o$ = long-term mean signal level

σ = the standard deviation of $\bar{R}_o$

The long-term mean signal level and standard deviation in eqn (2.10) depends upon base and mobile antenna heights, terrain irregularity, nature of the earth's surface and size, construction and density of buildings. $\bar{R}_o$ depends as well on distance between the mobile receiver and the base station. In general it will decrease more rapidly with distance as the receiver moves away from the base transmitter. It seems to be well approximated by an inverse fourth-power dependence[2,3] on the distance between the base station and the mobile receiver.

Prediction curves for the standard deviation (σ), based upon empirical data collected by Okumura[3] and others are shown in Fig 2.12. The increase in σ is negligible for frequencies up to 600MHz when it exhibits a more gradual but small increase.

2.6 Effect of Mobile Radio Propagation on Digital Modulation Systems

The commonly used measure of performance for digital modulation systems is the relationship between the probability of bit error, PE, and signal to noise ratio, γ. Expressions giving the relationship

between the two for different systems are well established. They are discussed in Chapter 3. They are calculated assuming a steady signal to noise ratio, no interference, and an ideal channel which does not introduce frequency or phase distortion and the noise is additive white and Gaussian. In the following the effects of mobile radio propagation impairments on the static probability of bit error Pe(γ)s are discussed.

2.6.1 Effect of Multipath Propagation

Because only narrow band digital modulation systems of 5kHz bandwidth are to be considered, the fading characteristics can be assumed nonselective. This can be justified by referring to Fig 2.11. In urban environments the product of maximum time delay spread and a 5kHz frequency separation is less than 0.1. Consequently, the signal level and phase statistics correlation coefficient will be very near to unity, certainly greater than 0.9.

The bit rate in such narrow channels is in the order of a few thousand bits per second, ie. the bit period is a fraction of a millisecond. This is a hundred times greater than the delay spread experienced in any class of the mobile radio environment. Hence, it can be stated that the received signal does not suffer from intersymbol interference, given that the transmitter and receiver filters do not introduce any.

The signal to noise ratio γ at the demodulator input is directly proportional to the received signal level assuming that the mobile radio channel noise is additive white and Gaussian. Thus, γ will have the same statistics as the received signal level.

In this analysis, the level crossing rate given in eqn (2.6) is assumed to be less than the message bit rate. Consequently, γ can be regarded effectively constant during each symbol period, although varying over a long succession of bits.

Fig 2.13 illustrates a typical situation for the signal to noise ratio, γ, of a fading signal. the value γ shown in the above figure will be crossed N_γ times per second and each fade below this level will last an average of $\bar{\tau}_\gamma$ seconds. N_γ and $\bar{\tau}_\gamma$ are obtained from eqns (2.6) and (2.7) respectively by substituting R_o^2 and R^2 by γ_o and γ. Thus the fraction of total message time spent below γ is equal to $\bar{\tau}_\gamma N_\gamma$. This can be repeated for the value $\gamma + \Delta\gamma$. The fraction of time spent between γ and $\gamma + \Delta\gamma$ is given by:

$$\bar{\tau}_{\gamma+\Delta\gamma} N_{\gamma+\Delta\gamma} - \bar{\tau}_\gamma N_\gamma$$

$$= e^{-(\gamma/\gamma_o)} \left[1 - e^{-\frac{\Delta\gamma}{\gamma_o}} \right] \qquad \ldots (2.11)$$

The series expression of $e^{-\frac{\Delta\gamma}{\gamma_o}}$ is:

$$e^{-\frac{\Delta\gamma}{\gamma_o}} = 1 - \frac{\Delta\gamma}{\gamma_o} + \frac{\left[-\frac{\Delta\gamma}{\gamma_o}\right]^2}{2!} + \frac{\left[-\frac{\Delta\gamma}{\gamma_o}\right]^3}{3!} + \ldots$$

and

$$\lim_{\Delta\gamma \to 0} e^{-\frac{\Delta\gamma}{\gamma_o}} = 1 - \frac{d\gamma}{\gamma_o} \qquad \ldots (2.12)$$

From (2.11) and (2.12) the fraction of time spent at $d\gamma$ is equal to:

$$\frac{1}{\gamma_o} \; e^{-\frac{\gamma}{\gamma_o}} \; d\gamma$$

The number of errors during this time is given by:

$$dN_B P_e(\gamma)_s \; \frac{1}{\gamma_o} \; e^{-\frac{\gamma}{\gamma_o}} \; d\gamma \qquad \ldots (2.13)$$

where dN_B is the total numbmer of transmitted bits during the time spent at $d\gamma$ and $P_e(\gamma)_s$ is the static probability of error at a signal to noise ratio γ.

The total number of errors during an average transmission period can be found by performing a double integration on eqn (2.13). The first is with respect to N_B for all values of N_B between 0 and N_B, where N_B is the total numbmer of transmitted bits during an average transmission period. The second integration is with respect to γ for all possible values between 0 and ∞, ie:

$$\text{total number of errors} = \int_0^{N_B} \int_0^{\infty} P_e(\gamma)_s \; \frac{1}{\gamma_o} \; e^{-\frac{\gamma}{\gamma_o}} \; dN_B d\gamma$$

$$= N_B \int_0^{\infty} \frac{1}{\gamma_o} \; P_e(\gamma)_s \; e^{-\frac{\gamma}{\gamma_o}} \; d\gamma \qquad \ldots (2.14)$$

The probability of error is defined as the total number of bits in error divided by the total number of transmitted bits in an average message. Thus, the probability of error under fading conditions $P_e(\gamma)_D$ can be found directly from eqn (2.14):

$$P_e(\gamma)_D = \int_0^\infty \frac{1}{\gamma_o} e^{-\gamma/\gamma_o} P_e(\gamma)_s \, d\gamma \qquad \ldots (2.15)$$

The same expression in (2.15) was achieved in the past by different authors using a different approach. That was averaging the steady-state error probability over the Rayleigh fading probability density function given by eqn (2.3).

Eqn (2.15) being independent of f_D agrees with the previously stated fact that the average time spent below a certain signal level is independent of f_D. The expression obtained in eqn (2.15) is used in the following chapter to calculate probability of error for different modulation techniques.

2.6.2 Effect of Random FM Noise

Random FM noise is a quantity independent of the signal strength as can be seen from the previous analysis. Hence, it contributes an irreducable probability of error. As has been shown earlier, random FM noise is inversely proportional to the ratio between baseband signal bandwidth and the maximum doppler shift. In digital modulation the baseband spectrum is directly proportional to the bit rate. Thus, it can be expected that the effect of random FM noise will become appreciable at low ratios of bit rate to maximum doppler shift.

It is not possible to find a general expression for the probability of error due to random FM noise as was the case in Rayleigh fading. The analysis will depend on the mechanism of demodulation and the result will vary accordingly. Therefore, it will be left until this is studied in the following chapter.

2.6.3 Effect of Long-Term Fading

Slow and shallow variations in the received short-term mean signal level which follow a lognormal distribution will put further constraints on the performance of digital modulation systems. Therefore, it is important for a system designer to estimate the degradation in system performance due to a composite probability distribution of the signal level derived from a short-term Rayleigh fading with superimposed long-term lognormal variations.

The degradation in performance may be measured by the increase needed in signal to noise ratio to maintain a constant probability of error (10^{-3} in this case), with respect to the pure Rayleigh distribution against the increase in standard deviation (σ) of the lognormal distribution, σ being the indication for deviation from pure Rayleigh distribution. The curve in Fig 2.14 was plotted under the above assumptions. Recalling Fig 2.12, σ in an urban environment is between 5dB and 6dB for frequencies below 1000MHz, thus the degradation in system performance could be expected to be around 7 to 8dB. The curve in Fig 2.14 was plotted following the analysis carried out by Hansen[14] and can be applied to any modulation technique.

2.7 Mobile Radio Interference

So far the inherent properties of mobile radio propagation and their effect on digital communication systems have been considered. There are other imposed environmental conditions which the transmission has to cope with. These are mainly man-made noise, especially ignition noise, co-channel interference and adjacent channel interference.

2.7.1 Ignition Noise

Automative ignition noise often dominates other noise sources at and above the VHF band, especially in urban areas[15]. The most serious ignition interference is due to one's own vehicle. This appears in a periodic waveform with irregular pulse amplitudes. This is clearly illustrated in Fig 2.15(b). It can be considerably attenuated by using different suppression techniques in the ignition system. The improvement is appreciated in Figs 2.15(c) and (d). This set of figures was obtained in [16] by observing the received signal on a spectrum analyser. The centre frequency was chosen in a "quiet" part of the VHF band around 80MHz.

Although a user can ensure suppression of his ignitionn system to a greater or lesser extent, he cannot expect other vehicles to be fitted with such components. The presence of other vehicles of differnt types moving with unequal speeds produces impulse trains which are random in period, amplitude and width. Often such impulses occur in groups with irregular group spacing. The duration of impulse groups vary from tens of microseconds to a few milliseconds. Within impulse groups individual impulses may have widths between 1 and 5 nanoseconds and a repetition rate of 30 to 300Hz. These

impulses can reach peak levels of 40dB above normal receiver signal levels. The impulse levels depend on the traffic density and may display 16dB daily variations. When passed through the receiver IF filter the impulses are lengthened. The resultant length will be equal to the inverse of IF filter bandwidth. However, assuming that ringing may occur, the length of this effect may be significantly longer.

2.7.2 Co-channel Interference

Because of the increasing demand on mobile radio channels, system designers have to allocate the same frequency bands to different users in different distant areas. This scheme is known as frequency re-use. The re-use distances are influenced by the amount of co-channel interference. If a high level of interference can be tolerated without seriously degrading the digital system performance, then frequency re-use distances can be reduced. The result will be a higher overall spectrum efficiency.

Thus, the chosen digital modulation system for mobile radio applications should have an equal or better resistance to co-channel interference compared with other systems. In Chapter 5 the degradation in probability of error performances of some digital modulation systems due to co-channel interference is compared.

2.7.3 Adjacent Channel Interference

Transmission in individual channels must be confined in definite frequency bands so that neighbouring channels do not suffer from adjacent interference. This can be achieved by proper alignment of

channels' frequency bands within a geographical area, a narrow frequency spectrum at the modulator output, a minimum out of band radiation due to non-linearities in the transmitter power amplifiers, stable crystal oscillators and proper filtering at the receiver input. The final line of defence can be guard or dead frequency bands in between adjacent channels. This can be expensive in terms of spectrum efficiency.

Even with the above precautions taken, adjacent interference may occur due to instability in crystals controlling carrier frequencies of different channels or in some cases faulty equipment.

A well designed digital modulation system should have a narrow frequency spectrum which falls sharply to prevent spillover to the adjacent channels. The resultant modulated signal envelope fluctuation should be small to accommodate for reasonable non-linearities in transmitter power amplifiers. The modulation mechanism should not affect the stability of carrier oscillator circuits. Finally, the system should be reasonably tolerant to adjacent channel interference.

This will ultimately lead to better utilisation of the available frequency spectrum by reducing the frequency difference between adjacent channels.

2.8 Conclusion

The two most important impairments in mobile-radio data transmission are short-term Rayleigh fading and ignition interference. The first will cause burst of errors when the signal

fades deeply. All digital modulation systems will be impaired. The most effective way to combat short-term fading is by the use of a diversity technique.

Errors due to ignition interference can be greatly reduced if proper VHF suppression in the ignition system of the operator vehicle is carried. Unfortunately a considerable number of errors will be caused by other vehicles' ignition systems.

Random FM noise represents a lower bound in system design. As will be seen, some modulation techniques will perform better than others in the presence of FM noise. But in all cases the ratio between the doppler shift and bit rate should be kept as small as practically possible.

Long-term fading will generally cause modest degradation in system performance compared with the short-term one. Its effect can be reduced by improving the area coverage.

Co-channel and adjacent channel interference are the only impairments on which the designer can exercise full control. A well engineered system will reduce their effects and efficiently use the frequency spectrum at the same time.

CHAPTER 2: REFERENCES

[1] Allen, G: "The application of sideband diversity to mobile radio", PhD Thesis, University of Bath, 1978.

[2] Allsebrook, K and Parsons, J D: "Mobile radio propagation in British cities at frequencies in the VHF and UHF bands", Proc.IEE, Vol.124, No.2, 1977.

[3] Okumura, Y et al: "Field strength and its variability in VHF and UHF land mobile service", Rev. Elec. Commun. Lab., Vol.16, September and October 1968.

[4] Ossanna, J F: "A model for mobile radio fading due to building reflections: Theoretical and experimental fading waveform power spectra", B.S.T.J., Vol.43, Nov.1964.

[5] Gilbert, E N: "Energy reception for mobile radio", B.S.T.J., Vol.44, Oc.1965.

[6] Clarke, R H: "A statistical theory of mobile radio reception", B.S.T.J., Vol.47, July 1968.

[7] Rice, S O: "Statistical properties of a sine wave plus random FM noise", B.S.T.J., Vol.27, Jan.1948.

[8] Jakes, W C: 'Microwave Mobile Communication', John Wiley & Son Inc., N.Y., 1974.

[9] Gans, M J: "A power spectral theory of propagation in the mobile radio environment", IEEE, Vol.VT-21, Feb.1972.

[10] Norton, K A et al: "The probability distribution of the amplitude of a constant vector plus a Rayleigh distribution vector", Proc.IRE, Vol.43, Oct.1955.

[11] Schwartz, M, Bennett, W R and Stein, S: 'Communication Systems and Techniques', McGraw-Hill Book Co., N.Y., 1966.

[12] Lee, W C Y: 'Mobile Communication Engineering', McGraw-Hill Book Co., N.Y., 1982.

[13] Reudink, D O: "Properties of mobile radio propagation above 400MHz", IEEE, Vol.VT-23, Nov.1974.

[14] Hansen, F and Meno, F I: "Mobile fading - Rayleigh and lognormal superimposed", IEEE, Vol.VT-26, No.4, Nov.1977.

[15] Skomal, E N: 'Man-Made Radio Noise', Van Nostrand Reinhold Co., 1978.

[16] Brain, M and Kent, A N: "Characterisation of impulsive VHF radio interference in motor vehicles", Proc. of the Conf. on Electromagnetic Compatibility, Guildford, England, 1978 (IEE, 1978).

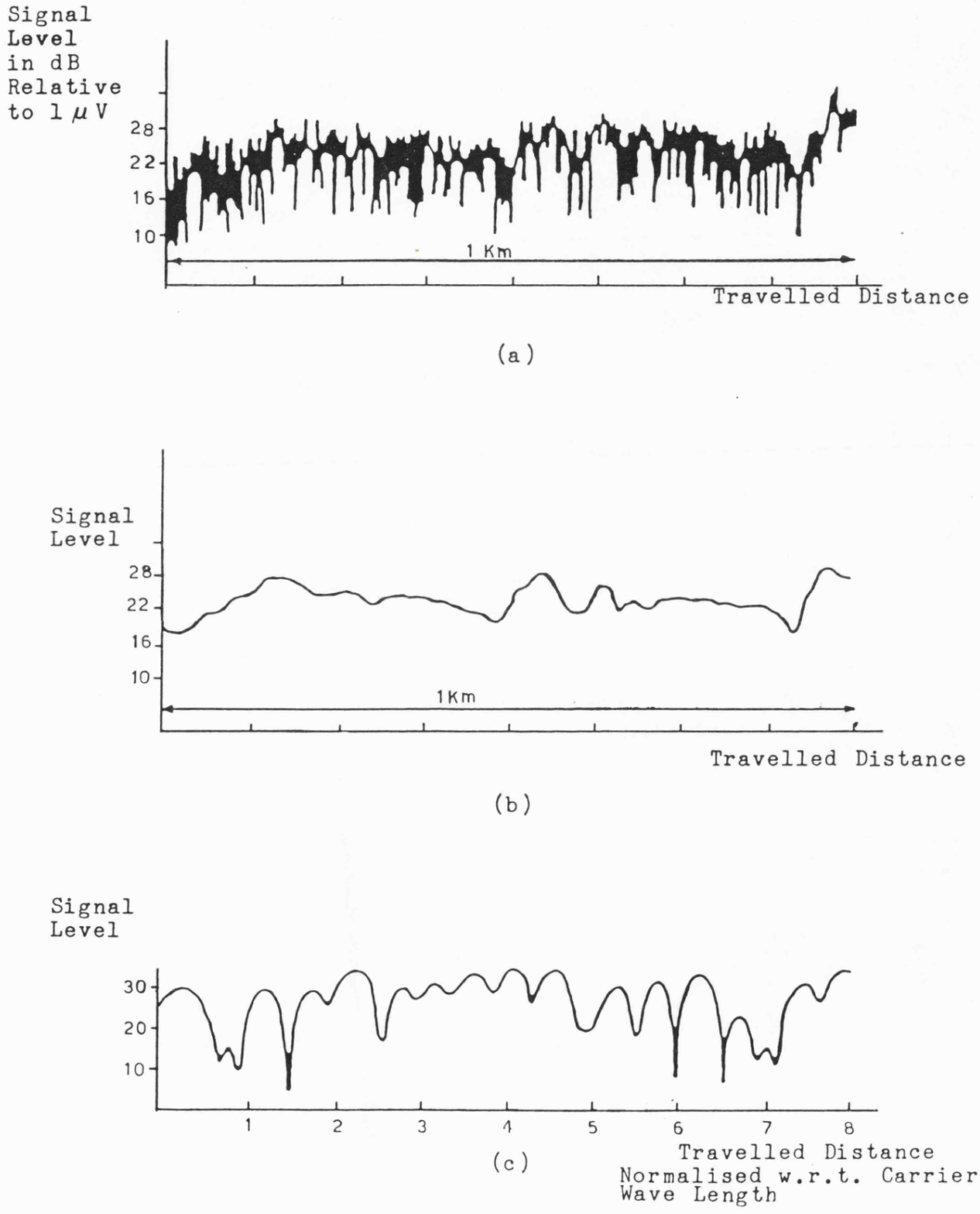

Figure 2.1 Typical Signal Level Recording at a Mobile Receiver.

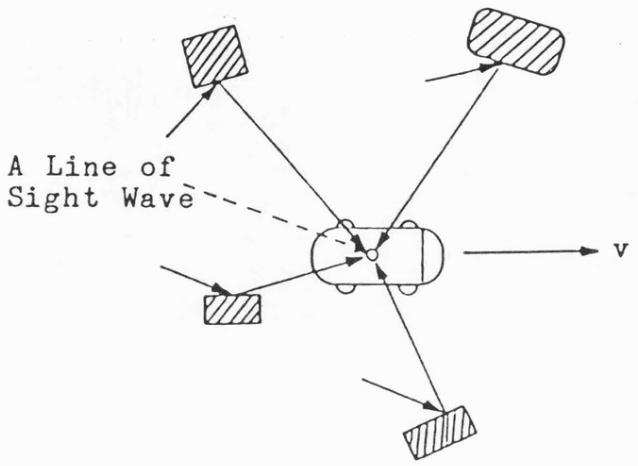

Figure 2.2 Multipath Phenomenon.

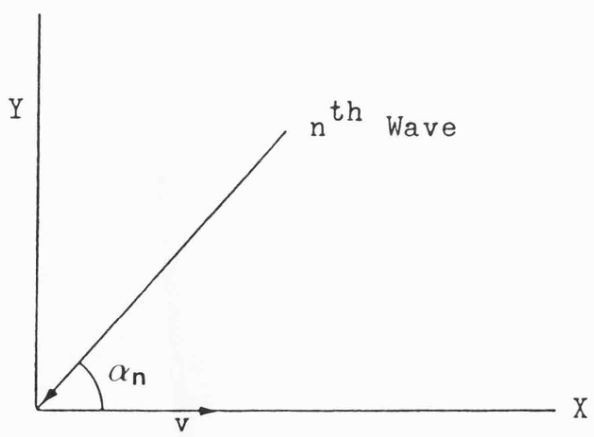

Figure 2.3 n^{th} Wave Component Arriving at the Mobile Antenna.

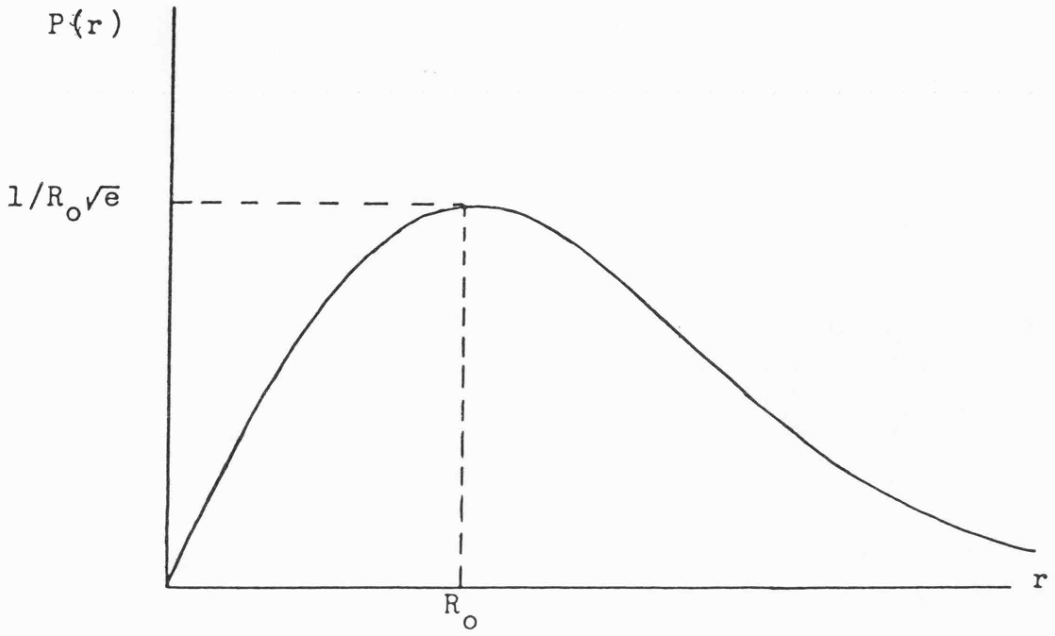

Figure 2.4 The Rayleigh Probability Density Function.

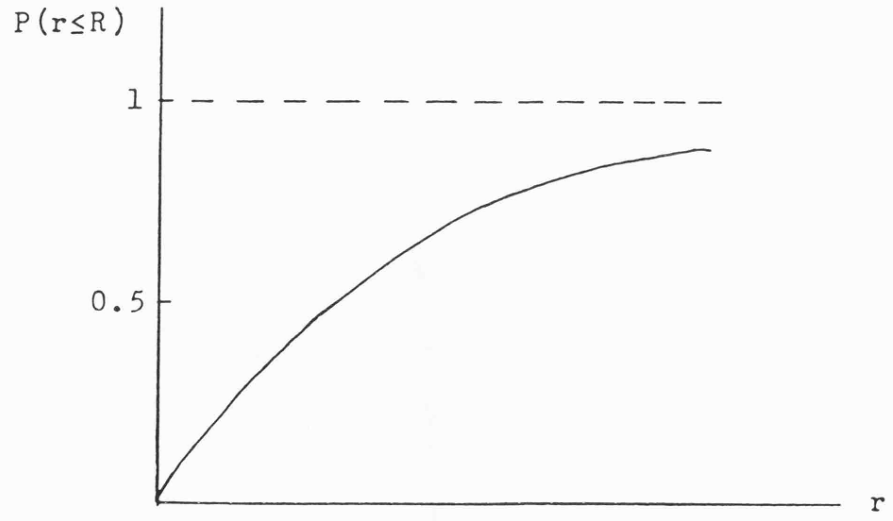

Figure 2.5 The Rayleigh Cumulative Distribution.

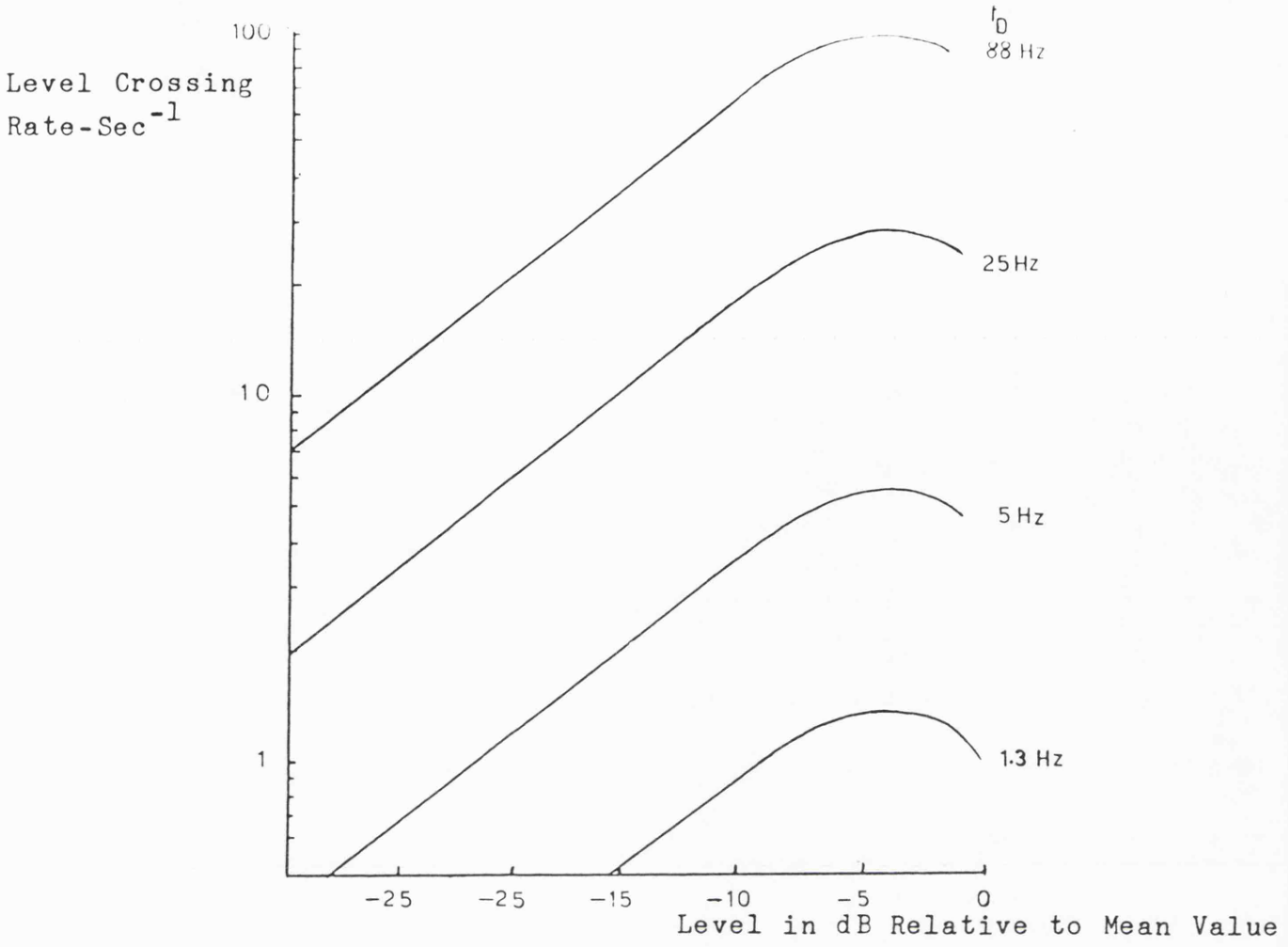

Figure 2.6 Level Crossing Rate.

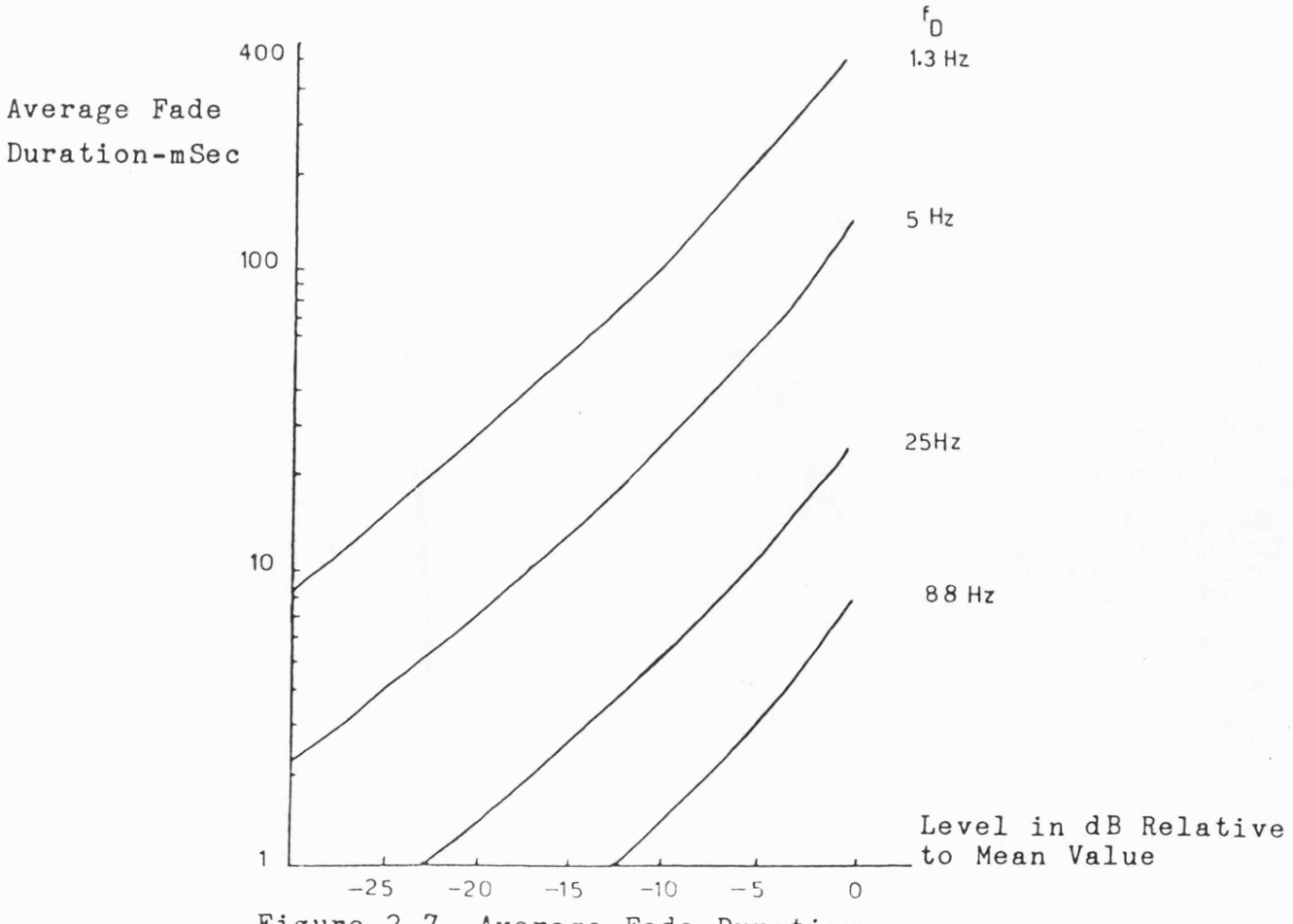

Figure 2.7 Average Fade Duration.

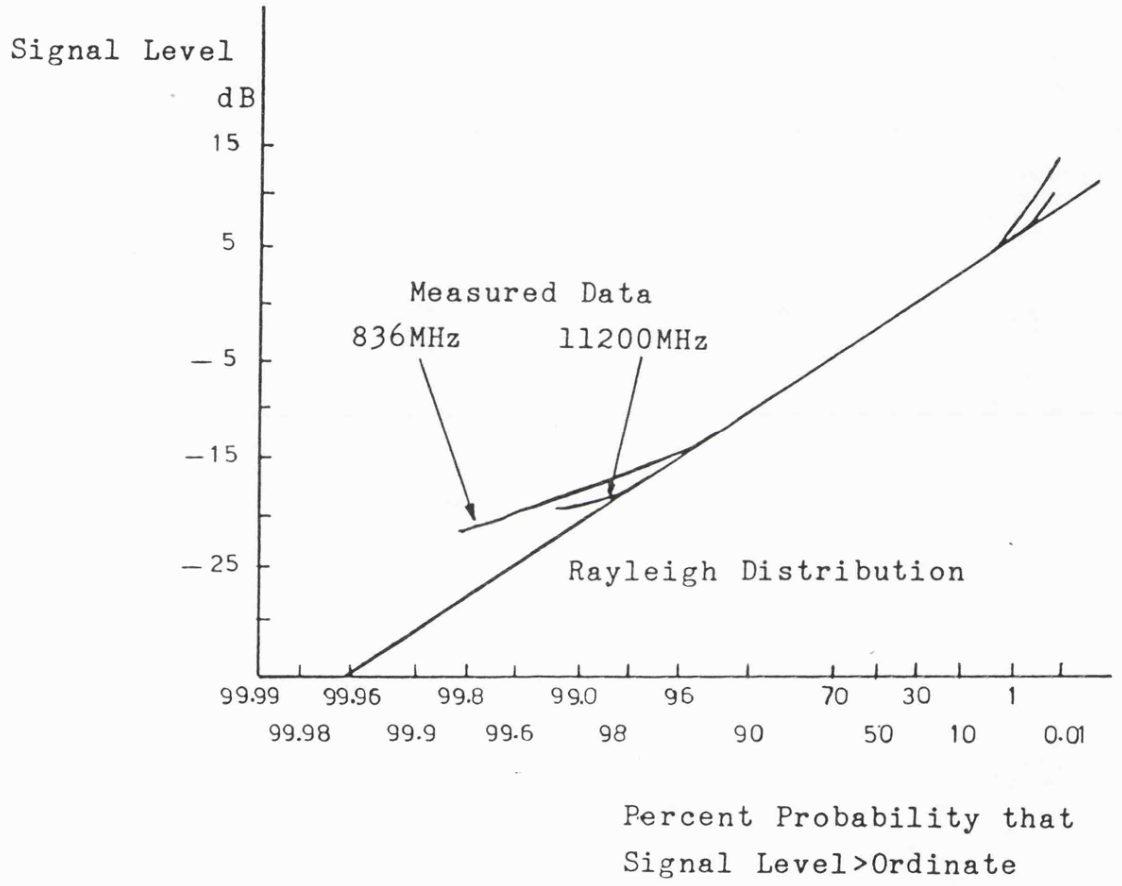

Figure 2.8 Agreement Between Measured Signal Level Distribution and Rayleigh Distribution.

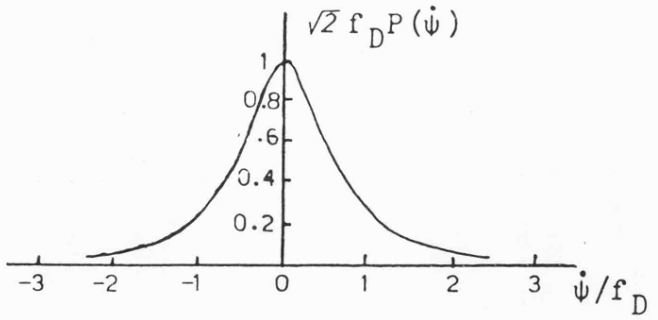

Figure 2.9(a) PDF of Instantaneous Frequency-$P(\dot{\psi})$.

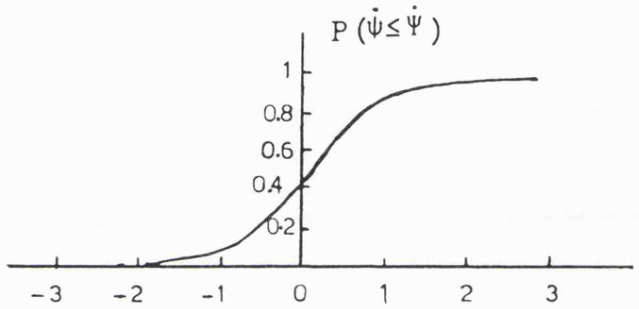

Figure 2.9(b) Cumulative Distribution of $P(\dot{\psi})$.

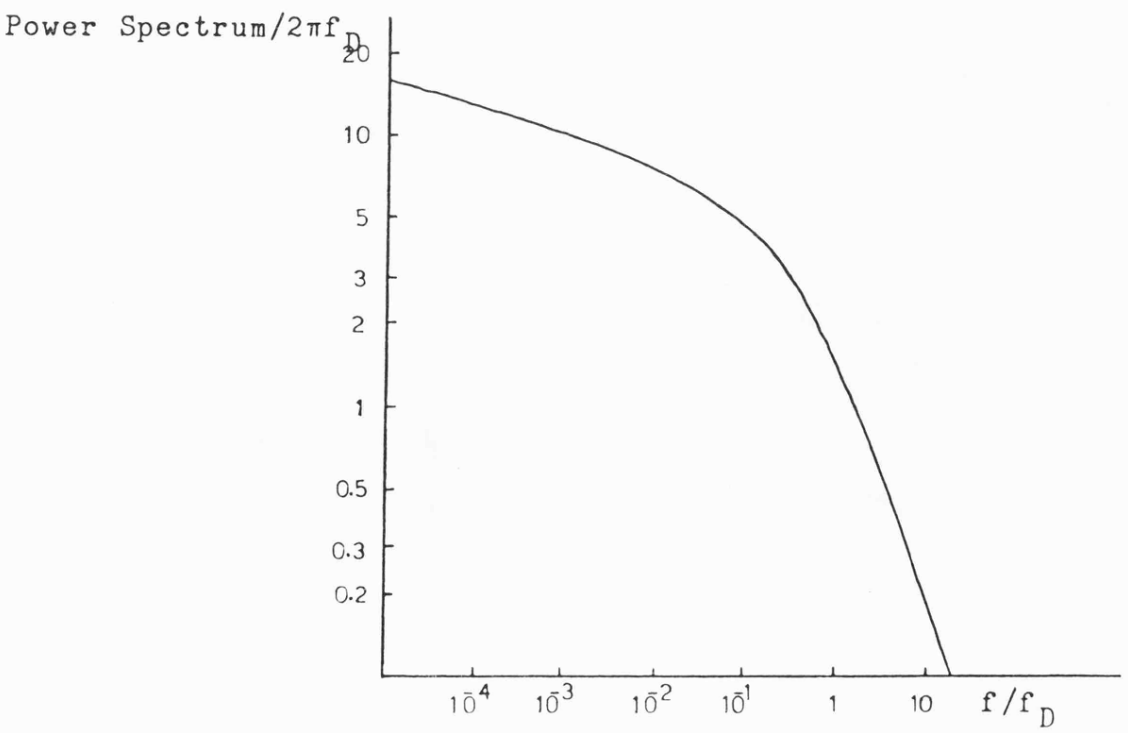

Figure 2.10 One Sided Power Spectrum of $\dot{\psi}$.

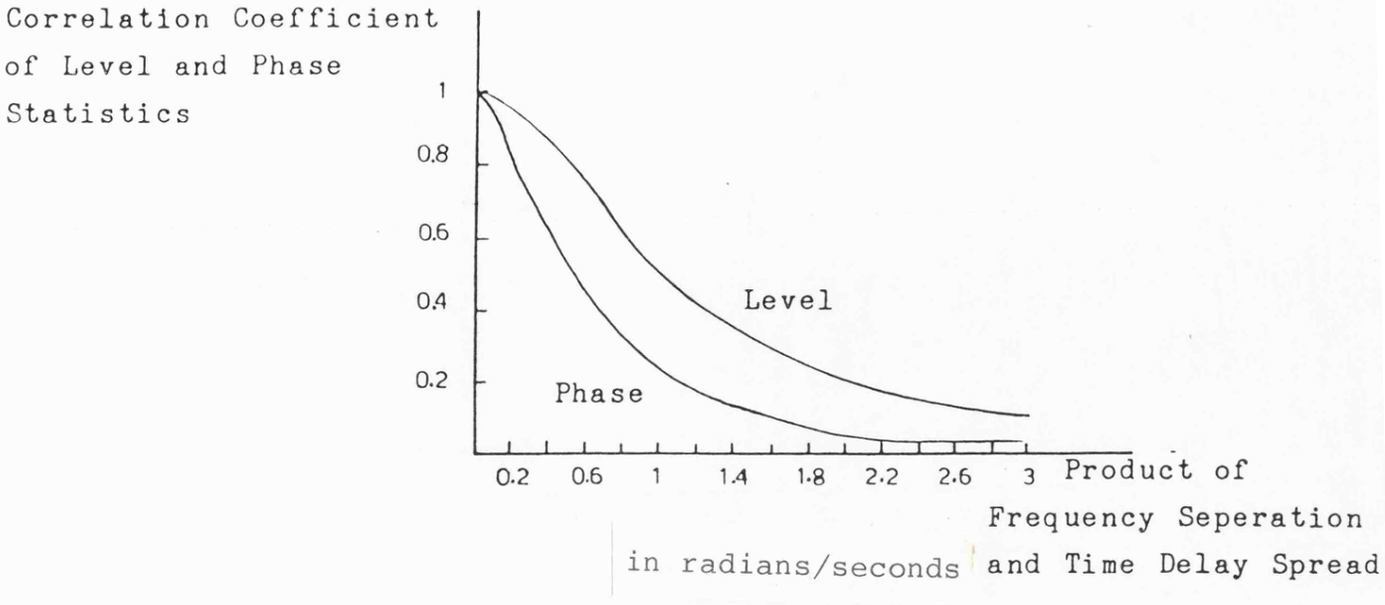

Figure 2.11 Plot of Level and Phase Statistics Correlation Coefficients Versus the Product of Time Delay Spread and Frequency Seperation.

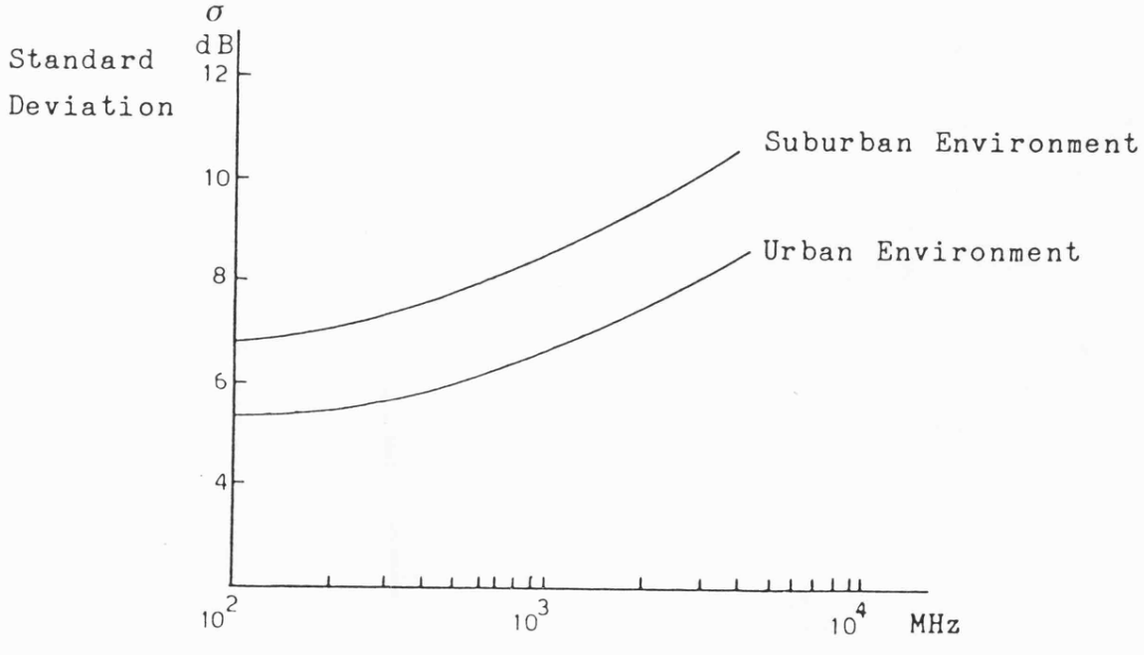

Figure 2.12 Prediction Curves for Standard Deviation σ of Long-Term Mean Signal Level.

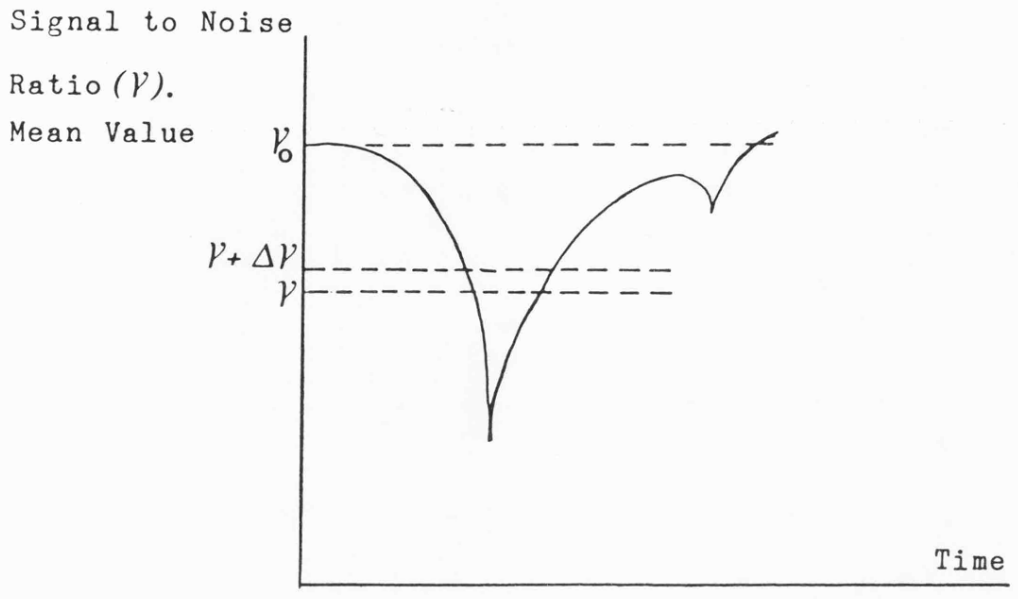

Figure 2.13 Reciever Signal to Noise Ratio in Fading Condition.

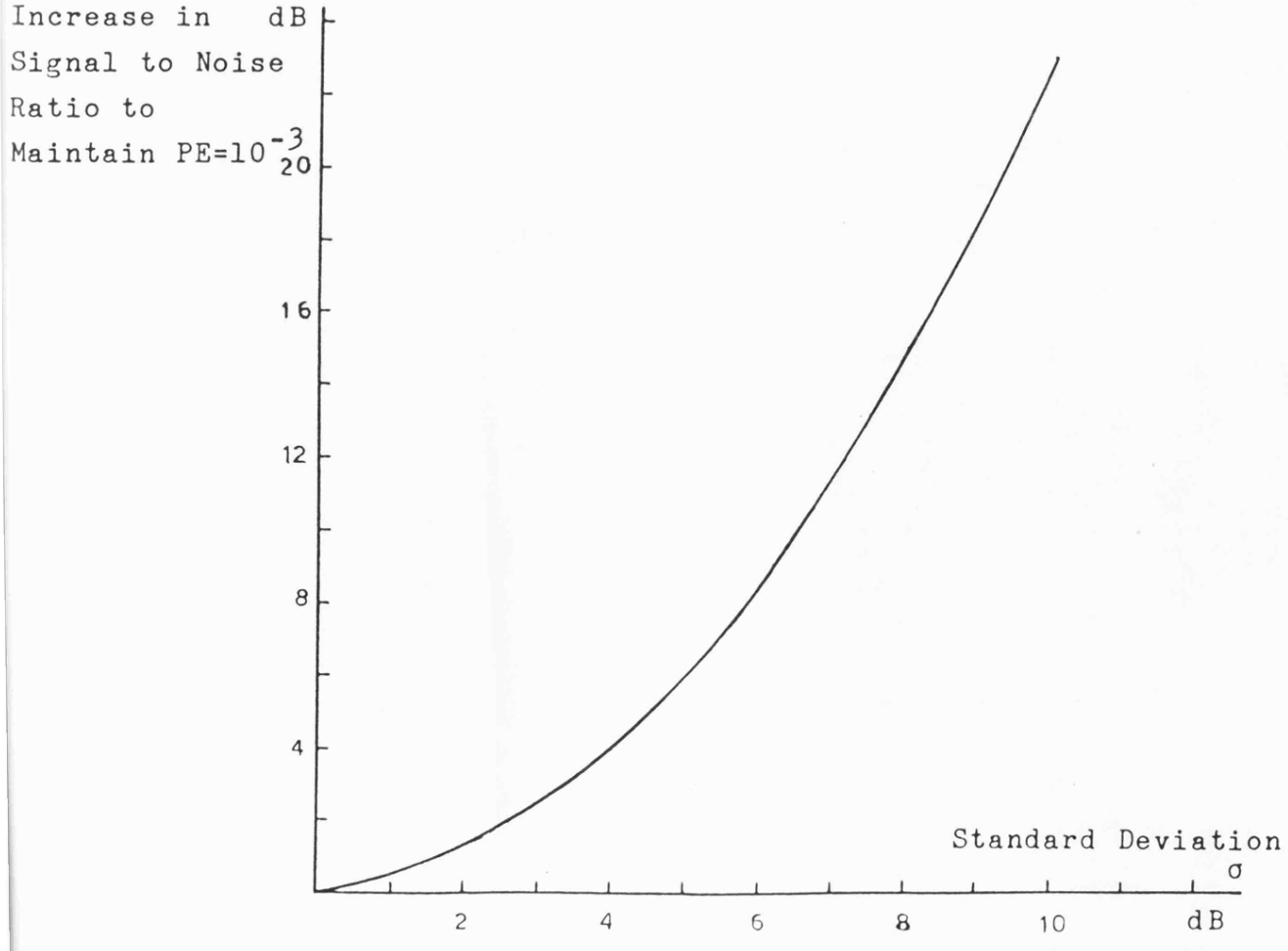

Figure 2.14 Performance Degradation due to Long-Term Fading.

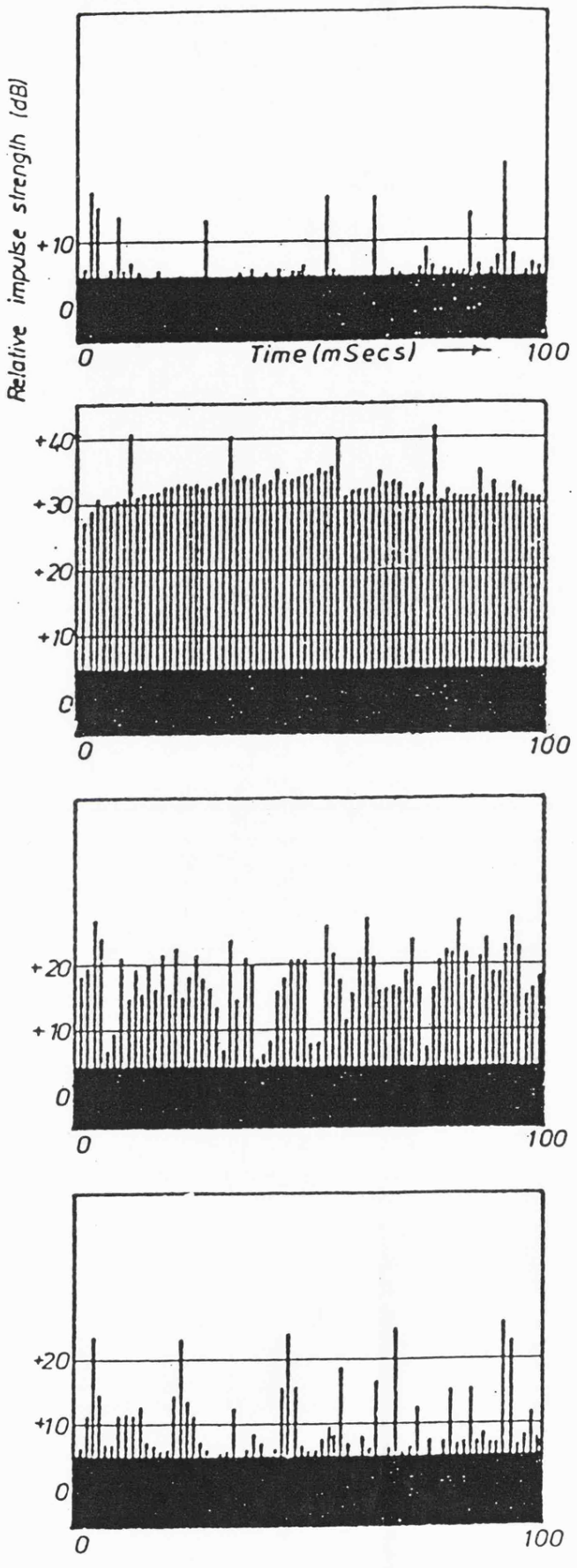

(a) Test Vehicle Engine not Running.

(b) Test Vehicle Engine Running (Un-Suppresed).

(c) Test Vehicle Engine Running-Fitted with VHF Suppresion Cmponents.

(d) Conditions as for c, but with a Capacitor Added to the Ignition Coil.

Figure 2.15 Ignition Noise.

CHAPTER THREE

NARROW BAND DIGITAL MODULATION SYSTEMS

3.1 Introduction

A carrier signal can be modulated with the data to be transmitted by varying one of its basic components. These are the amplitude, the phase and the frequency. Accordingly, digital modulation systems can be classified in three major groups. These are amplitude shift keying-ASK, phase shift keying-PSK, and frequency shift keying-FSK.

Minimum shift keying-MSK (also known as fast frequency shift keying) is unique in its properties. It can be viewed as a special case of the PSK or FSK families. Therefore, it will be discussed separately.

The advantage of using one modulation technique over the use of others depends on the nature of the application and the transmission media restrictions and impairments.

Because of the increasing demand for mobile radio channels in the UK, their bandwidth has been steadily decreased from 100kHz in the 1950s to 12.5kHz in the VHF band (68-174MHz) and 25kHz in the UHF band (425-470MHz) at the present time, with 12.5kHz channels being gradually introduced to the UHF band. Furthermore, research is currently being carried out to reduce channel bandwidth to 5kHz spacing. In addition, frequency re-use schemes are being employed in order to achieve a greater overall spectrum efficiency. Thus mobile

radio channels can be described as being both band and power limited. The power limitation results from the need to minimise co-channel interference in frequency re-use schemes and the limited power available to the transmitter/receiver at the vehicle.

Unfortunately spectrum efficiency and power efficiency are two conflicting demands in digital modulation systems. Therefore, the final choice should be based on a compromise between the two. Other factors which should be taken into consideration are error rate performance in the presence of fading and random FM noise, effect of bandlimiting on probability of error - PE - and generation of amplitude fluctuations, performance degradation in the presence of co-channel and adjacent channel interference and acceptable complexity of practical realisation.

ASK was one of the earliest forms of digital modulation used in wireless telegraphy because of its evident simplicity. If detected noncoherently (ie. by using envelope detector), the optimum decision threshold level is a function of the signal to noise ratio at the receiver and has to be adjusted continuously following changes in received signal level. This is practically very difficult to achieve in a fading environment. If coherent demodulation is used, ASK does not offer any advantage over FSK and PSK systems either in error performance or system implementation. Furthermore, to transmit 0.95 of the modulated signal energy a bandwidth of 2 to 3 times the modulating data bit rate is needed compared to less than one in the case of narrow band versions of PSK and FSK.

For the above reasons, discussion of ASK systems will not

proceed any further and attention is turned to PSK, FSK and MSK systems and their variants. These systems share two important features: constant signal envelope (prior to post modulation filtering) and fixed decision threshold which make them potential candidates for use in mobile radio digital transmission.

Of all PSK, FSK and MSK variants, only those which occupy a relatively narrow band without a great sacrifice in power performance will be considered.

In recent years, a number of new modulation techniques have been suggested for potential use in mobile radio. Most of these can be considered as variants of MSK modulation. They achieve better spectrum efficiency, in the sense of lower out of band radiation, than MSK. This is achieved with variable degrees of greater design complexity and deterioration in bit error rate performance and resistance to different types of interference and impairments. The most common of these systems will be discussed at the end of this chapter.

3.2 Generation and Power Spectral Density of PSK, FSK and MSK Systems

The general expression for a phase or frequency modulated carrier is:

$$S_C(t) = A_C\cos(2\pi f_C t + \phi(t) + \phi_O) \qquad \ldots (3.1)$$

where A_C, f_C and ϕ_O are the amplitude, frequency and initial phase at the start of modulation of the carrier respectively. ϕ_O can be assumed zero without loss of generality. $\phi(t)$ is the term proportional to the modulating data. The form it takes determines

and characterises the resultant modulation. Throughout this study the baseband modulating data format is assumed polar binary non-return to zero - NRZ.

Studying the power spectral density is important to evaluate bandwidth efficiency of different techniques and the proximity with which adjacent channels can be located. In this section the different methods used in generating PSK, FSK and MSK systems are discussed, together with their respective power spectral density functions - PSDF.

3.2.1 PSK Systems

The simplest form of PSK is binary PSK - BPSK. In BPSK $\phi(t)$ changes in discrete steps between 0 and π depending on whether a mark (+1) or a space (-1) is being transmitted. Thus, the BPSK waveform can be written as:

$$S_{BPSK}(t) = a_n A_C \cos 2\pi f_C t \quad nT_b \leq t \leq (n+1)T_b \quad \ldots (3.2)$$

where a_n represents the modulating data and is equal to ± 1 depending on whether a mark (+1) or a space (-1) is being transmitted, T_b is the bit period and n=1,2,3,... . Marks and spaces occur with equal probabilities.

A simple BPSK modulator is shown in Fig 3.1. An arbitrary data stream and the equivalent BPSK waveform are shown in Fig 3.2.

The time domain multiplication operation performed on the carrier in the above modulator is equivalent to the well-known double sideband suppressed carrier amplitude modulation (DSB-SC). Therefore, the PSDF of BPSK is a linear frequency translation of the

double sided baseband function. The PSDF of binary equiprobable NRZ signals is[1]:

$$P_{NRZ}(f) = \frac{2P}{f_b} \left[\frac{\sin \pi f/f_b}{\pi f/f_b} \right]^2$$

Thus, the PSDF of BPSK is given by:

$$P_{PBSK}(f) = \frac{2P}{f_b} \left[\frac{\sin \pi(f-f_c)/f_b}{\pi(f-f_c)/f_b} \right]^2 \qquad \ldots (3.3)$$

where P is the total signal power and f_b is the modulating data bit rate ($f_b = 1/T_b$). The spectrum of BPSK is given in Fig 3.3.

The frequency spectrum occupancy of BPSK signals can be halved by adding two BPSK signals each modulated by one of two quadrature carrier sinusoids. The resultant signal, known as quadrature PSK-QPSK, is thus composed of two orthogonal BPSK signals which can be separated at the receiver. The QPSK waveform can be written as:

$$S_{QPSK}(t) = A_c \left[aI \cos(2\pi f_c t) + aQ \sin(2\pi f_c t) \right]$$

where aI and aQ are the inphase and quadrature modulating data and can be equal to ±1 depending on the state of the data. Consequently, the QPSK signal can have one of the following four states:

$$A_c \left[+ \cos(2\pi f_c t) + \sin(2\pi f_c t) \right] \quad \text{if } aI = +1, \quad aQ = +1,$$

$$A_c \left[- \cos(2\pi f_c t) + \sin(2\pi f_c t) \right] \quad \text{if } aI = -1, \quad aQ = +1,$$

$$A_c \left[- \cos(2\pi f_c t) - \sin(2\pi f_c t) \right] \quad \text{if } aI = -1, \quad aQ = -1,$$

and $A_c \left[+ \cos(2\pi f_c t) - \sin(2\pi f_c t) \right]$ if aI = +1, aQ = -1.

Using trigonometric identities these states can be rewritten as:

$$\sqrt{2}\ A_c \cos(2\pi f_c - \pi/4) ,$$

$$\sqrt{2}\ A_c \cos(2\pi f_c - 3\pi/4) ,$$

$$\sqrt{2}\ A_c \cos(2\pi f_c - 5\pi/4) ,$$

and $\sqrt{2}\ A_c \cos(2\pi f_c - 7\pi/4)$.

Thus the carrier phase is equal to one of four discrete values, each representing a pair (aI, aQ) of data bits. The QPSK signal phasor diagram is shown in Fig 3.4.

Based on the above discussion a possible QPSK modulator structure is shown in Fig 3.5. The incoming data stream $\{a_n\}$ at the modulator input at a rate of f_b and is split in two streams $\{aI_n\}$ and $\{aQ_n\}$ consisting of odd and even bits respectively. The splitter also doubles the duration of each bit. This operation is demonstrated in Fig 3.6.

The resultant odd and even data go through two BPSK modulators derived by the inphase and the quadrature carrier signals. Finally the output of the modulators are summed together to produce the QPSK waveform which is shown in Fig 3.7.

The PSDF is the same as that of BPSK except for replacing f_b by $f_b/2$. The spectrum of QPSK signal is shown in Fig 3.3 for the same

number of bits transmitted per second as in the case of BPSK.

It is possible to further reduce the spectrum occupancy of PSK signal by increasing the allowable carrier phase states. However, this leads to an increase in the modulator/demodulator structure complexity and excessive deterioration in system error performance and resistance to co-channel interference when the number of phase levels exceeds 4 (ie. the QPSK case).

In QPSK instantaneous phase transition of π can take place when both bits in the input data pair change states. When the QPSK waveform is bandlimited these large phase jumps lead to large fluctuations in the signal envelope.

These fluctuations can be reduced by limiting allowable phase transitions to $\pi/2$. This is done by delaying the Q-channel data bits by T_b with respect to I-channel. This new configuration is shown in Fig 3.8, while its timing diagram is given in Fig 3.6 and is known as offset quadrature phase shift keying - OQPSK.

In OQPSK the modulating data pair cannot change simultaneously. Consequently the carrier phase changes at most by $\pi/2$. The waveform of OQPSK is shown in Fig 3.7.

The delay operation does not alter the unfiltered PSDF of QPSK. Hence, that of OQPSK is the same as QPSK given in Fig 3.3.

3.2.2 FSK Systems

FSK signals can be generated either by switching between two

independent oscillators or changing the freuqency of a single oscillator. In the first case the carrier can go through discontinuous phase transition during switching instants, while in the second case the phase is continuous even during the data transition instants.

Bennett and Rice[2] have shown that discontinuous phase transitions cause spreading of the PSDF of FSK signals and ultimately the spectrum falls off as the inverse square of the frequency. When phase transitions are continuous the resultant PSDF is more compact and ultimately falls off as the inverse fourth power of the frequency. Consequently, only the continuous phase case will be considered.

One way to produce continuous phase FSK signals - CPFSK - is by applying the baseband data to a voltage controlled oscillator - VCO. The VCO output during bit period, $nT_b \leq t \leq (n+1)T_b$, can be expressed as:

$$S_{CPFSK}(t) = A_c \cos\left[\left[2\pi f_c + a_n \frac{\pi h}{T_b}\right] t + \Phi_n\right]$$

$$nT_b \leq t \leq (n+1)T_b \qquad \ldots (3.4)$$

where h is the deviation ratio defined as the ratio between the difference of the mark frequency (fm) and the space frequency (fs) and the bit rate f_b,

$$h = \frac{fm - fs}{f_b} \qquad \ldots (3.5)$$

ϕ_n is a phase constant valid for $nT_b \leq t \leq (n+1)T_b$. The value of ϕ_n is determined by the requirement that the phase of the waveform be continuous at bit transition instants $t = nT_b$.

The excess carrier phase function $\phi(t)$ is given by:

$$\phi(t) = a_n \frac{\pi h}{T_b} t + \phi_n \qquad nT_b \leq t \leq (n+1)T_b \qquad \ldots (3.6)$$

Thus, when a mark is transmitted ($a_n = +1$) the carrier phase advances by πh while a space ($a_n = -1$) causes it to retard by πh. $\phi(t)$ is shown in Fig 3.9, assuming without loss of generality that the phase at the start of modulation is zero. Solid lines and dotted lines in Fig 3.9 correspond to transmission of marks and spaces respectively.

The phase continuity requirement during bit transitions results in the following recursive formula giving the value of ϕ_n:

$$\phi_n + a_n n\pi h = \phi_{n-1} + a_{n-1} n\pi h$$

or

$$\phi_n = \phi_{n-1} + (a_{n-1} - a_n) n\pi h \qquad \ldots (3.7)$$

For the special case when $h = 0.5$, the relevance of which will become evident later, eqns (3.4) and (3.7) become:

$$S_{CPFSK}(t) = A_c \cos \left[(2\pi f_c t) + a_n \frac{\pi}{2T_b} + \phi_n \right] \quad nT_b \leq t \leq (n+1)T_b$$

$$\ldots (3.8)$$

and

$$\phi_n = \phi_{n-1} + (a_{n-1} - a_n) \frac{\pi}{2} n \qquad \ldots (3.9)$$

Assuming that the value of ϕ_n at the beginning of modulation is equal to zero, and knowing that $(a_{n-1} - a_n)$ can only be 0, 2 or -2, then the value of ϕ_n is restricted to 0, π and modulo 2π.

Knowing that

$$\cos(x \pm n\pi) = \cos(x) \qquad \ldots (3.10a)$$

for n equal even integer numbers, and

$$\cos(x \pm n\pi) = -\cos(x) \qquad \ldots (3.10b)$$

for n equal odd integer numbers. Then if n is even, (3.9) becomes:

$$\phi_n = \phi_{n-1} \qquad \ldots (3.11)$$

and if n is odd it becomes

$$\begin{aligned} \phi_n &= \phi_{n-1} \pm \pi \quad \text{if } a_n \neq a_{n-1} \\ \phi_n &= \phi_{n-1} \quad \text{if } a_n = a_{n-1} \end{aligned} \qquad \ldots (3.12)$$

Bennett and Rice[2] have calculated the PSDF of CPFSK signal by taking the Fourier transform of its autocorrelation function. The general expression for the PSDF is given by:

$$P_{CPFSK}(f) = 2A_c^2 f_b \left\{ \frac{\sin^2\left[\pi \frac{(f-f_s)}{fb}\right] \sin^2\left[\pi \frac{(f-f_m)}{fb}\right]}{1-2\cos\left[2\pi \frac{(f-f_c)}{fb}\right] \cos(\pi h) + \cos^2(\pi h)} \right.$$

$$\left. * \left[\frac{1}{2\pi(f-f_s)} - \frac{1}{2\pi(f-f_m)} \right]^2 \right.$$

$$+ \frac{\sin^2\left[\pi\frac{(f+f_s)}{fb}\right]\sin^2\left[\pi\frac{(f+f_m)}{fb}\right]}{1-2\cos\left[2\pi\frac{(f+f_c)}{fb}\right]\cos(\pi h)+\cos^2(\pi h)}$$

$$* \left\{\left[\frac{1}{2\pi(f+f_s)} - \frac{1}{2\pi(f+f_m)}\right]^2\right\} \qquad \ldots (3.13)$$

Figs 3.10(a), (b) and (c) show the PSDF of CPFSK signal when h = 0.5, 0.7 and 1 respectively calculated from the above expression. The measured spectrum under the above conditions is shown in Fig 3.11. The CPFSK signal was produced by allowing a pseudo random data sequence (511 bits in length) to control the control voltage of a voltage controlled crystal oscillator - VCXO. The VCXO circuit is given in Appendix 4.5. The agreement between the measured spectrum and the theoretical one is evident.

From the above figures it is possible to conclude that for h < 1 the signal spectrum becomes more concentrated around the centre frequency as h decreases. Therefore, under this condition CPFSK signals become of potential importance for narrow band applications. In the remainder of this chapter CPFSK signals having h < 1 are termed narrow band CPFSK, NB-CPFSK.

3.2.3 MSK

As was stated previously, MSK can be considered as a special case of PSK or CPFSK. To demonstrate this property MSK is first defined in its PSK form; subsequently its relation with CPFSK will be

established.

A possible MSK modulator structure is shown in Fig 3.12. The incoming data enters the odd/even splitter at a rate of f_b and comes out at a rate of $f_b/2$. The Q-channel data (aQ_n) is delayed by T_b with respect to the I-channel data (aI_n). In the I-channel the data multiplies a sinusoidal reference, cos ($\pi/2$ $f_b t$), whose period is four times the original data period and its zero crossing coincides with the I-channel data transition instants. This operation results in a half sinusoidal pulse over intervals of $2T_b$. The pulse sign depends on the incoming data (aI_n) state. A similar operation is performed in the Q-channel except that the reference is phase shifted by $\pi/2$ to give sin($\pi/2$ $f_b t$). The above procedure is illustrated in Fig 3.13.

Finally, the I and Q channel pulses are multiplied by an inphase and a quadrature carrier waveform respectively. The results of multiplication are summed to give the MSK signal.

Recalling Fig 3.8 and the description of OQPSK, it is clear that MSK is equivalent to the latter but with the data pulses being sinusoidally weighted.

The MSK waveform can be expressed as:

$$S_{MSK}(t) = A_C \left[aI_n \cos\left[\frac{\pi}{2} f_b t\right]\cos(2\pi f_C t) + aQ_n \sin\left[\frac{\pi}{2} f_b t\right]\sin(2\pi f_C t) \right]$$

$$n T_b \leq t \leq (n+1) T_b \qquad \ldots (3.14)$$

Using trigonometric identities eqn (3.14) can be rearranged as:

$$S_{MSK}(t) = A_c \left\{ \left[\frac{1}{2} aI_n \left[\cos \left[2\pi \left[f_c - \frac{f_b}{4} \right] t \right] + \cos \left[2\pi \left[f_c + \frac{f_b}{4} \right] t \right] \right] \right] \right.$$

$$\left. + \left[\frac{1}{2} aQ_n \left[\cos \left[2\pi \left[f_c - \frac{f_b}{4} \right] t \right] - \cos \left[2\pi \left[f_c + \frac{f_b}{4} \right] t \right] \right] \right] \right\}$$

Replacing $\left[f_c - \frac{f_b}{4} \right]$ by f_s and $\left[f_c + \frac{f_b}{4} \right]$ by f_m, the above equations can finally be written as:

$$S_{MSK}(t) = \frac{A_c}{2} \left\{ aI_n \left[\cos(2\pi f_s t) + \cos(2\pi f_m t) \right] + aQ_n \left[\cos(2\pi f_s t) \right. \right.$$

$$\left. \left. - \cos(2\pi f_m t) \right] \right\} \qquad nT_b \leq t \leq (n+1)T_b \qquad \ldots (3.15)$$

Eqn (3.15) provides an alternative description of the MSK signal. Although aI_n and aQ_n have a constant value (± 1) over $2T_b$ period each, either of them can change value every T_b. Consequently and from eqn (3.15) the MSK signal can change frequency every T_b depending upon the values of aI_n and aQ_n. The relationship between aI_n, aQ_n and the resultant frequency is illustrated in Fig 3.14. Inspection of this figure indicates that a frequency f_s is transmitted during a time slot T_b if the I and Q data during this time

slot are equal, if they are unequal a frequency f_m is transmitted. The relation between f_m, f_s and f_b is:

$$\frac{f_m - f_s}{f_b} = \frac{1}{2} \qquad \ldots (3.16)$$

Based on the above discussion, eqn (3.14) can be rearranged and written as follows:

$$S_{MSK}(t) = A_c \left[\cos \left[2\pi f_c t + b_{2K} \frac{\pi}{2T_b} t + \psi_{2K} \right] \right]$$

$$2KT_b \leq t \leq (2K+1)T_b \qquad \ldots (3.17)$$

where the bit intervals and arrangement of data is depicted by the following.

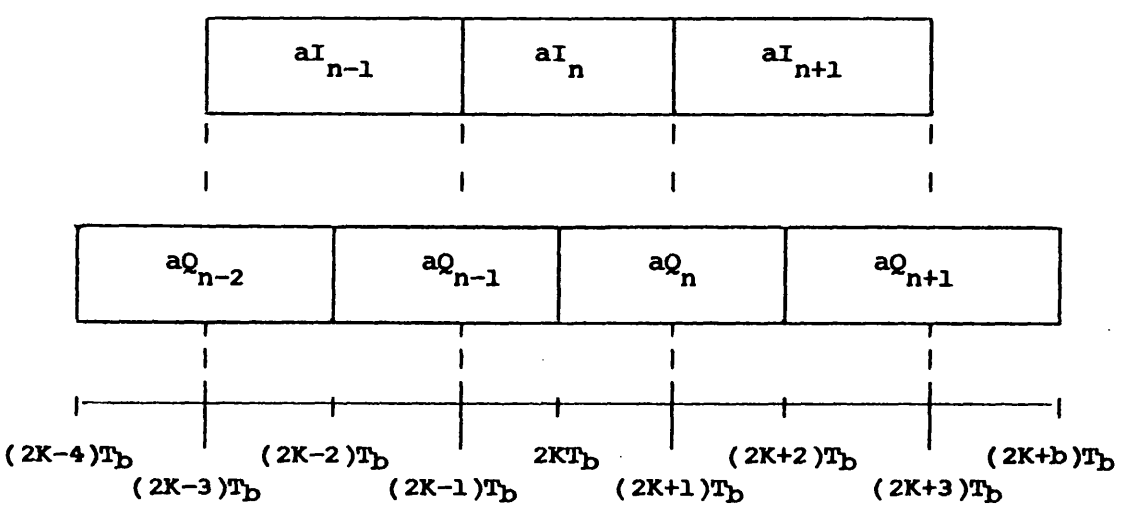

and

$b_{2K} = -aI_n \, aQ_n$

$\psi_{2K} = 0 \qquad$ if $aI_n = +1$

$= \pi \qquad$ if $aI_n = -1$

In the preceding interval, ie. $(2K-1)T_b \leq t \leq 2KT_b$:

$$b_{2K-1} = -aI_n \; aQ_{n-1}$$

$$\Psi_{2K-1} = 0 \qquad \text{if } aI_n = +1$$

$$= \pi \qquad \text{if } aI_n = -1$$

and in the following interval, ie. $(2K+1)T_b \leq t \leq (2K+2)T_b$

$$b_{2K+1} = -aI_{n+1} \; aQ_n$$

$$\Psi_{2K+1} = 0 \qquad \text{if } aI_{n+1} = +1$$

$$= \pi \qquad \text{if } aI_{n+1} = -1$$

In order to ensure that a one-to-one relationship exists between the data source output and the MSK modulator output frequency, some sort of coding should be applied to the data stream before the splitter. The encoder function is to compare the input to the modulator with the last transmitted bit, odd or even. If they are equal the next encoder output should be a space (-1) and if they are unequal it should be a mark (+1). This procedure is known as differential encoding and can be expressed as:

$$C_{n+1} = a_{n+1} \oplus C_n$$

where $\{C_n\}$ is the encoder output and $\oplus$ refers to the logical exclusive OR operation. The MSK data encoder is illustrated in Fig 3.15(a). The one-to-one relationship between the transmitted frequencies and the original modulating data resulting from the above encoding process is demonstrated in Fig 3.15(b).

From the above analysis MSK can be viewed as a form of FSK modulation whose deviation ratio h, defined by eqn (3.5) and given by eqn (3.16) for the MSK signal, is equal to exactly 0.5. Furthermore, it will be demonstrated in the following that the phase of the modulated carrier is continuous during bit transitions.

It follows from comparing eqn (3.8) and (3.17) that ϕ_n and a_n in the first are given by ψ_{2K} and b_{2K} in the second respectively. Hence, ψ_{2K} should satisfy both equations (3.11) and (3.12) before MSK may be considered as CPFSK.

The first condition (eqn (3.11)) is easily demonstrated by noticing that ψ_{2K} changes value according to changes in aI_n only, ie. at the beginning of odd time intervals. Thus,

$$\psi_{2K} = \psi_{2K-1} \qquad \ldots (3.18)$$

Replacing ϕ_n and a_n by ψ_{2K+1} and b_{2K+1} in eqn (3.9) gives:

$$\psi_{2K+1} = \psi_{2K} + (-aQ_n)(aI_n - aI_{n+1}) \frac{\pi}{2} (2K+1)$$

Recalling the previous remark concerning (3.10(a) and (b)) and eqn (3.18), the above expression can be reduced to:

$$\psi_{2K+1} = \psi_{2K-1} + (aI_n - aI_{n+1}) \frac{\pi}{2} \qquad \ldots (3.19)$$

ψ_{2K+1} in the above equation appears to depend not only on aI_{n+1} as previously stated for MSK, but also on aI_n and ψ_{2K-1}.

This apparent contradiction can be resolved by remembering that $\psi_{2K+1} = 0$ or π and that the initial reference values of ψ_{2K+1} and aI_n are zero and +1. Thus, and from the recursive nature of eqn (3.19), it can be stated that if $\psi_{2K-1} = 0$ or π aI_n is equal to +1 or -1 respectively. Hence, for $aI_{n+1} = +1$ and $\psi_{2K-1} = \pi$:

$$\psi_{2K+1} = \pi + (-1 - 1) \frac{\pi}{2} = 0$$

and, for $aI_{n+1} = -1$ and $\psi_{2K-1} = \pi$:

$$\psi_{2K+1} = \pi + (-1 + 1)\frac{\pi}{2} = \pi$$

Similarly, all other combinations will lead to the conclusion that:

$$\psi_{2K+1} = 0 \text{ or } \pi, \text{ for } aI_{n+1} = +1 \text{ or } -1$$

which resolves the contradiction stated before. Thus, it can finally be stated that MSK is equivalent to CPFSK signal having a deviation ratio equal to 0.5.

Consequently, an MSK signal can be generated either by using a CPFSK modulator whose deviation ratio is equal to exactly 0.5, or by using the quadrature modulation method explained at the beginning of this section.

The PSDF of an MSK signal is calculated from eqn (3.13) by substituting for h = 0.5. Alternatively, an approach similar to the one used to calculate the PSDF of BPSK can be used because the MSK signal can be described by a linear model. Both approaches lead to the following expression fro the PSDF of the MSK:

$$P_{MSK}(f) = \frac{8P}{f_b\pi^2} \frac{\left[1 + \cos 4\pi \frac{(f - f_c)}{f_b}\right]}{\left[1 - 16\left[\frac{f - f_c}{f_b}\right]^2\right]^2} \quad \ldots (3.20)$$

which is illustrated in Figs 3.3 and 3.10(a). The measured spectrum of CPFSK (h=0.5) shown in Fig 3.11(a) is also equivalent to that of an MSK signal.

3.3 Error Rate Performance of PSK, FSK and MSK Systems in Ideal Conditions

The commonly used measure of performance for digital modulation systems is the relationship between the probability of error and the signal to noise ratio assuming white Gaussian additive noise. The latter is usually expressed by its baseband equivalent (E_b/N_o) defined as the ratio between the average energy per bit to the one sided noise power spectral density as measured at the receiver input.

Ideal conditions refer to perfect transmitter and receiver circuit components and ideal transmission conditions where the only source of errors is additive random Gaussian noise. Furthermore, no error correcting codes are used.

The error performance depends on both the modulation technique and detection mechanism, and establishes a base line for comparison between the various methods. In the previous chapter it was referred to as $P_e(\gamma)$, where $\gamma = E_b/N_o$, and the same notation will be used throughout the remainder of this work.

Detection or demodulation methods can be classified in three major groups. These are coherent detection, differential detection and non-coherent detection. In the first, detection relies on precise knowledge of the phase and frequency of the carrier or reference signals. In the second, detection is accomplished by comparing the received signal by its delayed version. In the third, detection is based on amplitude or frequency information carried by the carrier signal, but no knowledge of the carrier phase is assumed.

3.3.1 PSK Systems

PSK signals can be demodulated using either coherent or differential detectors.

A possible coherent BPSK demodulator implementation is shown in Fig 3.16. This is also known as the correlation detector. The incoming signal is processed in the carrier recovery - CR - circuit to reproduce a phase-locked reference which is multiplied by the incoming signal ($S_r(t)$). The output of the multiplier is passed through an ideal integrator which is dumped every T_b seconds to prevent interference between adjacent bits. This latter operation is also referred to as integrate and dump - I&D. Finally, the output from the I&D, $S_d(t)$, is processed in a decision device. If $S_d(t) > 0$, then the decision is a mark; otherwise, a space is considered as the right decision.

In [3], the expression for $P_e(\gamma)_s$ for the above correlation receiver is shown to be:

$$P_e(\gamma)_s = \frac{1}{2} \operatorname{erfc} \sqrt{\frac{E_b(1-\rho)}{2N_o}} \qquad \ldots (3.21)$$

where erfc(.) is the complementary error function, and ρ is the correlation coefficient of the mark and space carrier waveforms which are assumed to have equal energy per bit. ρ is given by:

$$\rho = \frac{1}{E_b} \int_0^{T_b} S_m(t)\, S_s(t)\, dt \qquad \ldots (3.22)$$

where $S_m(t)$ and $S_s(t)$ are the mark and space waveforms resulting from the modulation process.

In BPSK $S_m(t)$ and $S_s(t)$ are given by:

$$S_m(t) = A_c \cos(2\pi f_c t)$$

$$S_s(t) = A_c \cos(2\pi f_c t + \pi)$$

The signal energy per bit is thus given by

$$E_b = \int_0^{T_b} S_m^2(t)\, dt = \int_0^{T_b} S_s^2(t)\, dt \qquad \ldots (3.23)$$

If $f_c >> 1/T_b$, the above integration yields:

$$E_b = \frac{A_c^2 T_b}{2} \qquad \ldots (3.24)$$

and the correlation coefficient becomes:

$$\rho = \frac{1}{E_b} \int_0^{T_b} \cos(2\pi f_c t) \cos(2\pi f_c t + \pi)\, dt$$

$$= -1$$

which is the minimum possible value for ρ. Thus, the probability of error of BPSK is given by:

$$P_e(\gamma)_s = \frac{1}{2} \operatorname{erfc} \left[\sqrt{\frac{E_b}{N_o}} \right] \qquad \ldots (3.24)$$

This represents the optimum error performance for all modulation and demodulation schemes when the signal is observed over one bit period.

In practice, regeneration of the carrier at the demodulator is accomplished by a square law or related non-linear operation (Costa's loop). In all these schemes the reference carrier is recovered with a

2-phase ambiguity (ie. it can be either $\cos(2\pi_c t)$ or $\cos(2\pi f_c t+\pi)$. Subsequently, the recovered data can be either all correct or all inverted. To overcome this problem without the need to transmit a reference carrier tone or a reference code word, differential encoding and decoding are used at the transmitter and the receiver. The encoder is similar to the one used to encode the data in MSK and given in Fig 3.15(a). The decoder performs the inverse logical operation and is given in Fig 3.17(a). The differential encoder/decoder operation is best explained by the example given in Fig 3.17(b).

The resolution of ambiguity occurs with a penalty in probability of error performance. If one demodulator output bit is in error the decoder output will tend to have double errors because two bits are compared for each output bit. Thus, the probability of error for differentially encoded BPSK-DEBPSK is given by:

$$P_e(\gamma)_s = 2P_e(1 - P_e) \quad \ldots (3.25)$$

where P_e is the probability of error of BPSK. For $P_e << 1$, eqn (3.25) can be reduced to:

$$P_e(\gamma)_s = 2P_e = \text{erfc}\sqrt{\frac{E_b}{N_o}} \quad \ldots (3.26)$$

Eqns (3.24) and (3.25) are illustrated in Fig 3.18.

A QPSK coherent demodulator is shown in Fig 3.19. If the carrier recovery circuit is assumed ideal there will be no crosstalk between the in-phase and quadrature channel and each branch becomes equivalent to a coherent BPSK demodulator having probability of error as given in eqn (3.24).

The carrier recovery technique is similar to the one employed in BPSK, except that the signals have to be quadrupled to remove the modulation. Hence, a 4-phase ambiguity results. Thus, depending on the phase of the recovered carrier the (aI, aQ) data pair at the modulator can be either:

$$(aI, aQ),\ (\overline{aI}, \overline{aQ}),\ (\overline{aQ}, aI) \text{ or } (aQ, \overline{aI})$$

at the demodulator output. The differential coding used in BPSK will give correct output only for the first two pairs. A differential QPSK encoder/decoder is given in [4] as:

Encoder:

$$AI_n = \overline{(aI_n \oplus aQ_n)}(aI_n \oplus AI_{n-1}) + (aI_n \oplus aQ_n)(aQ_n \oplus AQ_{n-1})$$

$$AQ_n = \overline{(aI_n \oplus aQ_n)}(aQ_n \oplus AQ_{n-1}) + (aI_n \oplus aQ_n)(aI_n \oplus AI_{n-1})$$

Decoder:

$$bI_n = \overline{(BI_n \oplus BQ_n)}(BI_n \oplus BI_{n-1}) + (BI_n \oplus BQ_n)(BQ_n \oplus BQ_{n-1})$$

$$bQ_n = \overline{(BI_n \oplus BQ_n)}(BQ_n \oplus BQ_{n-1}) + (BI_n \oplus BQ_n)(BI_n \oplus BI_{n-1})$$

where (aI_n, aQ_n) is the present (odd, even) encoder input (AI_n, AQ_n) and (AI_{n-1}, AQ_{n-1}) are the present and previous (odd, even) encoder outputs, (BI_n, BQ_n) and (BI_{n-1}, BQ_{n-1}) are the present and the previous (odd, even) decoder inputs and (bI_n, bQ_n) are the (odd, even) decoder outputs. In [5] it was shown that the probability of error of differential encoded DE-QPSK is the same as that of DE-BPSK.

In the case of OQPSK the introduction of delay in the Q channel at the transmitter is compensated at the receiver by changing the integration limits to coincide with bit transitions in both channels and the introduction of a time delay (T_b) in the Q-channel. This modification does not change the detection performance as compared with QPSK. The OQPSK differential encoder/decoder operations are given by[4];

Encoder:

$$AI_n = aI_n \oplus AQ_n$$

$$AQ_n = aQ_n \oplus \overline{AI}_n$$

Decoder:

$$bI_n = BI_n \oplus BQ_n$$

$$bQ_n = \overline{BI}_n \oplus BQ_n$$

where (aI_n, aQ_n) and (AI_n, AQ_n) are the (odd, even) encoder inputs and outputs and (BI_n, BQ_n) and (bI_n, bQ_n) are (odd, even) decoder inputs and outputs respectively. The OQPSK encoder/decoder structure is clearly much simpler than that of QPSK. The probability of error of DE-OQPSK is again the same as that of DE-BPSK.

A differential BPSK demodulator which avoids the use of a carrier recovery circuit is shown in Fig 3.20(a). The incoming differentially encoded BPSK signal is multiplied by its delayed replica at the receiver. As has been shown before, in differential encoded signals the data is carried in the relative phase between adjacent

bits. Thus the output from the lowpass filter circuit is proportional to the original modulating data. Similarly, QPSK can be detected using the differential demodulator shown in Fig 3.20(b).

The probabilities of error for both detector were analysed in [6]. The result for differentially detected BPSK, DBPSK, is:

$$P_e(\gamma)_s = \frac{1}{2} e^{-E_b/N_o} \qquad \ldots (3.27)$$

while that of DQPSK can be approximated by:

$$P_e(\gamma)_s = e^{-E_b/N_o} (1 - 1/\sqrt{2})2 \qquad \ldots (3.28)$$

Eqns (3.27) and (3.28) are plotted in Fig 3.18.

3.3.2 NB-CPFSK Systems

Demodulation of CPFSK signals can be accomplished by using coherent, differential or non-coherent mechanisms.

The block diagram of a coherent (correlator) CPFSK demodulator is shown in Fig 3.21. Two correlators are used, each detecting one of the received waveforms $S_m(t)$ and $S_s(t)$. Only one correlator was needed in BPSK because $S_m(t)$ and $S_s(t)$ were antipodal.

$S_m(t)$ and $S_s(t)$ in the case of CPFSK are given by:

$$S_m(t) = A_c \cos(2\pi f_m t)$$

$$S_s(t) = A_c \cos(2\pi f_s t)$$

If f_m and f_s are considered $>> 1/T_b$, then the energy per bit E_b is given by:

$$E_b = \int_0^{T_b} S_m^2(t)\,dt = \int_0^{T_b} S_s^2(t)\,dt$$

$$= \frac{A_c^2\,T_b}{2}$$

which is the same as that of BPSK. The CPFSK waveform correlation coefficient under the same assumptions is given by:

$$\rho = \frac{1}{E_b} \int_0^{T_b} \cos(2\pi f_m t)\cos(2\pi f_s t)\,dt$$

$$= \frac{\sin(2\pi(f_m - f_s)T_b)}{2\pi(f_m - f_s)T_b}$$

$$= \frac{\sin 2\pi h}{2\pi h} \qquad \ldots (3.29)$$

Eqn (3.29) is plotted in Fig 3.22.

The probability of error for coherently detected CPFSK signals can be calculated from eqn (3.21) by replacing ρ by its value given in eqn (3.29).

The correlation coefficient ρ is equal to zero, ie. $S_m(t)$ and $S_s(t)$ are orthogonal, if $h = n/2$ ($n=1,2,3,\ldots$) or f_m and f_s are spaced far enough apart. The probability of error under this condition is given by:

$$P_e(\gamma)_s = \frac{1}{2}\,\text{erfc}\left[\sqrt{\frac{E_b}{2N_o}}\right] \qquad \ldots (3.30)$$

Eqn (3.30) is illustrated in Fig 3.18.

It is interesting to notice that the minimum value of h for orthogonal signalling is 0.5, which is the reason for the name minimum shift keying given to CPFSK signal having h=0.5.

The minimum correlation coefficient for CPFSK is -0.21 and occurs at h=0.715. At this value the signal to noise ratio is about 1 dB less than orthogonal signalling for the same probability or error. Furthermore, in [7] it was demonstrated theoretically that by extending the observation period by 2 bits a performance equivalent to coherent BPSK can be achieved. This is done by using a correlation bank where all possible 4 bit reference patterns occurring in 2 consecutive bits are correlated with the received signal. The bit pattern that results in the largest correlation then provides the bit decision on the first of the two consecutive received bits. Extending the observation period to 3 bits yields another 0.9dB improvement, 5 bits gives another 0.2dB. However, there is no known self-reference recovery technique (ie. the reference is recovered from the modulated signal and not from an accompanying reference pilot) for CPFSK with h = 0.715. This is not the case when h = 0.5 where a reference recovery circuit can be devised as shall be demonstrated later.

The most analysed method of non-coherent CPFSK detection is that where detection is carried out by using two bandpass filters each centred around one of the two transmitted frequencies f_m and f_s. The filters are followed by envelope detectors and decision device. To prevent significant overlapping between the passbands of the two filters, the deviation ratio should be greater than unity, making this approach inappropriate for use with NB-CPFSK. Nevertheless, its

error rate performance is given in Fig 3.24 for comparison with other non-coherent detectors.

Alternatives to the non-coherent filter's detector, which eliminates the above constraint on h, are the limiter-discriminator and the differential detectors. Theoretical analysis of the probability of error performance of both detectors was carried out in [8] and the block diagrams are shown in Fig 3.23. The receiver's IF filters were assumed to have Gaussian amplitude characteristics and linear phase. The introduction of inter-symbol interference due to bandlimiting and its effect on probability of error was taken into account, but not that of delay distortion.

Fig 3.24 illustrates the results of the analysis for two values of h (0.7, 0.5) and an IF filter bandwidth equal to one (as normalised to the bit rate f_b). This value of B_{IF} gave best results compared with the other examined values which were 2 and 3. The two detectors have equal performances when h = 0.5. For h = 0.7 the performance of the limiter-discriminator detector improved, while that of the differential one deteriorated. The results show that the best setting for h in NB-CPFSK is 0.5 if differential detection is used and 0.7 if the limiter discriminator is used.

3.3.3 MSK

MSK being a NB-CPFSK signal can be detected using any of the methods discussed in the last section.

An MSK coherent demodulator structure which yields a performance equivalent to that of BPSK is shown in Fig 3.25. The incoming signal

is split into I and Q channels and correlated with recovered references $\cos(\pi/2\ f_b t)\ \cos(2\pi f_c t)$ and $\sin(\pi/2\ f_b t)\ \sin(2\pi f_c t)$ respectively. The correlators are followed by I & D, decision circuits and bit interleavers. The I & D operation timing is arranged to coincide with bit transitions in each channel as can be seen in Fig 3.25. Recalling eqn (3.14) and the subsequent description of MSK waveforms the received signal can be written as (without a noise term):

$$S_r(t) = A_c \left\{ aI_{-1} \cos\left[\frac{\pi}{2} f_b t\right] \cos(2\pi f_c t) + aQ_{-2} \sin\left[\frac{\pi}{2} f_b t\right] \sin(2\pi f_c t) \right\}$$

$$-T_b \leq t \leq 0$$

$$S_r(t) = A_c \left\{ aI_{-1} \cos\left[\frac{\pi}{2} f_b t\right] \cos(2\pi f_c t) + aQ_{-1} \sin\left[\frac{\pi}{2} f_b t\right] \sin(2\pi f_c t) \right\}$$

$$0 \leq t \leq T_b$$

The I-channel correlator output during the period $-T_b$ to $+T_b$ will clearly include only terms proportional to data bit aI_{-1}. Furthermore, the correlator/integrator structure is equivalent to the one described earlier in this chapter. Thus, in the I-channel the probability of bit error will be given by eqn (3.21).

The mark and space waveforms are given by:

$$S_m(t) = +A_c \cos\left[\frac{\pi}{2} f_b t\right] \cos(2\pi f_c t)$$

$$S_s(t) = -A_c \cos\left[\frac{\pi}{2} f_b t\right] \cos(2\pi f_c t)$$

Thus, the energy per bit in a duration $2T_b$ is given by:

$$E_b = A_c^2 \int_{-T_b}^{T_b} \cos^2\left[\frac{\pi}{2} f_b t\right] \cos^2(2\pi f_c t)\, dt$$

Given that $f_c >> f_b$, then:

$$E_b = \frac{A_c^2 T_b}{2}$$

which is the same as that of BPSK.

$S_m(t)$ and $S_s(t)$ are antipodal signals, thus their correlation coefficient is equal to -1.

Thus, the probability of bit error for an I-channel correlator is equal to that of BPSK. A similar analysis for the Q-channel will lead to the same conclusion.

Viewing MSK signal as a NB-CPFSK, the above detection process is equivalent to observing the signal over a 2-bit period, and taking a decision on the bit transmitted at the beginning of the observation period as was discussed in the case of h = 0.715. Only 2 correlators are needed for the MSK case because the mark and space waveforms over 2 bit periods are antipodal.

A relatively simple technique for reference signal recovery, based on [9], is explained in the following. Squaring the MSK signal doubles its frequency and produces a CPFSK signal having h = 1. The

spectrum of CPFSK having h = 1 (also known as Sunde's FSK) contains spectral line components at $2f_m$ and $2f_s$ as can be seen in Figs 3.10 and 3.11. These two components are recovered in 2 phase-locked loops (PLL) as shown in Fig 3.26. The outputs from the PLLs are divided by two to give $\cos(2\pi f_c t + \pi/2\ f_b t)$ and $\cos(2\pi f_c t - \pi/2\ f_b t)$. The I and Q references are recovered by performing summation and subtraction operations on the above divider outputs.

Because of the 2-phase ambiguity inherent in the division operation, the divider outputs can have any one of the following combinations.

$+\cos(2\pi f_c t + \pi/2\ f_b t)$ and $+\cos(2\pi f_c t - \pi/2\ f_b t)$,

$-\cos(2\pi f_c t + \pi/2\ f_b t)$ and $-\cos(2\pi f_c t - \pi/2\ f_b t)$,

$-\cos(2\pi f_c t + \pi/2\ f_b t)$ and $+\cos(2\pi f_c t - \pi/2\ f_b t)$,

or $+\cos(2\pi f_c t + \pi/2\ f_b t)$ and $-\cos(2\pi f_c t - \pi/2\ f_b t)$.

Therefore, it is not possible to determine which of the summers performs the addition and which performs the subtraction. The summers outputs for the first two pairs of dividers outputs are given by:

$\pm\cos(\pi/2\ f_b t)\cos(2\pi f_c t)$ and $\pm\sin(\pi/2\ f_b t)\sin(2\pi f_c t)$

respectively, which is the case shown in Fig 3.26. The second pairs result in:

$\pm\sin(\pi/2\ f_b t)\sin(2\pi f_c t)$ and $\pm\cos(\pi/2\ f_b t)\cos(2\pi f_c t)$

Consequently, a transmitted data pair (aI, aQ) can be at the receiver I/Q channel outputs:

(aI, aQ), $(\overline{aI}, \overline{aQ})$, (aQ, aI) or $(\overline{aQ}, \overline{aI})$.

A straightforward differential encoding on the input serial data at the transmitter coupled with differential decoding performed on

the serial data (at the bit interleaver output) at the receiver will solve the above ambiguity problem, as long as the timing of I & D operations coincides with waveform zero crossings in both channels. The latter is guaranteed by recovering I & D timing signals simultaneously with the references at the output of the dividers as can be seen in Fig 2.26. Inversion in I/Q channel roles will lead to instantaneous and equivalent change in the timing signals, thus ensuring correct timing at all times.

The differential encoder/decoder for an MSK signal is given in Figs 3.15(a) and 3.17(a). This is the simplest coding scheme compared with QPSK and OQPSK, which is an unanticipated advantage of MSK.

The original data clock ($f_b = 1/T_b$) which controls the bit interleaver and all subsequent logical operations is recovered simultaneously with the references. The outputs from the PLLs are multiplied and then passed through a lowpass filter to give the clock signal $\cos(2\pi f_b t)$. The implementation of a coherent MSK demodulator based on the above discussion is described in the following chapter.

Finally, the probability of error of differentially encoded MSK-DEMSK is clearly equivalent to that of DEBPSK and DEQPSK and given in Fig 3.18.

3.4 Effect of Filtering on Narrow Band Digital Modulation Systems

Having established the ideal performance of different narrow band digital modulation systems, attention is turned to evaluate their performance in conditions usually encountered in the mobile radio

environment.

A major factor in studying the suitability of a digital modulation technique for mobile radio applications is its performance in the presence of narrow band filters. These are used to contain the radiated radio spectrum at the transmitter in a prespecified bandwidth and at the receiver to prevent adjacent channel interference and excessive noise from reaching the demodulator stages.

The performance of coherent MSK and OQPSK in the presence of a bandpass filter, followed by a hard limiter, was studied in [10] using computer simulation. The simulated transmitter and receiver filters were equivalent to a 7 pole, 0.1dB ripple Chebyshev. The study was intended to simulate conditions usually encountered in satellite communications. Nevertheless, the type of filter simulated is common to mobile radio application as well as the hard limiting operation. The latter will be present at the receiver to remove the amplitude fluctuations before detection. It can also be found at the transmitter if high efficiency Class C power amplifiers are used. The results of the simulation are shown in Fig 3.27. The curves show the variation of performance degradation as a function of the filter noise bandwidth (normalised to bit rate) for the indicated constant value of probability of error. Performance degradation is defined as the increase in signal to noise ratio (in dB) required on the simulated filter bandwidth to achieve the desired probability of error over that required on an infinite bandwidth to achieve the same probability of error.

The performance curves show that for values of filter bandwidth greater than 1.1 (the filter bandwidth B_{IF} is normalised with respect to the data bit rate) MSK is superior to OQPSK. For B_{IF} less than 1.1 OQPSK starts to outperform MSK, however both systems begin to suffer severe degradation, especially MSK.

In a similar study Morais and Feher[11] compared the performances of QPSK, OQPSK and MSK. The degradation in performance as a function of B_{IF} is shown in Fig 3.27 for the three systems for a probability of error equal to 10^{-4}. The simulated filter was 4-pole Chebyshev and described as having relatively mild in-band phase distortion. This explains the lesser degradation experienced in [11] as compared to [10]. Performance curves given by [11] show a slight advantage for MSK over OQPSK and QPSK until B_{IF} is equal to approximately 0.85 where the latter starts to outperform the other two.

Differential detection performance of PSK and CPFSK systems will suffer from the delay distortion introduced by the narrow band IF filter. A typical IF filter group delay characteristic is shown in Fig 5.7. This shows that the type of distortion introduced can be approximated by quadratic delay distortion.

The effect of such distortion on the performances of PSK and CPFSK systems have been calculated in [12] and [13] respectively. The results of the above calculations are shown in Fig 3.28. Also shown in the latter figure is the performance degradation of CPFSK when detected by a limiter-discriminator as given in [13]. The degradation in performance is defined as the increase in signal to noise ratio (in dB) required at the detector input to compensate for

the effect of group delay distortion. The amount of distortion is specified by the increment in delay, d, measured in bit intervals, T_b, between the centre and the edge of the transmission band. The superiority of CPFSK with differential detection over all other schemes is evident from the above figure.

The narrow band filter at the transmitter will introduce amplitude fluctuations in the prefilter constant signal envelope. If the signal is passed through a non-linear power amplifier the side-lobes which have been attenuated by the filter will be restored to approximately their original values, thus suppressing the filter action and reintroducing out of band radiation.

The worst amplitude fluctuations will occur in BPSK and QPSK when the carrier phase goes through $\pm\pi$ transitions consequently causing the filtered signal envelope to go to zero. By reducing the maximum allowable transitions in the carrier phase to $\pm\pi/2$ these envelope zero crossings are prevented in OQPSK.

The maximum envelope fluctuations in filtered OQPSK and MSK depend on the filter characteristics and bandwidth. These fluctuations have been analysed through computer simulation in [14] for an OQPSK signal. The filter considered was a 6-pole Butterworth. For a value of 3dB bandwidth equal to $2.4f_b$, the percentage of amplitude fluctuation, defined as the percentage of the ratio of the difference between the maximum and the minimum signal amplitudes to the maximum signal amplitude, was 66%. Fig 3.29 shows a photograph representing the waveform of an MSK signal passed through an 8-pole crystal filter (the filter characteristics are given in Fig 5.7),

whose 3dB bandwidth equals twice the bit rate. The amplitude fluctuation percentage for the filtered MSK signal is 19%. This represents a great improvement in the case of MSK compared with OQPSK, in spite of the former's filter tighter characteristics.

3.5 Effect of Fading and Random FM Noise on Error Performance of PSK, CPFSK and MSK Systems

It was shown in Chapter 2 that the probability of error in non-selective slow Rayleigh fading conditions could be calculated by substituting for the probability of error under additive white Gaussian noise conditions in equation (2.15) and performing the integration.

Thus, for coherent detection of DEQPSK, DEOPQSK, DEMSK and DEBPSK, the probability of error in slow fading conditions is given by:

$$P_e(\gamma)_D = \int_0^\infty \frac{1}{\gamma_o} e^{-\gamma/\gamma_o} \operatorname{erfc}(\gamma)\, d\gamma$$

$$= 1 - \frac{1}{\sqrt{1 + 1/\gamma_o}} \qquad \ldots (3.31)$$

where γ_o is the average signal to noise ratio at the detector input averaged over the Rayleigh fading.

Similarly for DPBSK:

$$P_e(\gamma)_D = \int_0^\infty \frac{1}{\gamma_o} e^{-\gamma/\gamma_o} \frac{1}{2} e^{-\gamma} d\gamma$$

$$= \frac{1}{2} \quad \frac{1}{1 + \gamma_o} \qquad \ldots (3.32)$$

and for DQPSK:

$$P_e(\gamma)_D = \int_0^\infty \frac{1}{\gamma_o} \; e^{-\gamma/\gamma_o} \; e^{-\gamma(1-1/\sqrt{2})} \; d\gamma$$

$$= \frac{1}{1 + \gamma_o \, (1 - 1/\sqrt{2})2} \qquad \ldots (3.33)$$

while for coherent orthogonal CPFSK:

$$P_e(\gamma)_D = \int_0^\infty \frac{1}{\gamma_o} \; e^{-\gamma/\gamma_o} \; \frac{1}{2} \, \text{erfc}(\gamma/2) \, d\gamma$$

$$= \frac{1}{2} \left[1 - \frac{1}{\sqrt{1 + 2/\gamma_o}} \right] \qquad \ldots (3.34)$$

These equations (3.31) to (3.34) are plotted in Fig 3.30. When CPFSK signals are detected using limiter-discrimination and differential detectors under the above conditions (non-selective slow Rayleigh fading) the probabilities of error are given by[15] as:

$$P_e(\gamma)_D = \frac{1}{2} \left[1 - \frac{\sqrt{3} \; \gamma_o \, h}{(\gamma_o + 1)^{1/2} \, (1 + 3\gamma_o h^2)^{1/2}} \right] \qquad \ldots (3.35)$$

limiter-discriminator

$$P_e(\gamma)_D = \frac{1}{2}\left[1 - \frac{\gamma_o \sinh \pi}{[(\gamma_o+1)^2 - \gamma_o^2 \cos^2 h\pi]^{1/2}}\right] \quad \text{differential detector} \qquad \ldots (3.36)$$

Equations (3.35) and (3.36) are plotted in Fig 3.30 for the special case h = 0.5 (MSK case).

An important conclusion which can be made by investigating Fig 3.30 is that the signal to noise ratio advantage of coherent systems in non-fading conditions over non-coherent and differential detectors does not hold when the transmitted signal is subjected to slow fading conditions.

The slow Rayleigh fading assumption becomes invalid if the maximum doppler shift f_D approaches the data bit rate (ie. fast fading conditions). Under this condition random FM noise will introduce a limiting error rate that is independent of the signal to noise ratio, as was indicated in the last chapter. Thus, in fast Rayleigh fading environment the total probability or error could be approximated by[16]:

$$P_{et} = P_e(\gamma)_D + P_e(f_D/f_b) \qquad \ldots (3.37)$$

where the first term represents the probability of error due to the slow non-selective Rayleigh fading condition and given by equations (3.31) to (3.36) for different modulation and demodulation schemes. The second term represents the irreducible probability of error due to random FM noise.

Jakes[16] has shown that $P_e(f_D/f_b)$ for DBPSK is approximated by:

$$P_e(f_D/f_b) = \frac{\pi^2}{2}\left[\frac{f_D}{f_b}\right]^2 \quad \ldots (3.38)$$

It is possible to calculate $P_e(f_D/f_b)$ for DQPSK by considering its demodulators as being composed of two independent DBPSK ones each functioning at half the bit rate (Fig 3.20). Thus, the probability of bit error due to random FM noise for differentially demodulated QPSK, ie. DQPSK, can be given by:

$$P_e(f_D/f_b) = 2\pi^2\left[\frac{f_D}{f_b}\right]^2 \quad \ldots (3.39)$$

The $P_e(f_D/f_b)$ for CPFSK signals detected by limiter-discriminator and differential detectors was shown in [15] to be approximately given by:

$$P_e(f_D/f_b) = \frac{1}{2}\left[\frac{f_D}{hf_b}\right]^2_{\text{Limiter-discriminator}} \quad \ldots (3.40)$$

$$P_e(f_D/f_b) = \frac{\pi^2}{2}\left[\frac{f_D}{f_b \sin\pi h}\right]^2_{\text{Differential detector}} \quad \ldots (3.41)$$

From this it is evident that if differential detection is used, minimum error rate will be achieved for NB-CPFSK ($h < 1$) if $h = 0.5$, ie. the MSK case. Furthermore, from eqns (3.38) and (3.39), under the above condition, $P_e(f_D/f_b)$ for NB-CPFSK is equivalent to that of DBPSK and considerably less (0.25) than that of DQPSK.

In order to clarify the error rate performance of coherent detection in the presence of random FM noise, it is necessary to solve the tracking behaviour of the reference recovery circuit, usually a

phase-locked loop, in such conditions. This is a problem which has not yet been solved. However, a qualitative comparison between different coherent systems can be made.

A starting assumption in this comparison is that the degradation in error rate performance for any system due to random FM noise depends on the PLL tracking performance. Furthermore, increasing the loop natural frequency relative to the maximum doppler shift will improve the performance in such conditions. This is substantiated by results obtained in Chapter 5.

Reference signals in BPSK and MSK are obtained through a doubling operation which inherently leads to doubling of the maximum doppler shift, f_D. In QPSK and OQPSK the received signals are quadrupled to obtain the reference. Thus, to achieve the same degree of immunity to random FM noise the loop natural frequency in the latter two will have to be twice that of the BPSK and MSK.

For all systems the phase reference signal to noise ratio is inversely proportional to the loop noise bandwidth and hence its natural frequency[5,17]. Consequently, QPSK iand OQPSK phase reference SNR will be half that of MSK and BPSK.

The performance degradation due to a noisy phase reference has been given in [18] for BPSK, QPSK and OQPSK and in [19] for MSK. The results are summarised in Fig 3.31 and show the better performance of MSK as compared to OQPSK and QPSK.

Consequently, it is possible to conclude that MSK is capable of

achieving the same degree of immunity to random FM noise as QPSK and OQPSK, but with considerably less overall error rate performance degradation due to phase reference noise. BPSK in such conditions will give the best performance.

3.6 Comparison Between Narrow Band Digital Communication Systems

BPSK, QPSK, OQPSK, NB-CPPSK and MSK modulation techniques have been discussed and their performances evaluated in some typical mobile radio applications. The object of the following comparison is to demonstrate the superiority of MSK over the other techniques, especially PSK ones, for use in mobile radio data transmission applications.

Even though BPSK performs better than QPSK and OQPSK in some situations, its wide frequency spectrum makes it unsuitable for narrow band applications.

Compared to QPSK and OQPSK, MSK spectrum falls off much more rapidly. For large values of $f-f_c/f_b$ (Fig 3.3), the MSK spectrum falls off at a rate proportional to $(f-f_c/f_b)^{-4}$ compared to $(f-f_c/f_b)^{-2}$ for QPSK and OQPSK. Thus, if no filtering is used, channels could be spaced very much closer together in MSK compared to the others. To demonstrate the above advantage of MSK, White[20] has performed an analysis of the effects of worst-case crosstalk between two adjacent channels. He concluded that for a 1dB signal to noise ratio performance degradation and 10dB relative interference level (power ratio between adjacent channel and in-channel) the channel spacing for MSK, QPSK, OQPSK and BPSK should be $2.5f_b$, $13.5f_b$, $14f_b$ and $19f_b$, where f_b is the data bit rate, respectively. The analysis

assumed a linear additive white Gaussian channel with ideal coherent demodulation.

However, the main lobe of MSK is wider than that of QPSK and OQPSK, the first nulls falling at $(f-f_c)/f_b = 0.75$ and 0.5 respectively. This explains the slightly earlier rapid deterioration in MSK coherent demodulation performance compared to QPSK and OQPSK when tight filtering is applied ($B_{IF} < f_b$) as can be seen in Fig 3.27[10].

If coherent demodulation with differential data coding is used and ideal or non-selective slow Rayleigh fading conditions are assumed, MSK and all PSK systems will have the same performance. Nevertheless, when performance is considered in fast Rayleigh fading conditions, MSK could be expected to outperform QPSK and OQPSK as discussed previously.

If MSK and QPSK were demodulated using differential detectors in the presence of non-selective slow Rayleigh fading, the superiority of MSK becomes evident as can be seen in Fig 3.30. To achieve the same error performance DQPSK needs 2dB more average signal to noise ratio than DMSK. Furthermore, the irreducible probability of error due to random FM noise in the case of DMSK is 0.25 that of DQPSK. In addition, as can be concluded from Fig 3.26, DQPSK suffers severe and rapid degradation in the presence of delay distortion compared with the much smaller and more gradual degradation of DMSK.

Bandlimited MSK signals suffer much reduced signal envelope fluctuations compared with any other bandlimited PSK signals. Even

though a linear power amplifier has to be used to prevent spectrum side-lobe regeneration, the linearity constraints on the amplifier for the MSK signal is much less than for the PSK system.

Although co-channel interference effects were not discussed in this chapter, comparison between MSK measured performance degradation due to such conditions and published data on PSK systems is given in Chapter 5.

MSK, being a CPFSK signal, can be detected using narrow band analogue FM detectors. Thus, a simple data demodulator can be built which doubles as an analogue FM detector. This property is not shared with other PSK systems.

Increasing the deviation ratio in CPFSK systems decreases the number of errors due to random FM noise if a limiter discriminator detector is used, as can be seen from eqn (3.40). For h=0.7, the number of errors is approximatly half that for h=0.5. However, if differential detection is used optimum performance is achieved in both slow fading and random FM noise conditions if h=0.5.

The major advantage of CPFSK-h=0.5, ie. MSK, is the existence of a self-reference recovery technique for coherent reception. This is not the case with other NB-CPFSK signals (h<1).

3.7 Improving MSK Spectrum Efficiency

Improving the spectrum properties of MSK signals has received a great deal of attention in recent years.

Several techniques to produce an optimum pulse shape, ie. the shape which produces an MSK signal having a fast spectrum fall-off, have been suggested[21,22]. Unfortunately, all these techniques tend to produce a wider main lobe spectrum than MSK, thus worsening the performance when the signal is bandlimited[23].

A second approach to achieve higher spectrum efficiency in MSK is partial response signalling, where the data pulses are carefully shaped and stretched over more than one bit interval, according to certain rules prior to modulation. This leads to a family of modulation techniques which produces different degrees of spectrum compactness. Until the present time, the maximum spectrum efficiency has been attained in [24], where the resultant modulation is named, Tamed Frequency Modulation (TFM). The spectrum of TFM is shown in Fig 3.32, together with that of MSK. The improvement in spectrum efficiency in TFM is evident. Howver, this is achieved with a much more complicated modulator structure.

Coherent demodulation implementation of TFM is described in [24] and is identical to the MSK demodulator including the reference recovery circuit. The error rate performance of TFM was shown to be 1dB worse than MSK[24].

Partial response signalling results in a multi-level eye pattern when a frequency discriminator is used to detect the signal, as can be seen in Fig 3.33 for the TFM case. Therefore, a major disadvantage of TFM and all other partial response systems, is the severe deterioration in error performance if non-coherent or differential detectors are used. The simulated static error performance of a

limiter discriminator TFM detector[25] has shown that at 10^{-4} error rate TFM the detector requires 10dB signal to noise ratio more than DEMSK.

The performance of differentially demodulated TFM was analysed in [26] in the presence of slow Rayleigh fading. To achieve 10^{-2} error rate the signal to nosie ratio has to be 55dB, ie. 32dB more than DMSK. Hence, it is impractical to use non-coherent or differential detectors for demodulating TFM and other partial response MSK systems in mobile radio applications.

3.8 Conclusions

The superiority of MSK as compared to other conventional narrowband digital modulation systems for mobile radio applications has been demonstrated. Furthermore, the same coherent MSK demodulator can be used to detect highly spectrally efficient TFM signals with 1dB penalty in system performance.

All the above factors substantiate the importance of investigating the practical MSK modulation performance in the land mobile radio environment.

CHAPTER 3: REFERENCES

1. Bennet, W R and Davey, J R: 'Data Transmission', McGraw-Hill Book Company, New York, 1965.
2. Bennet, W R and Rice, S O: "Spectral density and autocorrelation functions associated with binary frequency shift keying", B.S.T.J., Sept., 1963.
3. Haykin, S: 'Communication Systems', John Wiley & Sons Inc., USA, 1978.
4. Feher, K: 'Digital Communications - Satellite/Earth Station', Prentice-Hall Inc., N.J., 1983.
5. Spilker, J J: 'Digital Communication by Satellite', Prentice-Hall Inc., N.J., 1977.
6. Lucky, R W, Salz, J and Weldon Jr., E J: 'Principles of Data Communication', McGraw-Hill Book Company, N.Y., 1968.
7. Osborne, W P and Luntz, M B: "Coherent and non-coherent detection of CPFSK", IEEE, Vol.COM-22, No.8, 1974.
8. Simon, M K and Wang, C C: "Differential versus limiter-discriminator detection of narrow-band FM", IEEE, Vol.COM-31, No.11, 1983.
9. Rudi de Buda: "Coherent demodulation of frequency-shift keying with low deviation ratio", IEEE Trans. on Communication, June 1972.
10. Gronemeyer, S A and McBride, A L: "MSK and offset QPSK modulation", IEEE, Vol.COM-24, No.8, 1976.
11. Morais, D H and Feher, K: "The effect of filtering and limiting on the performance of QPSK, offset QPSK and MSK systems", IEEE, Vol.COM-28, No.12, 1980.
12. Sunde, E D: "Pulse transmission by AM, FM and PM in the presence of phase distortion", B.S.T.J., March 1961.

13. Anderson, R R, Bennett, W R, Davey, J R and Salz, J: "Differential detection of binary FM", B.S.T.J., January 1965.

14. Moreno, L: "Sensitivity of PSK modulation techniques to non-linear distortions", IEEE, Vol.COM-27, No.5, 1979.

15. Hirade, K, Ishizuka, M, Adachi, F and Ohtani, K: "Error-rate performance of digital FM with differential detection in land mobile radio channels", IEEE, Vol.VT-28, No.3, 1979.

16. Jakes Jr., W C: 'Microwave Mobile Communications', John Wiley & Sons, N.Y., 1974.

17. Cruz, J R and Simpson, R S: "Minimum shift-keying signal detection with noisy reference signals", IEEE, Vol.COM-26, No.6, 1978.

18. Rhodes, S A: "Effect of noisy phase reference on coherent detection of offset-QPSK signals", IEEE, Vol.COM-22, No.8, 1974.

19. Matyas, R: "Effect of noisy phase references on coherent detection of FFSK signals", IEEE, Col.COM-26, No.6, 1978.

20. White, B E: "A worst-case cross talk comparison among several modulation schemes", IEEE, Vol.COM-25, No.9, 1977.

21. Amoroso, F: "Pulse and spectrum shaping in the minimum (frequency) shift keying (MSK) format", IEEE, Vol.COM-24, No.3, 1976.

22. Deshpande, G S, and Wittke, P H: "Optimum pulse shaping in digital angle modulation", IEEE, Vol.COM-29, No.2, 1981.

23. Pasupathy, S: "Minimum shift keying: a spectrally efficient modulation", IEEE Communication Magazine, Vol.17, No.4, 1979.

24. de Jager, F and Dekker, C B: "Tamed frequency modulation: a novel method to achieve spectrum economy in digital transmission", IEEE, Vol.COM-26, No.5, 1978.

25. Chung, K S and Zegers, L E: "Generalised tamed frequency modulation", Philips Journal of Research, 165-177, 1982.

26. Elnoubi, S and Gupta, S C: "Error rate performance of non-coherent detection of doubinary coded MSK and TFM in mobile radio communication systems", IEEE, Vol.VT-30, No.2, 1981.

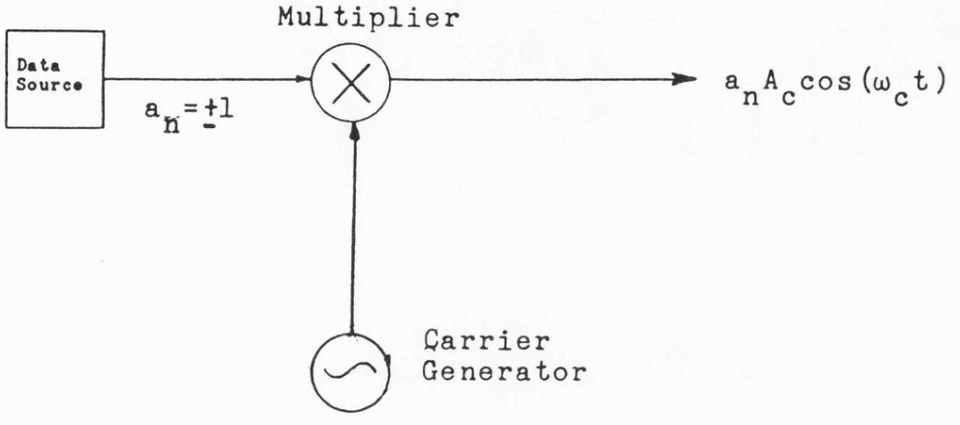

Figure 3.1 BPSK Modulator

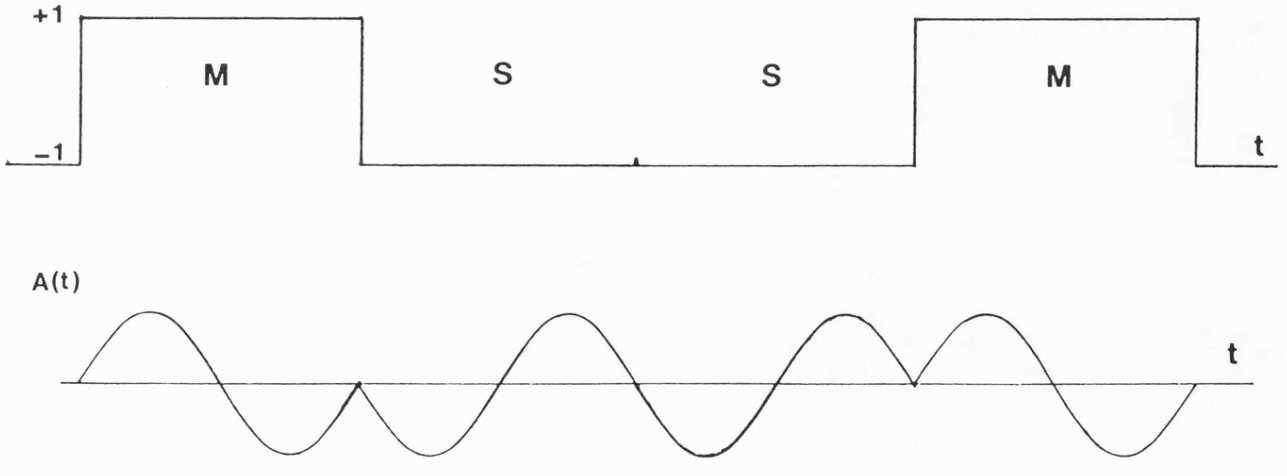

Figure 3.2 BPSK Waveform

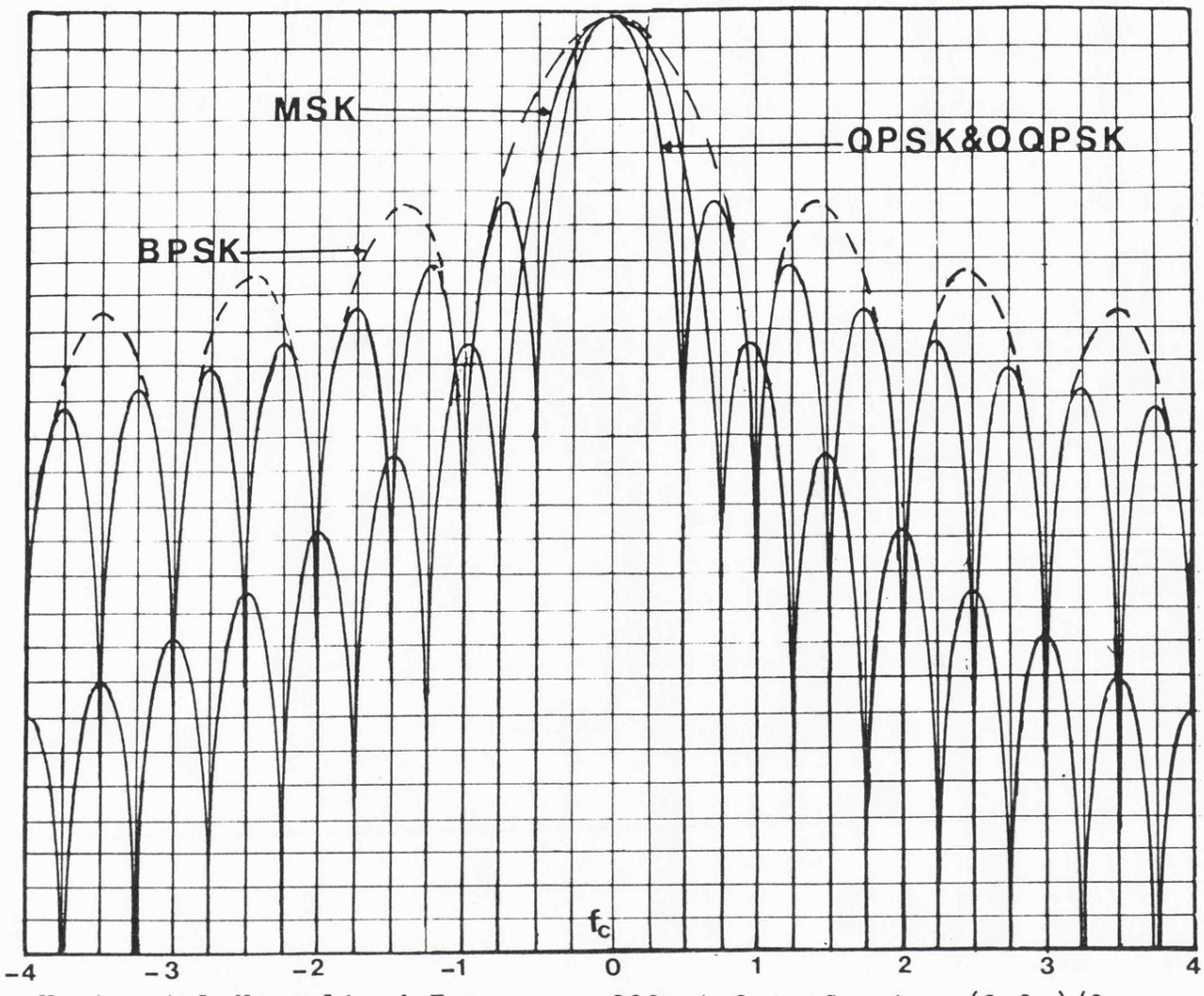

Horizontal:Normalised Frequency Offset from Carrier-$(f-f_c)/f_b$.
Vertical : 2.5dB/Division.

Figure 3.3 Theoretical PSDF of BPSK, QPSK, OQPSK & MSK .

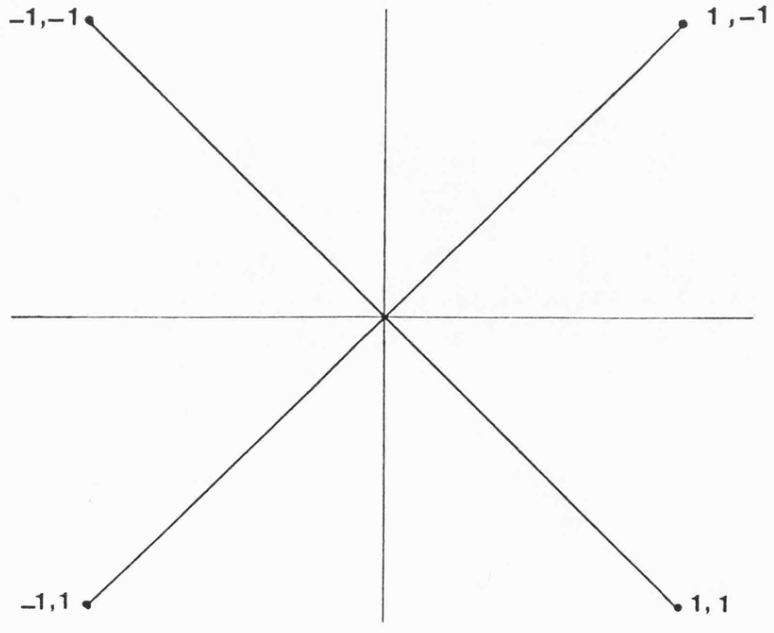

Figure 3.4 QPSK Signal Phasor Diagram.

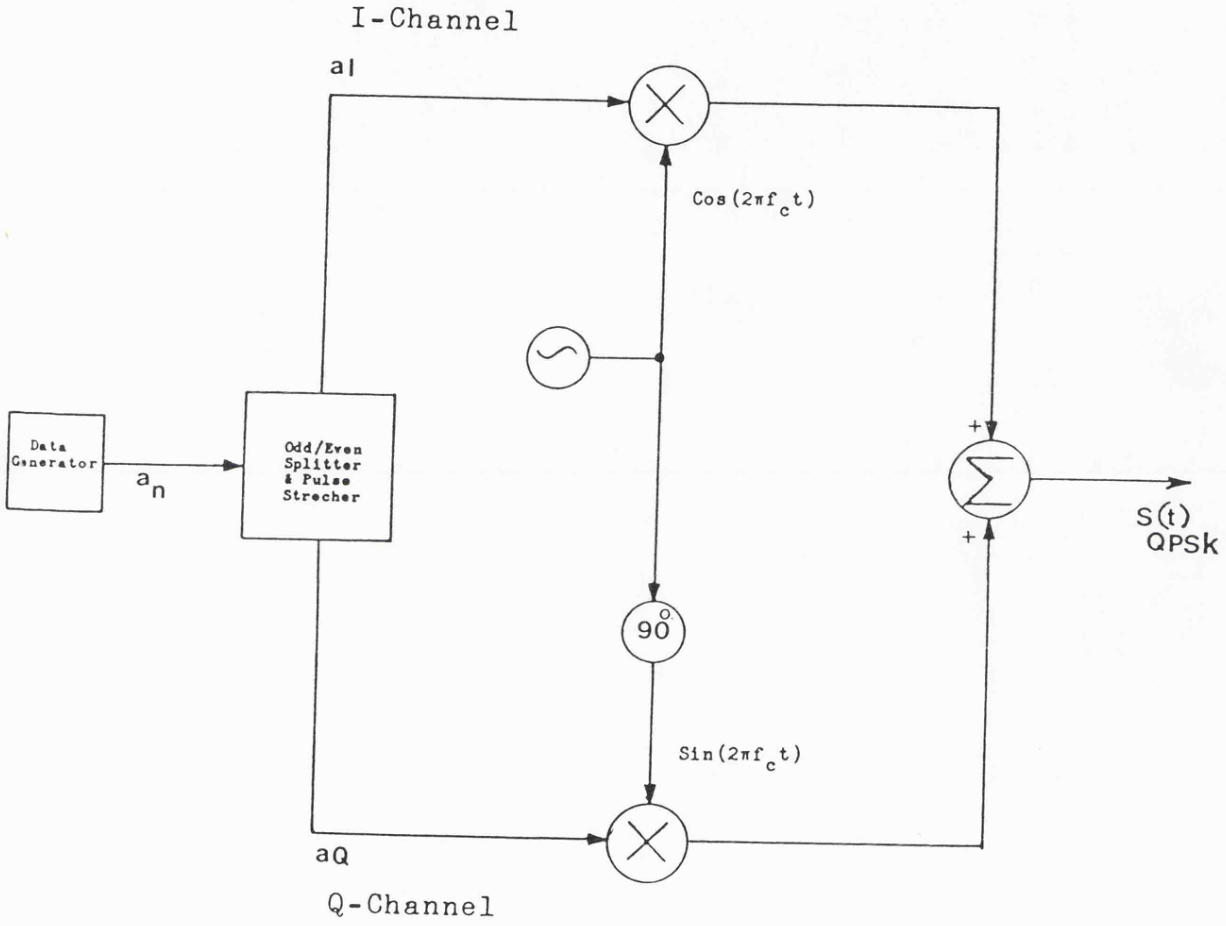

Figure 3.5 QPSK Modulator Structure.

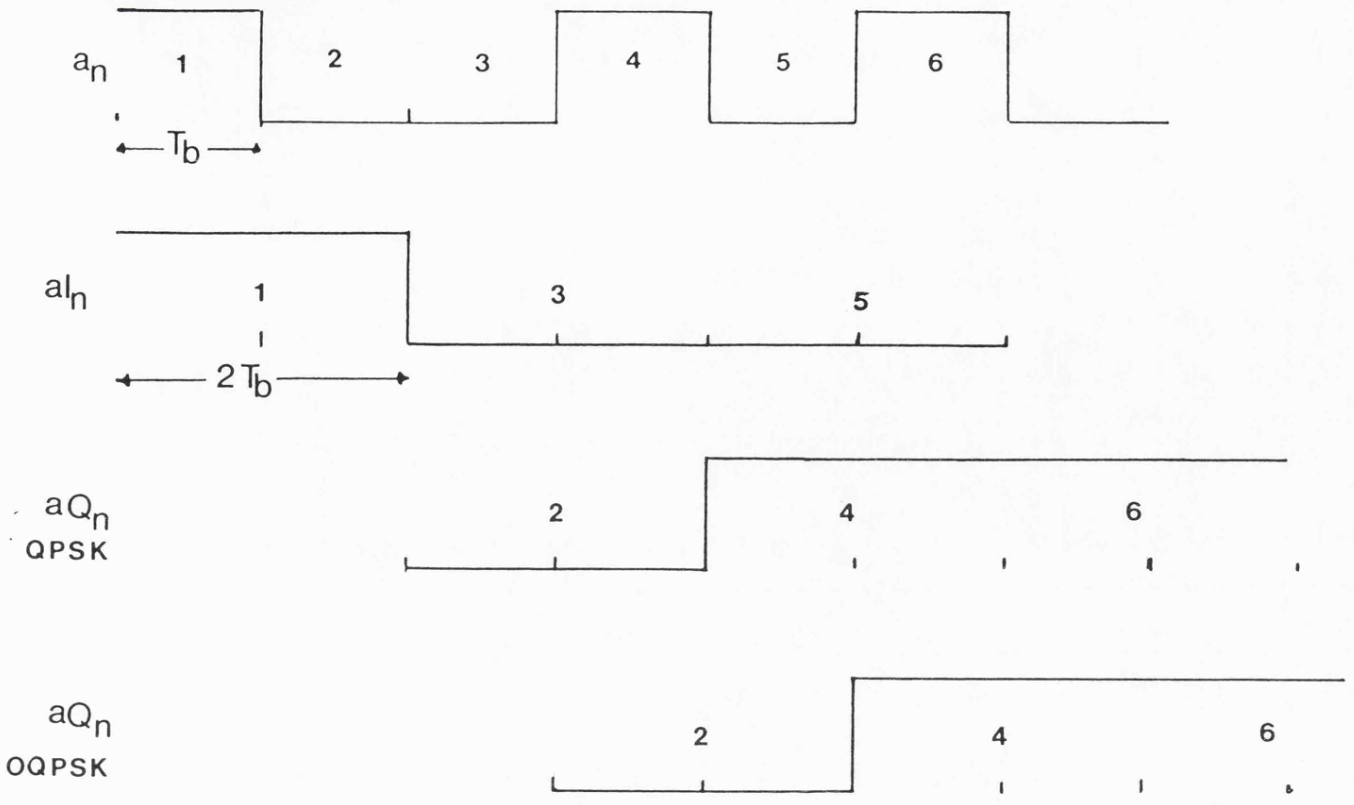

Figure 3.6 Data Timing in QPSK and OQPSK.

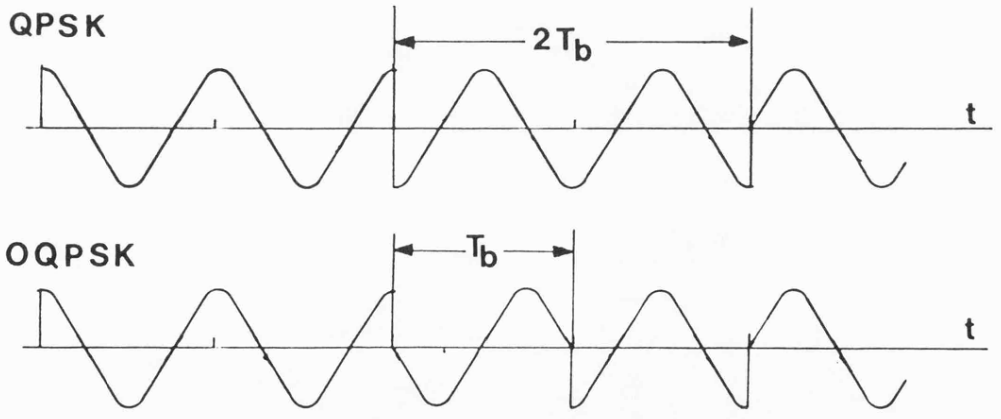

Figure 3.7 QPSK and OQPSK Waveforms.

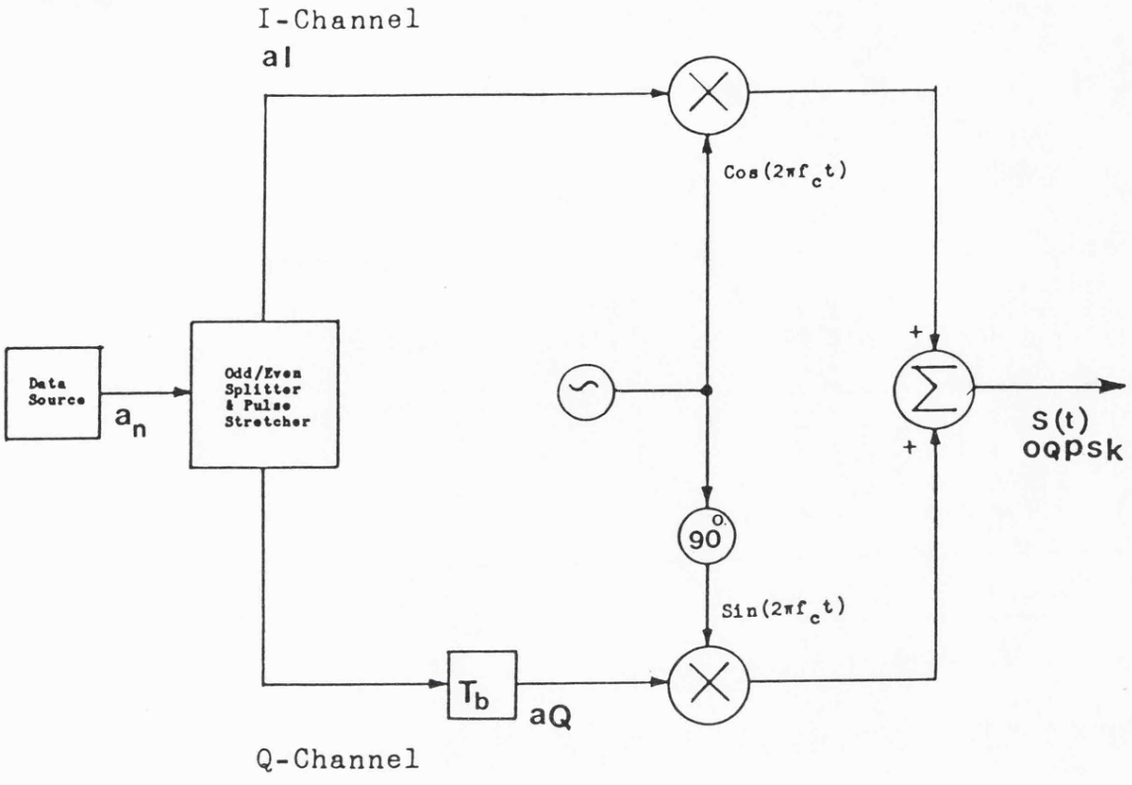

Figure 3.8 OQPSK Modulator Structure.

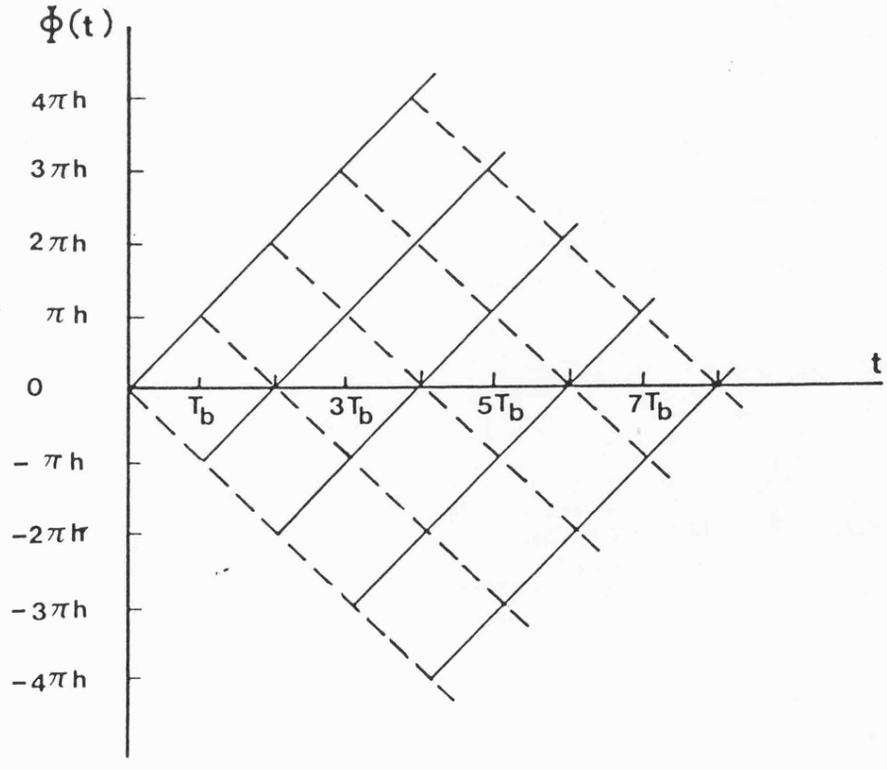

Figure 3.9 Excess Phase of the CPFSK Carrier.

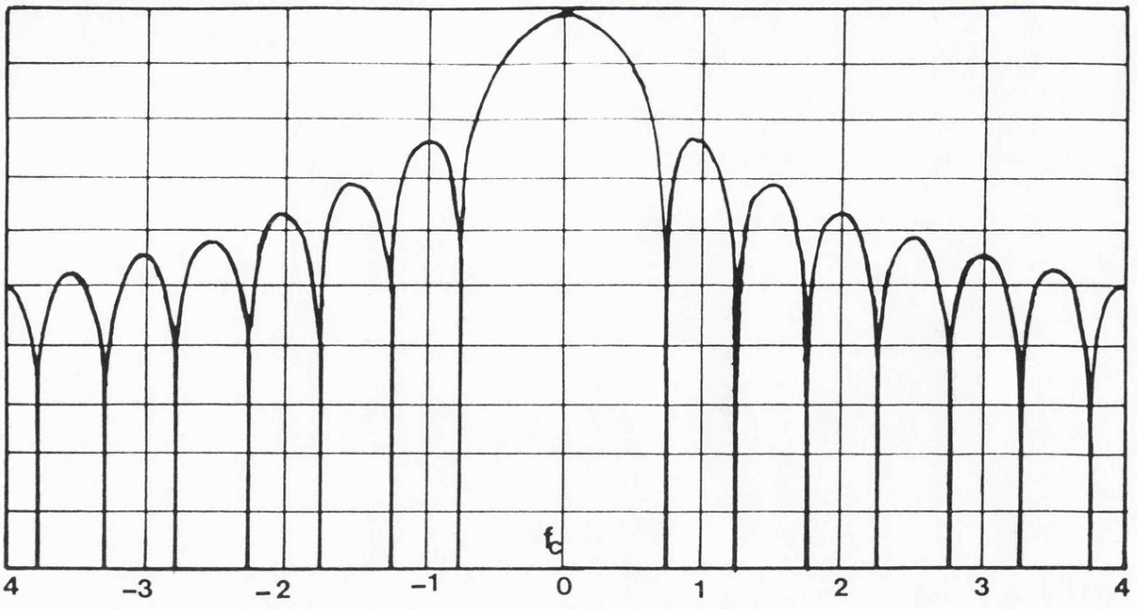

Horizontal:Normalised Frequency Offset from the Carrier-$(f-f_c)/f_b$.
Vertical Scale:10dB/Division.

(a) h= 0.5 .

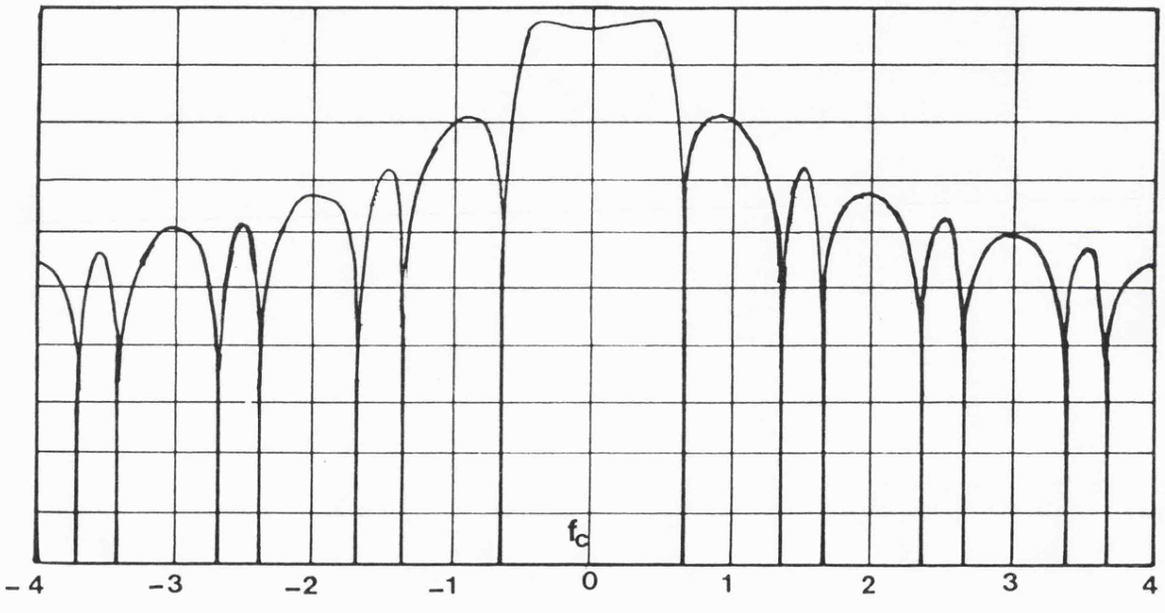

Horizontal & Vertical as in (a)

(b) h= 0.7 .

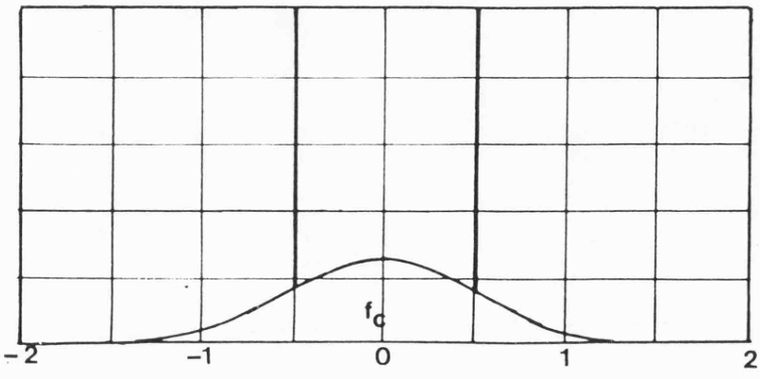

Horizontal:as in (a)— Vertical Scale: Linear.

(c) h= 1.0 .

Figure 3.10 Theoretical PSDF of CPFSK Signals.

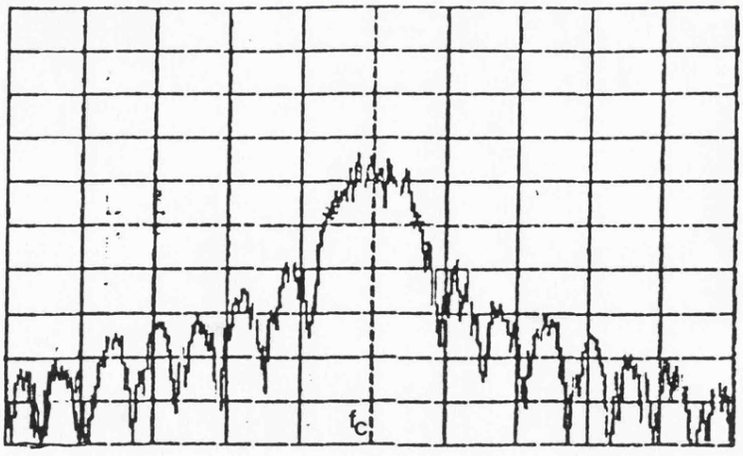

Horizontal: 2KHz/Div.- f_b=2.4KHz - f_c=10.7MHz.
Vertical : 10dB/Div.

(a) h = 0.5 .

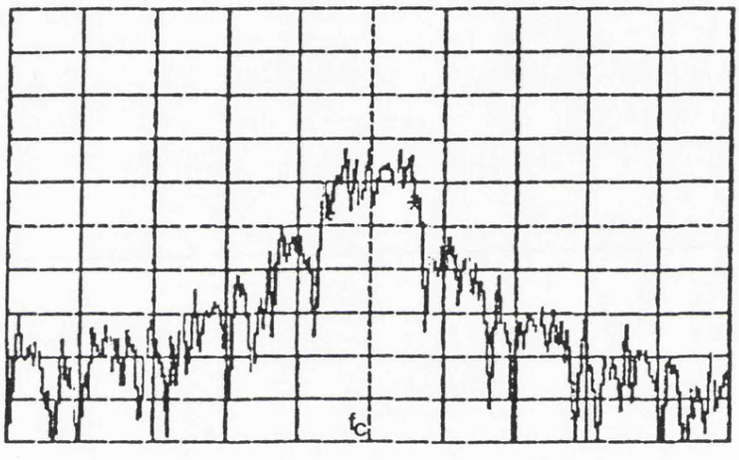

Horizontal & Vertical as in (a).

(b) h = 0.7 .

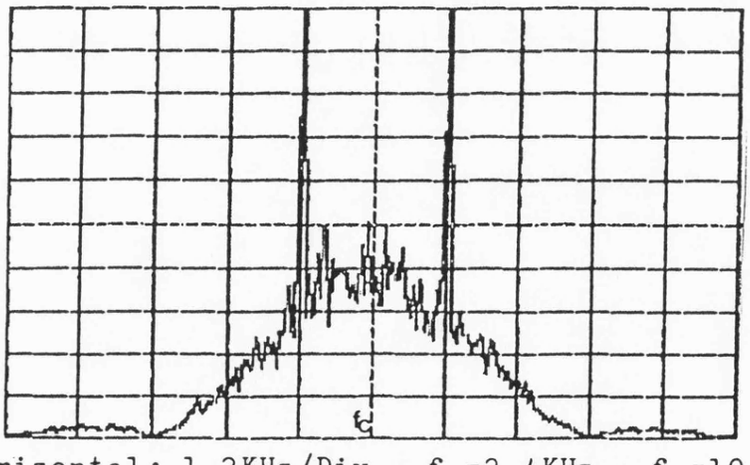

Horizontal: 1.2KHz/Div.- f_b=2.4KHz - f_c=10.7MHz.
Vertical : Linear Scale.

(c) h= 1.0 .

Figure 3.11 Measured CPFSK Spectrum.

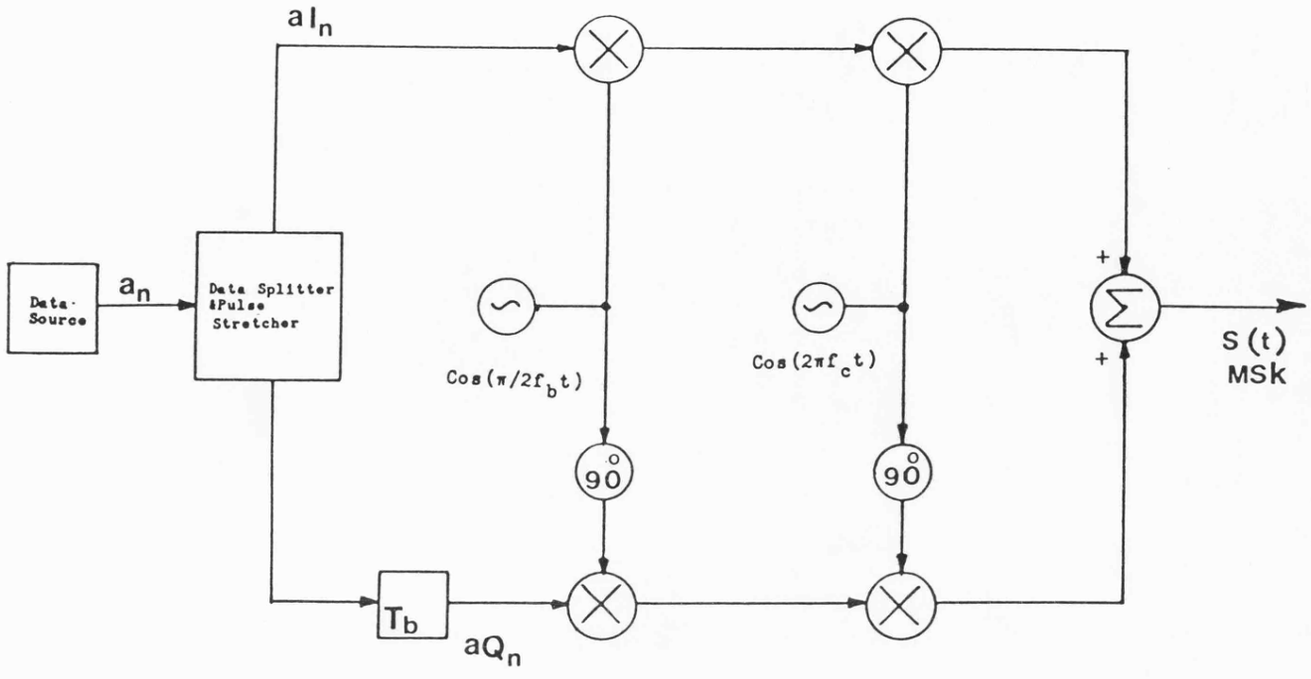

Figure 3.12 MSK Modulator Structure.

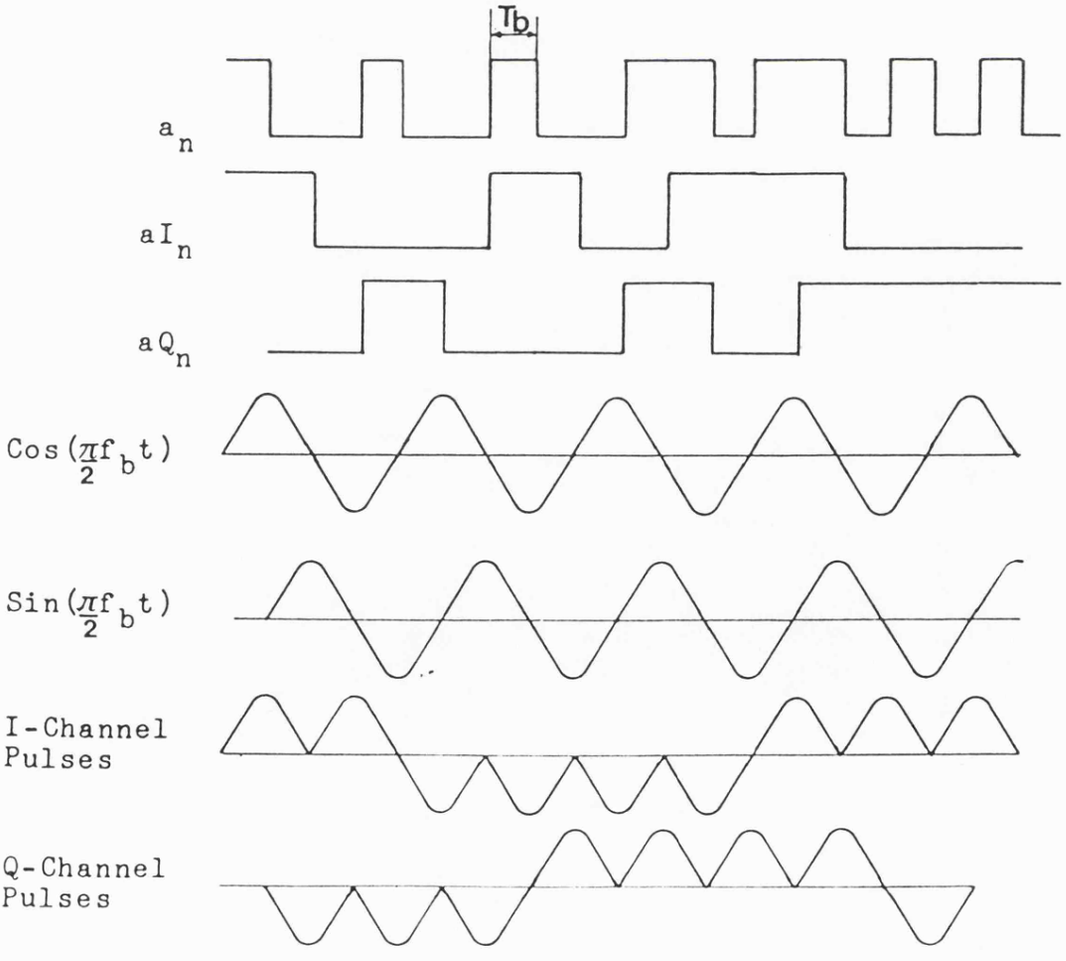

Figure 3.13 MSK Modulator Data Pulses.

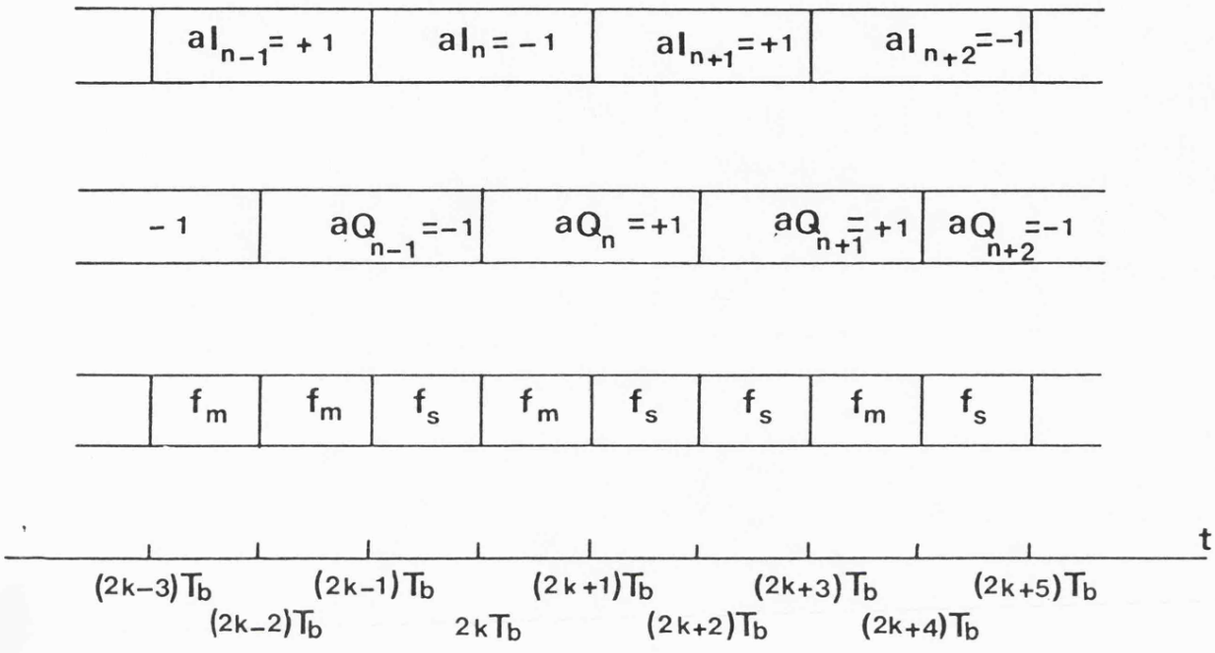

Figure 3.14 Relationship between the Transmitted Data and the Output Frequency of the MSK Modulator.

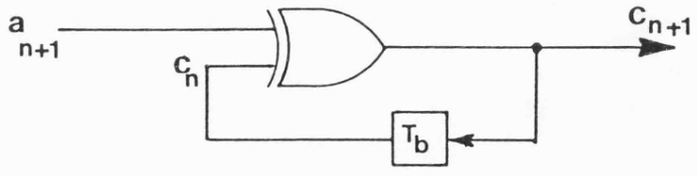

(a) Encoder.

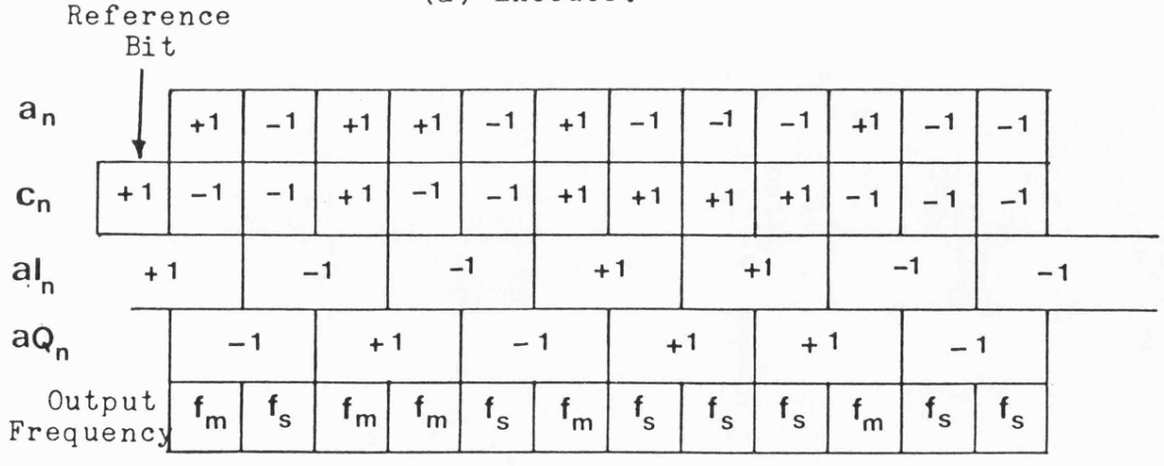

(b) Encoding Procedure.

Figure 3.15 MSK Data Encoding.

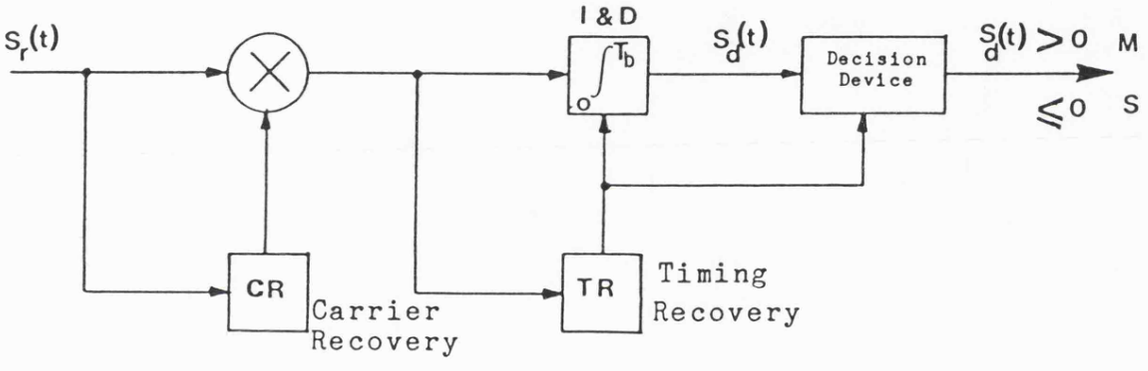

Figure 3.16 Coherent BPSK Demodulator.

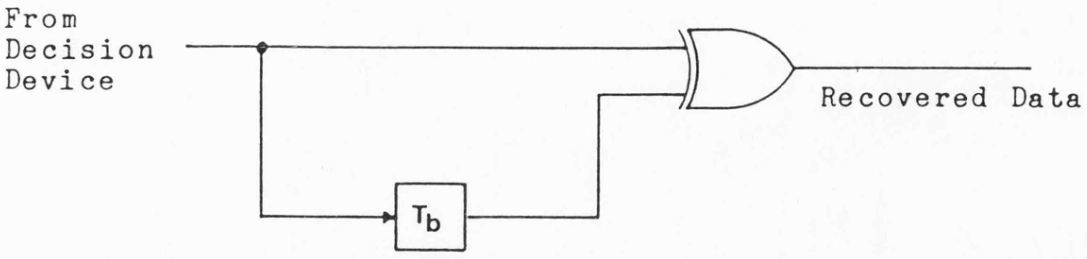

(a) Differential Decoder

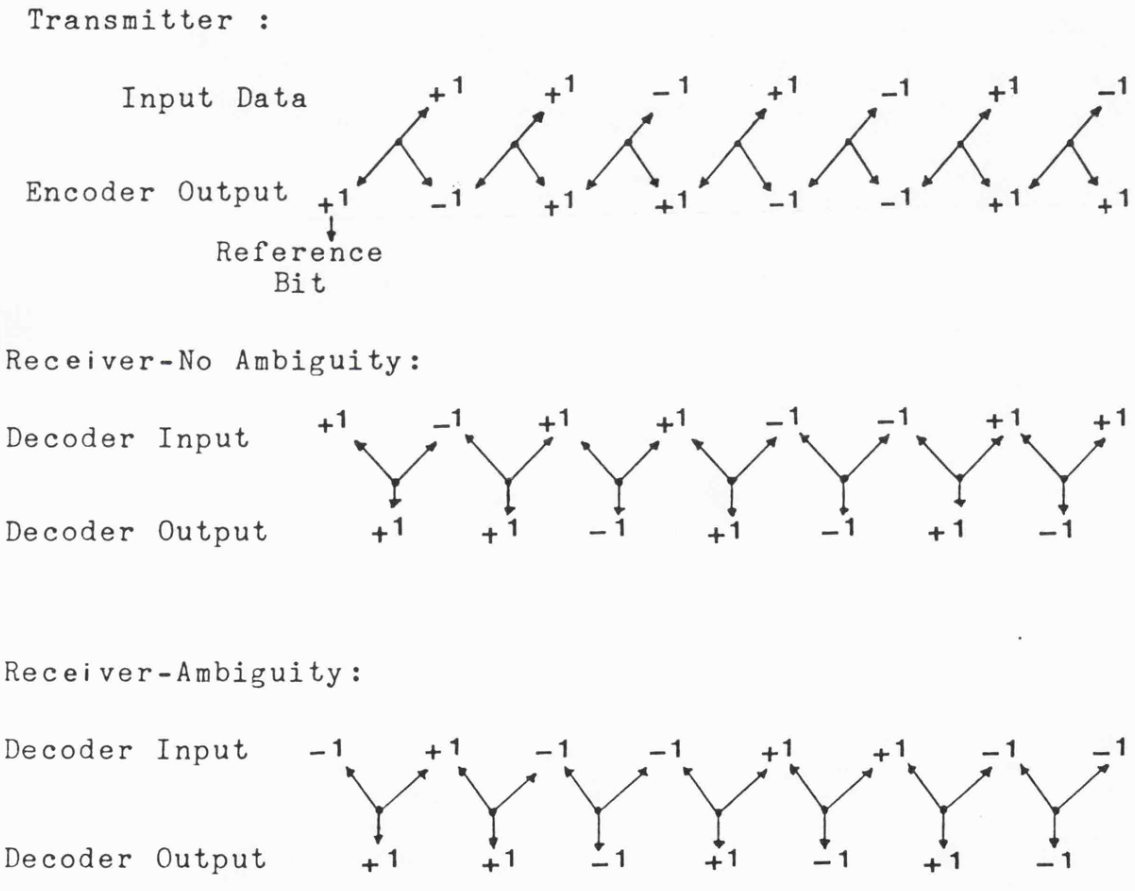

(b) The Principle of Differential Encoding/ Decoding Operation.

Figure 3.17 Differential Encoding/Decoding Process.

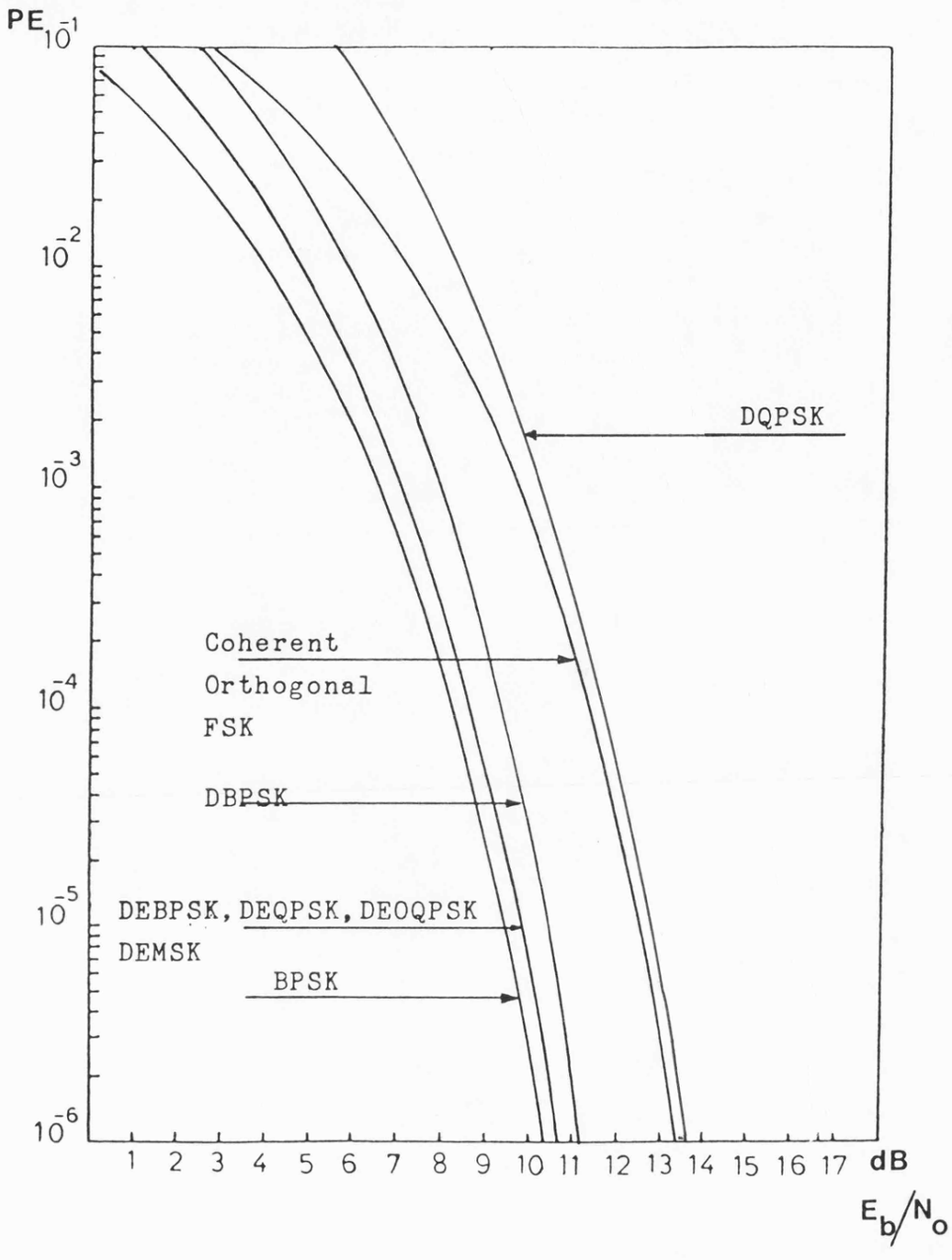

Figure 3.18 Theoretical PE Versus (E_b/N_o) of Different Digital Modulation/ Demodulation Techniques.

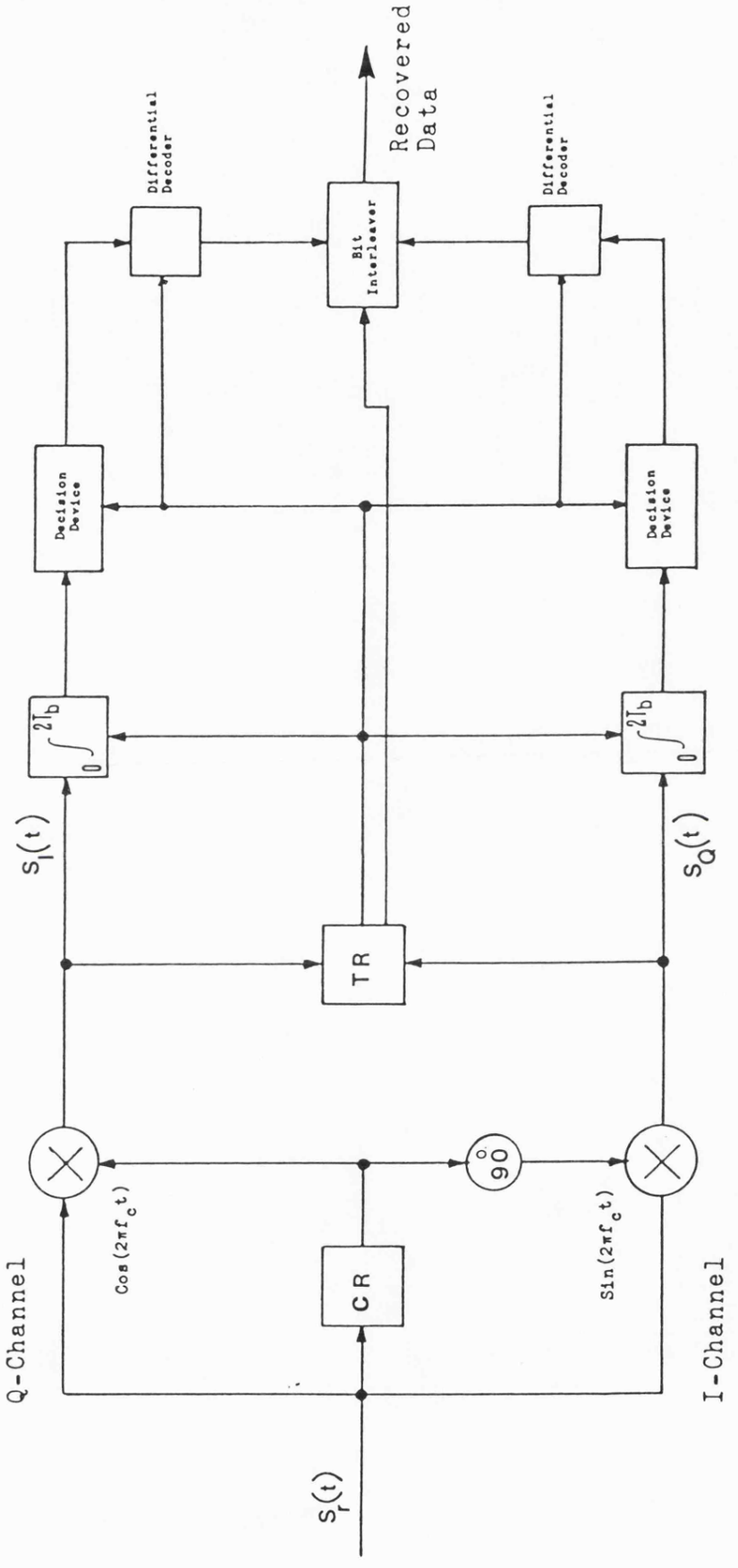

Figure 3.19 QPSK Coherent Demodulator.

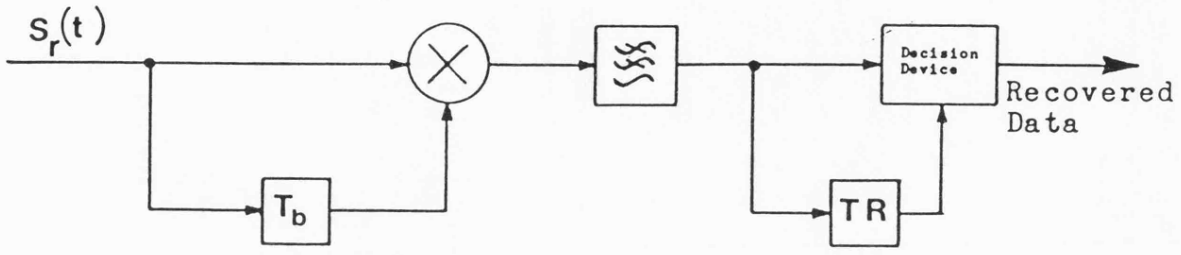

Figure 3.20(a) BPSK Differential Demodulator.

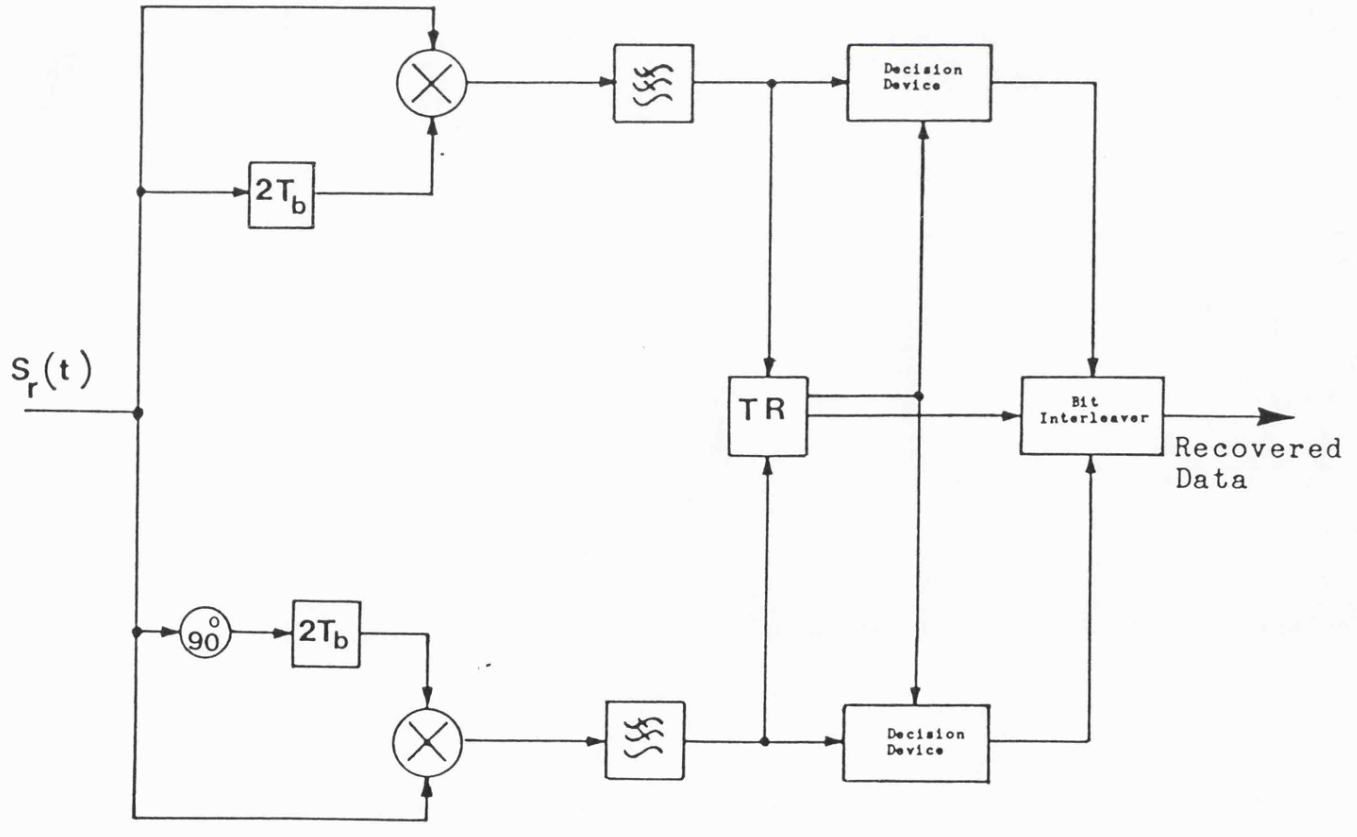

Figure 3.20(b) QPSK Differential Demodulator.

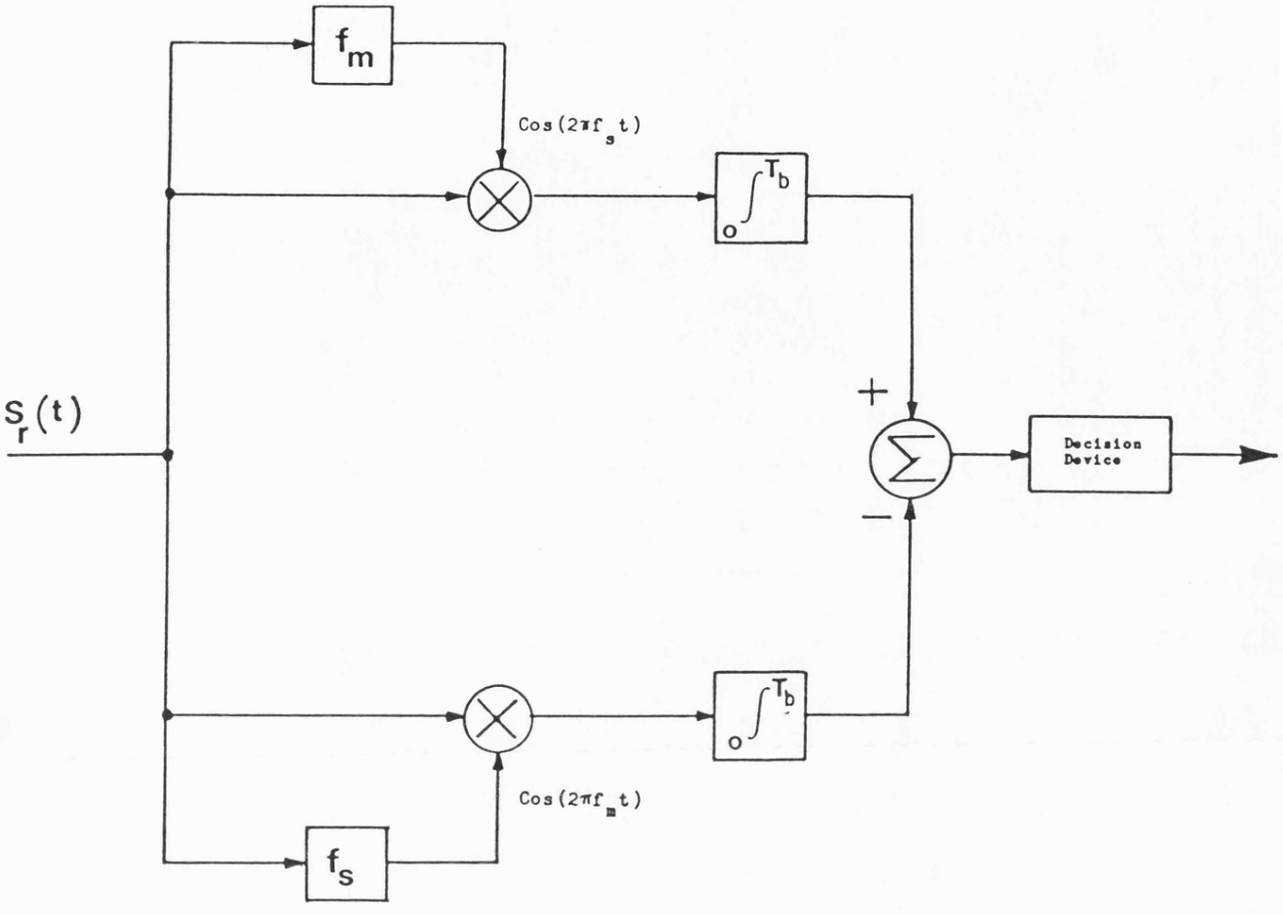

Figure 3.21 FSK Coherent Demodulator.

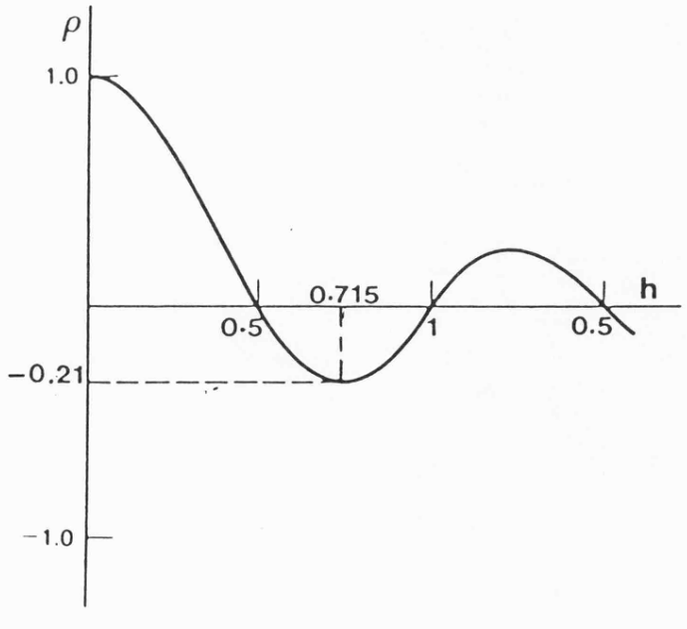

Fi Figure 3.22 FSK Waveform Correlation Coefficient Versus Deviation Ratio.

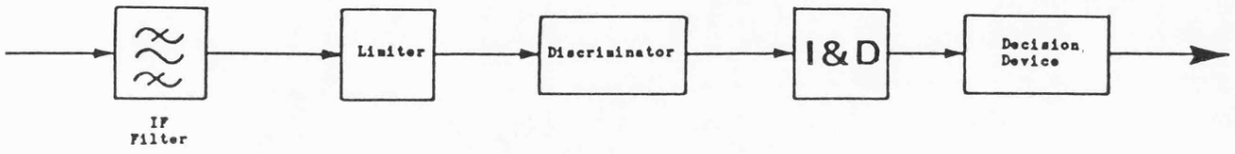

(a) Limiter-Discriminator Detector.

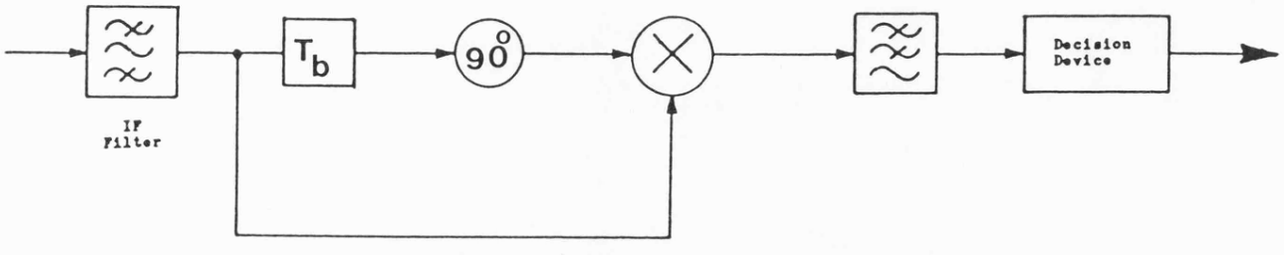

(b) Differential Detector.

Figure 3.23 Limiter-Discriminator & Differential CPFSK Detectors.

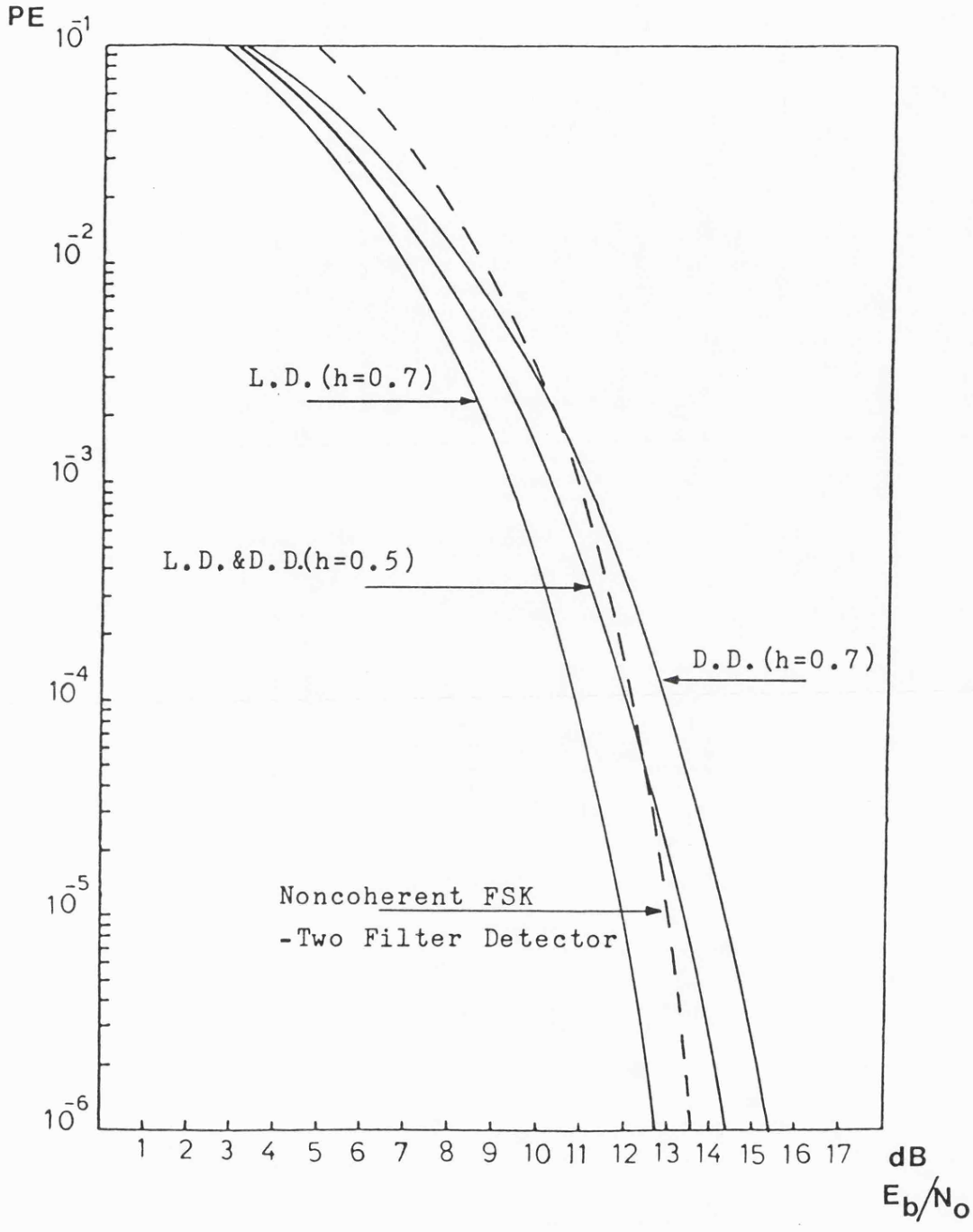

Figure 3.24 Theoretical Performances of Limiter-Discriminator (L.D.) & Differential (D.D.) NB-CPFSK Detectors.

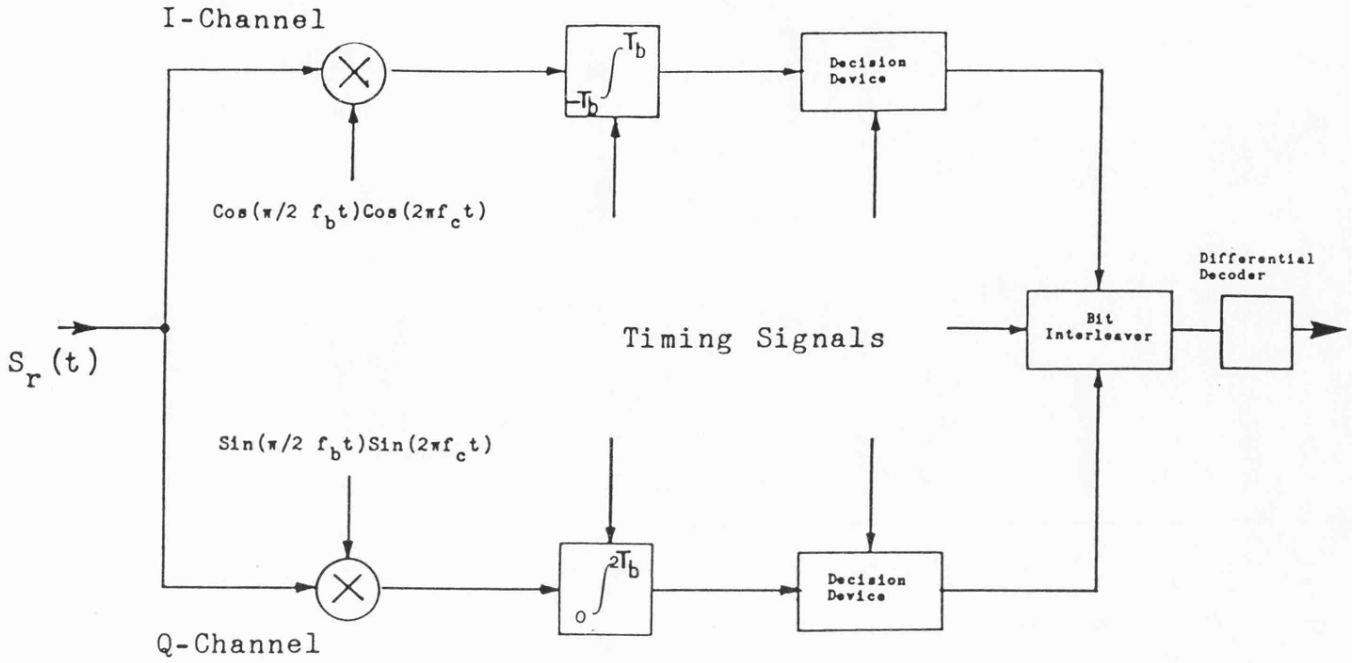

Figure 3.25 MSK Coherent Demodulator.

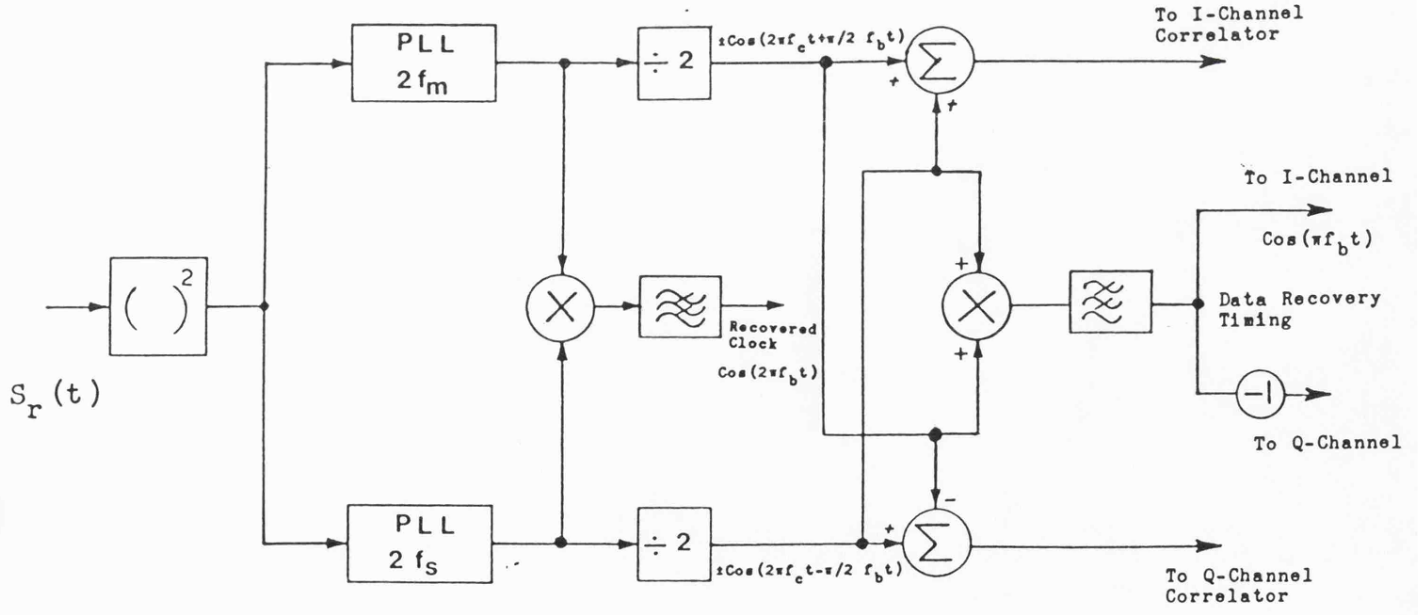

Figure 3.26 MSK References Recovery Circuits Block Diagram.

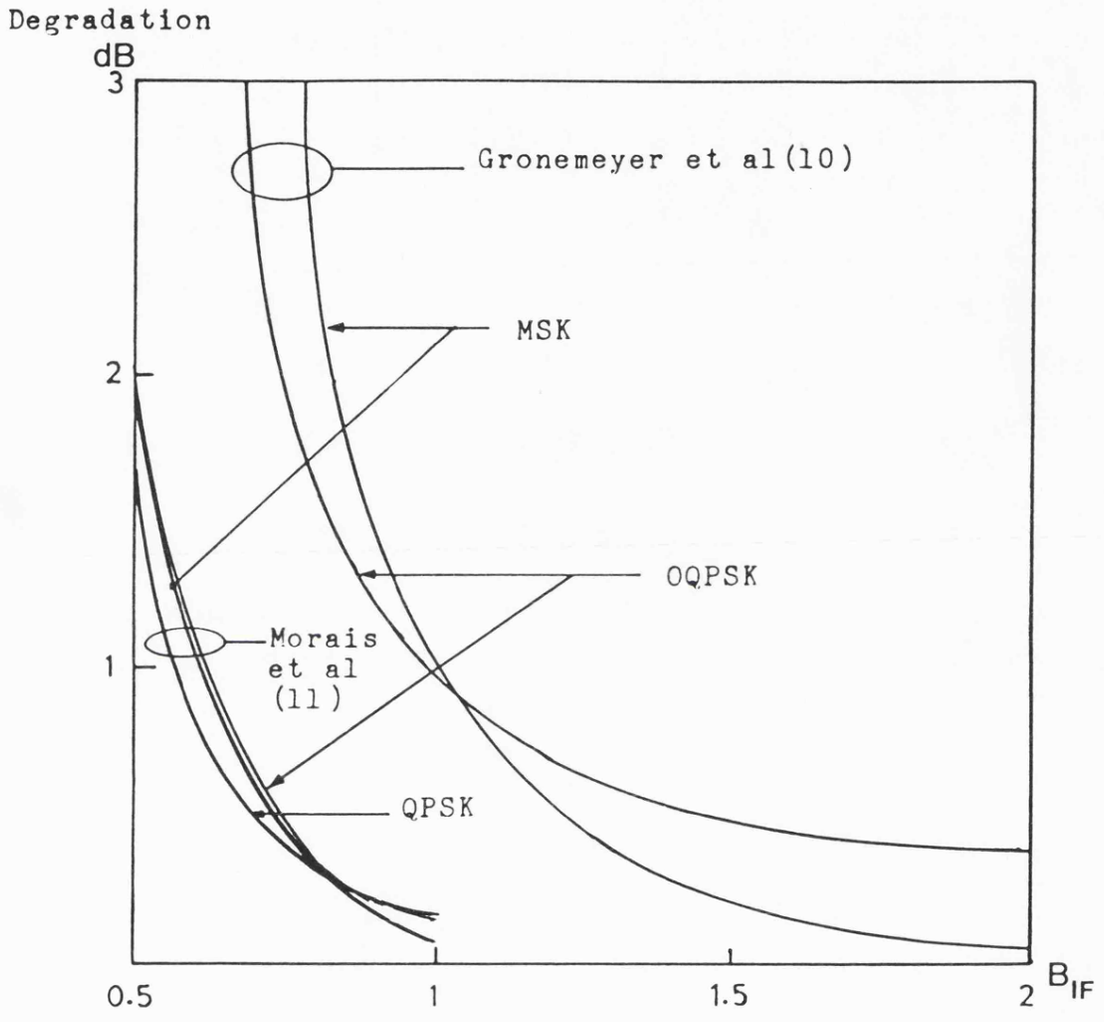

Figure 3.27 Effect of Bandlimiting on Performance Degradation of Coherent QPSK, OQPSK&MSK - PE=10^{-4} .

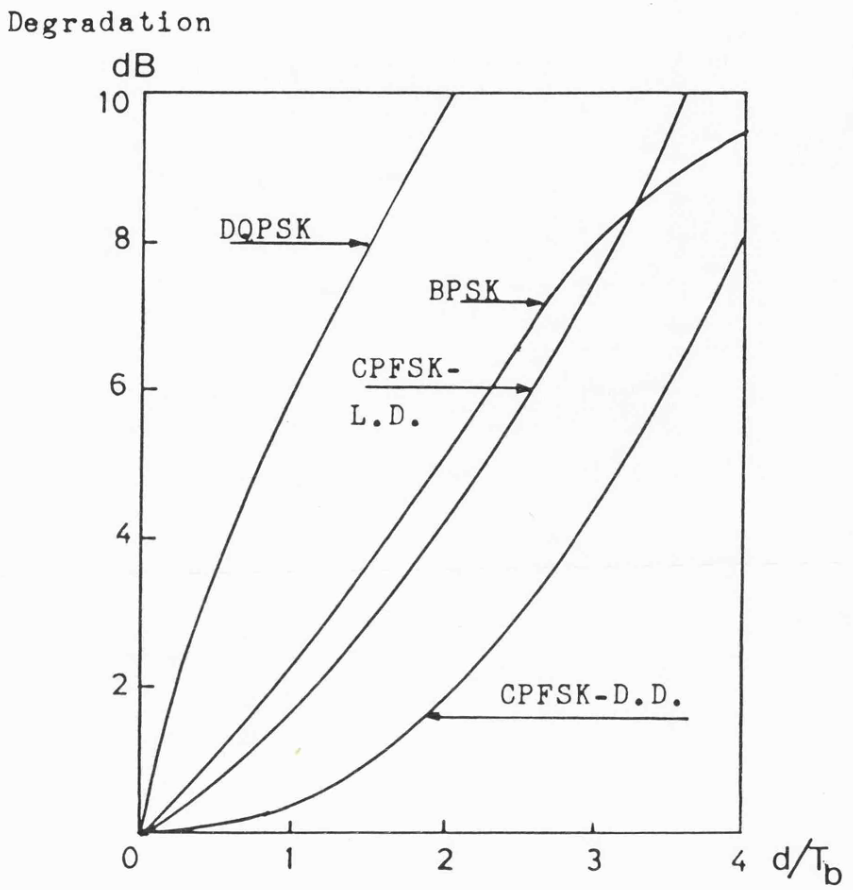

Figure 3.28 Effect of Delay Distortion on Differential Detction of BPSK , QPSK & CPFSK(D.D.) and Limiter-Discriminator Detection of CPFSK(L.D.).

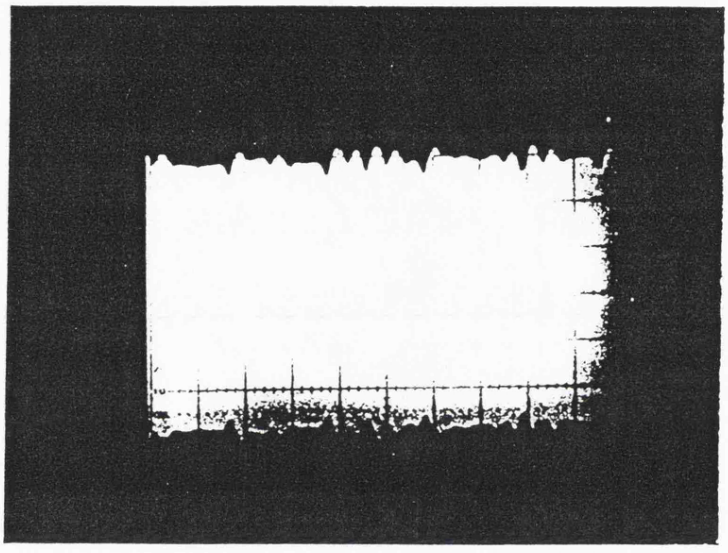

Figure 3.29 Bandlimited MSK Signal Waveform- $B_{3dB} = 2f_b$.

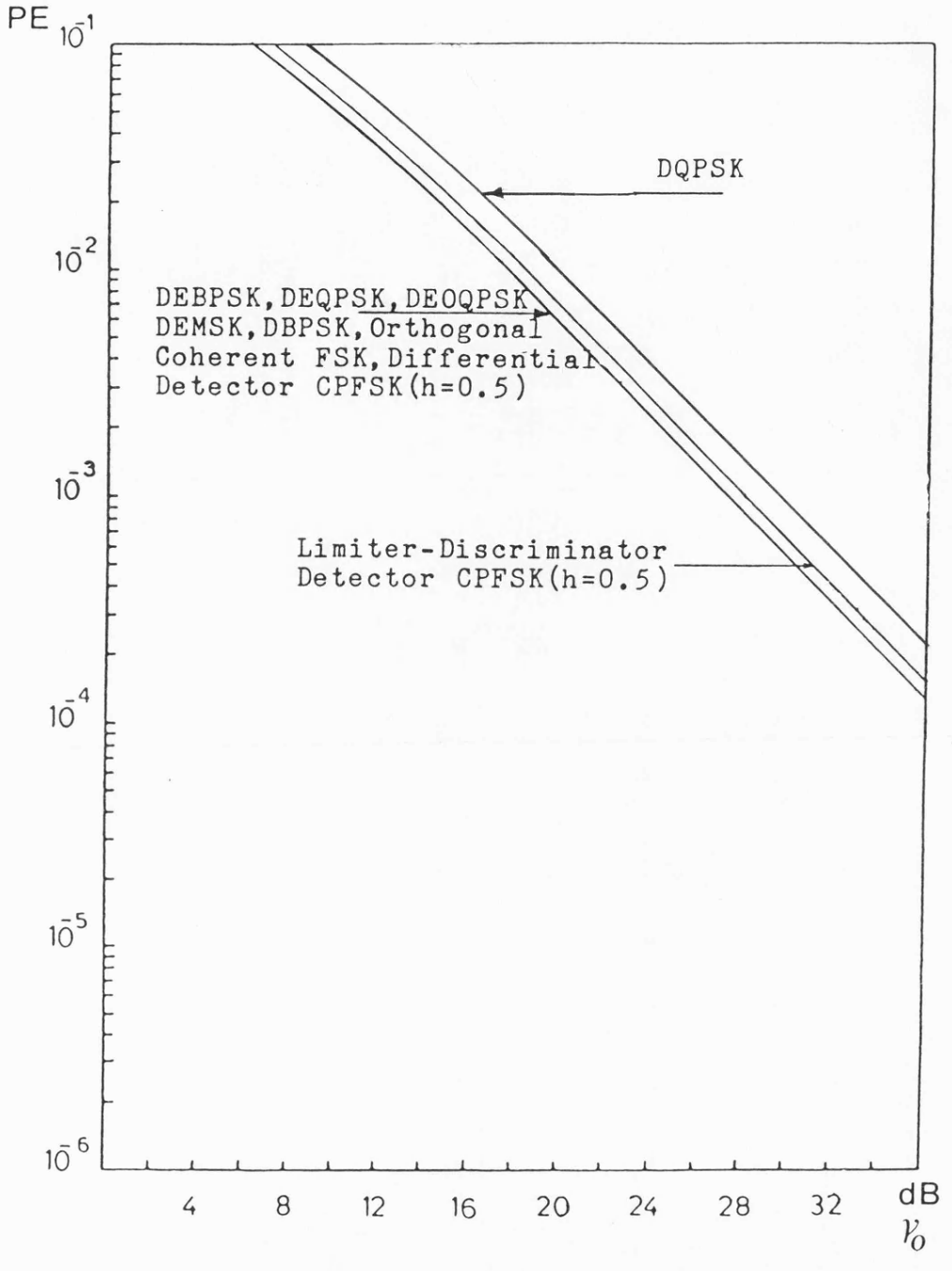

Figure 3.30 Probability of Error of Different Modulation/Demodulation Schemes in Presence of Slow Nonselective Rayleigh Fading.

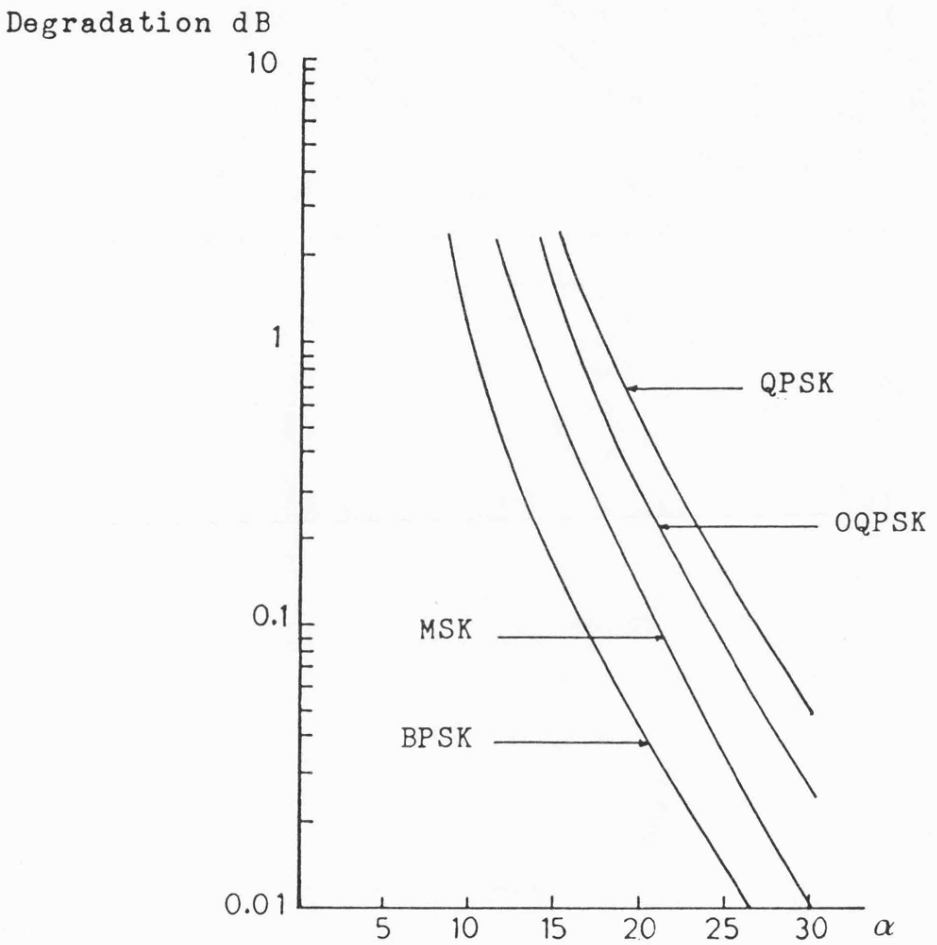

Figure 3.31 Performance Degradation as a Function of Phase Reference Signal to Noise Ratio , PE = 10^{-3}.

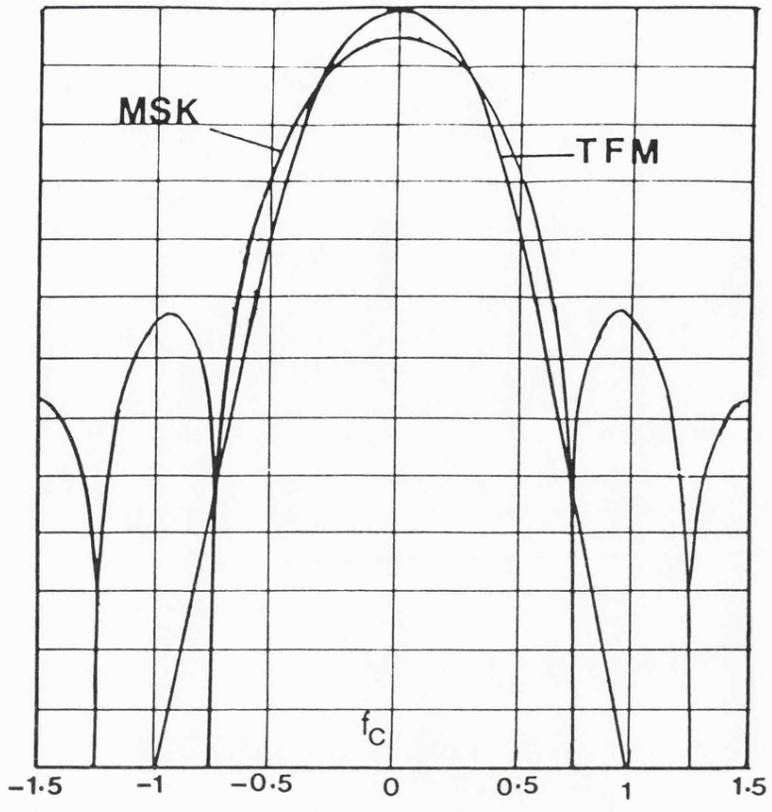

Horizontal: Normalised Frequency Offset from Centre- $(f-f_c)/f_b$, Vertical: 5dB/Div.

Figure 3.32 TFM Signal Spectrum.

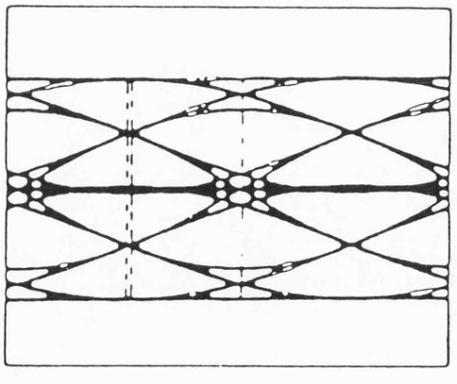

Figure 3.33 Eye Pattern at The Output of a Frequency Discriminator for TFM Signal.

CHAPTER FOUR

MSK MODULATOR-DEMODULATOR DESIGN

4.1 Introduction

The most commonly used analogue modulation technique over mobile radio channels until now has been frequency modulation (FM). There are two possible ways to introduce digital transmission into such a system. The first is shown in Fig 4.1(a), where the data modulates a base-band carrier, ie. an audio sub-carrier, which is treated in the following transmitter stages as an analogue signal. At the receiving end the digital signal is processed for detection at the output of the FM demodulator.

The second scheme, shown in Fig 4.1(b), is implemented by by-passing the analogue modulation circuitry in the equipment. The data directly modulates an RF carrier which can be the IF of the equipment.

While the first scheme offers compatability with existing equipments, it uses the available frequency spectrum inefficiently. Direct modulation improves the spectrum efficiency by a factor greater than 2 compared with indirect FM modulation.

Therefore, the MSK modulator carrier frequency was chosen to be 10.7MHz, which is a widely used IF in radio equipment. The demodulator input frequency is also 10.7MHz, however, the detection processses are carried out after mixing down the signal to 455kHz.

The modulator and demodulator were designed to operate at a data rate of 2.4Kbit/second. However, they can easily accommodate other values of bit rates.

4.2 Modulator Design

In the previous chapter it was shown that the MSK signal can be generated either by directly applying the data signal to the control votlage of a voltage controlled oscillator (VCO) or by using a quadrature modulation method. Although the first approach appears simpler, it suffers from two major drawbacks - instability and inflexibility.

Even though stability can be greatly improved by using a voltage controlled crystal oscillator (VCXO), it is a well known fact[1] that pullability and stability are two opposing requirements, and even in a crystal oscillator the stability suffers as the pullability is increased. Furthermore, the overall frequency deviation ratio (h) stability depends on that of the VCXO circuit and the amplitude of the modulating voltage. Changes in either due to temperature variations and/or fluctuations in predetermined modulating voltage levels, ultimately lead to a change in h.

As previously explained, MSK coherent demodulation relies in its references and clock recovery on a frequency doubling operation to produce a Sunde's CPFSK signal (h=1). Hence deviation from h=0.5 at the transmitter is doubled at the receiver and will adversely affect the recovery circuit and consequently the overall demodulator performance.

In some applications, especially prototype design and testing, it is desirable that the modulator could be easily modified to transmit data at different bit rates. In order to keep h=0.5, the peak deviation frequencies (f_m and f_s) of the VCXO will have to be carefully readjusted when the bit rate is changed. Furthermore, changing the carrier frequency to accommodate for different IF values used by different radio sets would practically mean designing and adjusting a new VCXO.

The quadrature modulation approach avoids the above disadvantages. The carrier frequency is generated by an ordinary crystal oscillator and does not suffer from potential instability due to the pulling operation. Furthermore, the carrier frequency can be simply changed by switching in a different oscillator. The only constraint is that the carrier frequency $f_c >> f_b$, which is always true for mobile radio applications. In addition, the modulator is designed to accommodate a certain range of bit rates by a simple adjustment procedure. The design can easily be modified to allow a wider range as will be explained.

The quadrature modulator is an exact realisation of the description of the MSK signal generation given in Chapter 3.2.3 and Fig 3.12. The detailed modulator block diagram is illustrated in Fig 4.2. The incoming data is first differentially encoded. The encoding procedure serves two functions: to produce a one-to-one relationship between the original data and the resultant modulated signal frequency, thus a non-coherent detector can be used without the need for further signal decoding and together with a differential decoder at the coherent receiver to resolve the recovered reference

phase ambiguity. The data splitter performs three functions simultaneously: odd-even data splitting, bit interval stretching to $2T_b$, and introduction of a T_b delay in the quadrature data stream aQ. The differential encoder and splitter circuit function diagram is given in Fig 4.3(a). In the above figure, (1),(2),(3),(4) and (5) are all D-type flip-flops. The splitter operation is explained by its timing diagram illustrated in Fig 4.3(b).

The sinusoidal data weighting reference, $\cos(\pi/2\ f_b t)$, is generated by passing ϕ_3, which is formed from the master clock as shown in Fig 4.3, through a low pass filter. The filter is an 8th order 0.5dB ripple Chebyshev and has a 3dB cut-off frequency of 0.7kHz, thus producing a sinusoidal signal from the input 0.6kHz square wave with practically no harmonic components. Following the filter a phase adjustment circuit is used to compensate for the phase shift in the filter and ensure that the input square wave and the output sinusoidal wave zero crossings coincide. Finally, the reference is passed through a 90° phase shift circuit to produce the quadrature channel data weighting reference. Both phase adjustment and 90° shift circuits are all-pass first order active networks and are given in Appendix 4.1. The range of bit rates the modulator can accept is governed by the low pass filter cut-off frequency. Using the above filter, the modulator produced an MSK signal with bit rates ranging from 1kb/sec (ie. f_b = 1kHz) to 2.6kb/sec. The only adjustments needed are those of the phase adjustment circuit and the 90° phase shift circuit to bring I and Q channels, references and data in phase coincidence. This is a simple procedure and carried by changing one multi-turn variable resistance in each as explained in Appendix 4.1. Bit rates outside the above range could be

accommodated by changing the low pass filter or more practically by using switched capacitor filters whose cut-off frequency is controlled by the value of their clock frequency. The latter can be provided by the clock ϕ_3 through a frequency multiplier as illustrated in Fig 4.2 by the dotted lines. The phase adjustment circuits can be designed to accommodate a wide frequency range.

The sinusoidal weighting reference multiplication by the data is accomplished by applying the references to an inverter/non-inverter circuit whose action is controlled by the data. Inversion is equivalent to a multiplication by a space bit (-1) and non-inversion is equivalent to a multiplication by a mark bit (+1). The inverter/non-inverter circuit is explained in Appendix 4.2. The I and Q channels' inverter/non-inverter outputs are shown in the photograph in Fig 4.4. The modulating data is a pseudo random sequence of a length 511 bits at a rate of 2.4kb/sec.

A crystal oscillator generates a signal whose frequency is 4 times the carrier frequency, ie. 42.8MHz. This frequency is then divided by 4 using high speed TTL D-type flip-flops to produce two carrier signals in quadrature as shown in Fig 4.5. This method of generating the carrier signals guarantees quadrature relationship independent of its frequency and values of the passive components which would have to be used otherwise. Because of the large difference between the carrier frequency and the modulating data bit rate, the phase relationship between them can be ignored.

The sinusoidal weighted data and the carrier signal of I and Q channels are applied to two balanced modulators acting as multipliers

as shown in Fig 4.2. The balanced modulator circuit is given in Appendix 4.3.

Finally, the MSK signal is generated by adding the outputs of the two balanced modulators in a resistive summer which is followed by a buffer amplifier. The final MSK modulator output waveform is shown in the photograph in Fig 4.6. The modulating data is a 511 bits (length) pseudo random sequence whose bit rate is 2.4kb/sec.

The power spectral density of the above modulator output signal is illustrated in the spectrum analyser trace in Fig 4.7(a) and (b) for two values of bit rate: 1.2 and 2.4 kbit/sec. The agreement between the modulator output spectrum and the theoretical MSK signal spectrum given in Fig 3.3 is evident.

4.3 Demodulators' Front-End

The MSK demodulators accept the signal after being converted down to 10.7MHz. Their front-ends are those of a conventional low-power narrowband FM IF integrated circuit (IC). The IC used is MC3359[2] and is designed primarily for use in voice communication, but is also finding a place in narrow band data communication applications. It includes an oscillator, a mixer, a limiting amplifier and a quadrature frequency discriminator. The received 10.7MHz MSK signal is converted down in the mixer to 455kHz and passed through a conventional bandpass ceramic filter as shown in Fig 4.8. At the output of the bandpass filter the signal is separated either for coherent or non-coherent detection.

4.4 Non-Coherent Demodulator

Non-coherent MSK demodulation is accomplished in the final stages of MC3359. The output from the ceramic bandpass filter (Fig 4.8) is applied to a limiter amplifier, whose output drives a quadrature frequency discriminator detector. The recovered baseband signal is then amplified and passed through a low pass filter to remove high frequency components. The demodulated MSK signal eye pattern is shown in Fig 4.9 for a modulating data bit rate of 2.4kb/sec. The ceramic filter 3dB bandwidth equals approximately twice the bit rate.

After removing the DC voltage from the demodulated signal the data recovery is accomplished by passing the signal through an integrate and dump (I&D) circuit which acts as a post demodulation filter. The I&D output is then sampled and held (S&H) at the end of each bit interval. The S&H output is then applied to a threshold level detector (the threshold level is zero in this case) whose output voltage levels are that of a TTL signal. Finally, data decisions are taken at positive edges of the recovered clock and inverted to compensate for the inversion action of the I&D circuit. The data recovery circuit and its timing control diagram are illustrated in Figs 4.10(a) and (b).

The receiver clock which controls the data recovery operations, and any subsequent digital operations, is phase locked to the data transition edges in the demodulated signal as explained in the following section.

4.5 Clock Recovery Circuit Analysis

The clock recovery, ie. the synchronisation between the receiver and the transmitter clocks, is performed at baseband. The timing information contained in data transisions of the demodulated signal is used to synchronise, ie. phase-lock, a stable local clock reference.

The schematic diagram of the recovery circuit is shown in Fig 4.11.. Binary transitions in the baseband signal are detected and applied to a binary lead-lag detector. The other detector input is the local reference clock signal whose frequency is approximately equal to the transmitted bit rate f_b. The local clock is derived from a high frequency cystal oscillator whose output is frequency divided down in a programmable binary divider to produce f_b. The lead-lag detector compares the positive edges in the local clock with the transition edges in the demodulated signal. It has two outputs, the first indicates that the clock edges are leading the transitions and the second indicates the opposite. These are used as binary outputs which do not give an indication of the amount of phase difference between the signal transitions and the local clock.

The binary lead/lag signals from the detector are then applied to an up-down binary counter. The lead output causes counting up and vice-versa as shown in Fig 4.11. The counter has equal upper (2M) and lower (0) counting limits, when either is reached one of two mutually exclusive pulses each indicating one of the limits is produced. The counter limit pulses drive an OR gate whose output resets the up/down counter to its mid-point (M), where M is an integer.

The up/down counter averages the lead-lag information and thus allows the recovery circuit to ignore transitions in the received demodulated signal due to noise if a long total counting length (2M) is used.

The counter output pulses are used to update the phase of the local reference clock. If the upper counter limit is reached, which indicates that the clock is leading transition edges, the clock frequency is decreased by changing the frequency division ratio (N) of the programmable divider providing the local clock to (N+1). On the other hand, if the averaging up/down counter reaches its lower limit the division ratio is changed to (N-1). The change in division ratio lasts for a time interval equal to LT_b, where L is an integer. The timing is provided by a programmable timer which is initiated by either of the averaging counter two limits pulses which are available at the output of the OR gate as shown in Fig 4.11. After the time interval LT_b has elapsed, the division ratio is reset to its mid-value N.

For each lead or lag command, the phase retard or advance correction step is equal to 360/N degrees. During a time interval LT_b, the phase of the local clock is advanced or retarded by:

$$\Delta\Theta = \frac{360}{N} L \text{ degrees} \qquad \ldots (4.1)$$

Assuming that the received signal is a sequence of alternate marks and spaces, the recovery circuit will produce, in the absence of noise, a maximum of f_b/M adjustment commands per second, and for each command the phase is adjusted by $\pm\Delta\Theta$. Under these conditions, the maximum phase adjustment rate is $\pm\Delta\Theta\ f_b/M$ degrees per second.

Consequently, the maximum frequency difference, f_r, that can exist between the transmitter and receiver clocks without the recovery circuit going out of lock, is given by:

$$f_r = \pm \frac{\Delta\theta}{360} \frac{f_b}{M} \quad \text{Hz} \qquad \ldots (4.2)$$

where $\Delta\theta$ is given by eqn (4.1). Because the circuit achieves locking in discrete phase steps, then the minimum phase error it can attain is $\pm \Delta\theta/2$.

In the presence of noise, assuming that it will cause false lead/lag decisions at the output of the binary lead/lag detector with equal probabilities, the probability that the averaging counter will reach one of its limits due to false detector decisions, and thus possibly producing a wrong phase adjust command will decrease by increasing the total counter length (2M). However, increasing the counter length leads to a decrease in the locking bandwidth, as can be concluded from eqn (4.2), and an increase in the time needed for the circuit to achieve locking, if it is initially out of lock, ie. acquisition-time.

The choice of the recovery circuit parameters, $\Delta\theta$ and M, will depend on different factors. The phase correction step should be made as small as possible to minimise recovered clock phase jitter. In mobile radio transmission the signal is frequently lost during deep fades, therefore the recovery circuit should have as large as possible averaging counter length (M) to reduce the probability that a false command will reach the phase adjust circuit. If M is large enough the recovered clock will flywheel during periods of deep fades. However, the minimum circuit locking bandwidth (f_r) is

ultimately governed by the transmitter and the receiver clock oscillator's stabilities.

To decrease the acquisition time of the recovery circuit without compromising its performance when locking has been achieved, ie. tracking performance, it can be designed to have dual averaging counter length (M). A short one at the start of transmission to speed up acquisition and a long one after acquisition has been achieved for tracking purposes.

4.5.1 Clock Recovery Circuit Implementation

Based on the above description, a clock recovery circuit has been implemented using standard TTL integrated circuits[3]. The circuit function diagram is illustrated in Fig 4.12. The practical circuit realisation and the choice of its parameter values are explained in the following.

The demodulated baseband signal, after being converted to TTL voltage levels, is applied to a 2-input exclusive OR (EXOR) gate. the other gate input is the signal delayed version. The EXOR acts as a signal transition edge detector, as depicted in Fig 4.13. The binary lead/lag detector is composed of a D-type flip/flop, two 2-input AND gates and two inverters. The inverter's function is to compensate for the flip/flop propagation time delay. The detector operation is explained in Fig 4.13 and it can be concluded that it has a detection range of ±180°.

Each detector output triggers one of two one shot multivibrators (OMV) whose pulsewidths $\simeq T_b/100$. Each of the inverted multivibrator

outputs (Q) is applied to one of two 2-input OR gates. The other OR gate inputs are the output of a programmable pulse generator which is controlled by the acquisition control circuit. When the recovery circuit is in tracking mode the pulse generator output is disabled (low). The operation of acquisition control circuit is explained later.

In tracking mode each lead or lag pulse from the detector output causes one count step up or down respectively in the averaging counter. The averaging counter is composed of 12 stages by cascading three 4-stage synchronous counters, as shown in Fig 4.12. The mid-point counting length (M) is predetermined by programming the counter binary inputs A_o to A_{11}. The upper limit counting state is detected by programming X_o to X_{11} and monitoring the counter outputs Q_o to Q_{11}. The counters borrow outputs (B) are also monitored by a 3-input NOR gate to detect the lower counting limit (o). When either of the counting limits is reached the averaging counter is reset to its midpoint (M) by enabling the load input (L) as shown in Fig 4.12.

The local clock reference is produced by dividing down the output of a 12MHz crystal oscillator to 2.4kHz in two steps. The first is a division by 2500 (in the absence of phase adjust commands) in a 12-stage programmable binary divider (composed of three 4-stage synchronous unidirectional counters) and the second is a division by two in a D-type flip/flop to produce a symmetrical clock waveform. The funciton of the D-type flip/flop which precedes the division by two (Fig 4.12) is to produce a glitch-free signal.

Programming the divider is done by setting its binary program

inputs, A_0 to A_{11}, according to the following rule:

$$N = 4096 - K$$

wherew N is the required division ratio and K is the decimal value of the binary inputs. Hence to change the division ratio to N+1, K should be decreased by 1, and vice versa.

The divider inputs, A_0 to A_{11}, are the outputs, Q_0 to Q_{11}, of another set of 12 stage synchronous up/down counter (composed of three 4-stage synchronous up/down counters). The up/down counter binary program inputs, A_0 to A_{11}, are fixed so that when loaded they program the divider with a division ratio N. The latter is changed by applying the phase adjust command pulses to the counting inputs of the up/down counter. A phase advance pulse is applied to the counting up control input, consequently producing a division by (N-1). A phase retard pulse is applied to the count down input to change the division ratio to (N+1). The mutually exclusive phase command pulses are ored and used to trigger the programmable timer 1 as shown in Fig 4.12. At the end of the programmed time interval (LT_b) the timer produces a pulse which is applied to the load control input of the up/down counter. Thus, at the end of each phase adjust time interval (LT_b) the division ratio is reset to N. The programmable timer circuit is given in Appendix 4.

During tests to evaluate the non-coherent MSK demodulation performance the clock recovery circuit parameters were set to the following values:

$$L = 33 \quad \text{and} \quad 2M = 512$$

Thus, the phase adjust step, given by equation (4.1), is equal to:

$$\Delta\theta = \pm \frac{360}{5000} \times 33$$

$$= \pm 2.376 \text{ degrees}$$

The maximum locking bandwidth, given that the data is composed of a sequence of alternate markers and spaces, can be calculated from equation 4.2:

$$f_r = 0.062 \text{ Hz}$$

which closely agreed with practical measurements.

The above assumption for maximum locking bandwidth cannot be satisfied when transmitting bipolar non-return to zero (NRZ) random data. Given that marks and spaces occur in a random manner with equal probabilities, the number of transitions occurring per second can be assumed equal to $f_b/2$. Thus, the recovery circuit locking bandwidth under such conditions is equal to $f_r/2$, ie. ± 0.31. However, in practical situations long sequences of marks and spaces could take place, thus further reducing f_r. In tests, the data source used was a 511 bit length pseudo random data sequence. This sequence is recommended for data transmission tests by the CCITT[4] and it produces a maximum of nine consecutive marks or spaces and contains all possible eight bit data patterns. The maximum frequency difference between the transmitter and the receiver clocks was allowed to be approximately ± 0.024Hz. This represents a frequency stability of ±10 parts per million, which can be achieved by using standard crystal oscillator circuits[1].

To assess the tracking performance of the clock recovery circuit under the above conditions, error rate versus signal to noise ratio measurements were carried with the modulator clock hardwired to the

demodulator and also with the clock recovered at the demodulator. The tests were carried for the coherent (ω_n = 10,100) and noncoherent demodulators under non-fading and simulated Rayleigh fading conditions. The fading rates, expressed as the maximum doppler shift f_D, were 0.15Hz and 100Hz. No deterioration in error rate performance was noticed when the clock recovery circuit was used. The details of the experimental set-up and the results are given in Chapter 5. Furthermore, the circuit was flywheeling, ie. the receiver clock was drifting with respect to the transmitter one at a rate equal to their frequency difference, in the absence of a received signal during deep fades. This is because of the long averaging counter length used (512).

Operating the clock recovery circuit at higher bit rates is trivial. For a given bit rate and a required locking bandwidth, equations (4.1) and (4.2) can be used to determine the values of N, L and M. The upper bit rate (ie. clock frequency) limit on the circuit operation is governed by the maximum acceptable phase correction step, $\Delta\theta$, which does not cause excessive phase jitter. This can be reduced by reducing L as the clock frequency increases, nevertheless there will be a limit when L=1 and 360/N does not satisfy the condition on the phase jitter. Assuming the previous phase step of ±2.376°, this limit occurs at N ≃ 152. Using a 12MHz oscillator the bit rate should be lower than 78kHz. This is very much higher than the bit rates the land-mobile radio channels can support, even in the present time maximum channel bandwidth (25kHz).

4.5.2 The Acquisition Control Circuit

When the recovery circuit is in the tracking mode the acquisition control circuit is disabled and the programmable pulse generator

output (Fig 4.12) is low. In standby mode, the detection of a received signal triggers the acquisition control circuit . The received signal state detector is given in Fig 4.14 and is explained later. The triggering of the acquisition circuit initiates the programmable timer (2) (Fig 4.12), which produces a high state at its output lasting for a predetermined time interval equal to multiples of T_b. The timer output is applied to a 2-input AND gate whose other input is the output of a 2-input OR gate. The OR gate inputs are the mutually exclusive lead/lag detector output pulses. Consequently, the appearance of a lead or lag pulse during the acquisition time interval, which is controlled by timer 2, will trigger the programmable pulse generator as shown in Fig 4.12. The pulse generator is derived from a 12MHz signal provided by the crystal oscillator and it produces for each trigger pulse a pre-determined number of pulses P. Thus, during acquisition, for each lead or lag pulse the count in the averaging up/down counter is advanced or retarded by P steps (instead of one step during tracking), as can be concluded by investigating Fig 4.12. This effectively reduces the counting length to M/P and speeds up the acquisition time by a factor proportional to P. The maximum value of P is governed by the one shot multivibrators (OMV - Fig 4.12) output pulse width and can be 100 at most. The programmable timer 2 and pulse generator circuits are explained in Appendix 4.4

At the start of a transmission the maximum phase excursion the clock recovery circuit should go through to achieve locking is 180°. Hence, the maximum acquisition interval time, T_A, is given by:

$$T_A = \frac{180}{\Delta\Theta \frac{f_b}{M} P \pm \text{phase drift rate (degrees/sec)}} \text{ seconds}$$

. . . (4.3)

where $\Delta\Theta (f_b/M)P$ represents the rate of phase correction and the ± sign in the denominator depends on whether the phase drift and the correction steps are in the same (+) or opposite (−) directions. Thus T_A, using the previous circuit parameters ($\Delta\Theta$ = 2.376°, M = 256), while the acquisition circuit is inactive (P=1), assuming that a preamble signal composed of a sequence of alternate marks and spaces at the beginning of transmission at a rate of 2.4kbit/sec and given a maximum frequency difference of ±0.024Hz between the receiver and transmitter clocks, is equal to 5.83 seconds or 13.16 seconds depending on whether the phase drift and correction steps are in the same or opposite directions respectively. It is evident from equation 4.3 that T_A can be decreased by increasing P. The decision on a value of P and consequently T_A depends on the user choice and type of data application.

The acquisition circuit, in addition to its importance at the start of transmission, can also play a useful role during tracking. This role is a result of the fading nature of mobile radio transmission. When the signal goes through a deep fade, the local clock will flywheel during the fade period. The bit integrity of the received signal will be maintained as long as the receiver clock does not go through a cycle slip with respect to the transmitter clock. In the above circuit cycle slip would occur if the local clock drifts for more than ±180°. Assuming a frequency difference of ±0.024Hz, this cycle slip takes place if the received signal remains absent for more

than 20 seconds. A deep fade duration of 20 seconds, although possible, cannot be considered as a common occurrence. However, deep fades of several seconds duration can occur, leading to a proportional phase drift (at 0.024Hz frequency difference the phase drifts at a rate of 8.6°/sec). Thus, when the signal recovers from a relatively long fade there will be a re-acquisition time lapse during which bit errors result from the excessive timing error. The reacquisition time can be reduced by resetting the recovery circuit to the stand-by mode whenever the loss of signal is detected. The loss of signal detection is performed by the same circuit which detects the signal prsence and whose action is explained in the following section.

When the acquisition circuit is used to speed up phase locking after a deep fade, the acquisition time should be made proportional to the fade duration. This will prevent an increasing number of false lead-lag commands being produced if the recovery is immediately followed by another, not necessarily deep, fade. A fade duration estimator circuit which would control the programmable timer 2 can be built around the signal state detector explained in the following section.

The Rayleigh fading simulator used in testings has a minimum fading rate (expressed as the maximum doppler shift f_D) of 0.15Hz. Tests have shown that at this fading rate the acquisition circuit would not contribute in improving system error rate performance. However, in practical situations where deep fades can last for several seconds, its contribution in improving digital receptioin performance is evident.

4.5.3 Received Signal State Detector

Fig 4.14 illustrates the signal state detector function diagram. Its operation is based on a race between two positive edge triggered counters, one counting clock pulse and the other counting transitions in the demodulated baseband signal. In high signal to noise ratio conditions, the clock counter will be counting faster than the signal transition counter. As the signal to noise ratio decreases, extra pulses due to noise appear in the demodulated signal and the latter counter starts counting faster than the first.

The detector counters, which are 12 stages long, are designed to have each two predetermined counting limits. One in each is activated while the circuit is in stand-by mode, and the other while it is in tracking mode. The first should be short to minimise detection time. The counting limits during tracking should be made longer to prevent the signal detector from changing its state when the signal suffers from a deep but relatively short fade which does not cause excessive phase drift, and thus causing an interruption of the message until signal presence detection is re-established. The operation of the signal state detector can be understood by studying Fig 4.14. The choice of counting limits depends on the average number of transitions caused by the noise in the demodulated signal in conjunction with the type of data coding used and data application.

4.6 Coherent Demodulator Design

The coherent MSK demodulator structure and its references recovery circuit were previously studied in Chapter 3. Their block diagrams are given in Figs 3.25 and 3.26 respectively. The following

practical realisation of the coherent MSK demodulator is based on the above study.

4.6.1 Refrences and Clock Recovery

At the MSK receiver front-end output (Fig 4.8), the signal is converted to TTL voltage levels before processing for reference recovery. The signal squaring, ie. frequency doubling, is performed in a 2-input EXOR gate, whose inputs are the signal and its delayed version. The time delay is accomplished by passing the received signal through six cascaded inverters as shown in Fig 4.15. The amount of time delay is not critical, as the phase detectors used in the reference recovery circuit base their decisions on the phase difference between the signal's negative edges irrespective of their waveforms. The signal frequency spectrum at the output of the digital frequency doubler is illustrated in Fig 4.16(a), where the modulating data is a pseudo random sequence (511 bits) and in Fig 4.16(b) where the modulating data is a sequence of alternate marks and spaces. In both spectrum traces the modulating data bit rate is 2.4kbit/sec. The MSK signal was produced using the quadrature modulator explained at the beginning of this chapter. The agreement between the practical spectrum of the squared MSK signal and the theoretical and practical frequency spectrums of Sunde's FSK signal (CPFSK-h=1) given in Fig 3.10(c) and Fig 3.11(c) respectively is evident.

The coherent demodulator reference frequencies, represented by spectrum line components at twice the mark and space MSK signal frequencies (911.2 and 908.8kHz respectively) in Fig 4.16(a) are recovered in two phase locked loops, each centred around one of the

frequencies. By investigating Fig 4.16(b), which represents a worst case operation condition from frequency selectivity point of view, it is possible to conclude that acquisition and tracking bandwidths of each loop should be smaller than $\pm f_b/2$. This requirement is essential to prevent either of the loops from falsely locking to the carrier frequency or other clock related harmonic components in the modulated MSK signal. Furthermore, to prevent the VCO frequency from drifting outside the pre-specified loop bandwidth, it should be a voltage controlled crystal oscillator, VCXO, which provides the best possible stability compared to LC or RC based oscillators.

The block diagram of a customary second order phase locked loop having an active low pass filter and which incorporates a divider of division ratio X at the output of the VCO is shown in Fig 4.17. The closed loop transfer function is well known[5,6] to be equal to:

$$G(s) = \frac{2\eta\omega_n s + \omega_n^2}{s^2 + 2\eta\omega_n s + \omega_n^2} \qquad \ldots (4.4)$$

where η is the loop damping factor and ω_n is its natural frequency and are given by:

$$\omega_n = \left[\frac{K_\phi K_o}{X} \quad \frac{1}{R_1 C} \right]^{1/2} \text{ rad/sec} \qquad \ldots (4.5)$$

$$\eta = \frac{R_2 C}{2} \left[\frac{K_\phi K_o}{X} \quad \frac{1}{R_1 C} \right]^{1/2} \qquad \ldots (4.6)$$

In equations (4.5) and (4.6), K_ϕ is the phase detector conversion gain in volts per radian, K_o is the VCO conversion gain in radians per second per volt, X is the divider division ratio and R_1, R_2 and C are

the active filter component values as indicated in Fig 4.17. Equations (4.5) and (4.6) represent the phase locked loop design equations. The loop characteristics, although will differ depending on the type of phase detector used, are completely described by ω_n, η, K_ϕ, K_o and X.

The division by X is usually accomplished using binary dividers and hence can only have an integer value. Therefore, when a VCXO is used its centre frequency (determined by the crystal resonance frequency) should be an integer multiple of the reference frequency. In MSK reference recovery, although for some values of bit rates it is possible to find standard commercial crystals that satisfy the above condition for $2f_m$ or $2f_s$, it is difficult to find one which satisfies it for both or two crystals each for one of them. Thus, in most cases at least one will have to be especially ordered, if not two. Furthermore, once the VCXO's crystals are chosen, the bit rates the demodulator can accept cannot be easily changed except within the very restricted limits which changing X may offer.

To overcome these limitations, an uncommon phase locked loop structure was used for MSK reference recovery. The complete PLL circuit function diagram is illustrated in Fig 4.18. The only difference between this loop structure and that of the common PLL shown in Fig 4.17 is the use of a frequency synthesiser as a divider in place of a simple binary divider. The use of a frequency synthesiser allows the division by a fractional number instead of only integers in case of a simple binary divider. The synthesiser output frequency f_V is given by:

$$f_V = \frac{J}{H} f_O \qquad \ldots (4.7)$$

where f_O is the VCXO frequency and J and H are the division ratios of the programmable binary dividers as indicated in Fig 4.17. The VCXO, whose circuit is given in Appendix 4.5, uses a standard commercial 10.7MHz crystal. The dividers used can be programmed to have a division ratio varying between 1 to 256 in the case of the J divider and 1 to 4096 in the case of the H divider. Thus, by properly choosing the values of J and H, it is possible for the loop to lock to a wide range of reference frequencies.

The frequency synthesiser PLL is a HEF4046 single chip PLL[7]. Its VCO is of an RC type whose gain factor is very much higher than that of the main loop. The loop filter component values were adjusted so that the synthesizer loop natural frequency is very much greater than that of the main loop and at the same time having a damping factor which causes neither oscillatory nor slow transient performance. Consequently, the synthesiser loop acquisition and tracking bandwidth are much larger than that of the main loop.

The two MSK references ($2f_m$ and $2f_s$) recovery loops are exactly equivalent except for the divider's settings J and H. For a modulating data rate of 2.4kbit/sec, $2f_m$ and $2f_s$ at the input of the recovery PLL's are equal to 911.2 and 908.8 respectively. The division ratios, J and H, were set to 58 and 681 in the case of $2f_m$ and 49 and 577 in the case of $2f_s$ respectively. The measured VCXO-synthesiser combination frquency versus voltage characteristics in both loops are given in Fig 4.19. The vertical axis represents the difference between the loop's centre frequencies, $2f_m$ (911.2kHz) and

$2f_s$ (908.8kHz), and the frequency corresponding to the control voltage value given in the horizontal axis. From Fig 4.19 an approximate value for the gain factor K_o/X is 314 radians/second/volt for both loops. Furthermore, it is possible to conclude that the maximum tracking and acqusition loops bandwidths, governed by the loop dynamic range, is equal to 700Hz.

The phase detector (PD) used in the main loop is a Motorola MC4044 IC[8]. This is a tristate sequential phase-frequency detector which provides the PLL with a frequency acquisition aid[4] and thus improves the overall demodulator performance in fading conditions. The detector gain factor K_ϕ as given in [8] is equal to 0.12 volts per radian.

Given the above values of K_o/X and K_ϕ (315, 0.12), equations (4.5) and (4.6) were used to calculate the loop filter component values (R_1, R_2 and C) for prespecified values of ω_n and η. The loop damping factor was fixed at 0.7 which represents a compromise between fast transient response and oscillatory transient response. To evaluate the effect of references recovery PLL characteristics (described by ω_n after fixing η, K_o, K_ϕ and X in equations (4.5) and (4.6)) on MSK demodulator performance under different transmission conditions, the filter components were calculated for four values of ω_n, 100, 50, 20 and 10 rad/second. For ω_n > 100 the loop characteristics were limited by its dynamic range, while for ω_n < 10 by the DC offsets instabilities in the operational amplifiers used.

The phase locked loop's outputs, $2f_m$ and $2f_s$, are then processed to produce the reference signals for coherent MSK demodulation, as

shown in Fig 4.15. The two outputs are first divided by 2 using D-type flip/flops whose outputs are summed in two wide band operational amplifiers (op-amp). The two inputs of one of the summers are the non-inverted outputs from the two dividers. The other summer inputs are the non-inverted output of one of the dividers and the inverted output of the other divider, as can be seen in Fig 4.15. Thus, one of the summers is performing the summation while the other is performing the addition to produce I and Q channel reference signals.

The I&D, S&H and bit interleaver timing signal is recovered by applying the non-inverted divider's outputs to a 2-input EXOR gate which performs the multiplication operation. The EXOR gate output is then passed through an RC low pass filter to remove high frequency components and the low frequency signal ($f_b/2$) is applied to TTL voltage levels converter before using it to control the timing of data recovery operations illustrated in Fig 4.20.

The data receiver clock (f_b) which samples the bit interleaver output and controls the differential decoding process and any subsequent digital processing can be recovered by multiplying the two PLLs' output as shown in Fig 3.26. However, in the fading environment as the received signal disappears during deep fades the recovered clock signal will skip several cycles before the reference recovery phase locked loops re-establish locking. Consequently, receiver bit integrity will be lost during deep fades. To overcome this problem without the need to periodically transmit synchronisation words, the data receiver clock is recovered using the clock recovery circuit used in case of the non-coherent receiver. The reference signal

supplied to the clock recovery circuit is the low pass filtered EXOR gate output $f_b/2$ used for the data recovery operation timing. This signal is equivalent to a sequence of alternate marks and spaces and produces f_b transitions per second when passed through the clock recovery circuit data transition detector. Hence, the recovery circuit maximum locking bandwidth will be given by equation (4.2) and is equal to ±0.062Hz for a 2.4kbit/second data signal and the recovery circuit parameters given previously, irrespective of the random modulating data.

4.6.2 Coherent Data Recovery

The data recovery circuit function diagram is illustrated in Fig 4.20. The recovered I and Q channel reference signals are multiplied with the 455kHz MSK signal using analogue multipliers. The multipliers' circuit is given in Appendix 4.6. The multipliers inverted and non-inverted outputs are then passed through passive RC filters to remove high frequency components and then applied to difference operational amplifiers. The coherently demodulated MSK I and Q channels baseband eye patterns appearing at the output of the difference amplifiers are shown in the photograph in Fig 4.21 for a 511 pseudo random modulating data having a 2.4kbit/second bit rate. The 455kHz ceramic IF filter 3dB bandwidth is equal to approximately twice the bit rate.

The baseband I-Q signals are then processed in two identical I&D and S&H circuits whose operation is similar to those used in the non-coherent demodulator. Following the S&H circuits the signal is applied to a threshold detector (zero level detector) whose output voltage levels are those of a TTL signal. The recovered I-Q data

outputs are then interleaved in the bit interleaver, whose output is sampled by the recovered data clock. Finally, the recovered data is differentially decoded to reproduce the original transmitted data as can be seen in Fig 4.20. The I-Q channels operation and their relative timing are given in Fig 4.22, together with the bit interleaver operation.

APPENDIX 4.1

PHASE SHIFT CIRCUIT

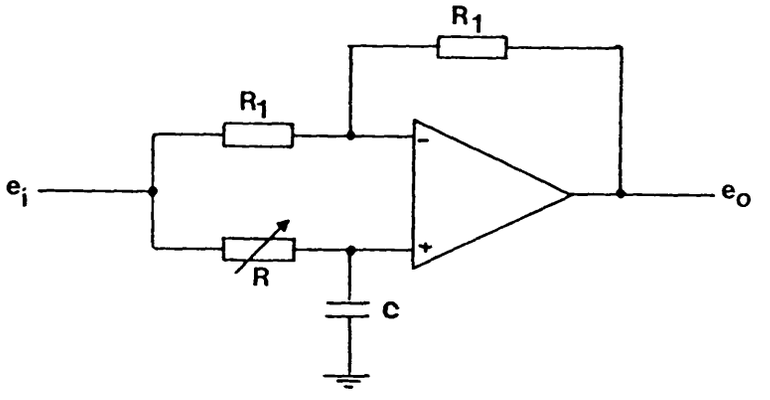

The voltage transfer function of the phase shift circuit is given by:

$$G(j\omega) = \frac{1 - jRC\omega}{1 + jRC\omega}$$

which represents that of a first order all pass network. The phase angle of the output voltage is given by:

$$\phi = \tan^{-1} \frac{-2RC\omega}{1 - R^2C^2\omega^2}$$

Thus, by changing the resistance R the output signal phase delay can be adjusted so as to bring the two signals in phase coincidence and hence compensating for the low pass filter (Fig 4.2) phase delay. Two cascaded stages were used for this purpose. In the second stage the resistance R is a multiturn variable resistance to accommodate for a range (1kHz-2.8kHz) of modulating data clock frequency.

The same circuit is also used to provide a 90° phase shift in the

Q-sinusoidal reference weighting signal with respect to the I-channel. A single stage is used with a multiturn variable resistor R to accommodate for a range (1kHz-2.8kHz) of modulating data clock frequency.

APPENDIX 4.2

INVERTER/NON-INVERTER CIRCUIT

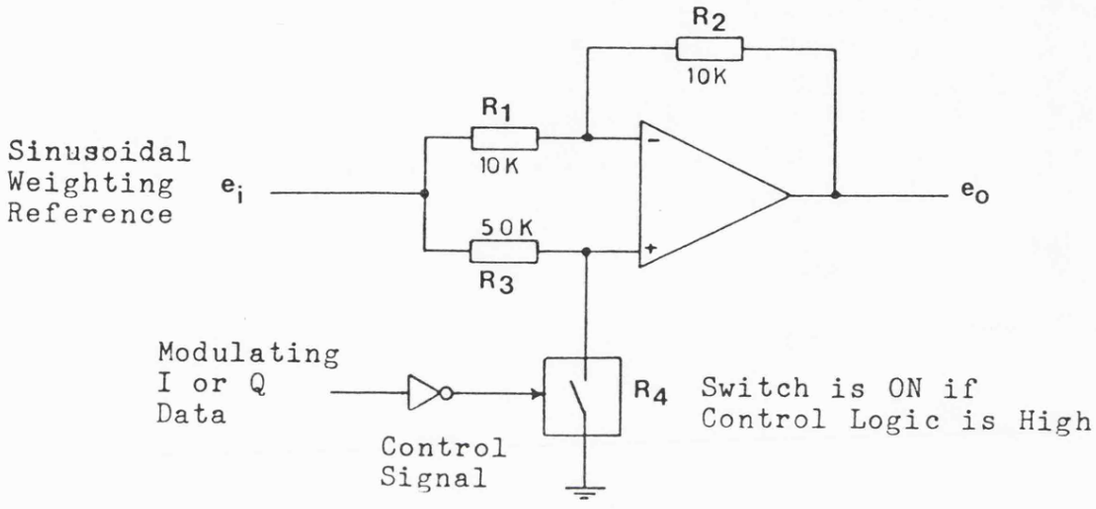

The relation between the output and input voltages of the inverter/non-inverter circuit is given by:

$$e_o = \frac{1 - \dfrac{R_1 + R_2}{R_2} \quad \dfrac{R_4}{R_3 + R_4}}{1 - \dfrac{R_1 + R_2}{R_2}} \; e_i$$

where R_4 represents the on or off resistance of the analogue switch. By choosing $R_1 = R_2$ the above equation becomes:

$$e_o = - \left[1 - 2 \frac{R_4}{R_3 + R_4} \right] e_i \qquad \ldots \text{(A4.2.1)}$$

When the analogue switch is in the ON position, $R_4 << R_3$ and equation A4.2.1 can be reduced to:

$$e_o = - e_i$$

ie. the input signal is multiplied by -1. When the analogue switch is in the OFF position, $R_4 >> R_3$ and equation A4.2.1 can be reduced to:

$$e_o = e_i$$

ie. the input signal is multiplied by +1.

Thus, by allowing the inverted binary I/Q data to control the switch action, the sinusoidal reference multiplication by the data is accomplished.

APPENDIX 4.3

MSK MODULATOR CARRIER MULTIPLIER

The sinusoidally weighted data multiplication by the carrier signal in the I and Q channels is accomplished by using a high frequency balanced modulator IC. This IC is an MC1496[2] and the multiplier circuit diagram is given in the following figure.

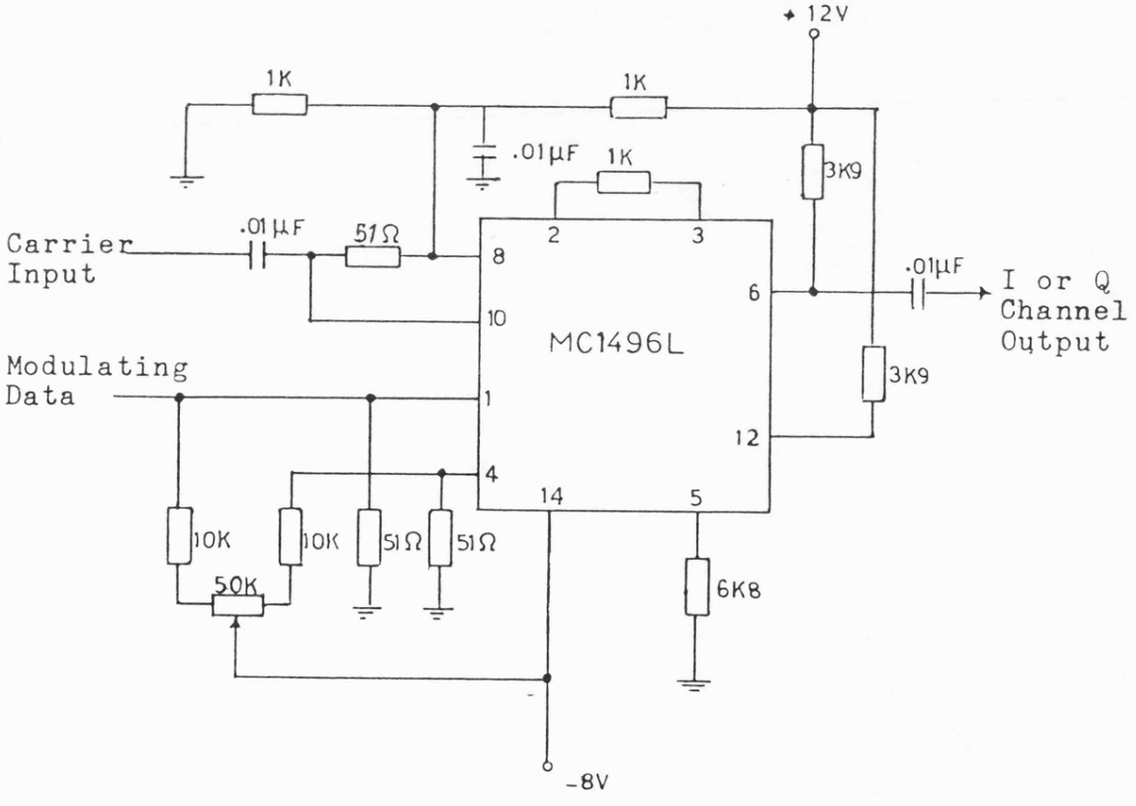

APPENDIX 4.4

PROGRAMMABLE TIMERS AND PULSE GENERATOR CIRCUIT

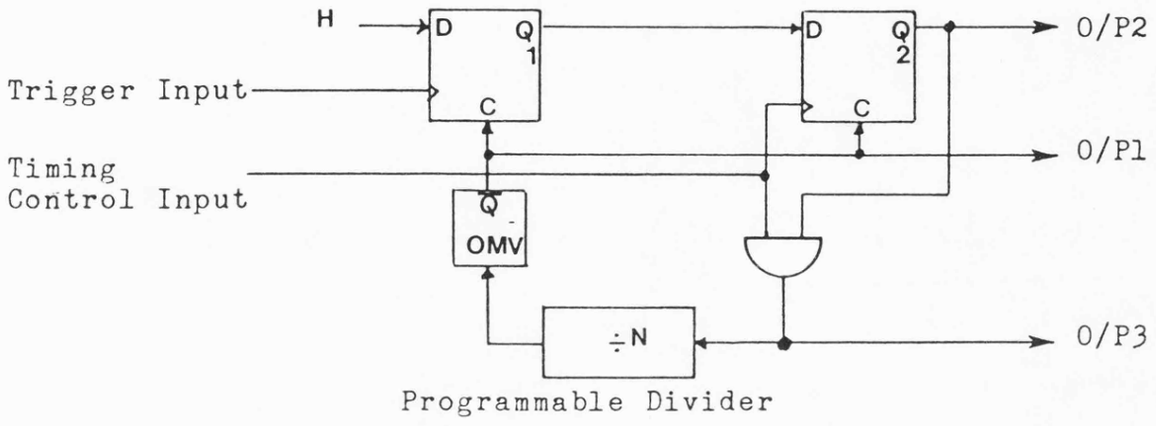

Programmable Divider

N.B. All Sequential Circuits are +ve Edge Triggered.

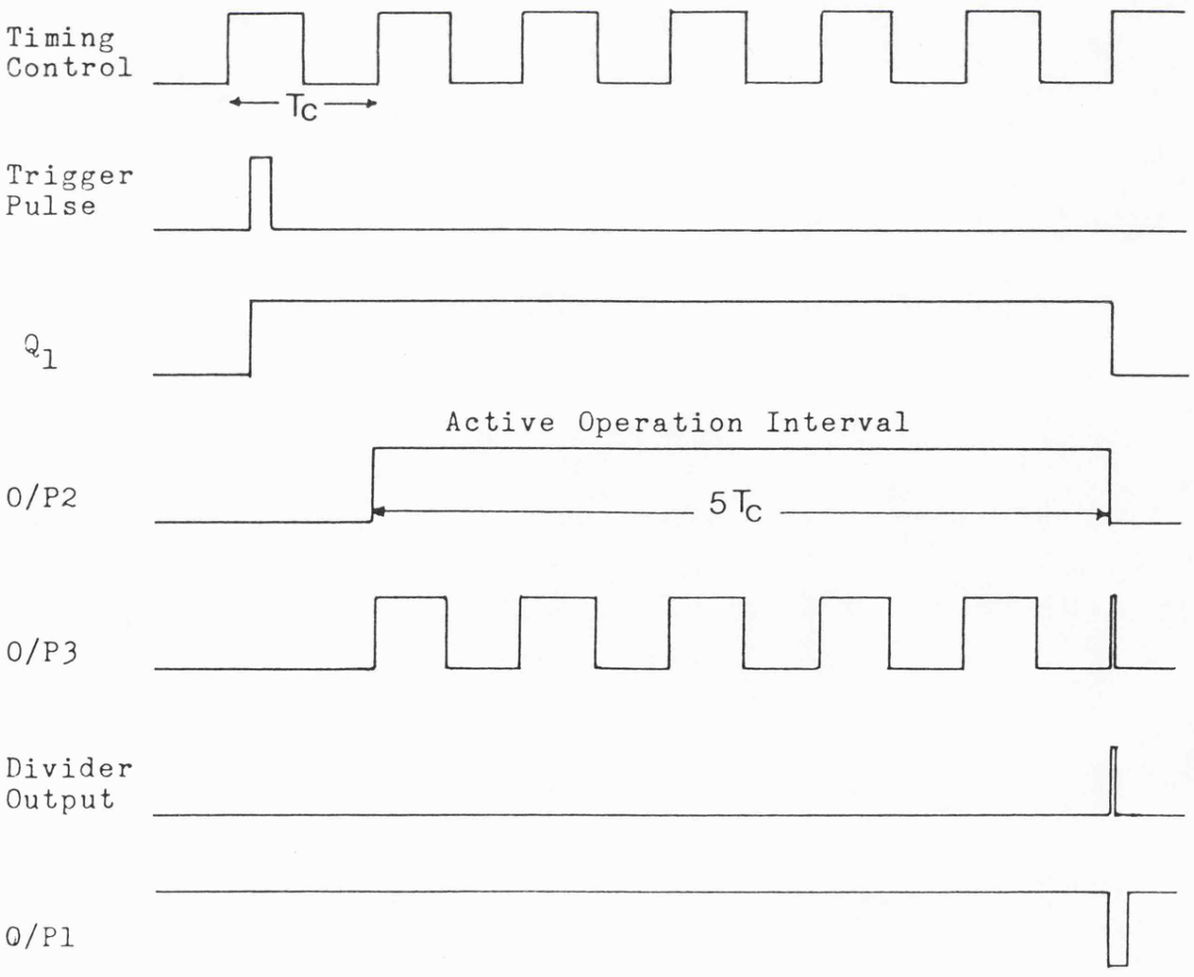

The programmable timers (1) and (2) and the programmable pulse generator in Fig 4.11 circuits are similar. The only difference between them lies in the output point used.

The above figures show the circuit function and timing diagrams. The circuit active operation period is controlled by the value of the programmable divider division ratio N. The timing diagram is shown for N=5. The control clock is the 2.4kHz local clock signal in the case of timers (1) and (2) and the 12MHz local oscillator output in the case of the programmable pulse generator as can be seen in Fig 4.12. The programmable timer (1) uses O/P1 while (2) uses O/P2. The programmable pulse generator uses O/P3.

APPENDIX 4.5

VOLTAGE CONTROLLED CRYSTAL OSCILLATOR

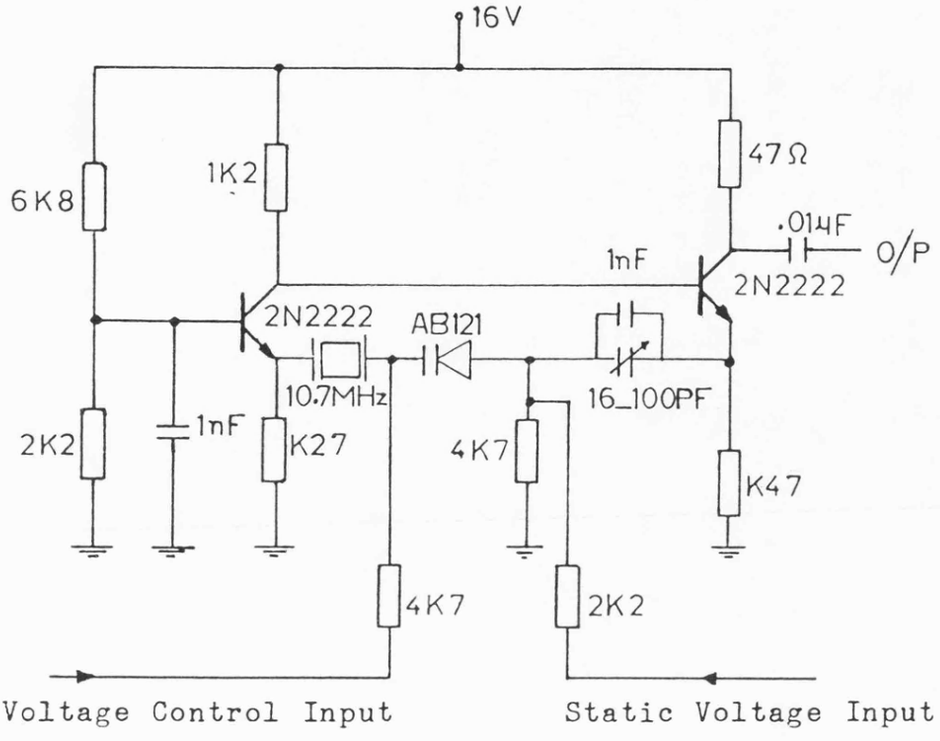

The static voltage is adjusted to make the VCXO centre frequency equivalent to the mid-control voltage value. The circuit was also used to produce the CPFSK signal shown in Fig 3.11 by applying the modulating data signal to the circuit control voltage. The deviation ratio is adjusted by changing the amplitude of the modulating data and the static voltage value.

APPENDIX 4.6

COHERENT DEMODULATOR-SIGNAL/REFERENCE MULTIPLIER

The circuit used to multiply the recovered I/Q references by the received MSK signal in the coherent demodulator (Fig 4.20) is based on an MC1495 IC which is a wideband monolithic four-quadrant analogue multiplier[2]. The following figure gives the multiplier circuit diagram.

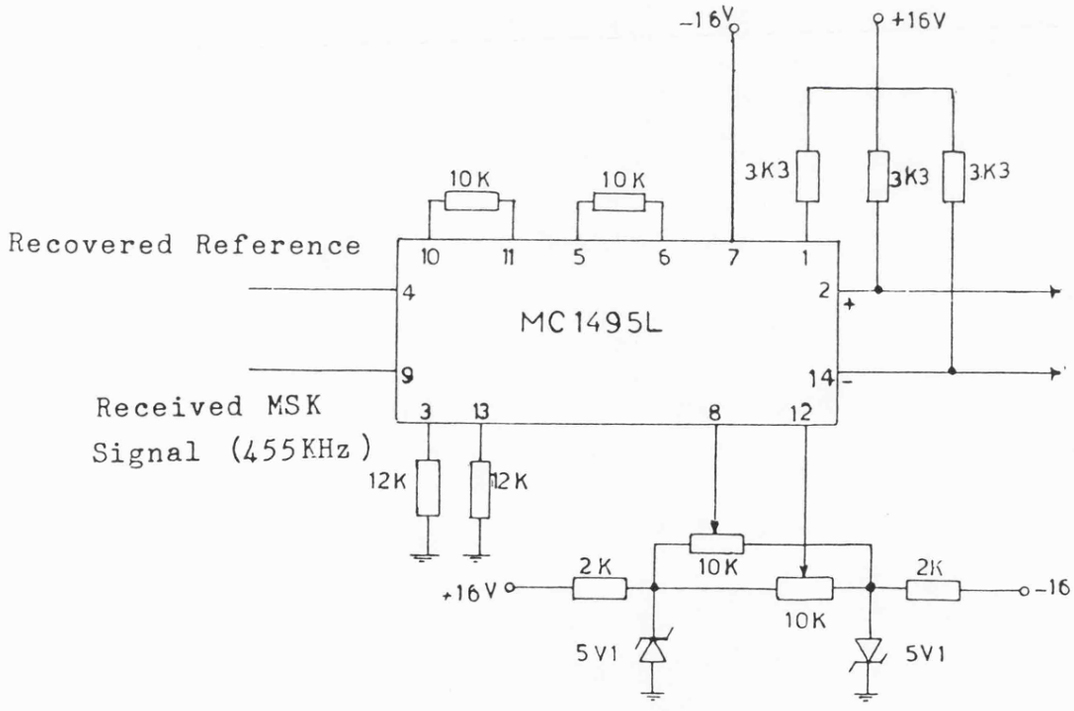

CHAPTER 4: REFERENCES

1. Frerking, M E: "Crystal oscillator design and temperature compensation", Van Nostrand Reinhold Company, 1978.
2. Motorola Linear Integrated Circuit, Data Book, 1981-82 edition.
3. The TTL Data Book for Design Engineers, Texas Instruments, 1980 edition.
4. Characteristics of Distortion and Error-rate Measuring Apparatus for Data Transmission, CCITT Recommendation, V.52, Vol.VIII.
5. Gardner, F M: "Phaselock techniques", John Wiley & Sons Inc., USA, 1979.
6. Rohde, V L: "Digital PLL Frequency Synthesizers - Theory and Design", Prentice-Hall Inc., 1983.
7. Mullard Technical Handbook, Book Four, Part Four, LOCMOS HE4000B Family Digital Integrated Circuits.
8. Phase-locked Loop Data Book, Motorola Inc., Second Edition, 1973.

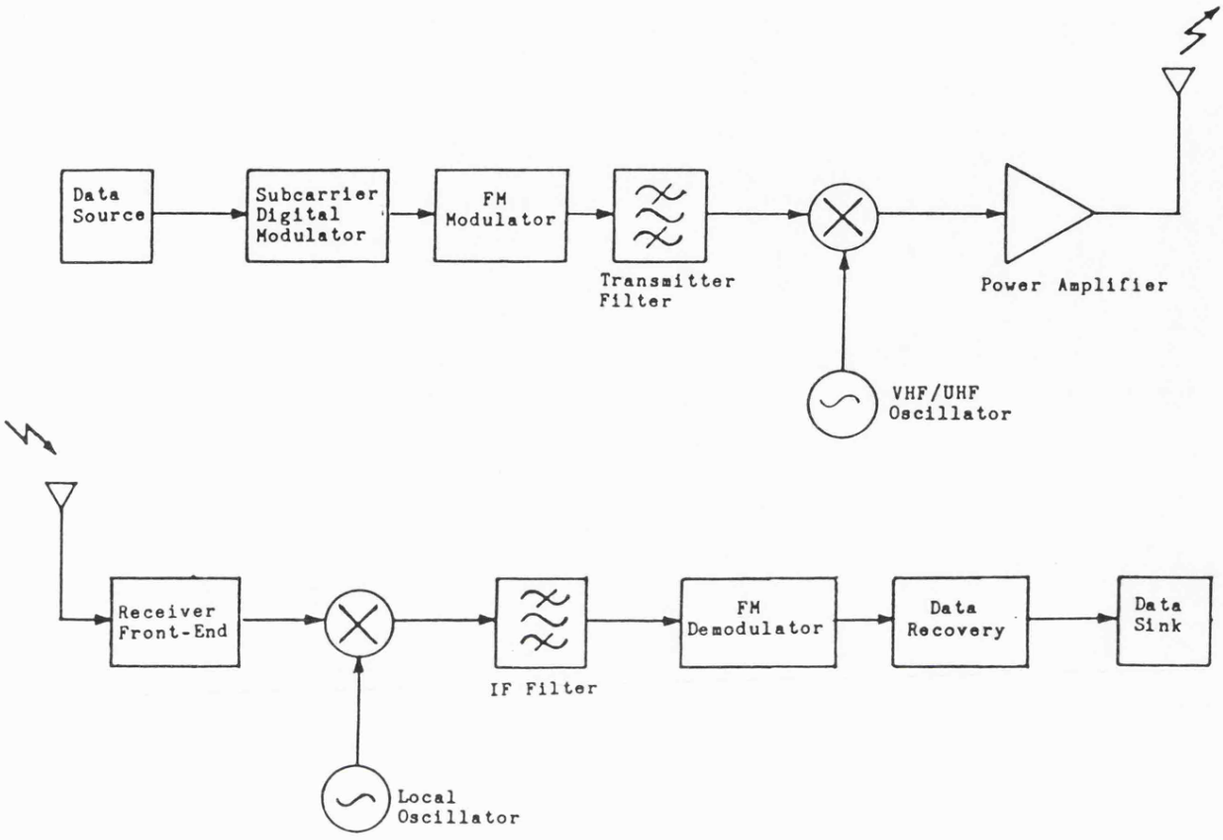

Figure 4.1(a) Indirect Modulation.

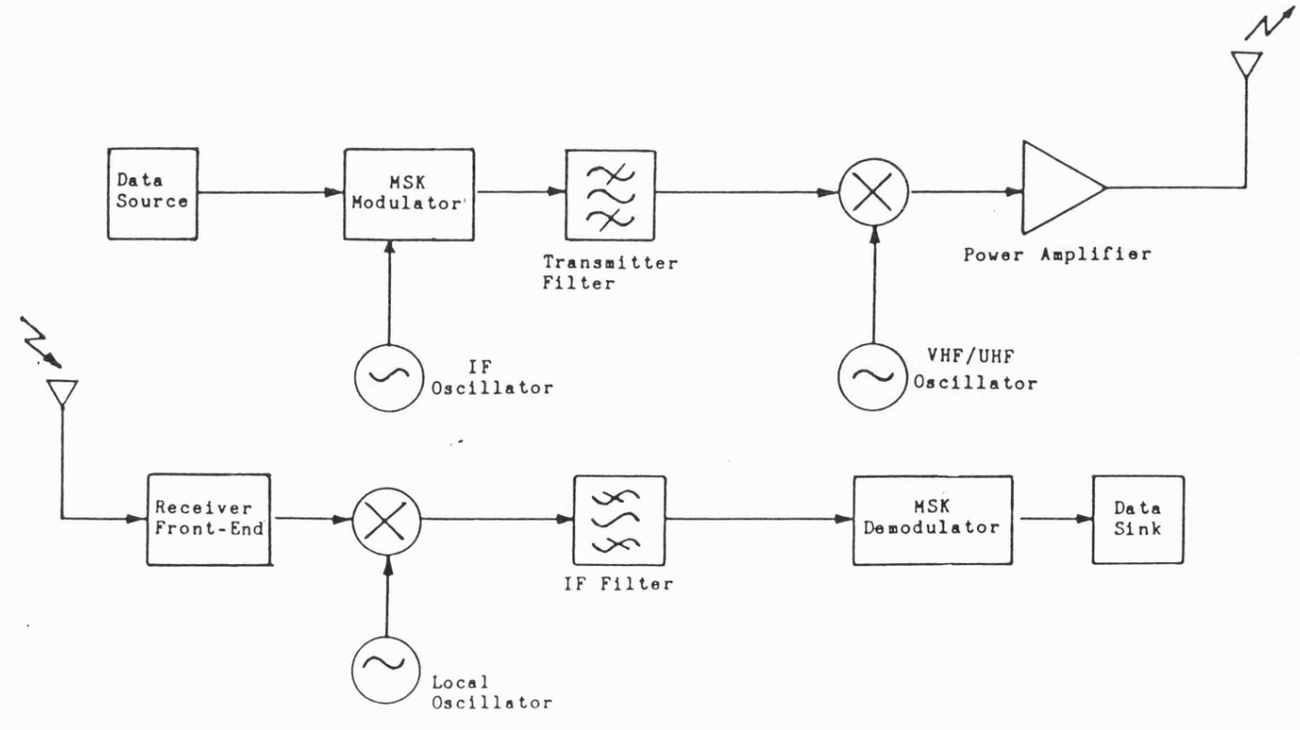

Figure 4.1(b) Direct Modulation.

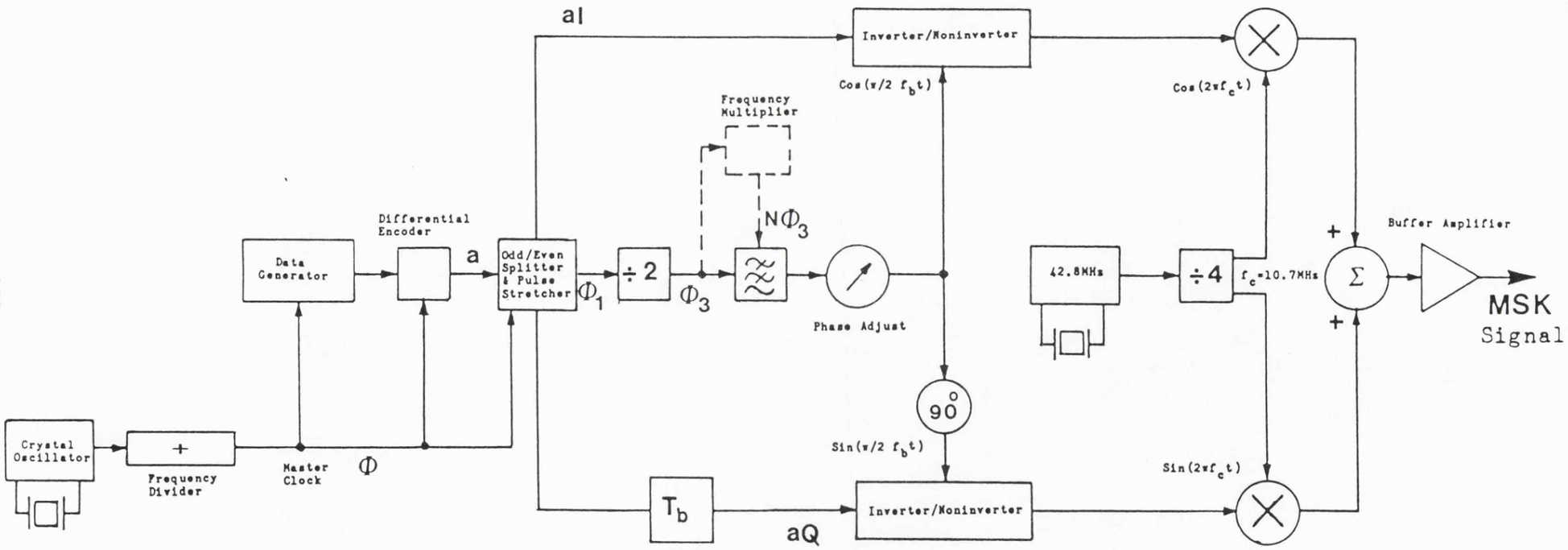

Figure 4.2 MSK Modulator Block Diagram.

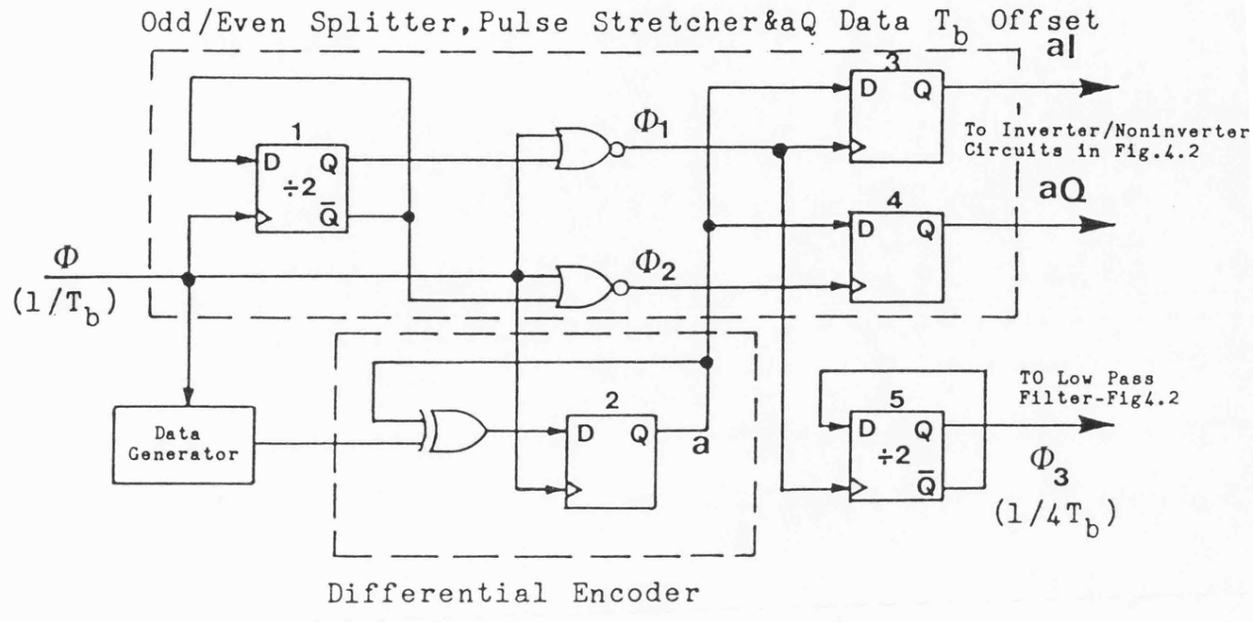

(a) Function Diagram.

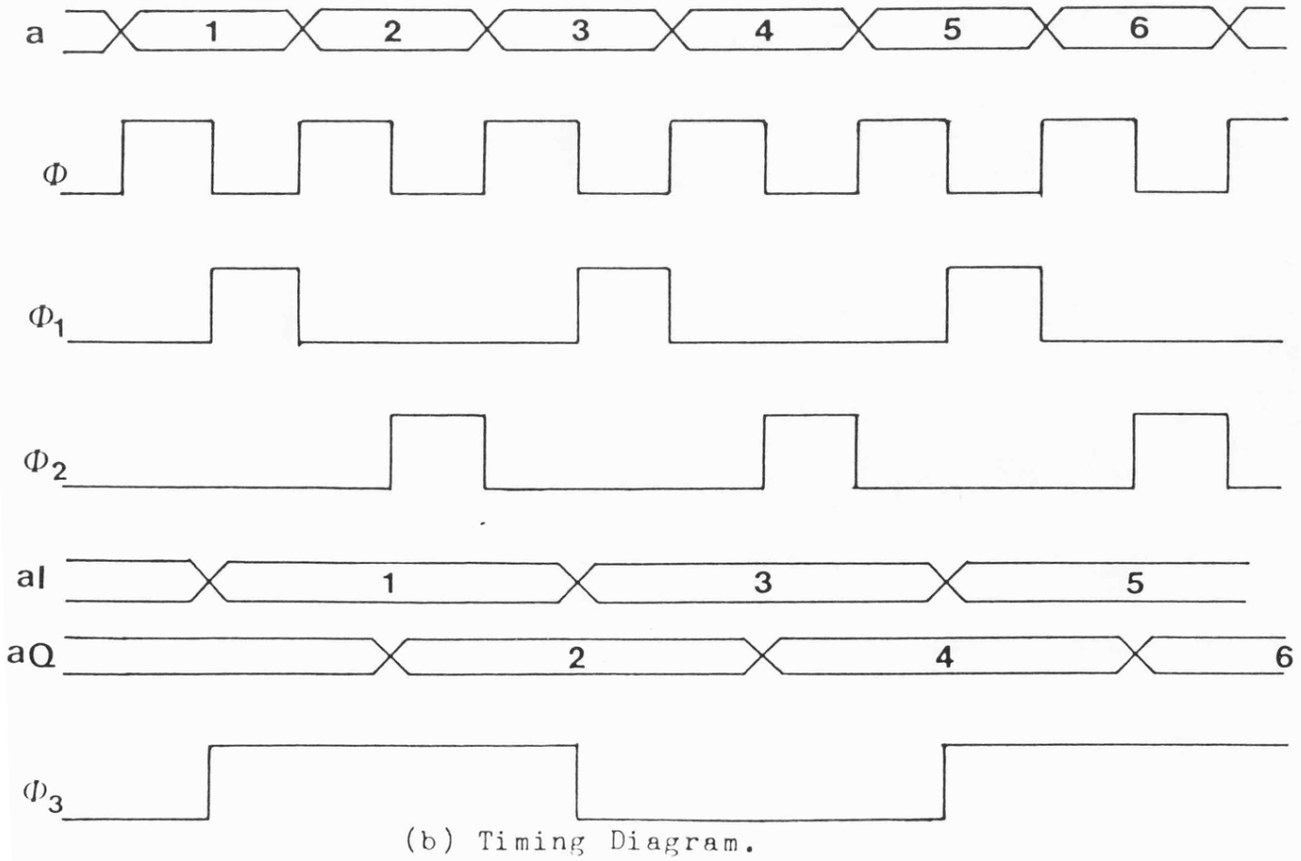

(b) Timing Diagram.

Figure 4.3 Modulator Data Splitter.

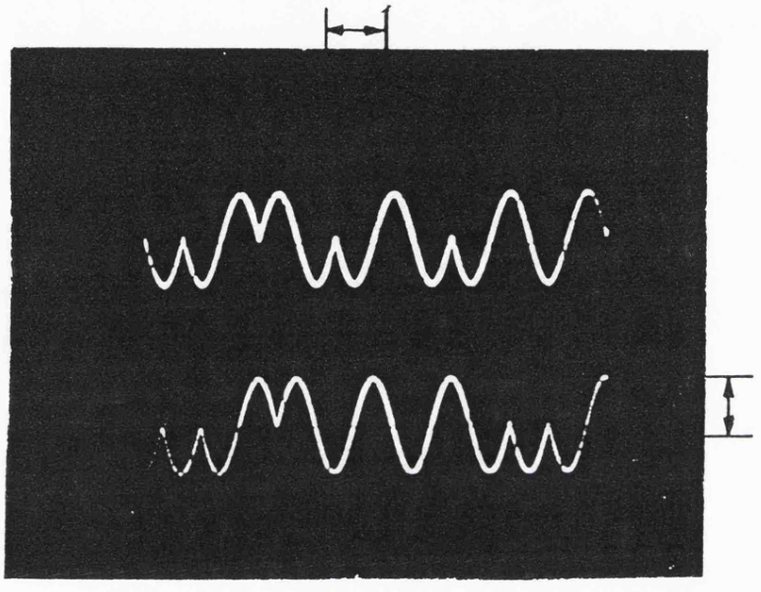

Horizontal: 1mSec/Div. - Vertical: 0.5V/Div.

Figure 4.4 I and Q Channels Sinusoidally Weighted Data.

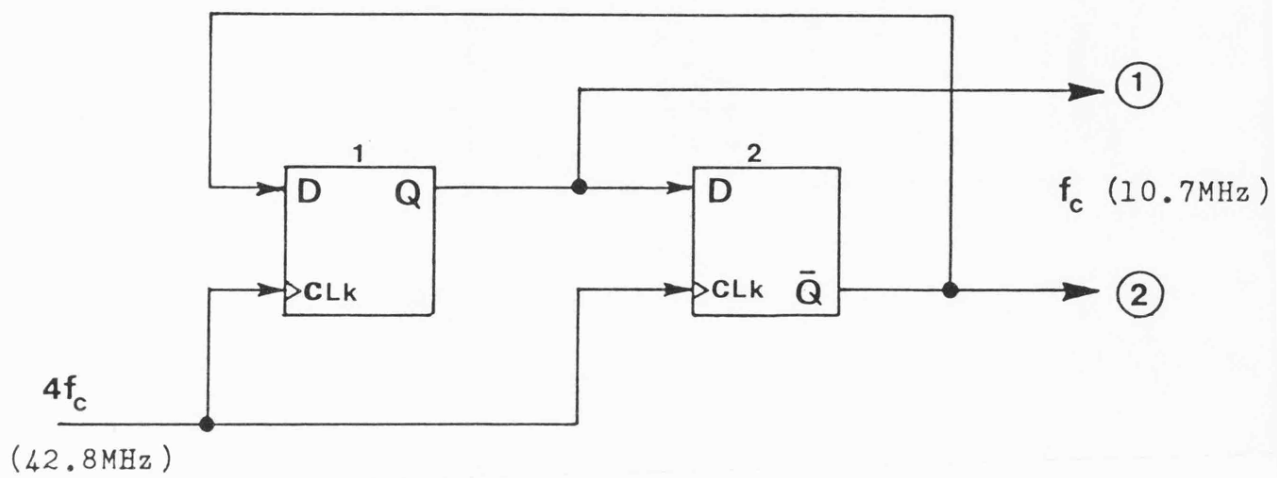

N.B. 1&2 are D Type Flip/Flops.

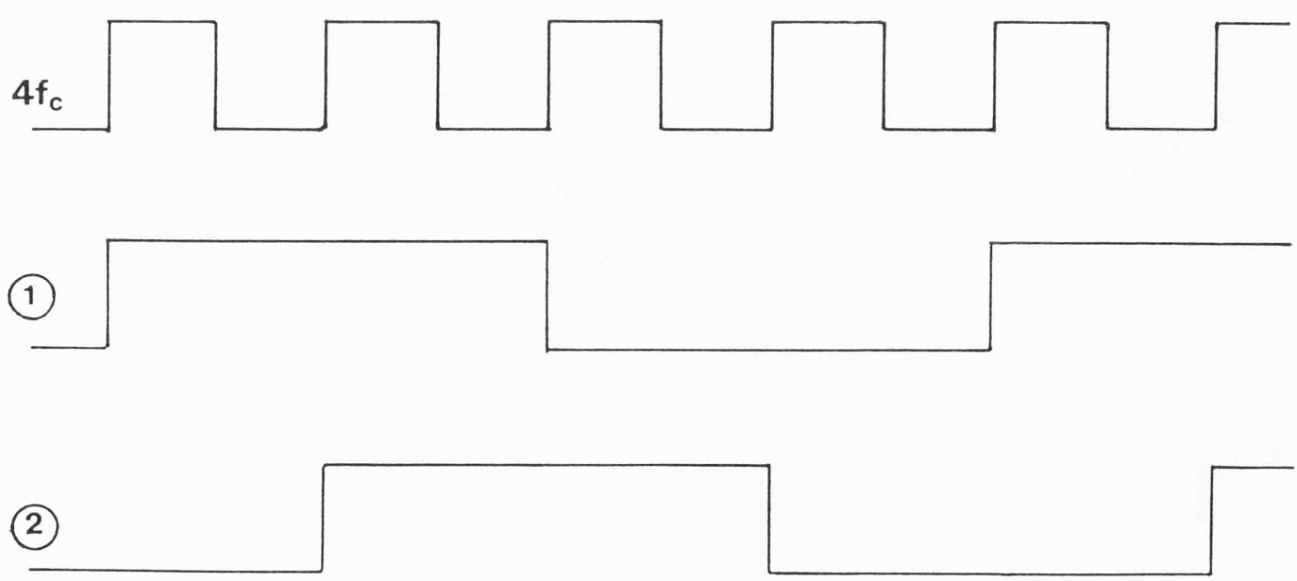

Figure 4.5 Inphase and Quadrature Carrier Generation.

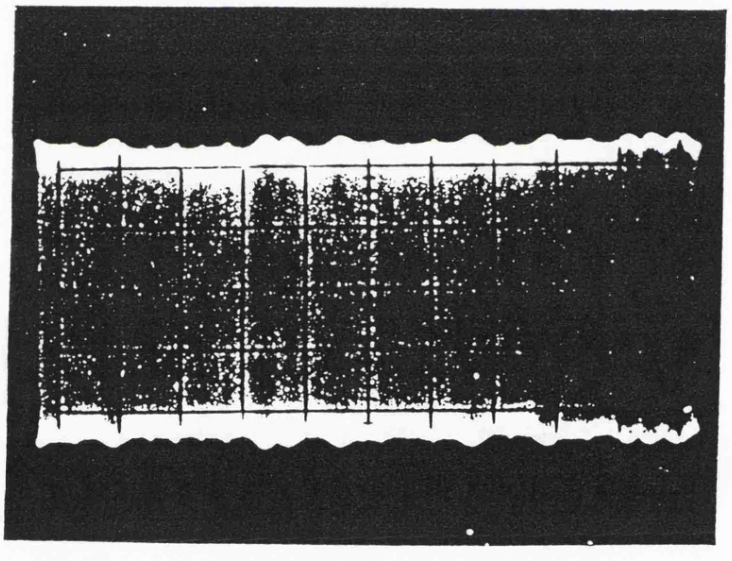

Figure 4.6 MSK Modulator Output Waveform.

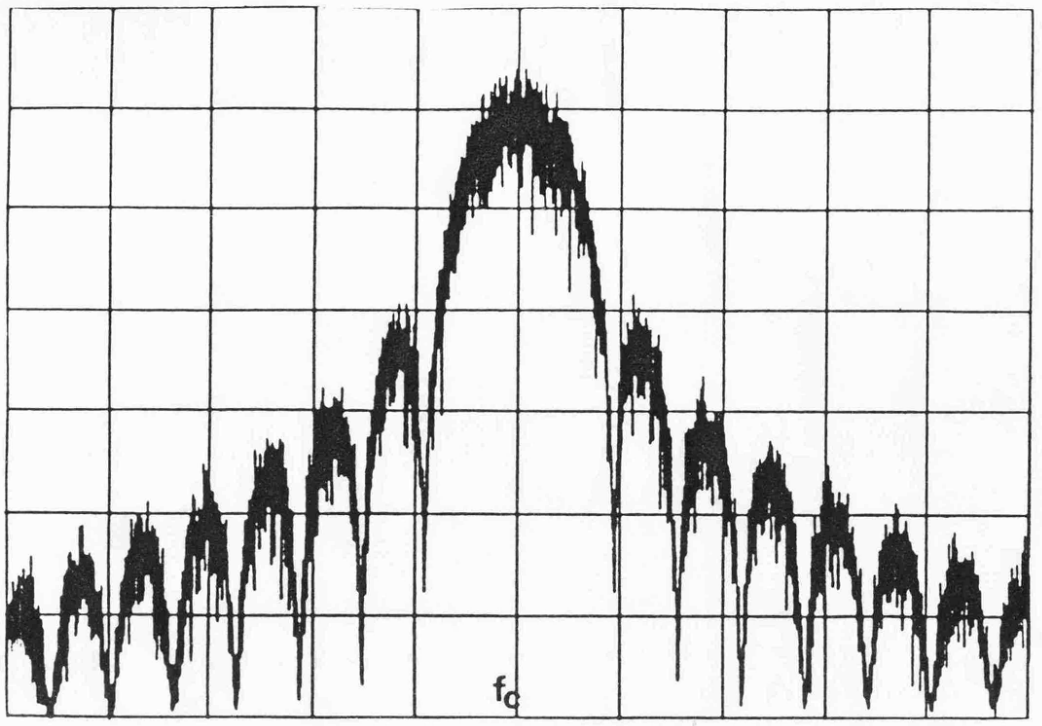

Horizontal: 1KHz/Div. , Centre Frequency: 10.7MHz ,
Vertical: 10dB/Div.

(a) Bit Rate (f_b)= 1.2KHz.

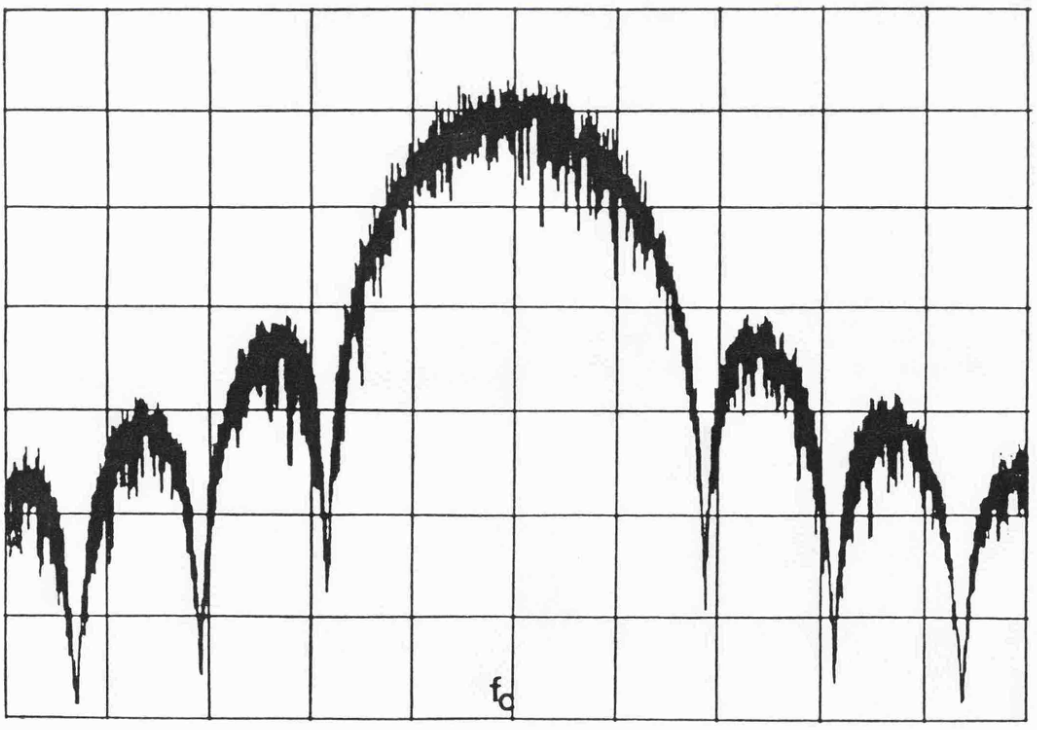

Horizontal , Centre Frequency & Vertical as in (a).

(b) Bit Rate (f_b)= 2.4KHz.

Figure 4.7 MSK Modulator Measured Output Frequency Spectrum.

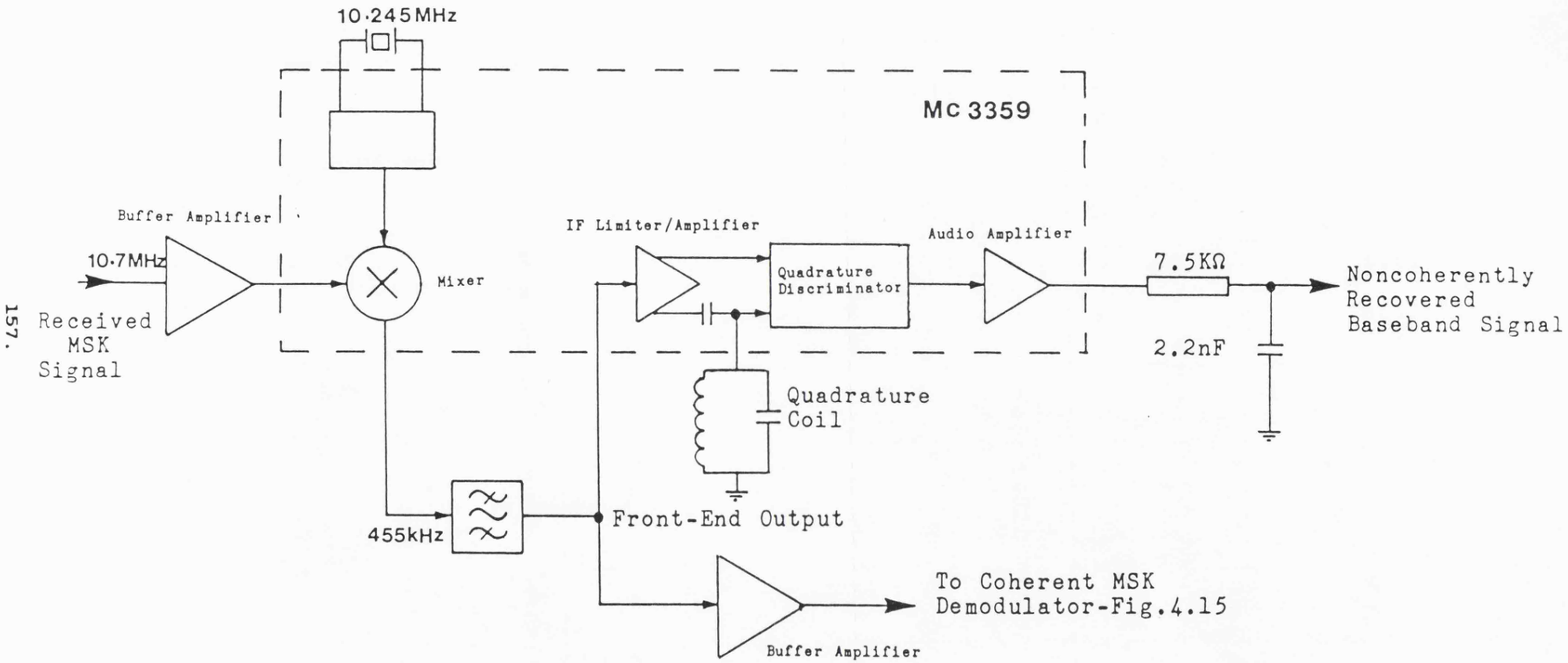

Figure 4.8 Demodulators Front-End & Noncoherent Detector.

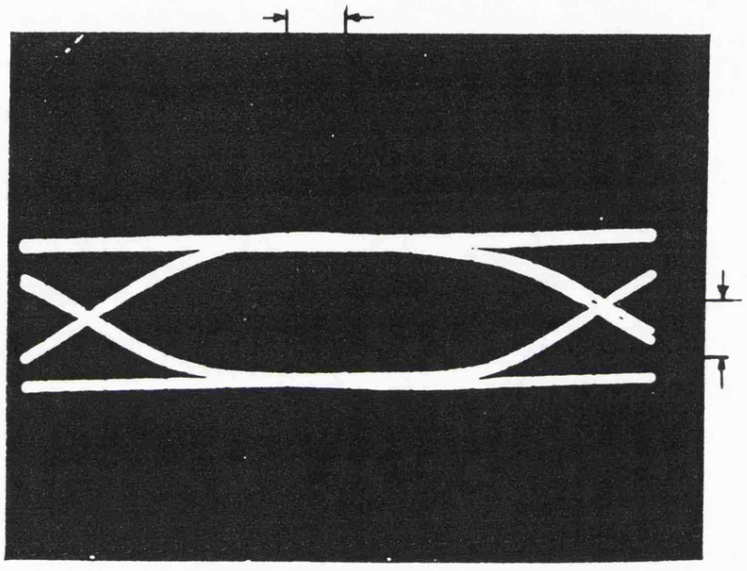

Horizontal : 0.05 mSec/Div.

Vertical : 0.5 V/Div.

Figure 4.9 Noncoherent MSK Demodulator Eye Pattern.

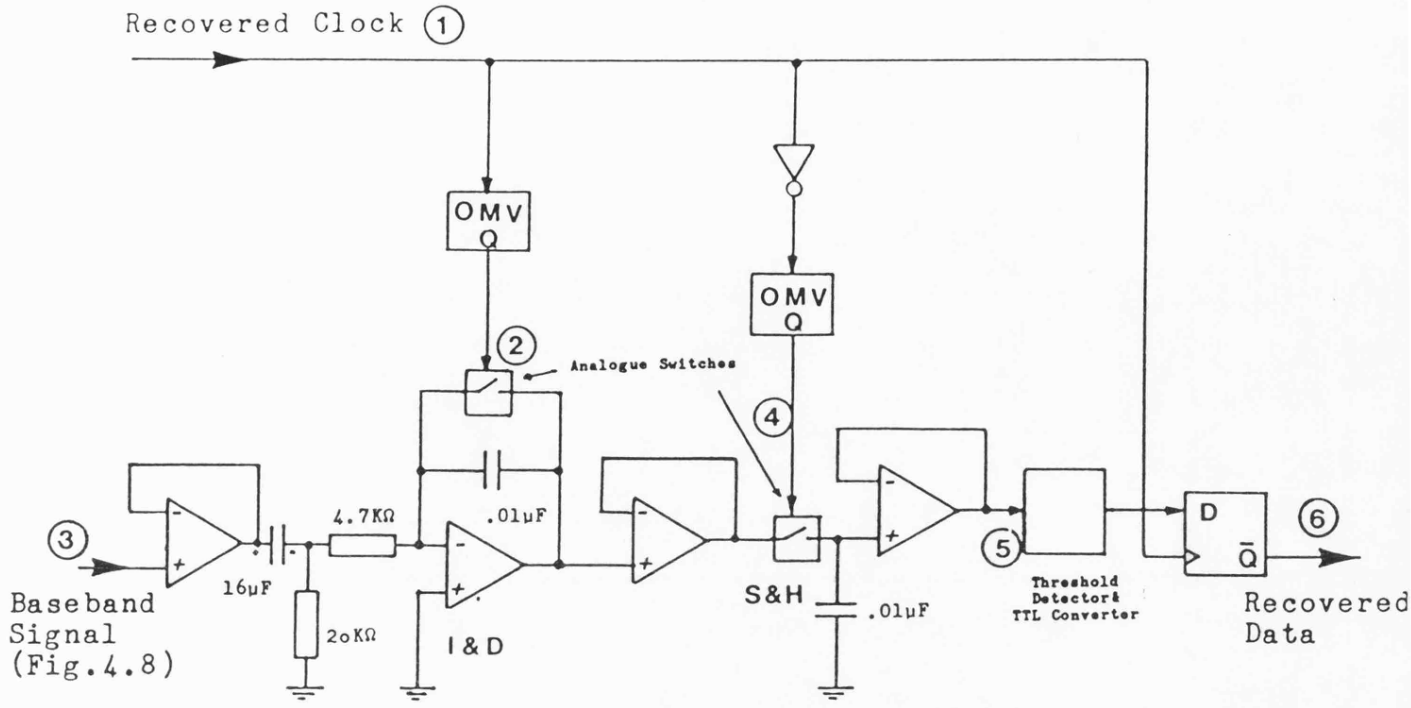

N.B. OMV is +ve Edge Triggered One Shot Multivibrator.

(a) Circuit Diagram.

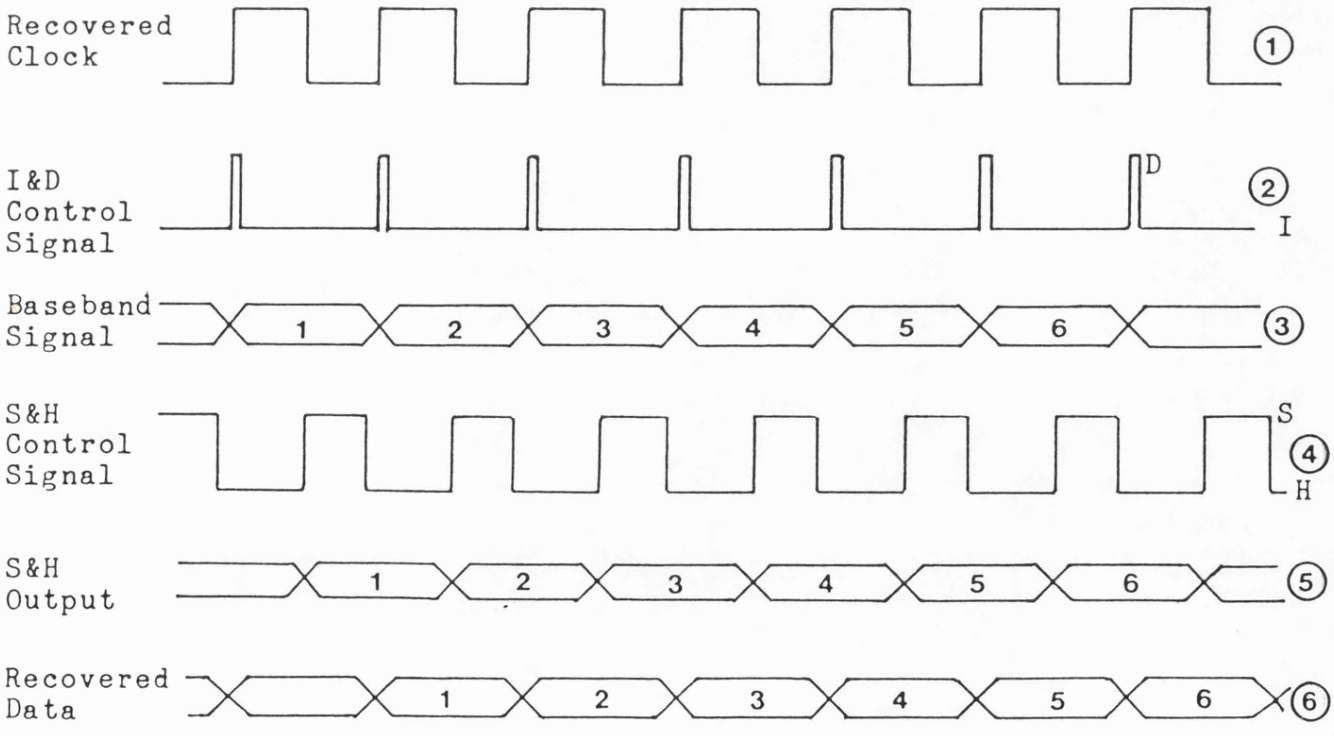

(b) Timing Diagram.

Figure 4.10 Data Recovery Circuit-Noncoherent Demodulator.

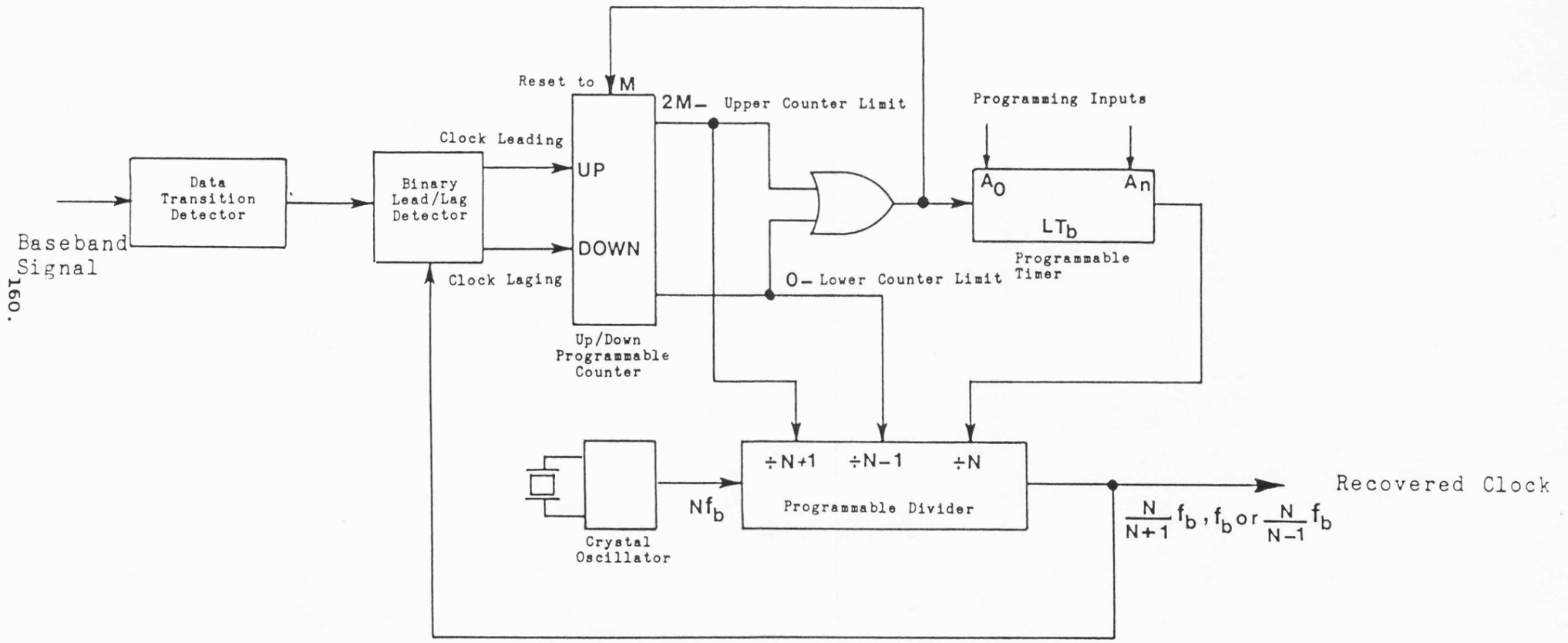

Figure 4.11 Clock Recovery Circuit Schematic Diagram.

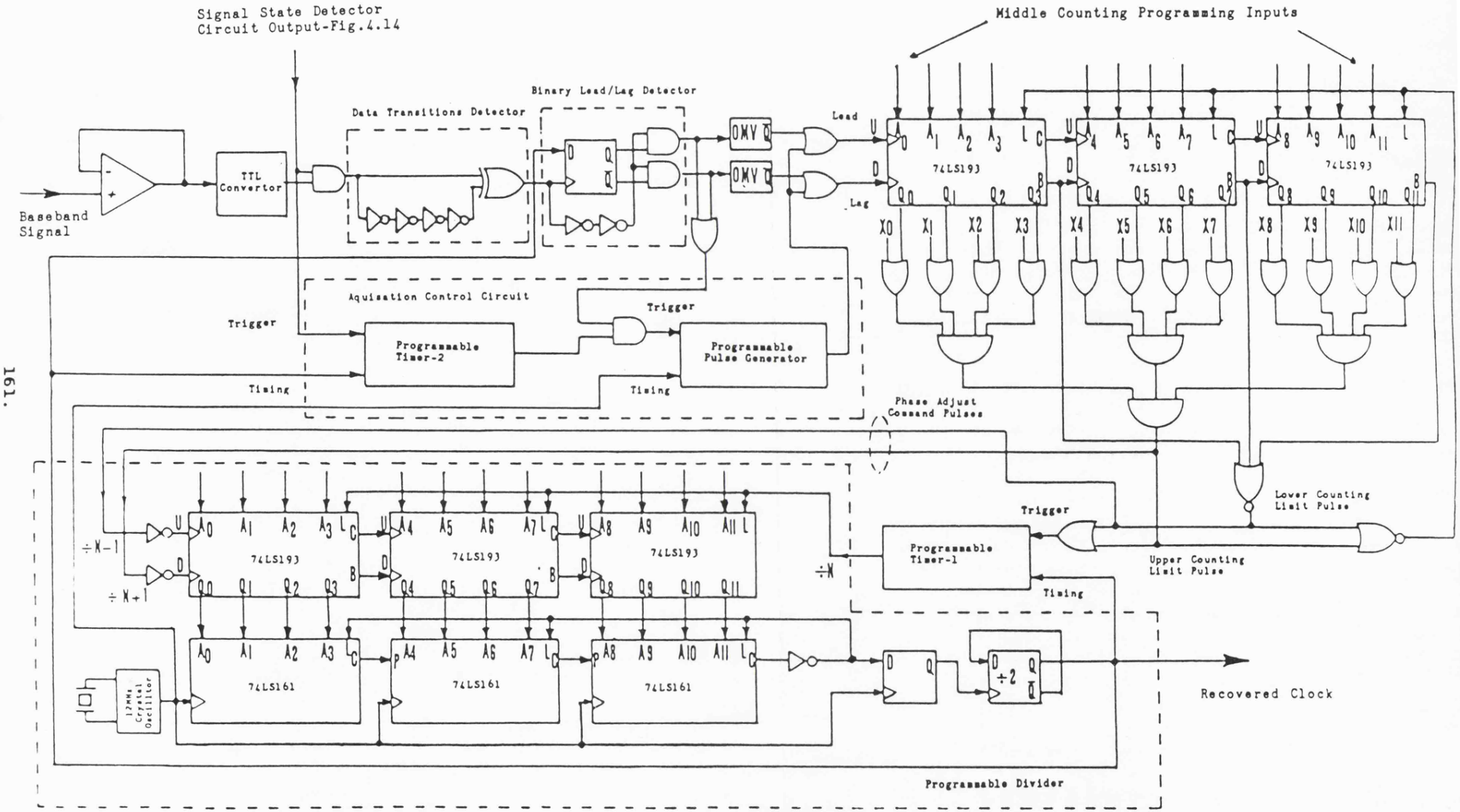

N.B. ALL Sequential Devices are +ve Edge Triggered

Figure 4.12 Clock Recovery Circuit Function Diagram.

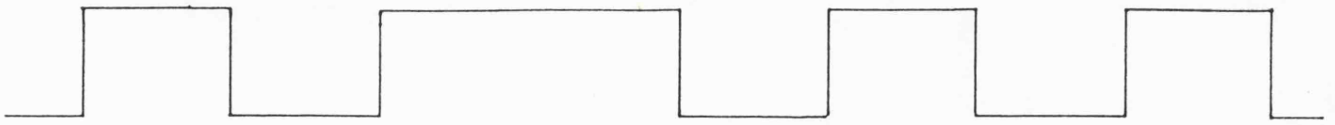

Baseband Signal-TTL Levels.

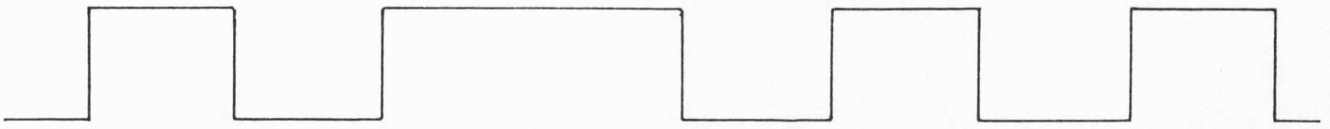

Delayed Baseband Signal.

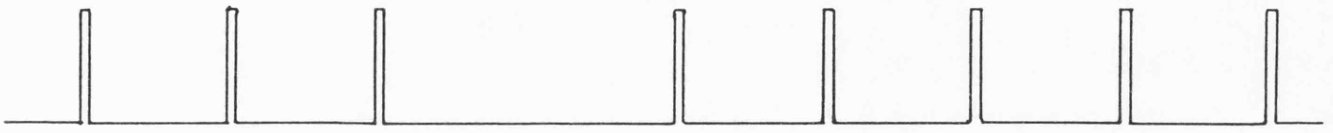

Transitions Detector Output.

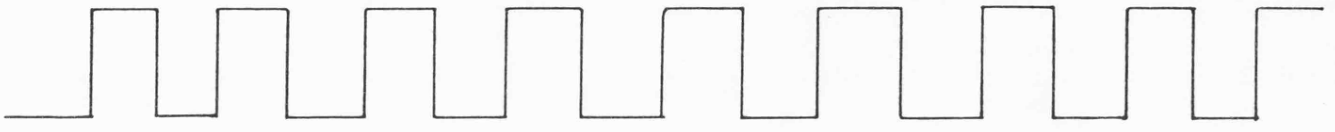

Recovered Clock Signal.

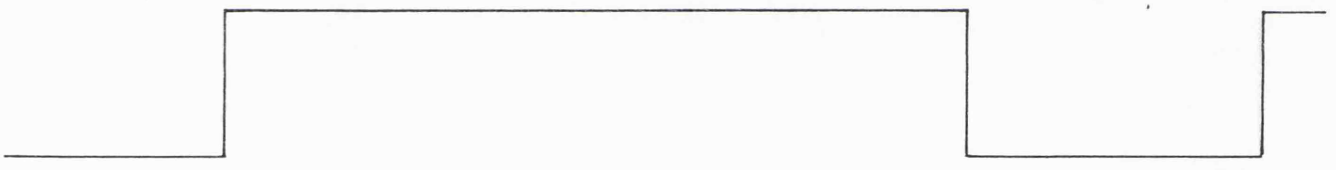

Detector Q Output.

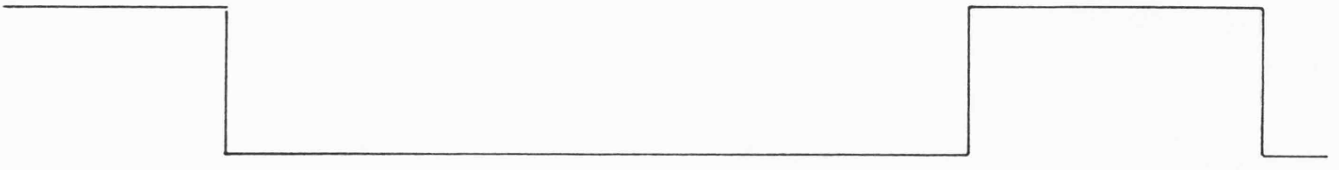

Detector $\overline{Q}$ Output.

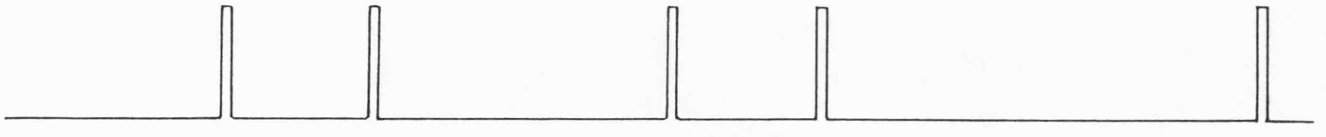

Lead Detector Output-Clock Edges Lead Baseband Transitions Edge.

Lag Detector Output- Clock Edges Lag Baseband Signal Transitions Edges.

Figure 4.13 Data Transition & Lead/Lag Detectors Signals.

Counting Length=4096- Binary Program Input Decimal Value.

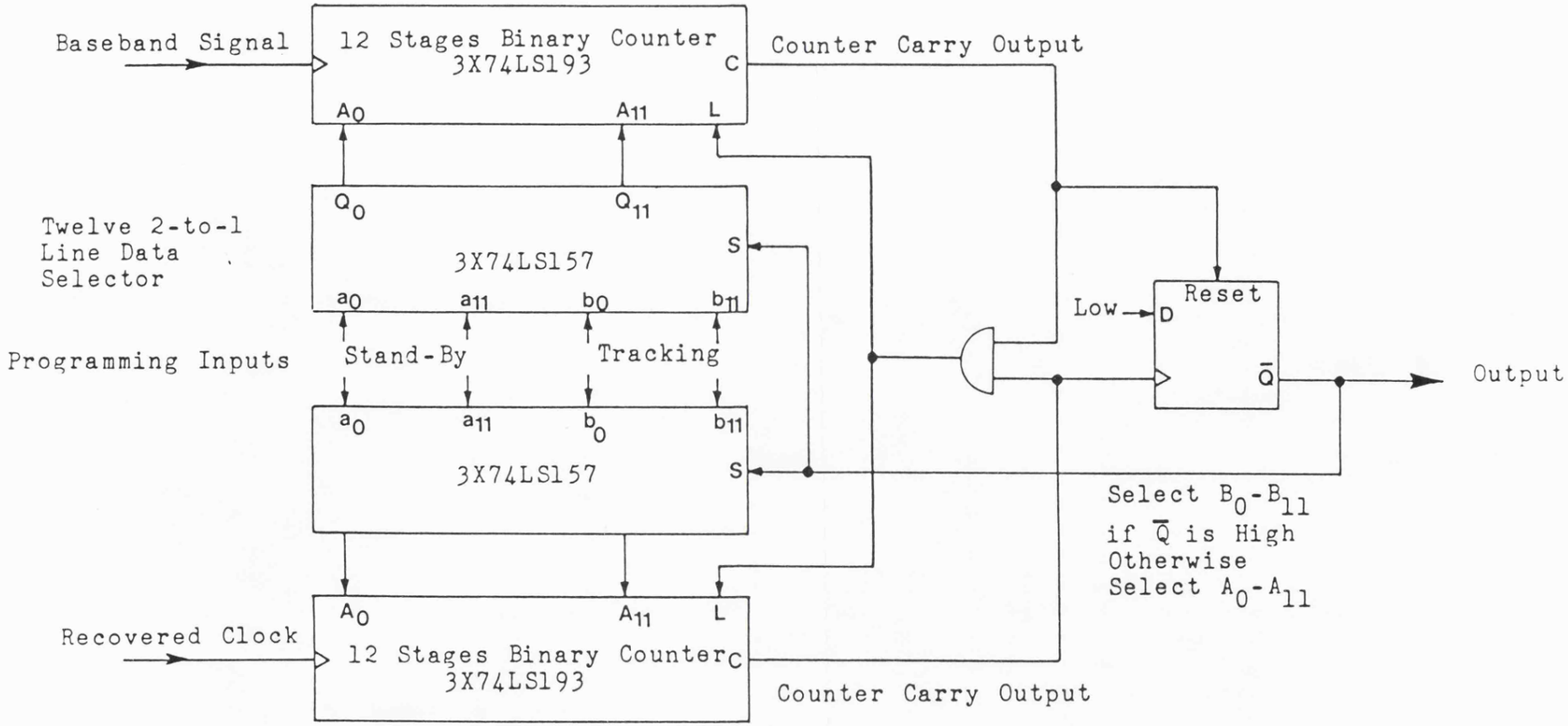

N.B. All Sequential Devices are +ve Edge Triggered.

Figure 4.14 Signal State Detector Circuit Block Diagram.

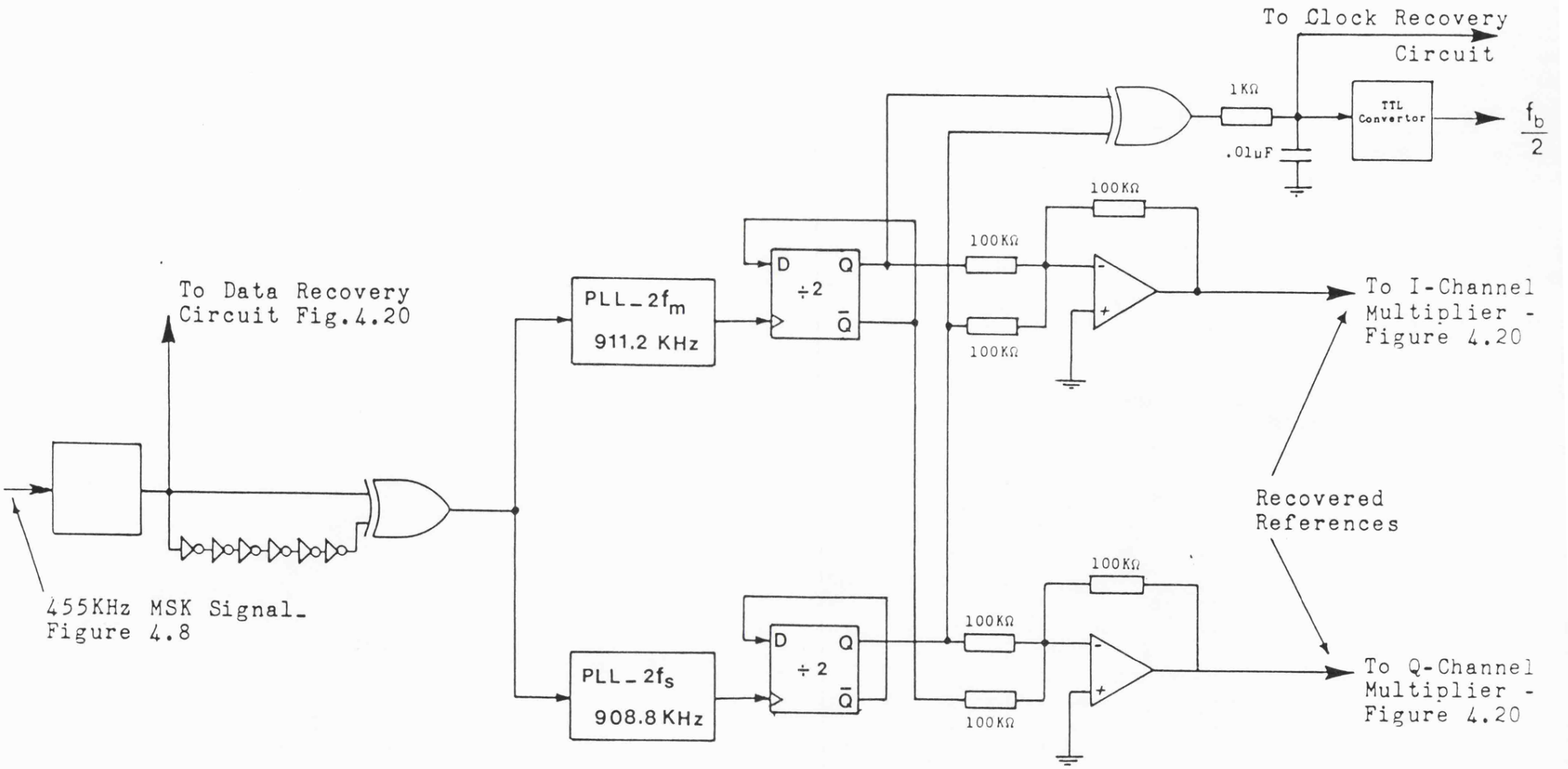

Figure 4.15 Coherent Demodulator References Recovery Circuit Function Diagram.

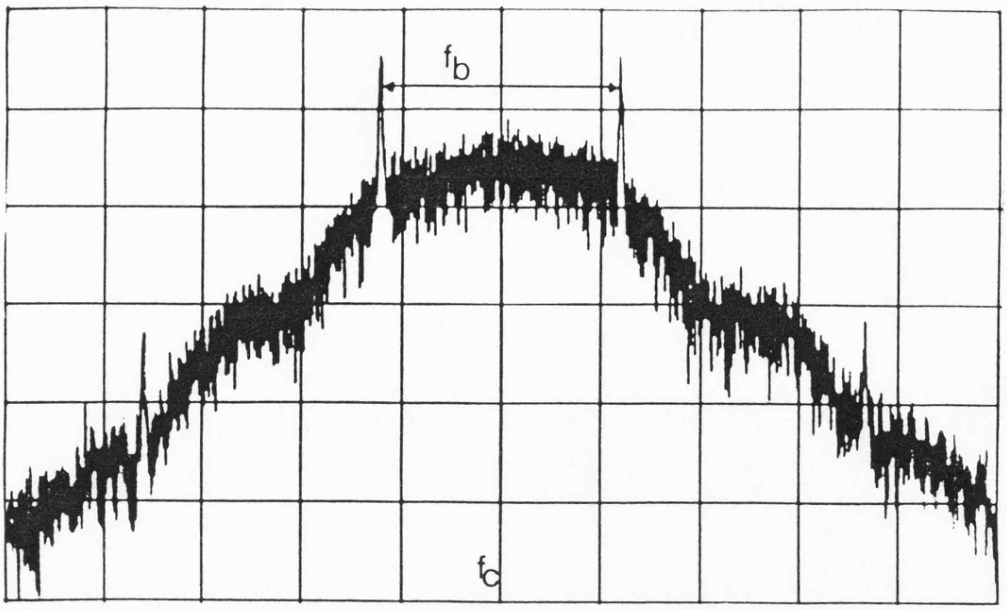

(a) Modulating Data is Random.

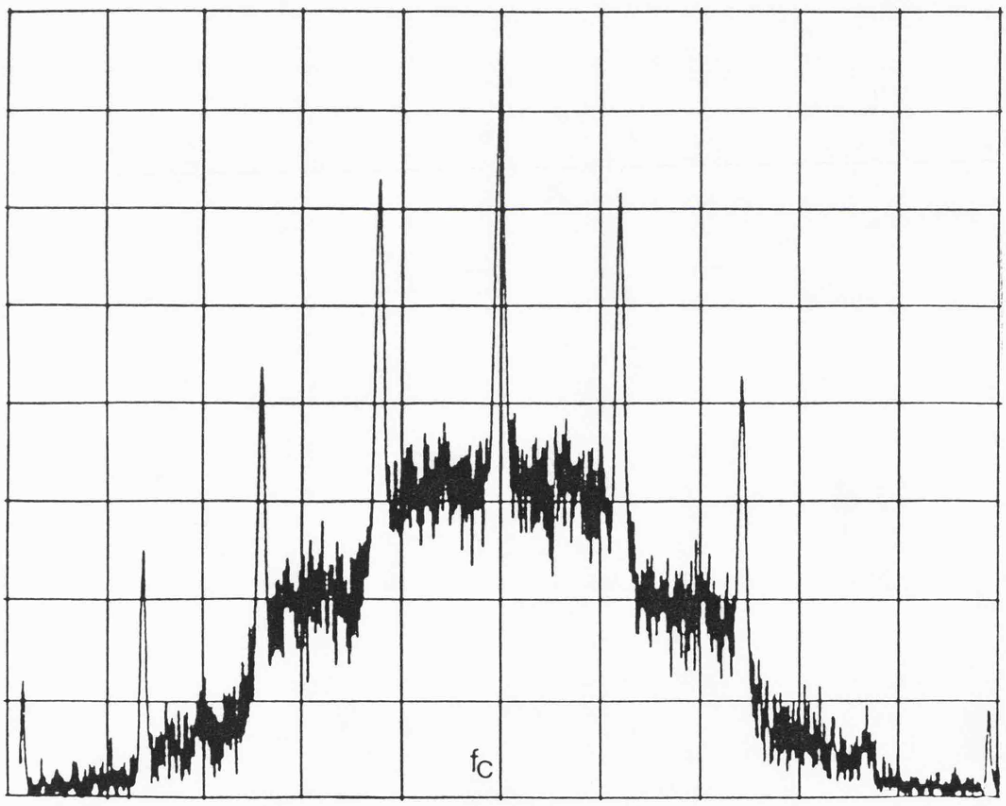

(b) Modulating Data is Alternate Marks & Spaces.

Horizontal:1KHz/Div.-Vertical:10dB/Div.-Centre Frquency:910KHz

Figure 4.16 MSK Signal Spectrum at the Digital Frequency Doubler Output.

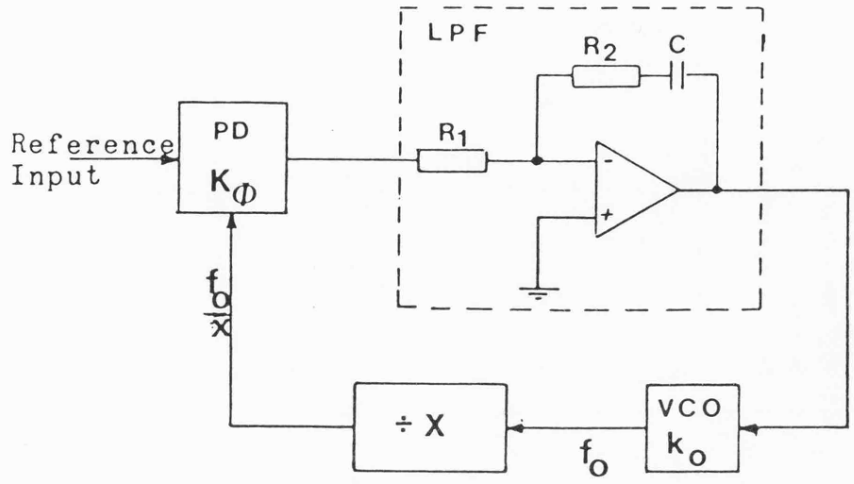

Figure 4.17 Second Order Phase Locked Loop.

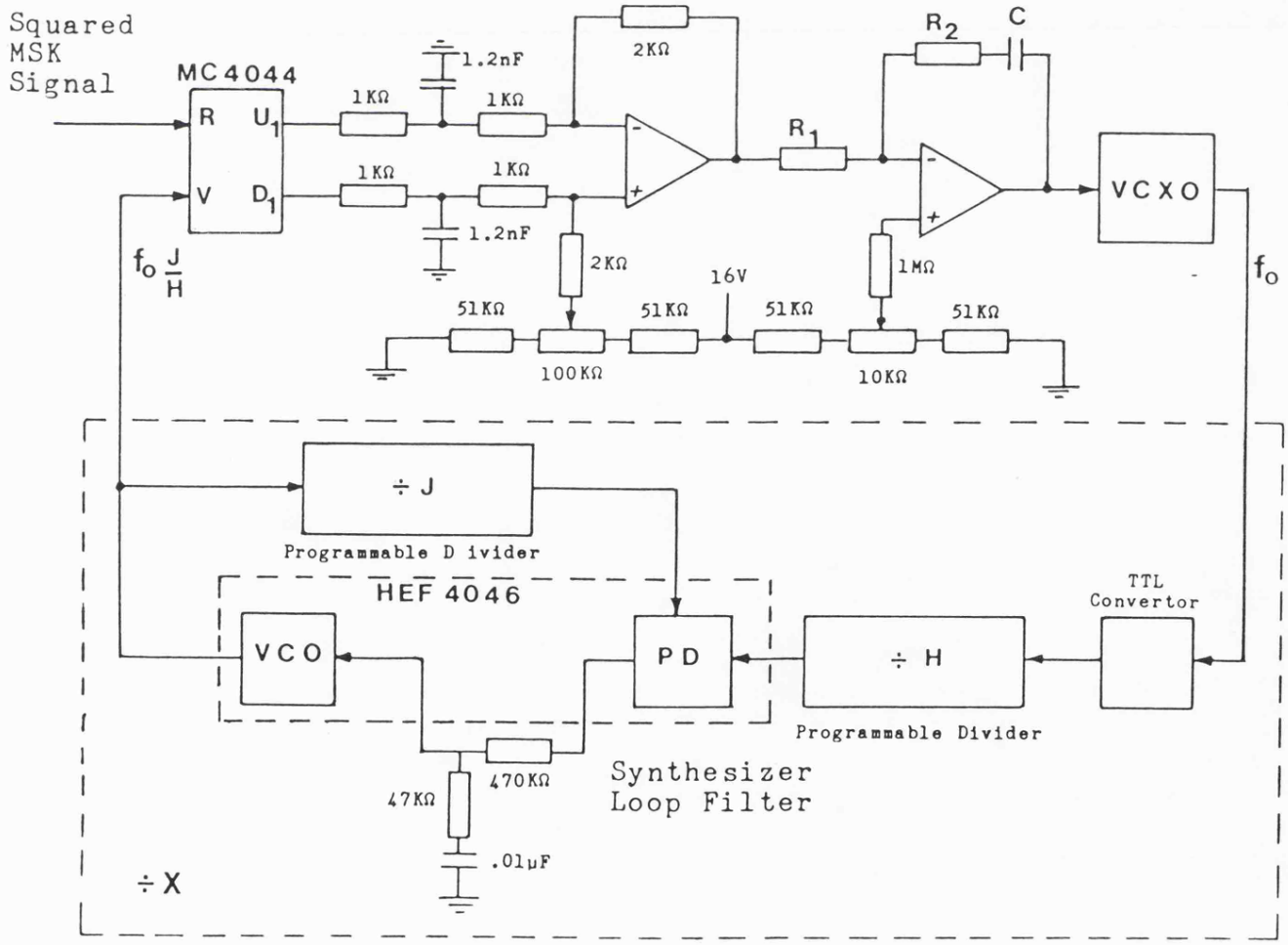

Figure 4.18 Reference Recovery Phase Locked Loop Circuit.

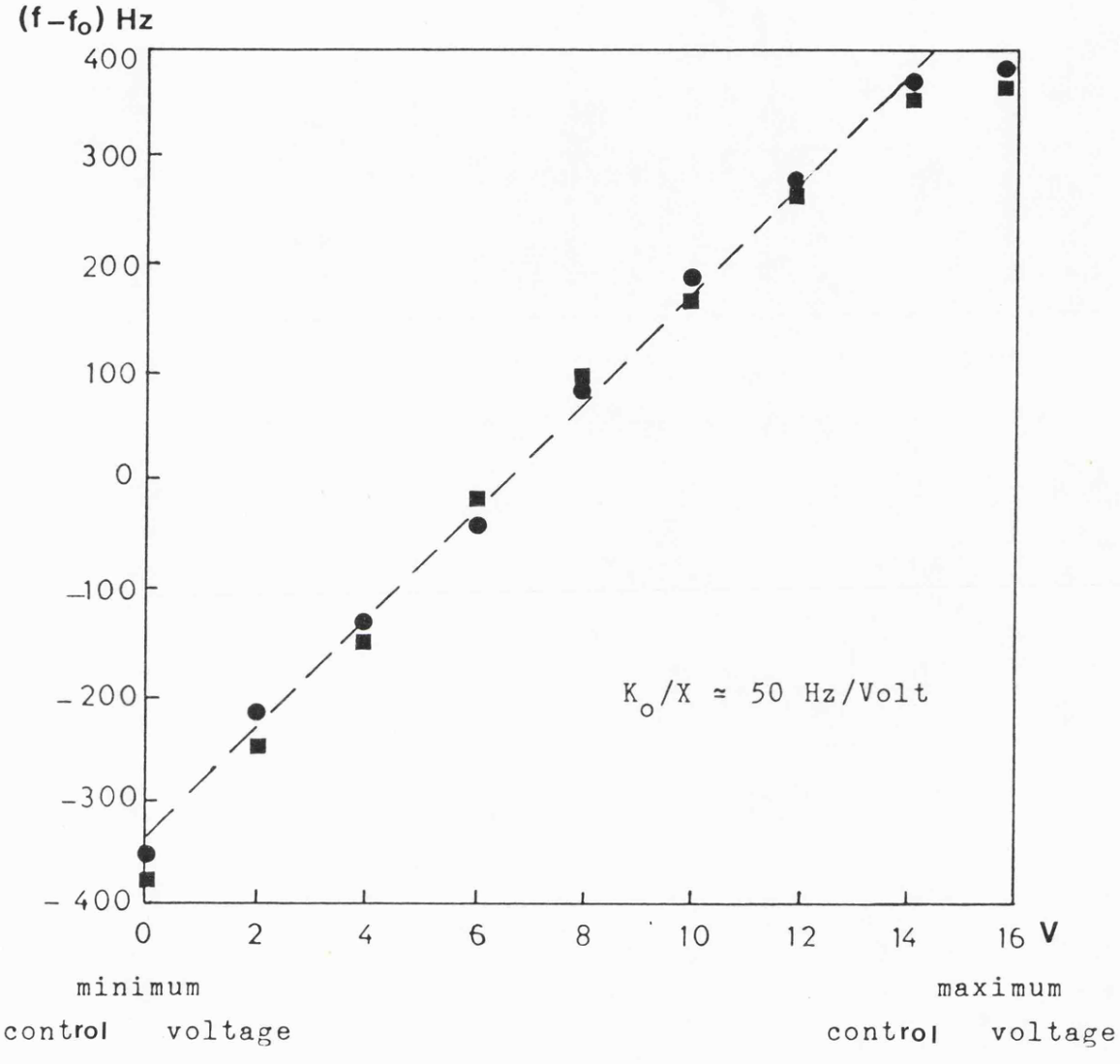

Figure 4.19 VCXO-Synthesizer Frequency Versus Control Voltage Charactarestics.

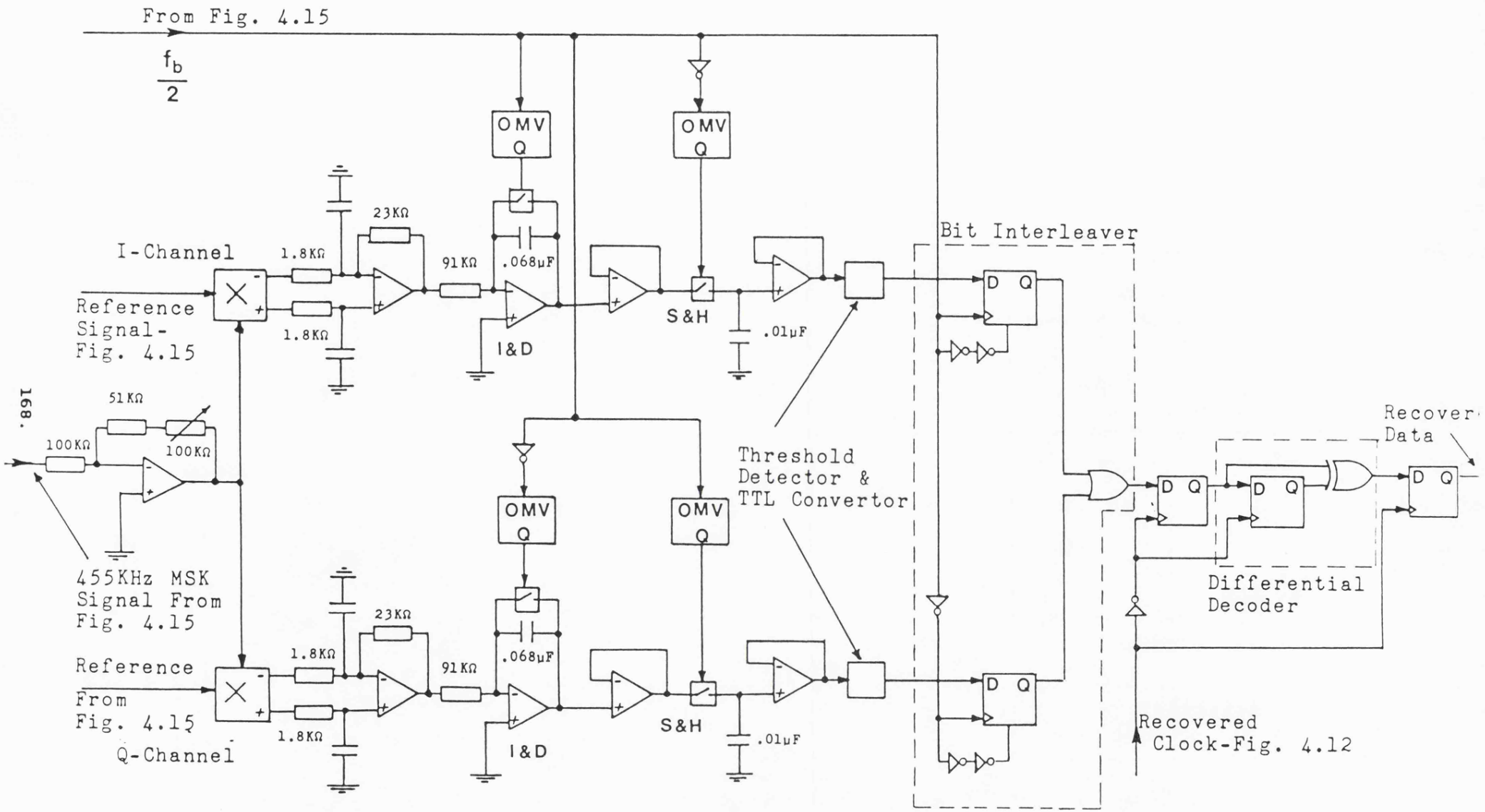

Figure 4.20 Data Recovery Circuit - Coherent Demodulator.

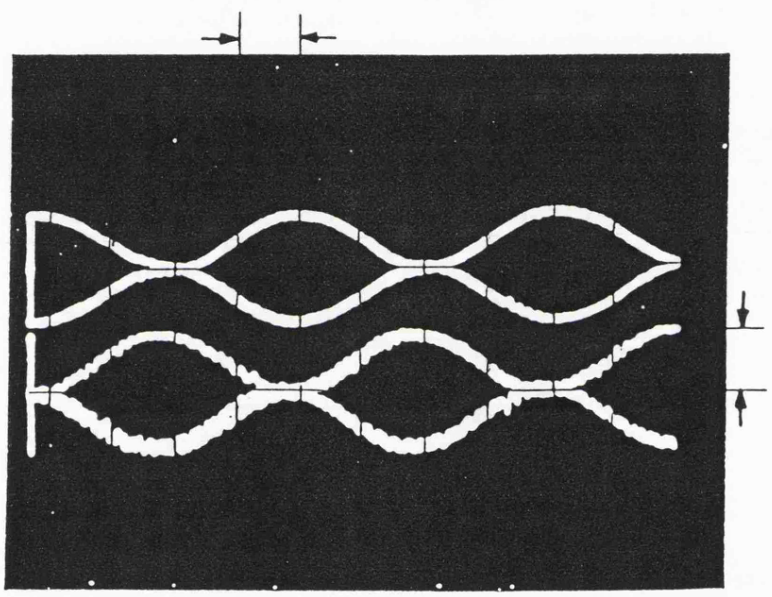

Horizontal : 0.2mSec/Div.

Vertical : 5V/Div.

Figure 4.21 Coherent MSK Demodulator I and Q Channels Eye Patterns.

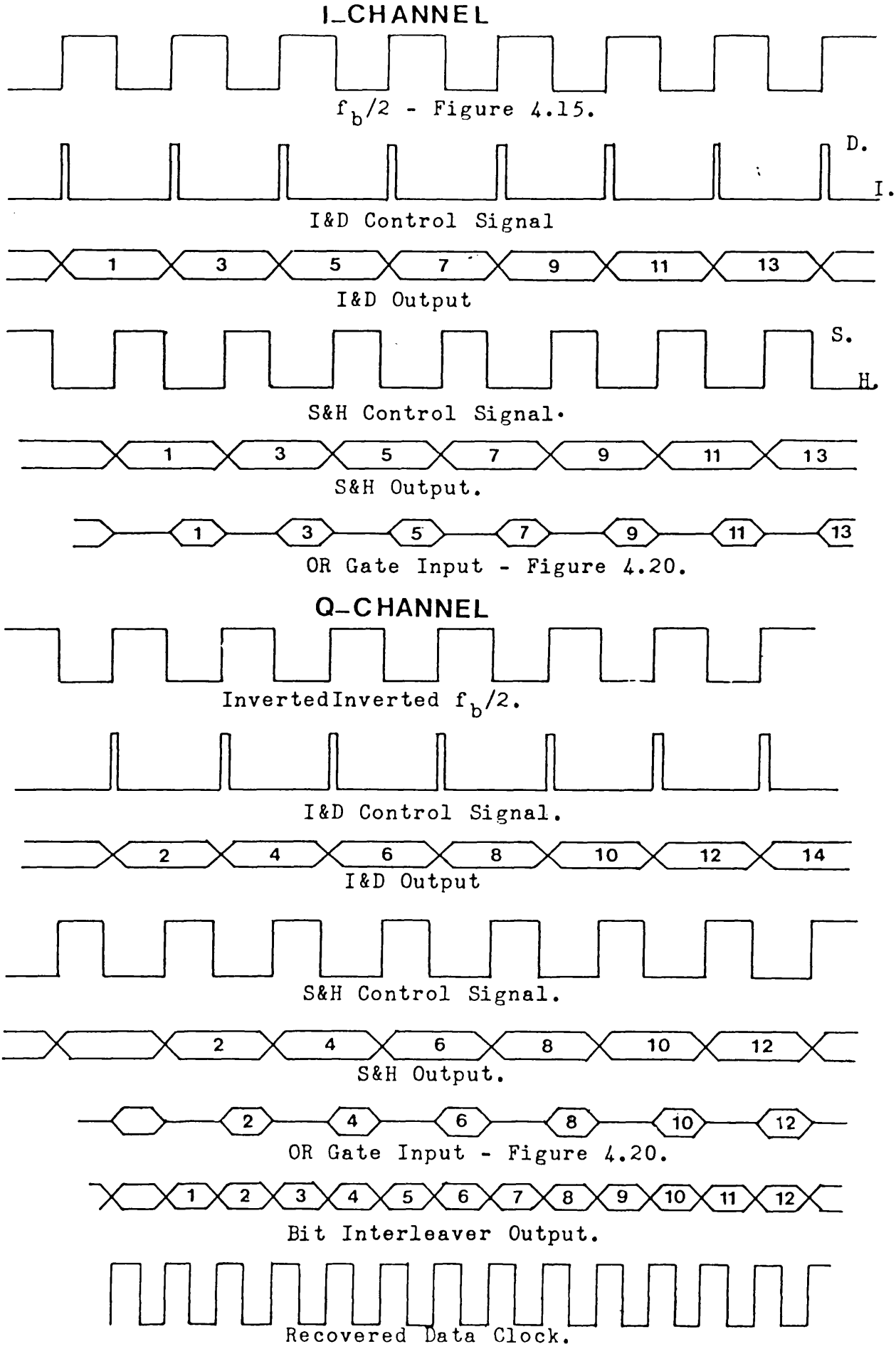

Figure 4.22 Coherent Demodulator Data Recovery Timing Diagram.

CHAPTER FIVE

MEASUREMENTS AND DISCUSSION OF RESULTS

5.1 Introduction

A wide range of bench tests, simulating typical mobile radio transmission conditions, was carried out to evaluate the performance of the MSK modulation scheme. MSK signal generation as well as coherent and non-coherent detection was accomplished using the modulator and demodulators discussed in the previous chapter. In this chapter the test conditions will be explained, and the results of the measurements discussed.

In all tests the noise introduced to the system was additive white Gaussian noise (AWGN). The noise is added to the MSK signal at the 10.7MHz input to the demodulator. The noise source used and its characteristics are discussed in Appendix 5.1.

A binary data transmission test set, model ICC-220 was used in all tests as a data source and for error counting. The modulator clock was supplied by the test set while at the demodulator the clock was recovered from the received signal. The clock recovery circuit was left in its tracking mode during all tests.

The data sequence used for test runs was a 511 bit pseudo-random sequence as recommended by the CCITT[1]. The transmission rate used in all tests was 2.4kbit/sec (ie. the clock frequency used was 2.4kHz) and the local receiver clock was adjusted to be within ±0.024 Hz of the transmitter clock. The number of bit errors was counted for 10^6 transmitted bits, which represents 7 minutes

transmission period at bit rate of 2.4kbit/sec. At low error rates (PE < 10^{-5}) the points shown in PE versus E_b/N_o curves represents the average of error counts in several 7 minute runs.

5.2 Signal to Noise Ratio Measurement

The received signal to noise ratio (SNR) was measured at the receiver 455kHz IF filter output, as illustrated in Fig 5.4. In order to compare the results of probability of error (PE) against SNR measurements with the theoretical data discussed in Chapter 3, the measured SNR was later reflected to its baseband equivalent E_b/N_o according to the following equation:

$$\frac{E_b}{N_o} = \frac{C}{f_b}\frac{B_N}{N} \qquad \ldots (5.1)$$

where

C = average carrier power or modulated signal average total power,

f_b = transmitted data bit rate,

N = average noise power measured at the IF filter output,

and B_N = IF filter noise equivalent bandwidth.

The filter noise equivalent bandwidth is shown in Fig 5.1 and is defined as the bandwidth of an ideal rectangular filter that would pass as much white noise power as the filter under consideration, their centre frequencies and maximum amplitude gain being equal[2]. Hence, the relation between B_N and the filter magnitude transfer function $|H(f)|$ is:

$$B_N = \frac{1}{|H(f_c)|^2} \int_0^\infty |H(f)|^2 \, df \qquad \ldots (5.2)$$

where $|H(f_c)|$ is the function value at the filter centre frequency.

The MSK demodulator 455kHz IF filter magnitude transfer function is shown in Fig 5.2. The filter noise equivalent bandwidth B_N was determined by calculating the area under the filter squared magnitude characteristics and finding the bandwidth of the rectangular filter whose centre frequency is 455 and magnitude transfer characteristics equal to $|H(f_c)|$ that delivers the same area. Accordingly, B_N was found to be approximately equal to 5.6kHz, ie. $B_N = 2.33f_b$ (f_b = 2.4kHz).

The MSK signal and noise voltages were measured at the IF filters output using an rms voltmeter as shown in Fig 5.4. Mathwich et al[3] have shown, by computing the fraction of the total modulated MSK signal power falling outside a certain bandwidth, that 99 per cent of the power of a non-filtered MSK signal is contained within a bandwidth of $1.15f_b$. Thus, given the wide bandwidth of the IF demodulator filter used, the average signal power at the filter output can be considered equal to that of the carrier. Consequently, E_b/N_o was calculated using equation (5.1) as follows:

$$\frac{E_b}{N_o} = 20 \log_{10} \left[\frac{(V_{rms})_{signal}}{(V_{rms})_{noise}} \right] + 10 \text{ Log}_{10} \left[\frac{5.6}{2.4} \right] \quad . . (5.3)$$

The same IF filter, whose characteristics are given in Fig 5.2, linear amplitude scale, and Fig 5.3, amplitude scale in dB, was used in all tests unless otherwise mentioned. Changing the SNR (hence E_b/N_o) was accomplished by varying the signal level whilst keeping the noise level at a constant value.

5.3 Wideband MSK Performance in the Presence of AWGN

Fig 5.4 illustrates the block diagram of the experimental set-up to measure PE versus E_b/N_o for a wideband MSK signal in the presence of AWGN. The PE was measured for both coherent and non-coherent demodulators. The IF filter amplitude and time delay characteristics are shown in Fig 5.3. Looking at the eye pattern of the non-coherent and the coherent demodulators, shown in Figs 4.9 and 4.21 respectively, reveals that no noticeable inter-symbol interference (ISI) is being introduced by the demodulator IF filter.

The results of the measurements are plotted in Fig 5.5 for the coherent demodulator, with the reference recovery PLL's natural frequency ω_n = 10rad/sec, and for the non-coherent demodulator. Also shown in this figure is the theoretical performances of ideal DEMSK (differentially encoded coherent MSK) and MSK using either limiter discriminator or differential detectors as given in [4].

At values of E_b/N_o > 8dB the coherent demodulator (ω_n = 10rad/sec) performance is approximately 0.8dB worse than the ideal coherent demodulator theoretical performance. The theoretical PE performance of DEMSK was calculated assuming an ideal reference recovery loop producing an infinite phase reference SNR (α). Cruz et al[5] have shown that when a second order phase locked loop is used and for high values of α, the signal to noise ratio in the case of MSK reference recovery can be approximated by:

$$\alpha = \frac{f_b}{4B_n \left[\frac{N_o}{E_b} + \left[\frac{N_o}{E_b} \right]^2 \frac{B_N}{2f_b} \right]} \qquad \ldots (5.4)$$

where f_b, E_b/N_o and B_N have been defined previously and B_n is the phase locked loop noise bandwidth. For the second order PLL shown in Fig 4.17, B_n is given by[6,7]:

$$B_n = \frac{\omega_n}{2}\left[\eta + \frac{1}{4\eta}\right] \text{ Hz} \qquad \ldots (5.5)$$

Using equations (5.4) and (5.5), α can be calculated for the MSK demodulator reference recovery PLL described in the previous chapter, assuming that the loop synthesiser acts as a simple frequency divider, for different values of ω_n and E_b/N_o. Hence for ω_n = 10 rad/sec and E_b/N_o = 8dB (ie. PE = 10^{-3}), α = 27.8dB.

Recalling Fig 3.31 giving the performance degradation as a function of α for MSK at PE = 10^{-3}, it is possible to conclude that at α = 27.8dB the performance degradation is around 0.02dB. Consequently, the 0.8dB difference between the ideal and practical coherent demodulator's performance can be mainly considered as an implementation loss. The further deterioration in the coherent demodulator performance due to increasing ω_n is shown in Fig 5.6.

Finally, it is possible to notice from Fig 5.5 that the performance of the non-coherent MSK detector (FM quadrature discriminator) is very close to the theoretical performance of either the limiter discriminator or differential detector as given in [4].

5.4 Effect of Bandlimiting on the MSK Signal

The use of a transmitter filter in order to limit the radiated signal spectrum will change the characteristics of the modulated signal. Bandlimiting will cause generation of amplitude fluctuations

in the originally constant amplitude MSK signal, the amount of fluctuation being dependent on the ratio between the filter bandwidth and the data bit rate. Furthermore, bandlimiting and delay distortion introduced by the filter will cause ISI, thus degrading the PE performance with different degrees depending on the demodulation mechanism and the filter characteristics.

The MSK signal was bandlimited by inserting a 10.7MHz crystal filter at the modulator output, followed by a buffer-amplifier stage. The filter used is a commercial 8 pole crystal filter of the type usually employed in SSB applications. From the filter characteristics shown in Fig 5.7 it is possible to conclude that the 3dB filter bandwidth (B_{3dB}) is equal approximately to 2.25kHz, and that the delay distortion introduced by the filter can be considered quadratic. The maximum delay distortion given by the difference in delay at mid-band and the edge of the transmission band (given by the 3dB point) is equal to approximately 1msec.

5.4.1 Generation of Amplitude Fluctuation

The bandlimited MSK waveform is shown in Fig 5.8 for three values of B_{3dB}/f_b ratio. The percentage of amplitude fluctuation, defined as the percentage of the ratio of the difference between the maximum and the minimum signal amplitudes to the maximum amplitude, is 19% for B_{3dB}/fB = 2 (ie. f_b = 1.125 kbit/sec), 26% for B_{3dB}/f_b = 1.5 (ie. f_b = 1.5 kbit/sec), and 48% for B_{3dB}/f_b = 0.94 (ie. f_b = 2.4kbit/sec). However, the latter is less than that of bandlimited OQPSK (66% - B_{3dB}/f_b = 2.4) discussed in Chapter 3.

The spectrum of the unfiltered MSK modulator output is shown in

Fig 5.9(a). The filtered MSK signal spectrum is illustrated in Fig 5.9(b). The same figure shows the signal spectrum after being passed through a VHF (165MHz) polar loop transmitter. The polar loop transmitter is a technique for power amplification, which has been developed at the University of Bath, that maintains amplification liearity while achieving the efficiency of a Class C power amplifier[8]. Finally, the spectrum of the filtered MSK signal at the output of a conventional Class C amplifier is illustrated in Fig 5.9(c). The reintroduction of out-of-band radiation, to a level approximately equal to that of the pre-filtered signal, is evident from this figure.

5.4.2 Bandlimited MSK Signal PE Performance

The same experimental arrangements shown in Fig 5.4, except for the inclusion of the crystal filter at the modulator output, were used to measure PE versus E_b/N_o of the bandlimited MSK signal. The measurements were carried out for both coherent and non-coherent demodulators.

The effect of filtering can be predicted by monitoring the demodulator's eye patterns. These are shown in Fig 5.10. The coherent demodulator eye patterns suffer slight distortion, thus slight performance degradation can be predicted. On the contrary, the non-coherent demodulator eye pattern opening has deteriorated severely, thus it is possible to conclude that the PE performance will similarly show severe degradation.

The measured PE versus E_b/N_o curves for both demodulators are shown in Fig 5.11. The coherent demodulator performance has been

degraded by approximately 1dB. This closely agrees with the theoretical value predicted by Fig 3.27 for the MSK signal. The non-coherent demodulator performance degradation is approximately 6dB at high E_b/N_o values. This is 0.6dB more than the theoretical value given in Fig 3.28 in case of a limiter discriminator detector for $d/T_b = 2.4$. However, this performance is still more than 4dB less than the theoretical performance degradation of DQPSK for the same amount of delay distortion as can be concluded from Fig 3.28.

Furthermore, by decreasing the bit rate to 1.5kbit/sec (ie. $B_{3dB}/f_b = 1.5$, $d/T_b = 1.5$) the performance can be expected to improve considerably. The reason for this is that at this filter bandwidth the MSK signal main lobe which contains more than 99% of the signal power[3] is being passed. The predicted improvement in performance is supported by the increased opening of the demodulator eye pattern illustrated in Fig 5.10(c) for $B_{3dB}/f_b = 1.5$.

5.5 Effect of Fading and Random FM Noise on PE Performance of MSK Modulation

A VHF (165MHz) Rayleigh fading simulator was used to study the effect of multipath transmission on PE performance of MSK modulation. The simulator was developed by the Wolfson research group at the University of Bath and is based on the simulation principle described in [9]. The output of the simulator represents the envelope and phase of a Rayleigh fading signal which is the condition frequently encountered in mobile radio transmission as was mentioned in Chapter 2.

Fig 5.12 illustrates the block diagram for the experimental

set-up to measure the system performance in the presence of simulated mobile radio multipath transmission.

To evaluate the performance of the polar loop transmitter when used for amplification of MSK signal, a set of PE versus E_b/N_o measurements was taken in the absence of the fading simulator. The results agreed closely with those shown in Fig 5.5. A second set of measurements was taken for the bandlimited MSK signal which agreed with those taken in the absence of the polar loop transmitter and shown in Fig 5.11. These measurements demonstrated the suitability of the polar loop technique for handling linear power amplification of the MSK signal.

The PE versus $(E_b/N_o)_o$ measurements were carried out for six different fading rates (defined as the maximum doppler shift, f_D) - 0.15, 1, 2, 10, 20 and 100 Hz. $(E_b/N_o)_o$ represents the base-band equivalent of the received SNR averaged over the Rayleigh fading level. An approximate measurement of this quantity was carried out by using an r.m.s. voltmeter which responds to the average value of the input signal and setting the fading simulator at its maximum rate value (150Hz). $(E_b/N_o)_o$ was later calculated according to equation (5.3).

The results of these measurements are plotted in Figs 5.13(a) to (f) for the coherent (ω_n = 10, 50 and 100) and non-coherent demodulators and the above values of fading rates. Also illustrated in these figures are curves showing the theoretical performance of DEMSK and DMSK (differentially demodulated MSK) and LDMSK (MSK demodulated using limiter-discriminator detector) as previously given

in Chapter 3 in fading and non-fading conditions. A close study of these figures (5.13(a) - (f)) leads to the following conclusions.

At low fading rates (f_D = 0.15, 1Hz), ie. slow fading conditions, the practical performance of the non-coherent detector is generally within 1-2dB of the theoretical performance of DMSK and LDMSK. The coherent demodulator is within 2-3dB of DEMSK. These differences between theoretical and practical results can be considered reasonable given the practical difficulty in accurately measuring the average value of (E_b/N_o). However, in general the non-coherent demodulator shows a slight advantage over the coherent one (all values of ω_n). This conclusion can be made because the PE measurements in all cases were taken for the same signal attenuator settings, ie. exactly equal $(E_b/N_o)_o$ values. This advantage can be explained by excess errors occurring during reacquisition intervals of the reference's recovery phase locked loops, taking place after the signal has been lost during a deep fade. The recovery is instantaneous in the case of the non-coherent detector. Furthermore, it is difficult to distinguish between the performance of the coherent demodulator for different values of ω_n. Although the recovery time will decrease as ω_n is increased, thus leading to less errors, the errors will be more at any fade level as ω_n increases. Thus, it can be expected that on average the same number of errors are produced for all values of ω_n considered. This remark is based on observing the results of the coherent demodulator plotted in Fig 5.13 and applies for the range of values of ω_n considered(10-100 rad/sec). Generalising this conclusion for values outside this range will need further investigation.

As the fading rate increases, the effect of random FM noise becomes apparent and ultimately leads to an irreducible error rate at high $(E_b/N_o)_o$ values as can be seen in Figs 5.13(c)-(f). The deterioration in PE performance starts at earlier values of f_D in the case of coherent demodulator compared to the non-coherent one, and at smaller values of ω_n than higher ones. However, at values of $(E_b/N_o)_o$ where the effect of signal level fading is predominant, the performance curves of both demodulators revert to the same pattern discussed previously.

To investigate the irreducible PE due to random FM noise the noise source was removed and the error rates were measured versus the fading rate. The results of these measurements are illustrated in Fig 5.14 for the coherent (ω_n = 10, 20, 50 and 100) and the non-coherent demodulators. Also shown in this figure are the theoretical performances of the limiter-discriminator and the differential detectors when used to demodulate an MSK signal in the presence of random FM noise, as given in equations (3.40) and (3.41) respectively. For values of $2f_D > 20$ the performance curve of the non-coherent demodulator lies between that of the limiter-discriminator and the differential detectors.

The differential detection operation relies on comparing the signal with its delayed version, ie. the demodulation reference is the delayed replica of the signal. Consequently, in the presence of random FM noise, where the signal phase changes its value in a random manner, the smaller the detector time delay element the quicker it will be able to track the random phase changes. The limiter-discriminator detection mechanism can be approximated by that of a

differential detector whose time delay element is zero[10]. This explains the better theoretical performance of the limiter discriminator detector as compared with the differential detector, whose time delay element is equal to T_b, as depicted in Fig 5.14.

The non-coherent demodulator, which is an FM quadrature discriminator detector, is equivalent to a differential CPFSK detector whose 90° phase shift circuit and delay line (Fig 3.23(b)) are the quadrature coil. The time delay generated by the quadrature coil used in non-coherent detection of the MSK signal is less than the bit interval T_b (T_b = 0.42 msec). Therefore its performance is better than the theoretical performance of the differential detector, but not as good as that of the limiter discriminator, for values of $2f_D > 20$.

For the same values of f_D ($2f_D > 20$) the performance of the coherent demodulator improves rapidly as f_D decreases in a pattern similar to that of the non-coherent demodulator, as can be seen in Fig 5.14. Furthermore, the number of errors at any value of f_D decreases as ω_n increases. This is a logical result and is explained by the fact that increasing ω_n speeds up the reference recovery phase locked loop's tracking of the random phase changes in the signal. However, for the highest value of ω_n (100 rad/sec), the coherent demodulator performance is considerably worse than that of the non-coherent demodulator.

A further increase in ω_n will close the gap between their performances as the loops response to the random phase changes will become quicker. In addition, it is possible that the frequency

synthesiser used as a frequency divider leads to a slower overall loop response to random phase changes. It can be expected that a loop with a simple binary divider would offer a better performance. Unfortunately, no experimental or theoretical data on the effect of reference recovery phase locked loops natural frequency on the peformance of coherent MSK in the presence of random FM noise is available. Therefore, it is not possible to establish a more precise conclusion on the performance of this particular loop structure in the presence of random FM noise.

For values of $2f_D < 20$ the improvement in performance of both demodulators as f_D decreases becomes much more gradual. This is due to the excess random phase changes generated by the fading simulator at these low values of f_D.

5.6 Effect of Co-Channel and Adjacent Channel Interference

The block diagram for the experimental arrangement used to study both co-channel and adjacent channel interference is shown in Fig 5.15. In both cases the interfering signal was assumed to be another MSK signal having the same bit rate (2.4kbit/sec). The interfering signal was generated by the VCXO, described in Appendix 4.5, adjusted to produce a CPFSK signal whose deviation ratio is 0.5 (ie. MSK signal). The modulating data was produced by a pseudo random sequence generator different from the one used to produce the in-channel data and having 1048575 bits sequence length. The generator clock was within ±0.4Hz of the in-channel data generator.

The centre frequency of the VCXO was adjusted to produce a

co-channel interference signal at exactly 10.7MHz. The frequency spectra of the in-channel and co-channel MSK signals are shown in Fig 5.16.

To simulate adjacent channel interference the VCXO centre frequency was adjusted to produce an MSK signal at 10.705MHz - ie. assuming 5kHz channel spacing. The frequency spectr of the in-channel and adjacent channel signals are given in Fig 5.17(a) and the spectrum of the signal at the demodulator front end input is shown in Fig 5.17(b).

Measurements of PE versus the ratio between the in-channel signal to the co-channel signal (I_n/C_o) and to the adjacent channel signal (I_n/A_d) were carried out for several values of E_b/N_o by fixing the in-channel signal level and varying the interfering signal level, as depicted in Fig 5.15.

The results of these measurements for the co-channel interference case are shown in Figs 5.18(a), (b) and (c) for the coherent demodulator ω_n = 10, ω_n = 100 and the non-coherent demodulator respectively. These results were used to plot curves giving the demodulator's performance degradation, defined as the increase in E_b/N_o needed to achieve the same PE in the presence and absence of interference. The degradation for PE = 10^{-6} is shown in Fig 5.19(a) for the coherent demodulator (ω_n = 10). Also shown in this figure is the theoretical degradation of BPSK and QPSK as given in [11]. MSK and QPSK have similar performances. However, the theoretical analysis of QPSK and BPSK assumed that the interfering signal is a single sinusoid and it was concluded in the same reference[11] that

an interference from a source having the power of a single sinusoid spread over the channel band is more damaging than a single sinusoid. Consequently, it is possible to conclude that the MSK demodulator will give relatively better resistance to co-channel interference than at least QPSK.

Degradation curves for PE = 10^{-4} were also plotted for the coherent demodulator (ω_n = 10, 100) and the non-coherent demodulator to compare their relative performances in the presence of co-channel interference. These curves appear in Fig 5.19(b) and show that the three cases have equal resistance to this type of interference.

The same measurement procedure, described for the co-channel interference case, was carried to study the effect of adjacent channel interference on the demodulator's performance. No filter was used to bandlimit the transmitted signal spectrum. Although this might not be the case in a practical situation, it allows to study the tolerance of both demodulators to interference and the role of the receiver IF filter in improving this tolerance.

The first set of measurements was taken using the same IF filter used throughout all the previous measurements. The results appear in Fig 5.20(a) for the coherent demodulator and Fig 5.20(b) for the non-coherent demodulator.

A second set of measurements was taken for a second IF filter whose 3dB bandwidth is approximately equal to the first one (4.8kHz) but has a much faster amplitude attenuation roll-off. The frequency spectrum appearing at the output of the two filters for an input white

noise signal is shown in Fig 5.21 for the two filters.

The second filter achieves higher selectivity while causing a slight distortion to the non-coherent eye pattern as can be seen from the photograph in Fig 5.22. However, it has no effect on its PE performance in the presence of AWGN. This is because the slight ISI action introduced by the filter is compensated by the smaller receiver noise bandwidth the latter provides.

The result of the measurements for the coherent demodulator (ω_n = 10, 100) and the non-coherent demodulator, when the second filter was employed, are shown in Figs 5.23(a), (b) and (c) respectively. The improvement in resistance to adjacent interference of both demodulators in the case of the second filter is clearly evident from these figures.

The performance degradation curves are illustrated in Fig 5.24 for PE = 10^{-4} in the case of the two filters. For a 2dB degradation, the I_n/A_d ratio will have to be -12dB in the case of the second filter compared with -7dB in the case of the first filter, when the coherent demodulator (ω_n = 10) is employed. This represents a 5dB advantage offered by the second filter. When the first filter was employed the degradation figures for the second and first filters are -10dB and -4.6dB, which represents a 5.4 advantage in the case of the second filter.

Another conclusion which can be drawn from Fig 5.24 is the improvement in immunity to adjacent channel interfrence offered by the coherent demodulator relative to the non-coherent. For a 2dB

degradation the coherent demodulator (ω_n = 10) can tolerate 2dB more interference than the non-coherent in the case of the second filter and 2.4 in the case of the first filter. Furthermore, decreasing ω_n increases the resistance to interference. This difference in performance is due to the better selectivity offered by the coherent demodulator as compared to the non-coherent demodulator and the improvement in this selectivity as ω_n decreases in the case of the first.

5:7 Effect of Ignition Interference

The nature of ignition interference renders a model of such an event difficult to define. However, as was mentioned in Chapter 2, ignition interference is characterised by bursts of impulsive noise which can reach a rate of 300Hz in each burst. The impulsive noise level can be up to 30dB higher than the white noise level at the receiver input in some cases. The effect of high energy impulses is to blank the received signal for an interval of time dependent on the receiver IF filter impulse response.

In order to compare the effect of such events on the demodulator performance, measurements of PE versus E_b/N_o were carried out while blanking the input signal by pulses having 0.05msec width and 300Hz repetition rate. Both demodulators have shown equal degradation in performance of 1dB for values of PE < 10^{-3}. However, when the pulse width was increased to 0.2msec (ie. $0.48T_b$) errors occurred at a rate approximately equal to the pulse rate regardless of the value of E_b/N_o. This observation agrees with previous experimental tests carried out in [12] and reported in [13] on differentially demodulated BPSK and non-coherent FSK. These tests led to conclude

that if a noise impulse of peak value equal to the signal end of length greater than half the data clock period, an error would occur regardless of the mode of data modulation. Hence it is possible to state that in such an environment other data modulation systems do not appear to have an advantage over MSK.

5.8 Discussion of Results

The performance of the coherent and non-coherent demodulators has been measured in the presence of different transmission conditions related to typical land mobile radio channels.

When tested in wideband non-fading conditions, the coherent demodulator had approximately 4dB advantage over the non-coherent. However, when operated in slow non-selective Rayleigh fading the difference between their performances disappeared as predicted by their respective theoretical performances illustrated in Fig 3.30. Furthermore, in these conditions, the non-coherent demodulator has shown, in general, an approximate 1dB advantage over the coherent, due to excess errors in the latter occurring during reacquisition intervals of the reference signals taking place after the signal is lost in a deep fade. The reacquisition of the non-coherent demodulator is almost instantaneous.

As the fading rate increases, the effect of random FM noise becomes more pronounced and the non-coherent demodulator emerges as the one having the superior performance. For $\omega_n = 100$ and $f_D = 10$ the coherent demodulator produces 25 times the number of errors produced by the non-coherent demodulator. Although the performance of the coherent demodulator in random FM noise will improve as ω_n is

increased beyond 100, it is not expected to become superior to that of the limiter-discriminator detector. The latter will give the fastest possible tracking performance under such conditions compared to any other demodulator, as can be concluded from the discussion on its detection mechanism given in this chapter. In this case the quadrature discriminator (ie. non-coherent) detector produces only 1.7 times the errors produced by the limiter-discriminator.

If adjacent channel interference takes place due to transmitter frequency instability and/or functioning with non-bandlimited transmitters, the coherent demodulator will give better performance. However, this advantage in performance is achieved at low values of ω_n. The degradation in the coherent demodulator performance approaches that of the non-coherent as ω_n increases, as can be seen in Fig 5.24. Due to the effect of random FM noise, it is unfavourable to operate the coherent demodulation with low values of ω_n. Consequently, it can be concluded that the use of the coherent demodulator as opposed to the non-coherent will not offer improved immunity to adjacent channel interference in a fading environment.

With regard to co-channel and impulsive interferences, both demodulators appeared to suffer an equal degradation in performance in both cases.

In the presence of severe bandlimiting and quadrature delay distortion (B_{3dB}/f_b = 0.94, d/T_b = 2.4) produced by the transmitter crystal filter, the coherent demodulator has shown 1dB deterioration in performance as compared to 6dB in the case of the non-coherent. However, by increasing the filter bandwidth to $1.5f_b$ (ie. d/T_b = 1.5)

the performance degradation of the non-coherent detector is expected to decrease substantially. Furthermore, by a proper design of the transmitter filter, its time delay distortion can be considerably decreased, thus decreasing the degradation in performance and allowing the use of a smaller filter bandwidth.

From the above discussion, the superiority of the non-coherent demodulator in non-selective Rayleigh fading is evident. The simplicity of the non-coherent demodulator structure also clearly favours its use in land mobile radio applications. While the non-coherent demodulation is accomplished using a single low power consumption chip and an external quadrature coil, the coherent demodulator needs a number of digital integrated circuits as well as two VCXO and other analogue circuits which constitute the reference recovery phase locked loops and the I/Q channels correlators (analogue multipliers). Accordingly the power consumption, which is an important consideration in vehicle mounted terminals, is much less in the case of the non-coherent demodulator. Furthermore, the non-coherent demodulator can be used to receive analogue voice signals as well as data signals, in present day channels.

An MSK signal modulated by 2.4kbit/sec data can be detected by the non-coherent demodulator with a small degradation in performance, if the transmitted signal is bandlimited by a filter similar to the one used during tests, if it has a bandwidth greater than $1.5f_b$. In this case the transmitted MSK signal occupies a bandwidth of 3.6kHz with out-of-band radiation at -70dB or less. This will leave 1.4kHz for use as guard bands in a 5kHz channel. However, the guard bands can be extended or alterantively the bit rate increased if a filter

having less delay distortion is used.

Extending these figures to the conventional channel bandwidths, this represents the transmission of 6kbit/sec with 3.5kHz guard bands in 12.5kHz channels and 12kbit/sec with 7kHz guard bands in 25kHz channels. The results of the measurements obtained in this chapter can be equally applied to these bit rates and channel bandwidths. The fading can still be considered non-selective because the MSK signal transmitted bandwidth at 12kbit/sec (18kHz) is well within the coherence bandwidth (26.5kHz) of urban and non-urban land mobile radio channels.

The practical extension of the modulator, demodulators and timing recovery circuit to work over these bit rates is trivial as was indicated in Chapter 4. The quadrature discriminator detector used for the non-coherent demodulation of the MSK signal is capable, in its configuration used during test, of demodulating FM signals having typical peak ot peak frequency deviation of ±3kHz, ie. it can demodulate MSK signals having a bit rate of up to 12kbit/sec. The peak frequency separation of the detector can be further widened by using a shunt resistance across the quadrature coil as indicated in the manufacturer's information sheet[14].

An investigation of equations (3.40) and (3.41) reveals that for the limiter-discriminator and the differential detectors, the irreducible probability of error due to the presence of random FM noise is inversely proportional to the squared value of the bit rate (f_b) in both cases. Consequently, it can be concluded that the number of errors produced by the non-coherent MSK demodulator at a certain

fading rate f_D in the presence of random FM noise will decrease as the bit rate increases at a rate proportional to $(1/f_b)^2$. Furthermore, as the bit rate increases, the ratio between the demodulator quadrature coil time delay and the bit interval will decrease and the non-coherent demodulator performance will further approach that of the limiter-discriminator.

For a fixed carrier frequency the worst-case of the irreducable error rate will take place at the highest vehicle speed. Assuming this to be 70 mile/hour, the fading rate in the VHF band (68-174MHz) will be (7.12-18.2Hz). Under these conditions, assuming that an MSK signal is being transmitted at a rate of 2.4kbit/sec (ie. 5kHz channel), the irreducible probability of error of the non-coherent demodulator, calculated from Fig 5.14, will be (3×10^{-5} - 2×10^{-4}) respectively. This will be reduced to approximately (4.8×10^{-6} - 3.2×10^{-5}) at 6kbit/sec (ie. 12.5kHz channel). In the UHF band (425-470MHz) the fading rate given a vehicle speed of 70 mile/hour will be (44.47-49Hz). The irreducible probability of error will be approxiamtely 1.5×10^{-3} at 2.4kbit/sec (ie. 5kHz channel), 2.4×10^{-4} at 6kbit/sec (ie. 12.5kHz channel) and 6×10^{-5} at 12kbit/sec (ie. 25kHz channel).

The average signal to noise ratio $(E_b/N_o)_o$ at the demodulator input is unlikely to be higher than 28dB, as this will require excessive transmitter power. For values of $(E_b/N_o)_o$ < 28dB the probability of error due to slow non-selective Rayleigh fading is higher than 10^{-3} (Fig 5.13(a),(b)). Therefore, under this condition and given the previous estimations of the non-coherent demodulator irreducible probability of error due to random FM noise, it can be

concluded that the random FM noise represents a lower bound on the non-coherent demodulator probability of error performance in all cases of bit rate and channel bandwidths except in the UHF band with a 5kHz channel (2.4kbit/sec). However, the non-coherent demodulator will almost produce the minimum irreducible probability of error compared to any other demodulator, unless diversity or another technique is used to reduce or eliminate the effect of random FM noise, where the benefit will be common to all demodulators. Furthermore, the introduction of 5kHz channels, when it takes place, is likely to start at the VHF band because it is easier to achieve the required frequency stability at this frequency as compared to the UHF band.

On the transmitter side the suitability of the polar loop transmitter for the linear power amplification of the MSK signal without causing any change in the demodulator's performance has been practically demonstrated. On the other hand, if a conventional linear power amplifier is to be used, the small envelope fluctuations of the MSK signal will relax the linearity requirement of the amplifier compared with conventional PSK systems.

Finally, as was mentioned in Chapter 3, the same coherent demodulator used for demodulating the MSK signal can be used with the highly spectrally efficent and constant envelope partial response, TFM signal[15] with a loss in performance due to the nature of the TFM signal of 1dB. However, postmodulation filtering of an MSK signal, together with a polar loop transmitter, can achieve the same ultimate objective of the TFM technique with simpler hardware and slightly narrower spectrum. The postfiltered MSK signal spectrum shows better

efficiency than the TFM signal as can be seen in Fig 5.9, and the polar loop transmitter will achieve the same power efficiency as that of a Class C power amplifier. The degradation in MSK performance for this severe band limiting is 1dB, thus making its performance equivalent to that of TFM. The addition of a single analogue IF signal processor in the case of the polar loop transmitter is considerably simpler than the amount of digital and analogue signal processing circuits described in [15] needed to achieve precise partial response signalling. Furthermore, in the case of TFM coherent demodulation is essential to achieve acceptable performance even in static (ie. non-fading) conditions. This is not the case in MSK where non-coherent detection can be employed even when the signal is bandlimited.

Furthermore, because of the relatively rapid MSK signal spectrum fall-off, the transmitter filter does not have to have a very sharp attenuation at the passband edge, as is the case with the filter used during tests. Hence, it is possible to design a post-modulation filter having more gradual out-of-band attenuation characteristics and consequently less delay distortion, which can ultimately result in an MSK signal whose spectrum efficiency approaches that of TFM without seriously degrading the non-coherent demodulator performance.

APPENDIX 5.1

THE WHITE GAUSSIAN NOISE SOURCE

The white Gaussian noise was obtained at low frequency by operating a Zener diode near the cut-off voltage. This method produces white noise over a wide band which is very close to Gaussian[9]. The noise was later amplified and mixed up with a 10.6MHz carrier (produced by a crystal oscillator) to produce the noise signal at 10.7MHz. A 10.6MHz frequency was used for mixing to exclude the possibility of carrier component interfering with the 10.7MHz MSK signal. The spectrum analyser trace shown below represents two overlapped traces. The first shows the filtered MSK signal spectrum, and the second demonstrates the signal plus noise spectrums both at the receiver input. The white noise property, ie. the flat frequency spectrum, of the source over the bandwidth of interest is evident from this figure.

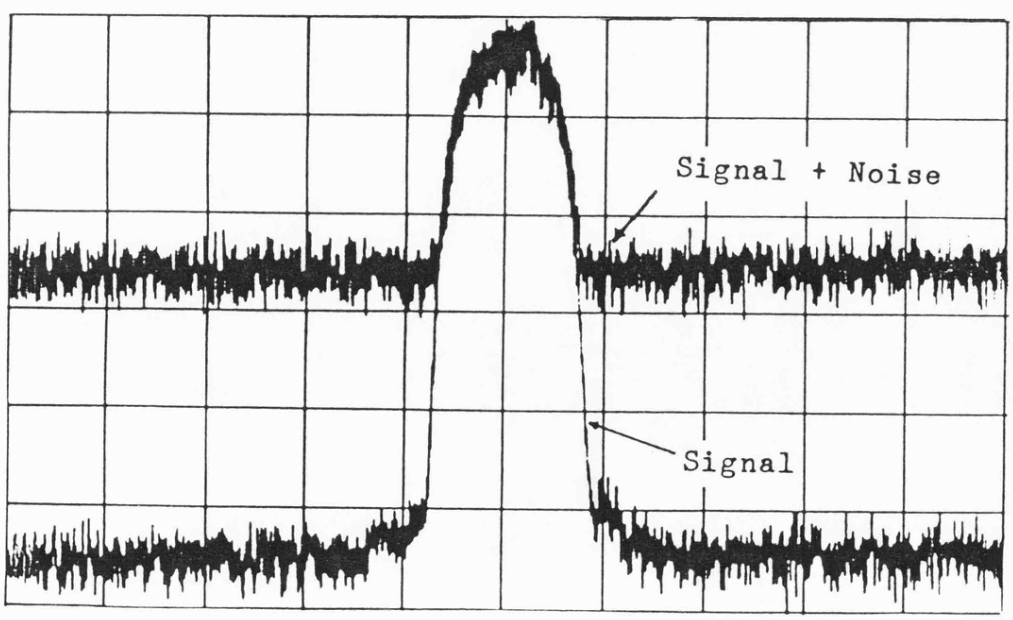

CHAPTER 5: REFERENCES

1. CCITT, Characteristics of distortion and error-rate measuring apparatus for data transmission, Volume VIII - Recommendation V.52.
2. Carlson, A B,: 'Communication systems - an introduction to signals and noise in electrical communication', McGraw-Hill Book Company, 1968.
3. Mathwich, H R, Balccewicz, J F, Hechat, M: "The effect of tandem band and amplitude limiting on the E_b/N_o performance of minimum (frequency) shift keying (MSK)", IEEE, Vol.COM-22, No.10, 1974.
4. Simon, M K, Wang, C C: "Differential versus limiter-discriminator detection of narrow-band FM", IEEE, Vol.COM-31, No.11, 1983.
5. Cruz, J R and Simpson, R S: "Minimum shift-keying detection with noisy reference signals", IEEE, Vol.COM-26, No.6, 1978.
6. Gardner, F M: 'Phaselock Techniques', John Wiley & Sons Inc., 1979.
7. Rohde, V L: 'Digital PLL frequency synthesizers - theory and design', Prentice-Hall Inc., 1983.
8. Petrovic, V and Gosling, W: "A radically new approach to SSB transmitter design", Conf. on Radio Transmitters and Modulation Techniques, IEE, London, England, 1980.
9. Arnedondo, G A, Chriss, W H and Walker, G H: "A multipath fading simulator for mobile radio", IEEE, Vol.COM-21, No.11, 1973.
10. Anderson, R R, Bennett, W R, Davey, J R and Salz, J: "Differential detection of binary FM", The Bell System Technical Journal, January 1965.
11. Spilker, J J: 'Digital communications by satellite', Prentice-Hall Inc., 1977.

12. Garrett, A R: "The effect of impulsive noise on a radio data receiver", MSc Thesis, University of Bath, 1976.

13. Allen, G: "The application of sideband diversity to mobile radio", PhD Thesis, University of Bath, 1978.

14. Linear Integrated Circuits, Motorola Semiconductors, 1981-82.

15. de Jager, F and Dekker, C B: "Tamed frequency modulation: a new method to achieve spectrum economy in digital transmission", IEEE, Vol.COM-26, No.5, 1978.

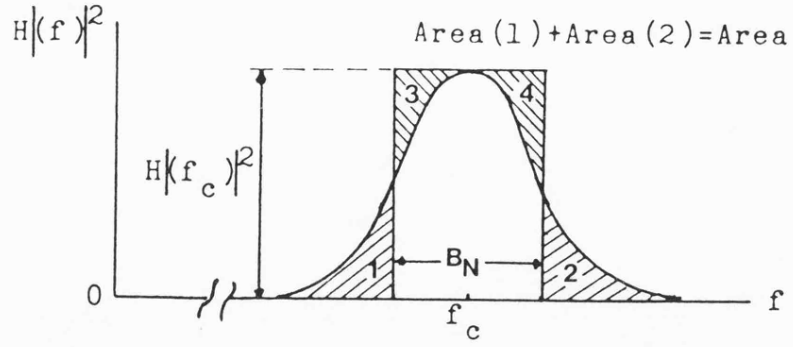

Figure 5.1 Noise Equivalent Bandwidth B_N of a Bandpass Filter.

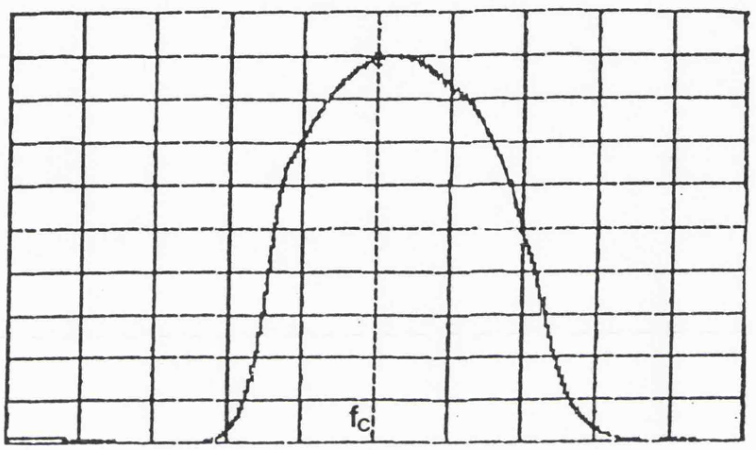

Centre Frequency f_c= 455KHz , Horizontal: 2KHz/Div.
Vertical: Linear Scale.

Figure 5.2 MSK Demodulator IF Filter Amplitude Characteristics |H(f)|.

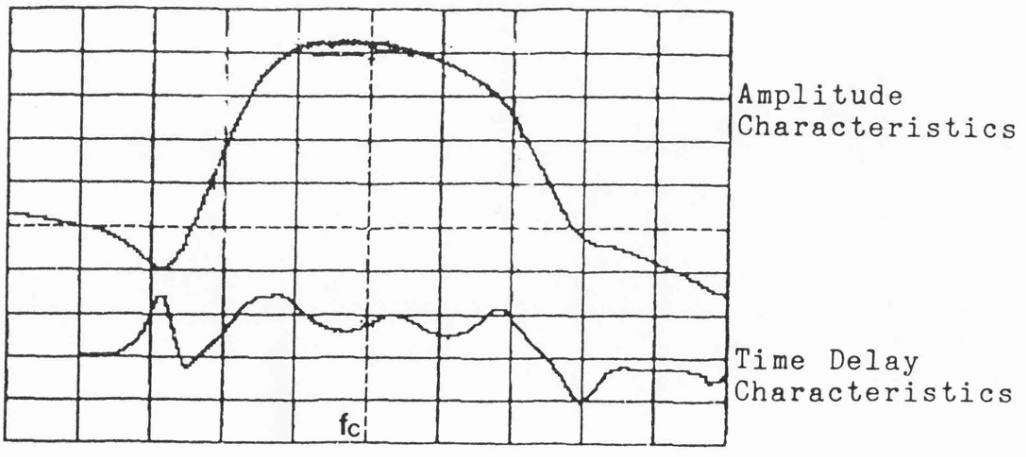

Centre Frequency f_c=455KHz , Horizontal: 2KHz/Div.
Vertical:Amplitude-10dB/Div. , Time delay-200nSec/Div.

Figure 5.3 MSK Demodulator IF Filter Characteristics.

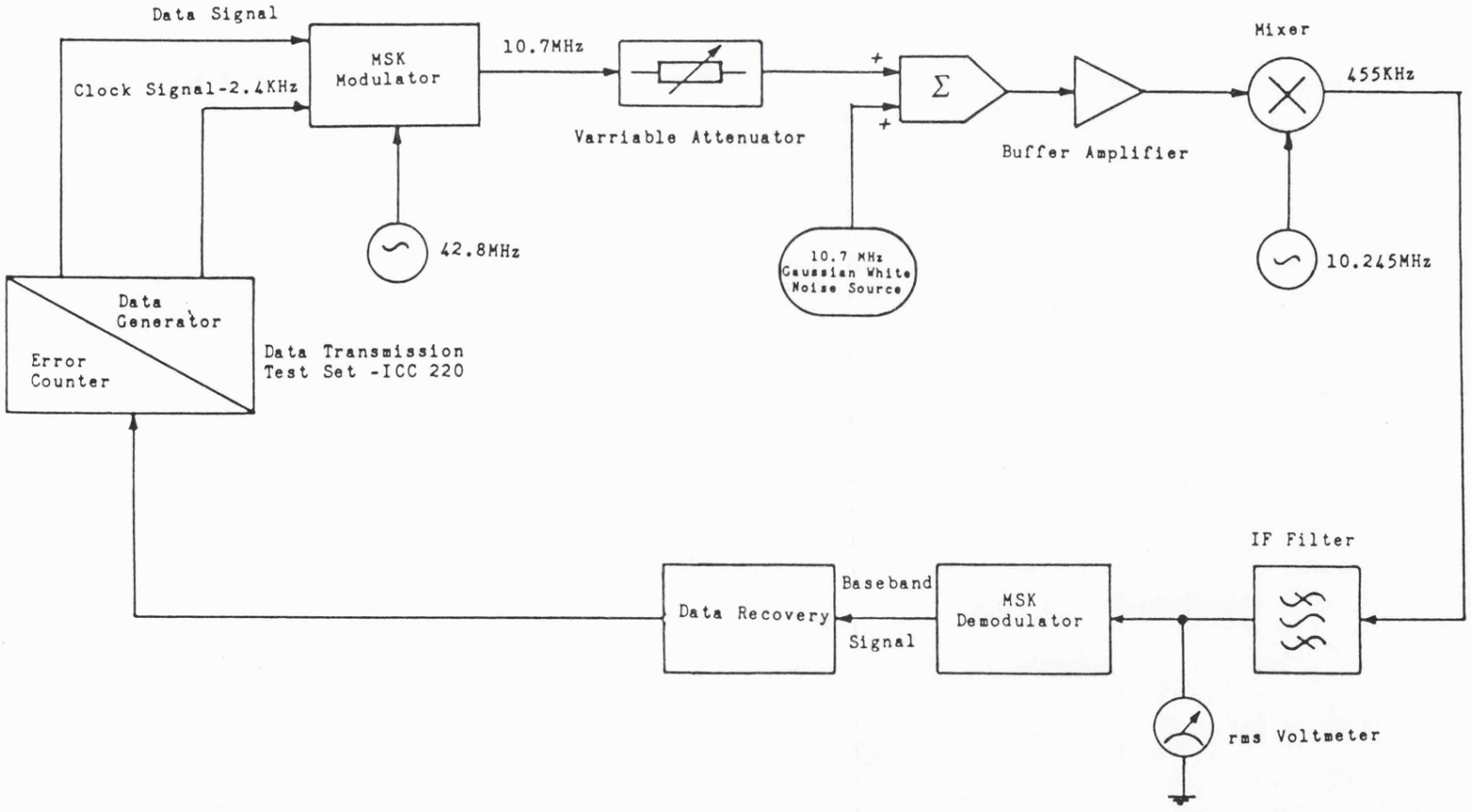

Figure 5.4 Block Diagram of Experimental set-up to Measure MSK System Wideband Performance in Presence of AWGN.

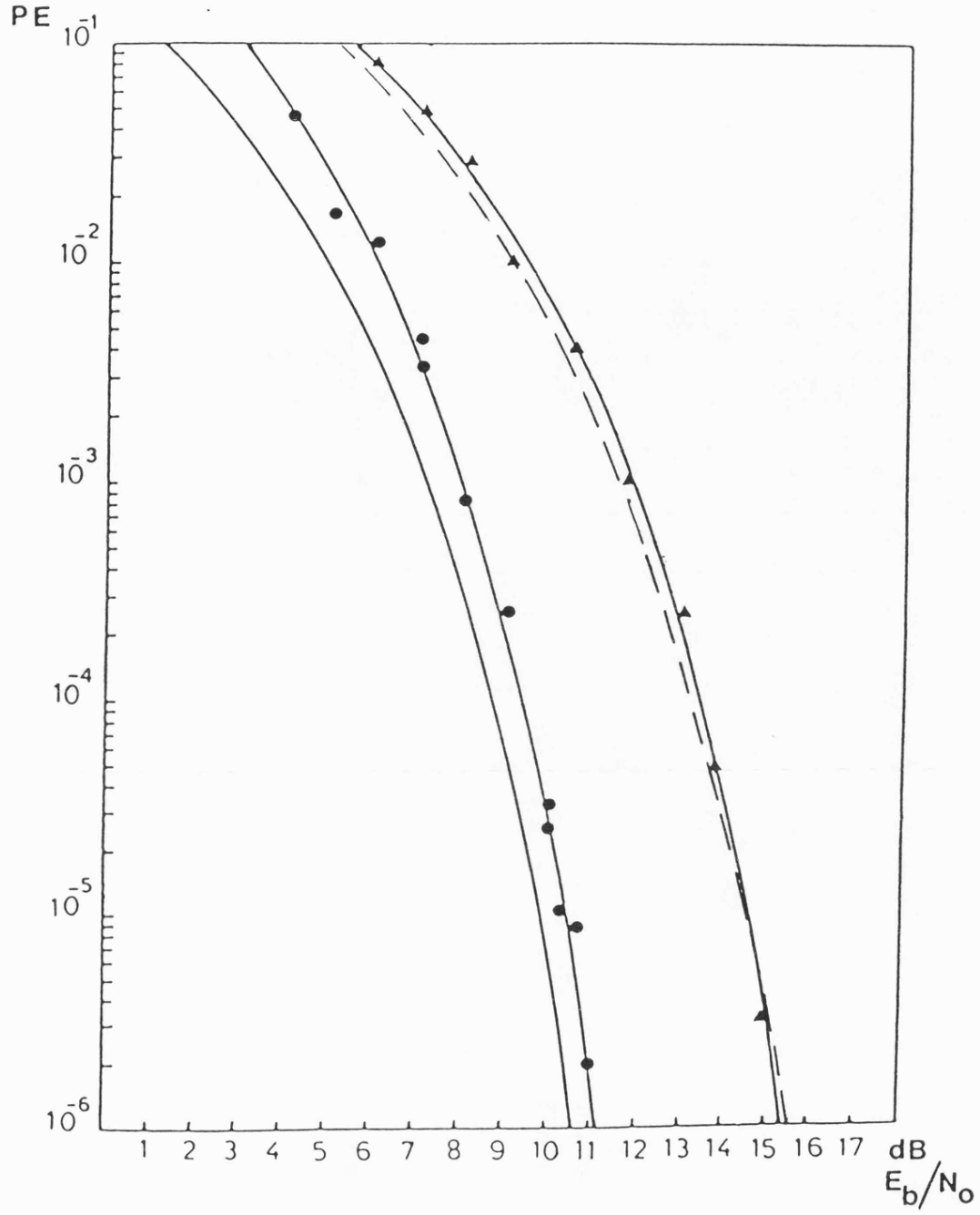

Practical : ● Coherent Demodulator-ω_n= 10 rad/Sec.

▲ Noncoherent Demodulator-B_N= 2.33 f_b.

Theoretical:——— DEMSK.

------- Limiter Discriminator & Differential Detectors-CPFSK(h=0.5)-B_N= 2 f_b.

Figure 5.5 Theoretical & Practical Performances of MSK in Presence of Additive White Gaussian Noise (AWGN).

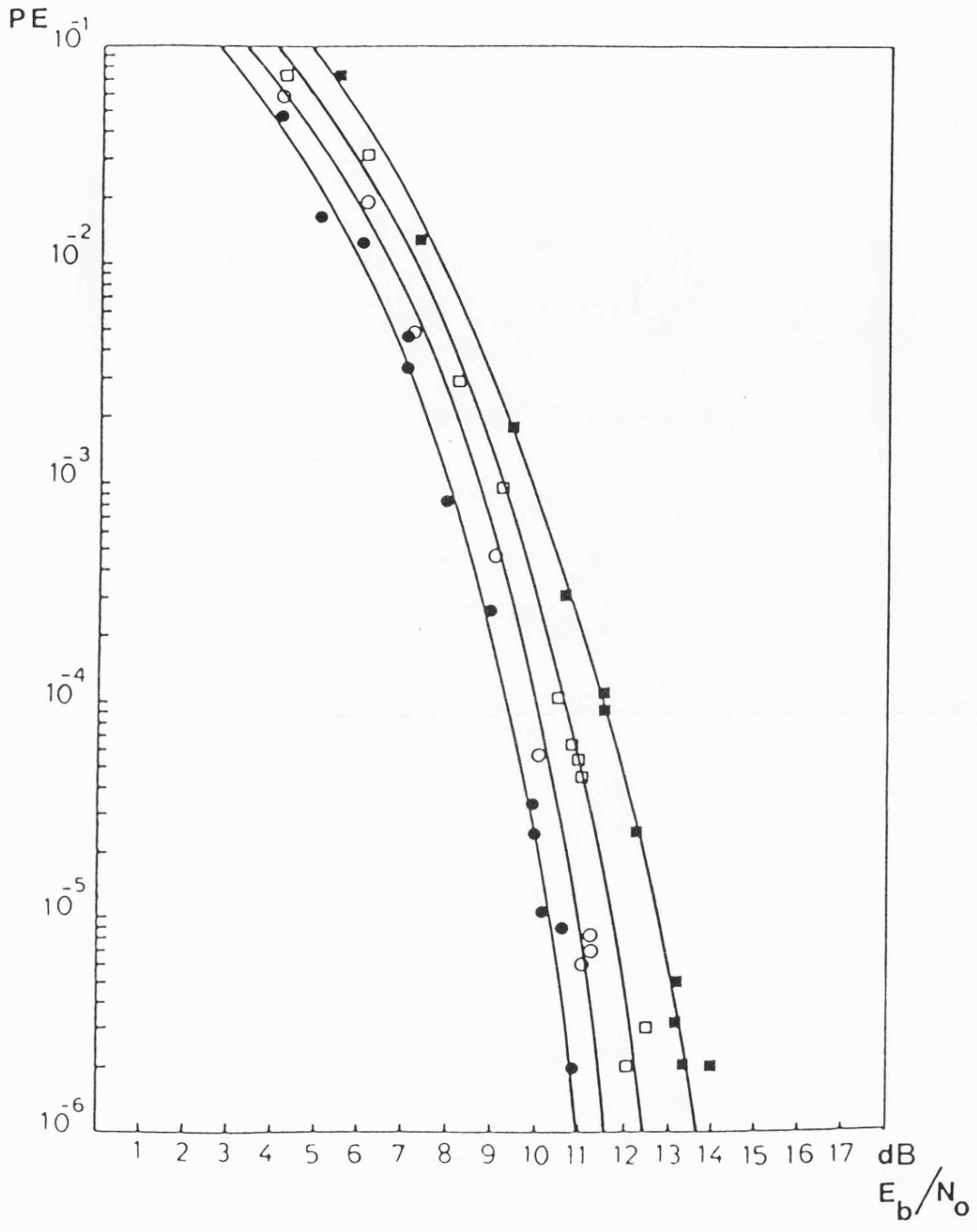

● ω_n=10.0 , ○ ω_n=20.0 , □ ω_n=50.0 , ■ ω_n=100.0 rad/Sec.

Figure 5.6 MSK Coherent Demodulator Performance for Different Values of Reference Recovery PLL's Natural Frequency- ω_n.

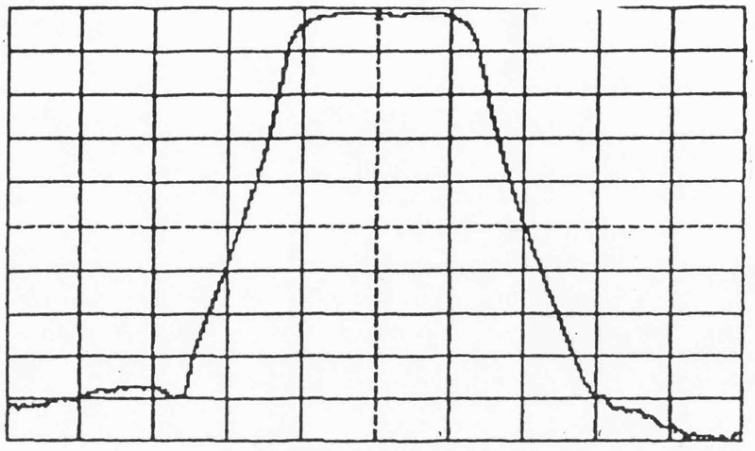

Centre Frequency:10.7MHz , Horizontal:1KHz/Div.
Vertical:10dB/Div.

(a) Amplitude Characteristics.

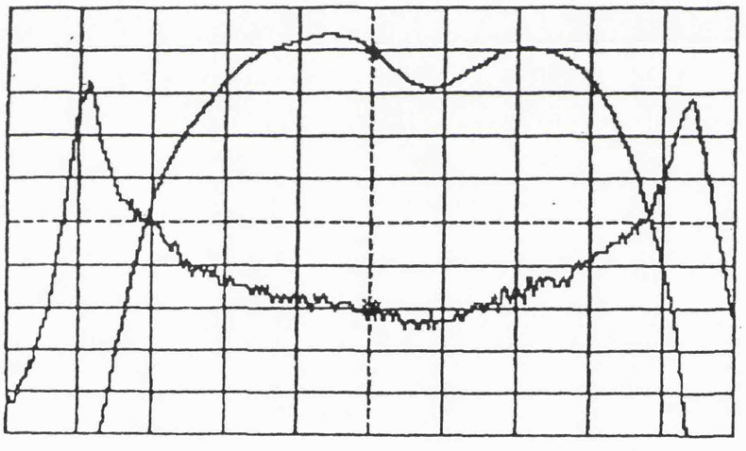

Amplitude.

Time Delay.

Centre Frequency: 10.7MHZ , Horizontal: 300HZ/Div.
Vertical:Amplitude-0.5dB/Div. ,
Time Delay- 200μSec/Div.

(b) Detailed Amplitude & Time Delay Characteristics.

Figure 5.7 Transmitter Filter Characteristics.

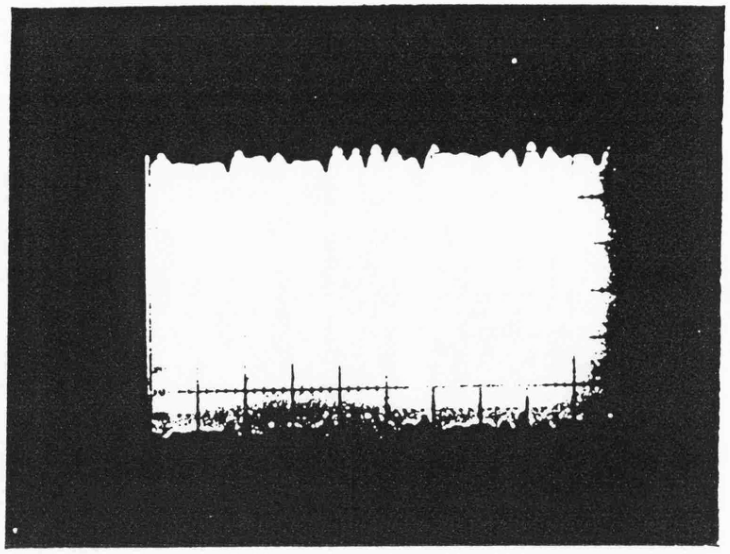

(a) $\frac{B_{3dB}}{f_b} = 2$

(f_b = 1.125 Kbit/Sec)

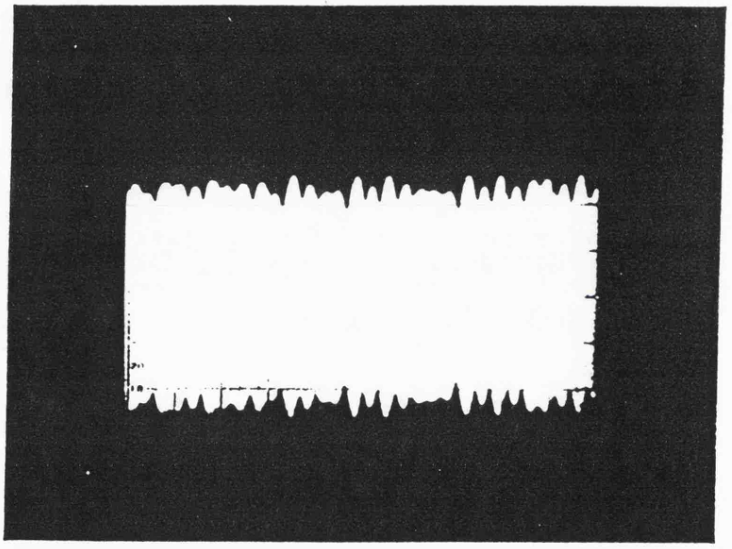

(b) $\frac{B_{3dB}}{f_b} = 1.5$

(f_b= 1.5 Kbit/Sec)

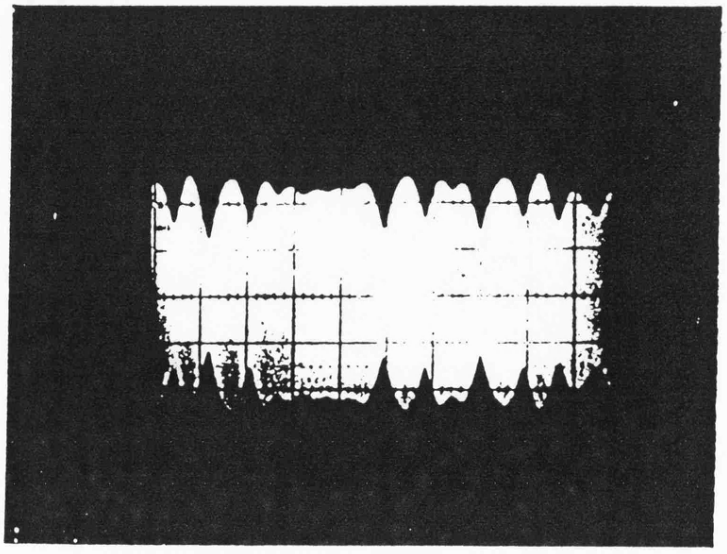

(c) $\frac{B_{3dB}}{f_b} = 0.94$

(f_b= 2.4 Kbit/Sec)

Figure 5.8 Bandlimited MSK Waveform

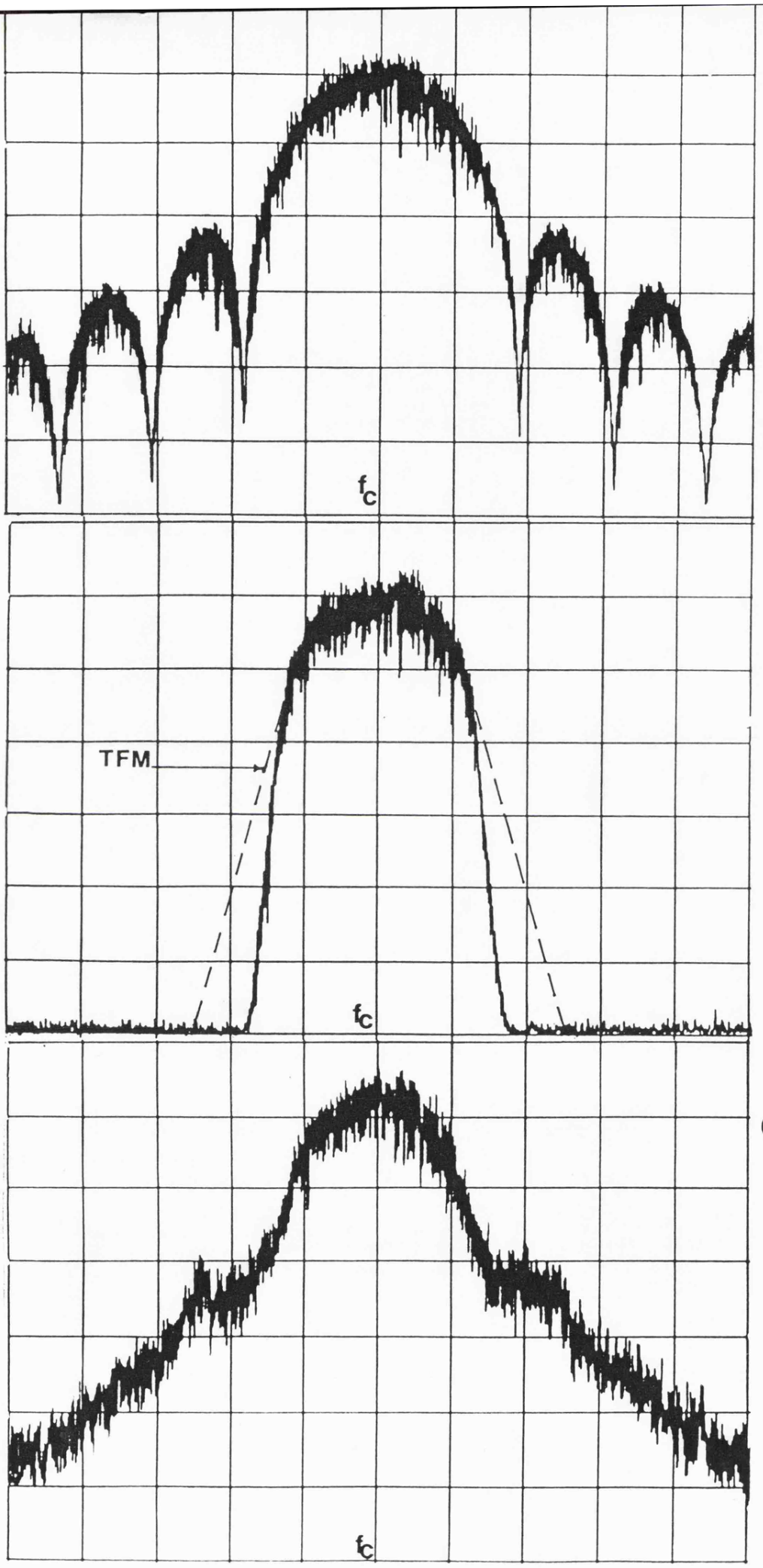

(a) Unfiltered MSK Signal Spectrum. f_c=10.7MHz

All Traces: Horizontal-1KHz/Div. Vertical-10dB/Div.

(b) Filtered MSK Signal Spectrum at The Input & Output of a Polar Loop Transmitter. $B_{3dB}=0.94f_b$ f_c=165MHz Transmitter Power=15Watts (rms)

(c) Filtered MSK Signal Spectrum at a Class C Power Amplifier Output. f_c=165MHz

Figure 5.9 MSK Signal Spectrum.

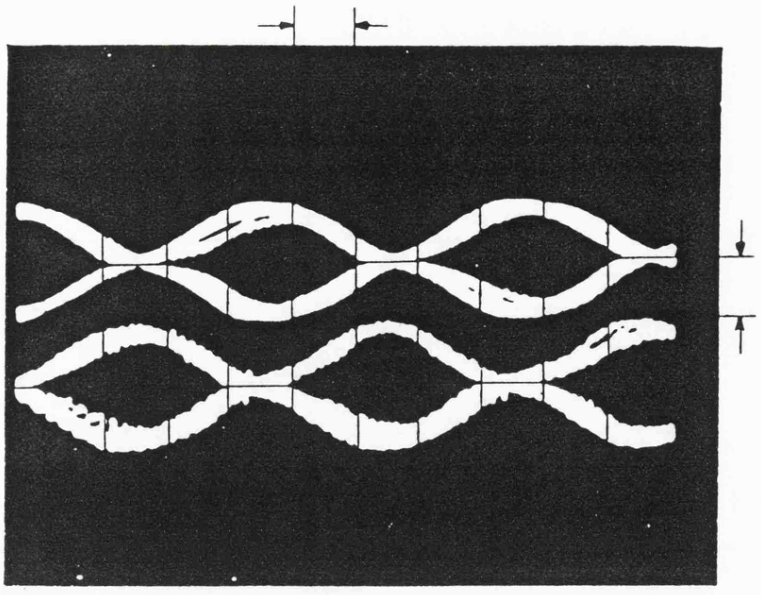

(a) Coherent Demodulator

$\frac{B_{3dB}}{f_b} = 0.94$, $\frac{d}{T_b} = 2.4$

(f_b = 2.4 Kbit/Sec.)

Horizontal: 0.2 mSec/Div.

Vertical : 5V/Div.

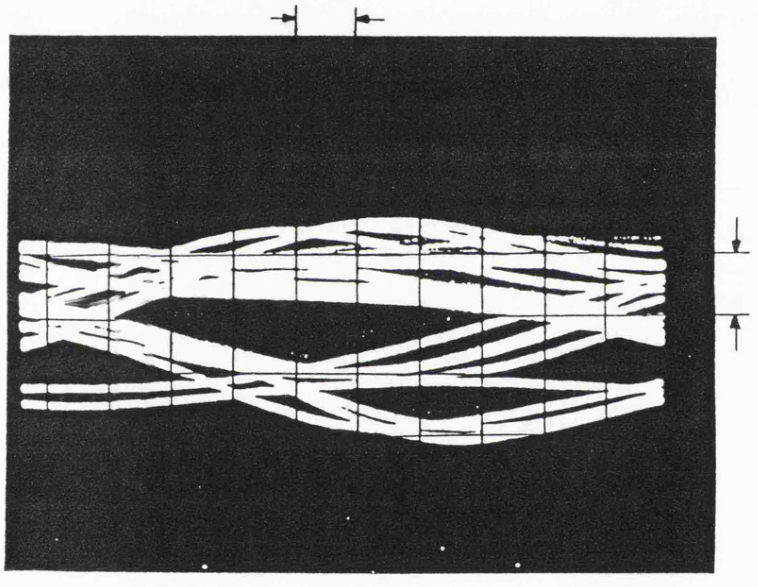

(b) Noncoherent Demodulator

(f_b = 2.4 Kbit/Sec.)

Horizontal: 0.05mSec/Div.

Vertical : 5V/Div.

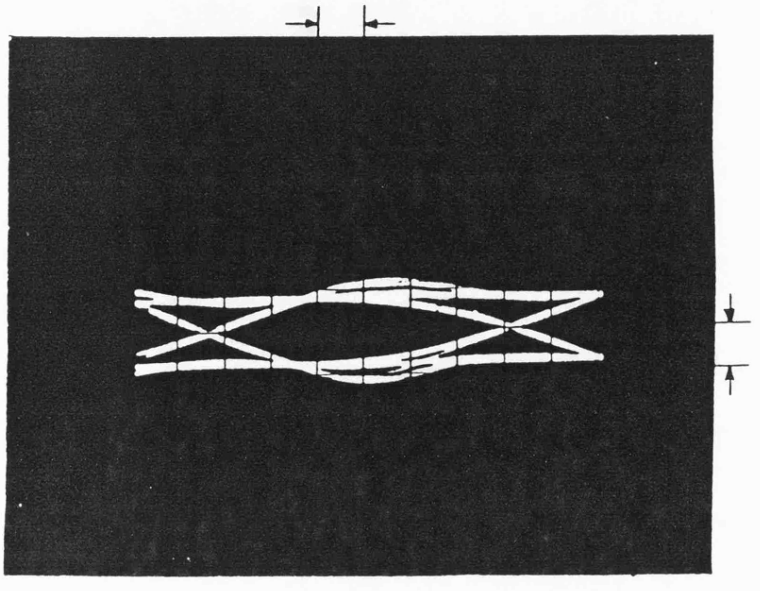

(c) Noncoherent Demodulator

$\frac{B_{3dB}}{f_b} = 1.5$, $\frac{d}{T_b} = 1.5$

(f_b = 1.5 Kbit/Sec.)

Horizontal: 0.1 mSec/Div.

Vertical : 0.5 V/Div.

Figure 5.10 MSK Demodulator Eye Patterns—Bandlimited Signal.

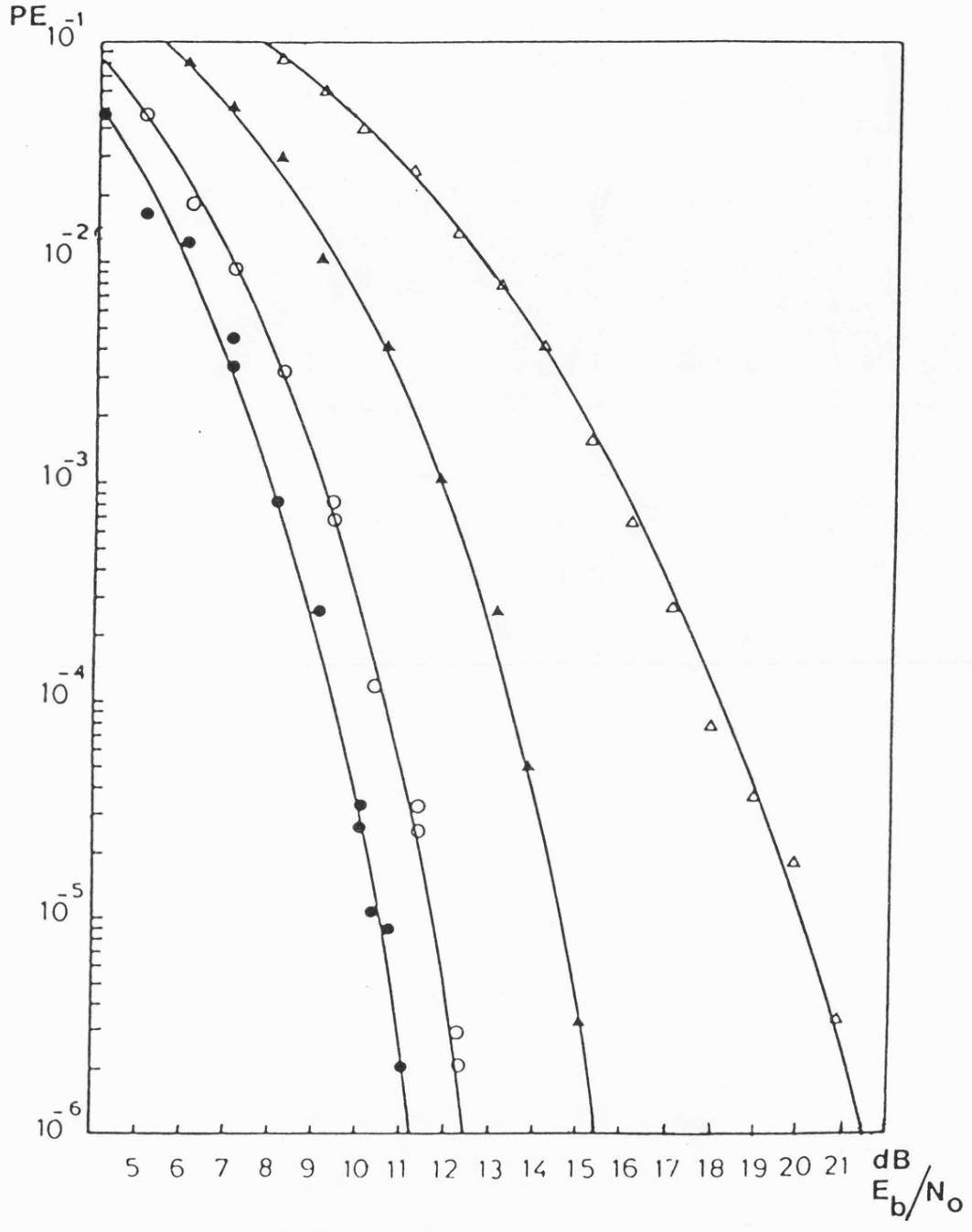

Coherent : ● Unfiltered Signal , ○ Filtered Signal.

Noncoherent: ▲ Unfiltered Signal , △ Filtered Signal.

Figure 5.11 Performance of Bandlimited MSK—
$B_{3dB}/f_b=0.94$, $d/T_b=2.4$.

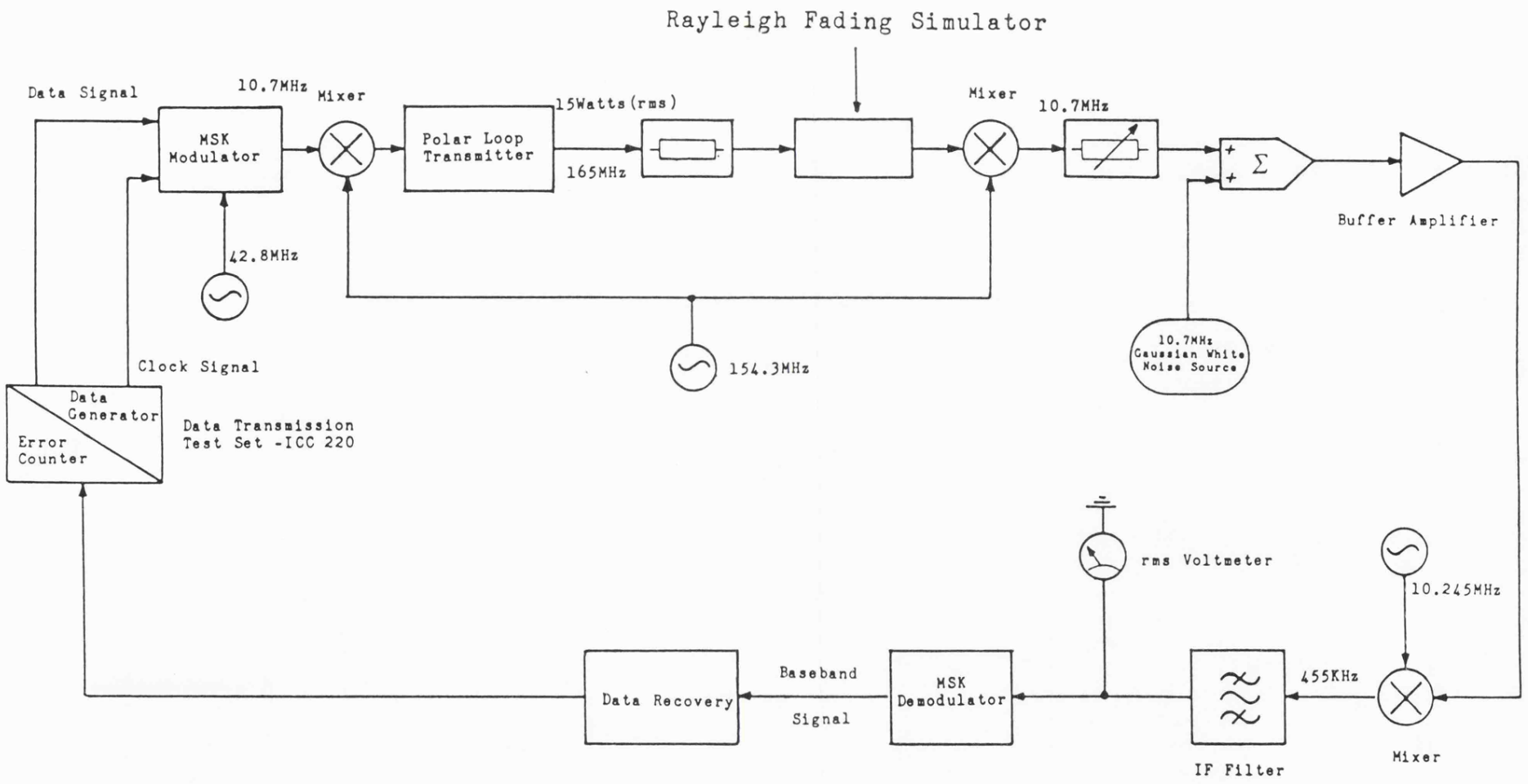

Figure 5.12 Performance Measurment in Presence of Simulated Rayleigh Fading Condition.

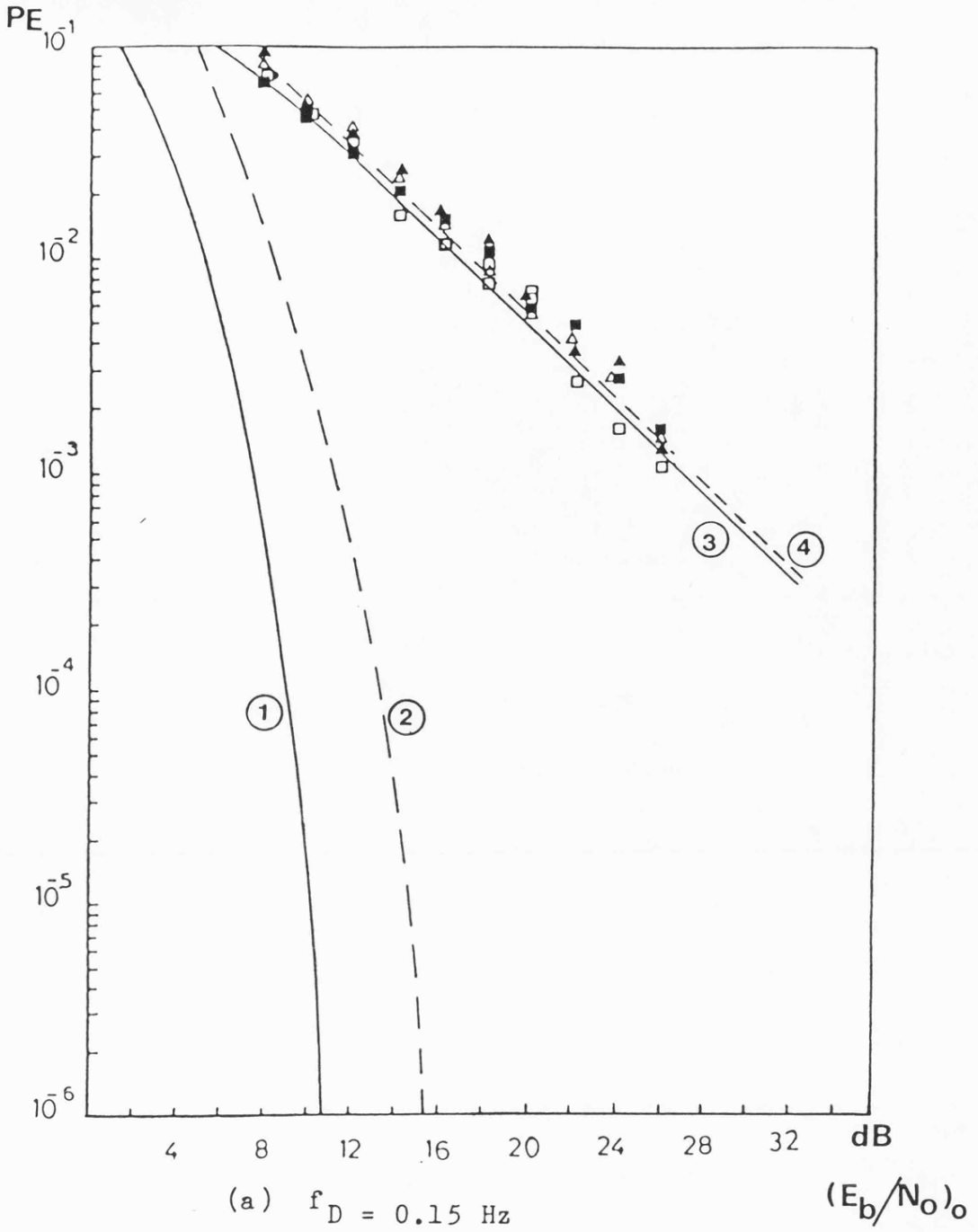

(a) $f_D = 0.15$ Hz

Practical: Coherent: ■ ω_n=10, ▲ ω_n=50, △ ω_n=100 rad./Sec.

Noncoherent: □

Theoretical: ① DEMSK-no Fading.

② Limiter Discriminator & Differntial Detectors CPFSK(h=0.5)-no Fading.

③ DEMSK & Differntial Detector-Fading.

④ Limiter Discriminator Detector-Fading

Figure 5.13 PE Versus $(E_b/N_o)_o$ in Presence of Simulated Slow Nonselective Rayleigh Fading.

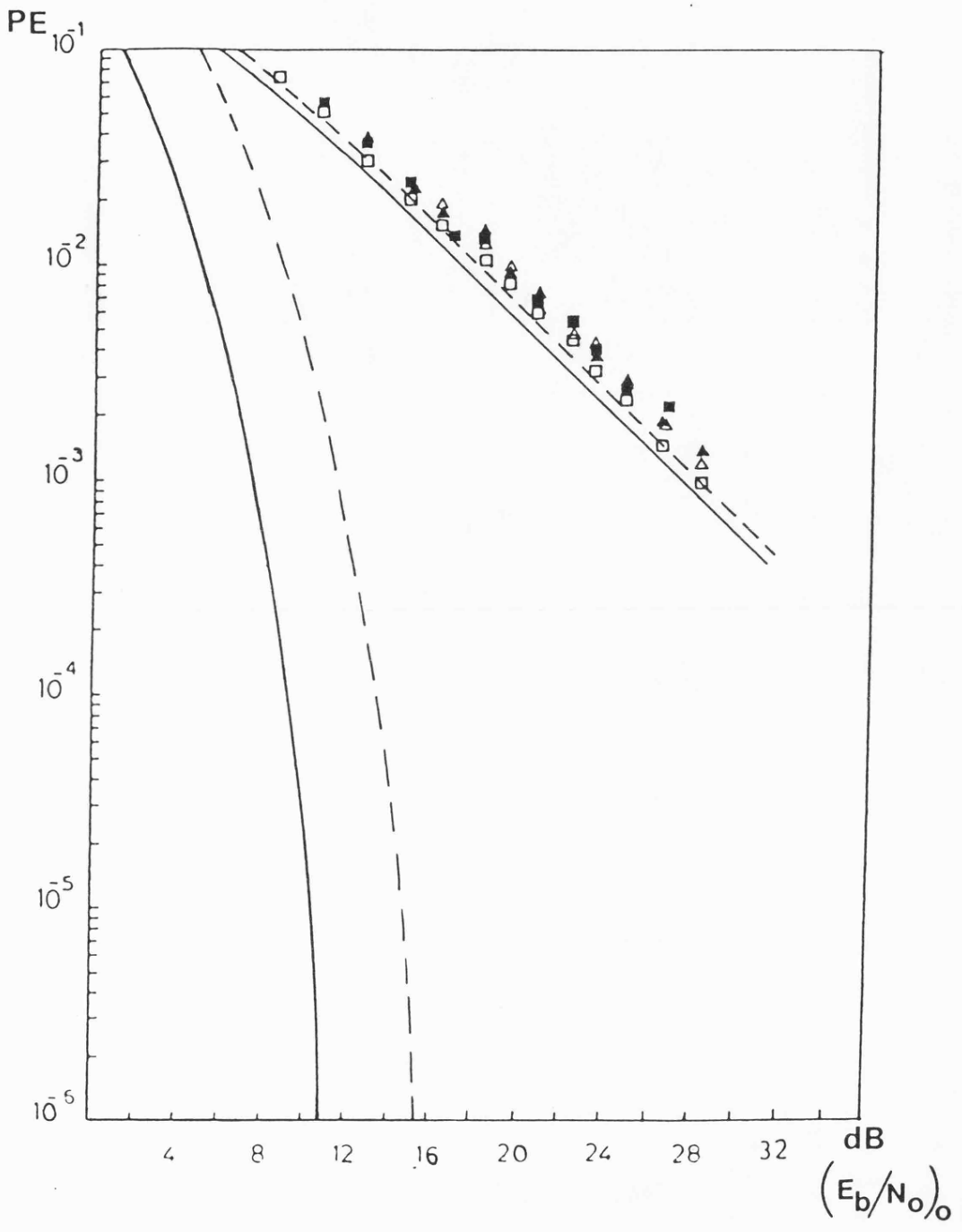

Figure 5.13(b) f_D= 1.0 Hz

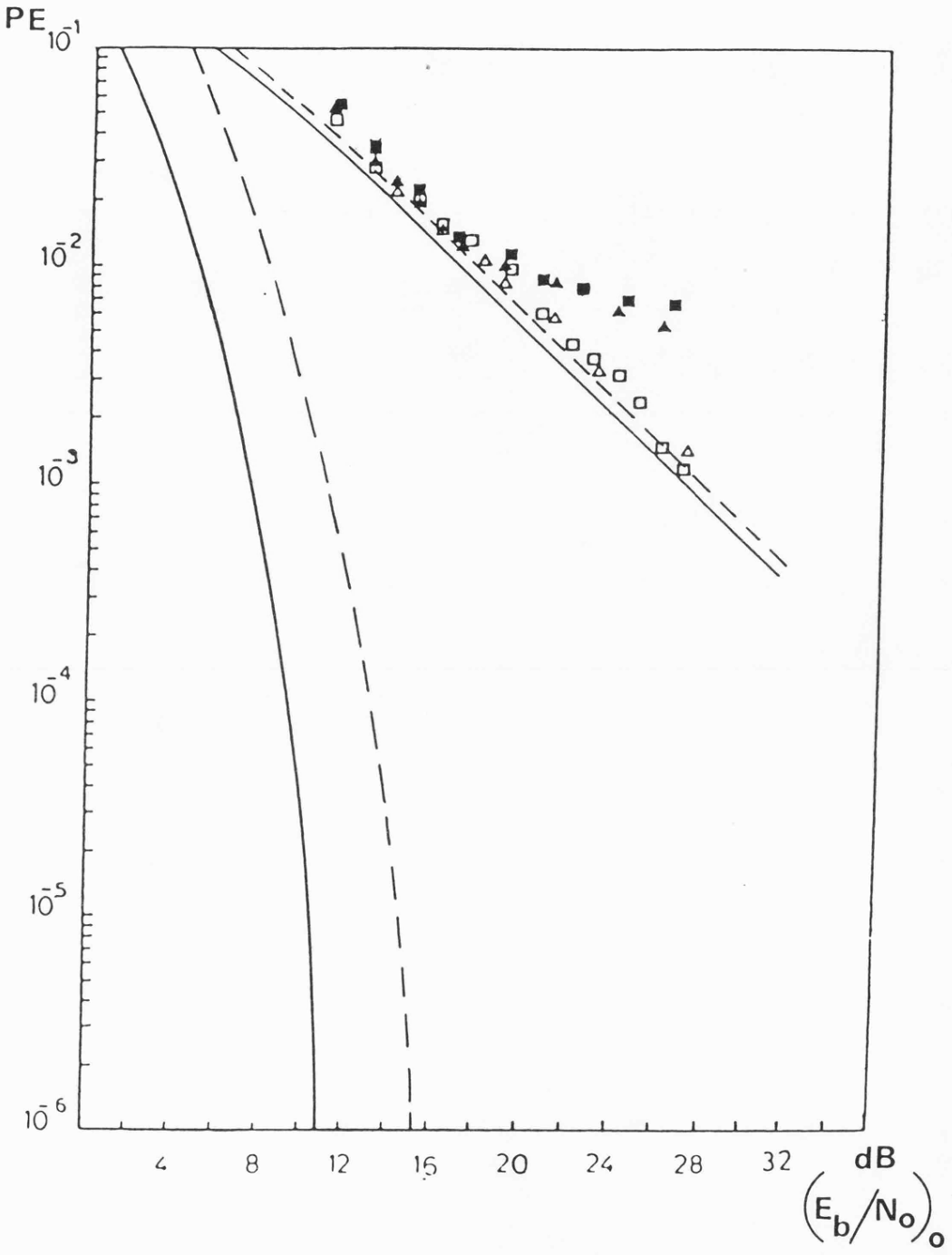

Figure 5.13(c) f_D= 2.0 Hz

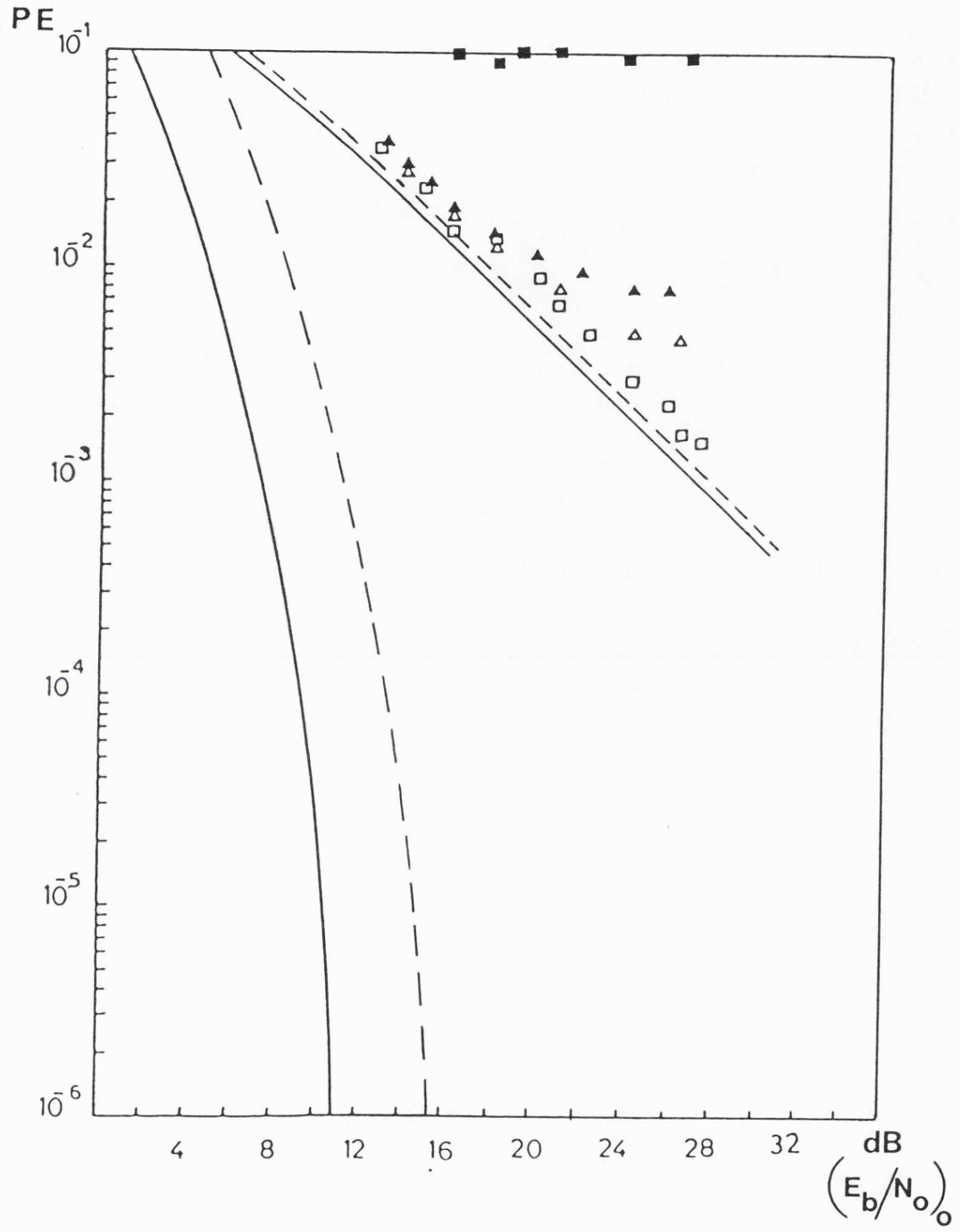

Figure 5.13(d) f_D= 10.0 Hz

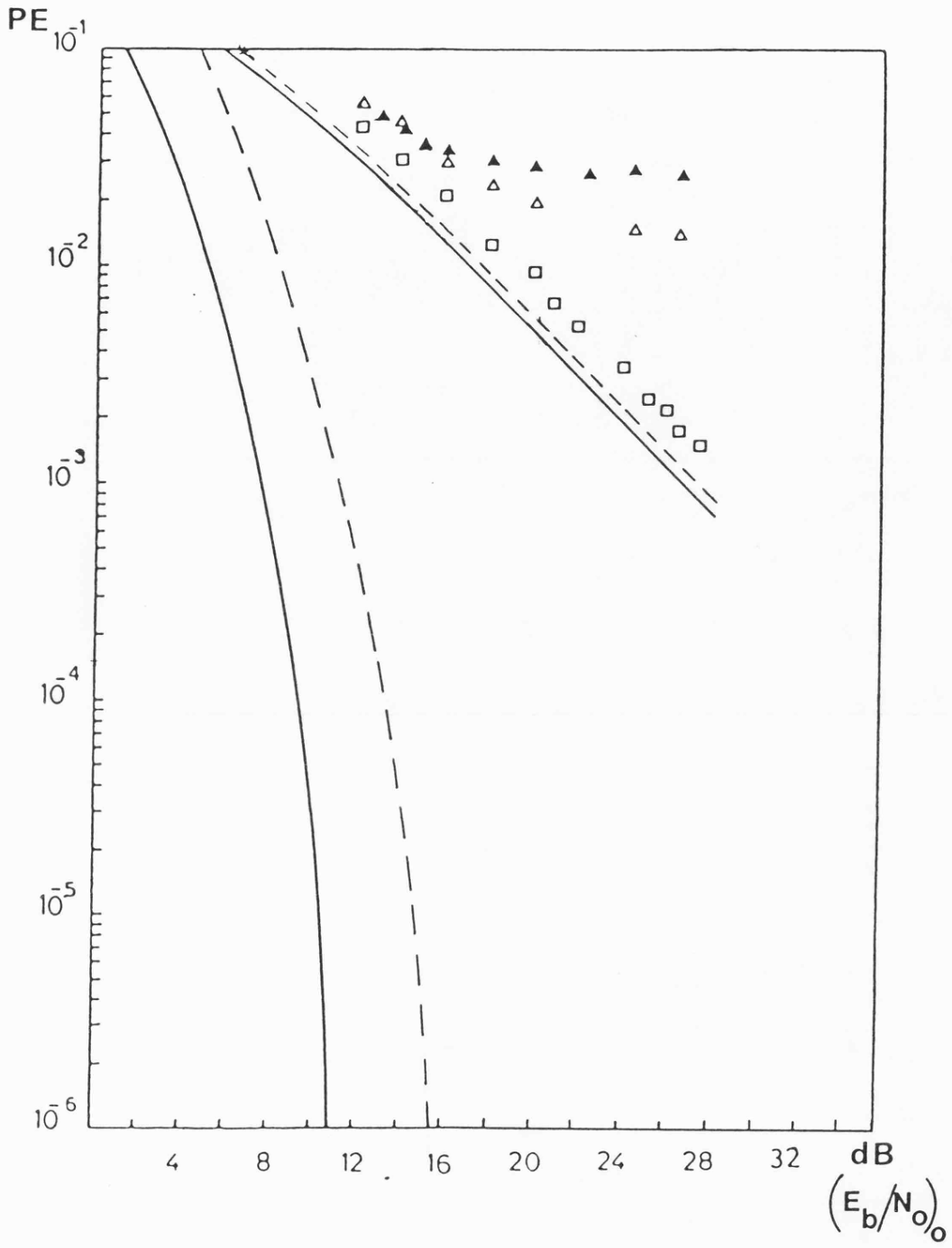

Figure 5.13(e) f_D= 20.0 Hz

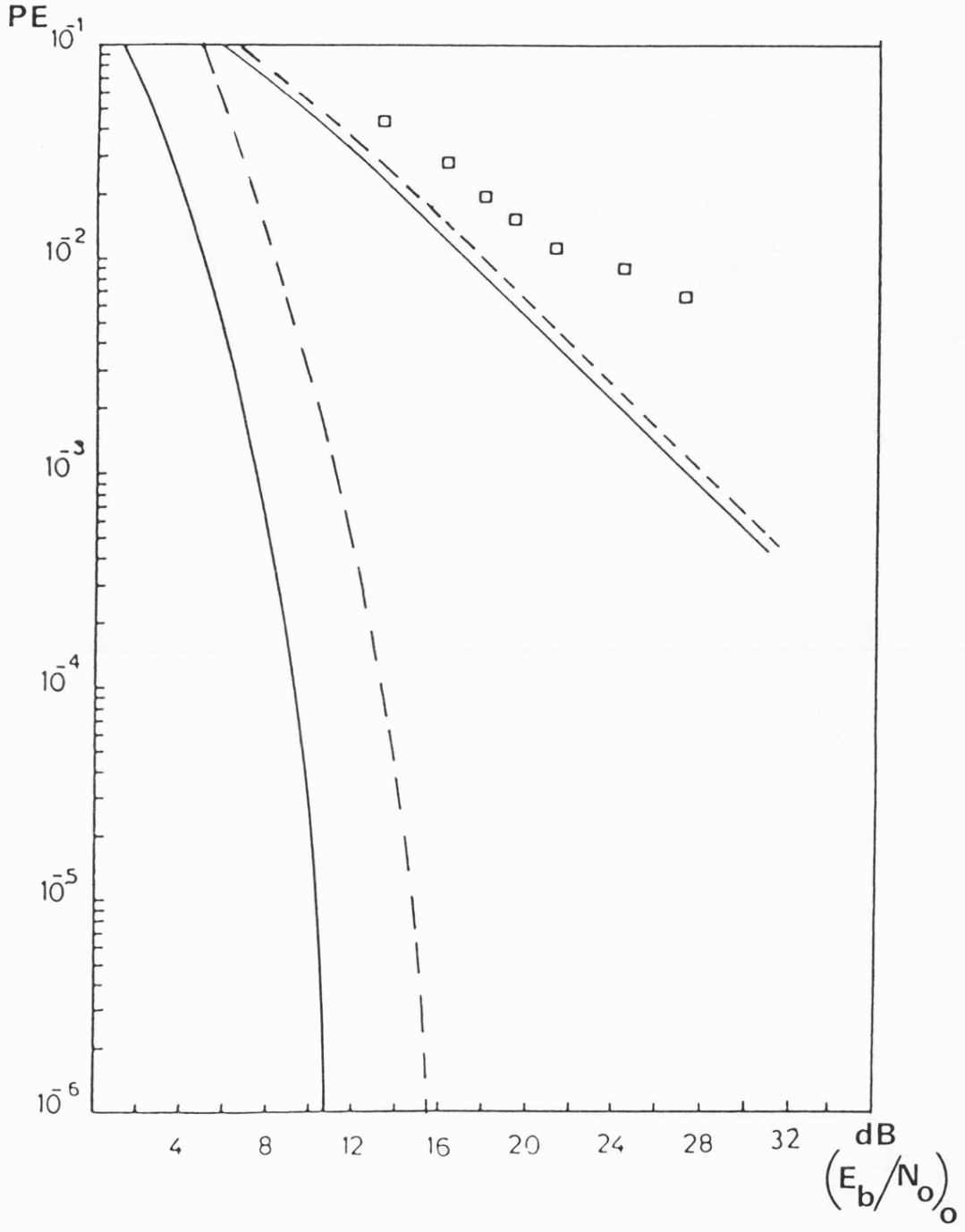

Figure 5.13(f) f_D= 100.0 Hz

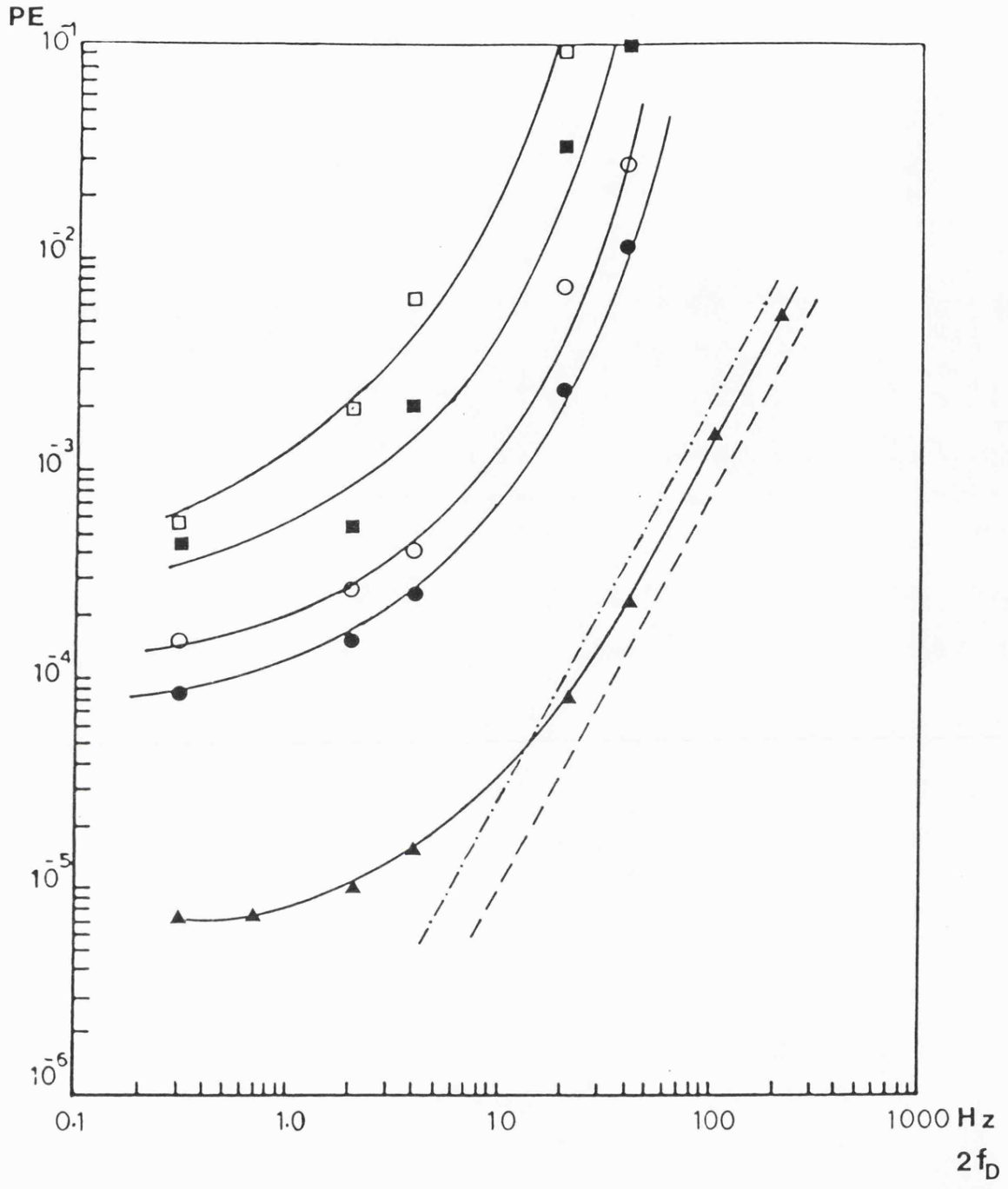

Coherent : ω_n=100 ● , ω_n=50 ○ , ω_n=20 ■ , ω_n=10 □

Noncoherent : ▲

Theoretical :------ Limiter-Discriminator Detector.

------- Differential Detector.

Figure 5.14 Effect of Random FM Noise on Practical and Theoretical Performance of MSK Demodulators.

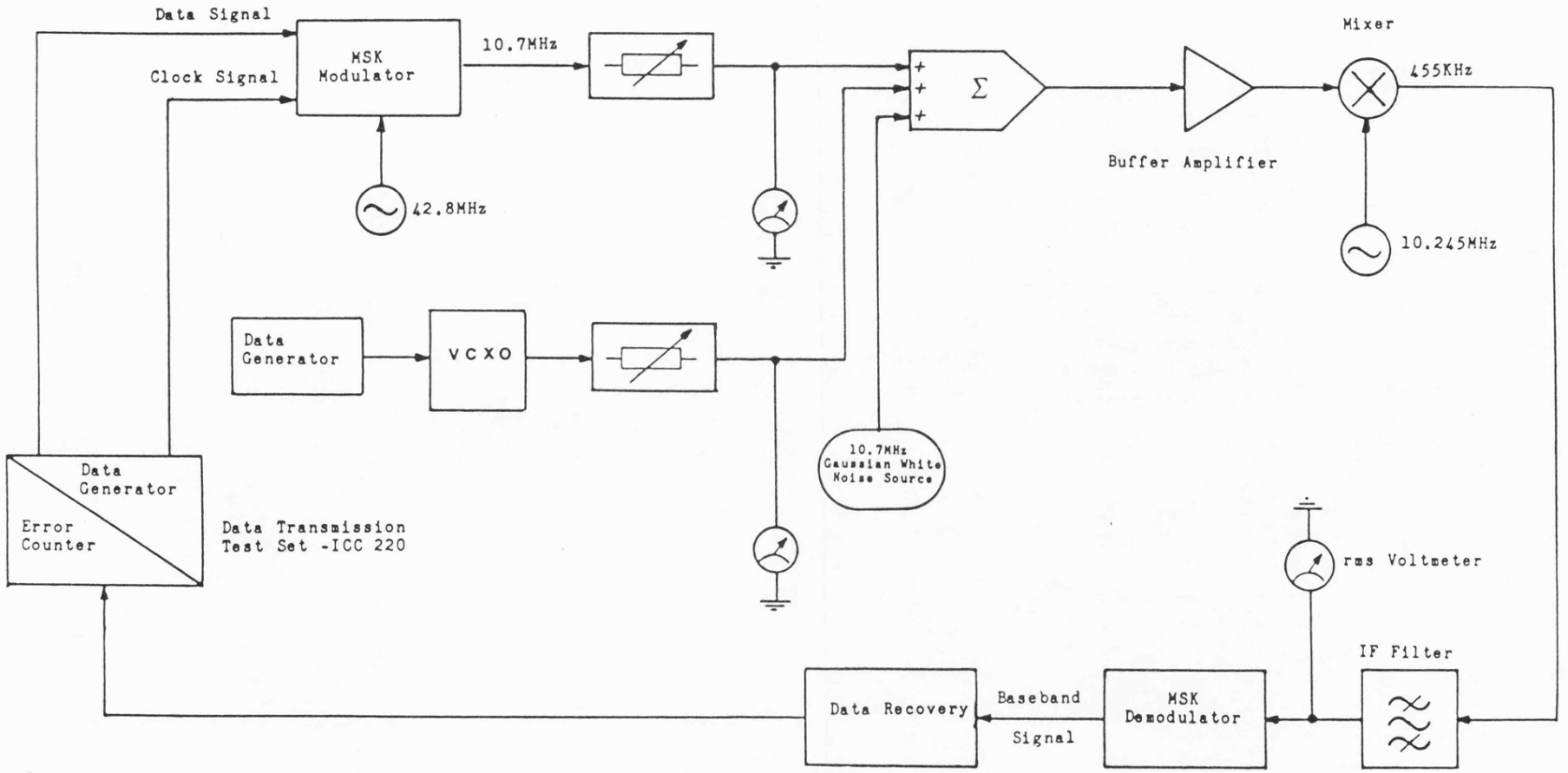

Figure 5.15 Block Diagram of Performance Measurments in Presence of Cochannel or Adjacent Channel Interference.

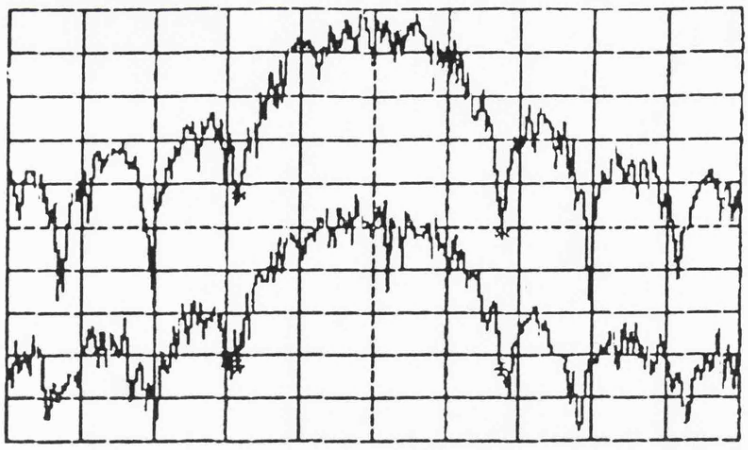

Centre Frequency:10.7MHz, Horizontal:1KHz/Div.,
Vertical:10dB/Div.

Figure 5.16 Inchannel and Cochannel Signals Spectrums.

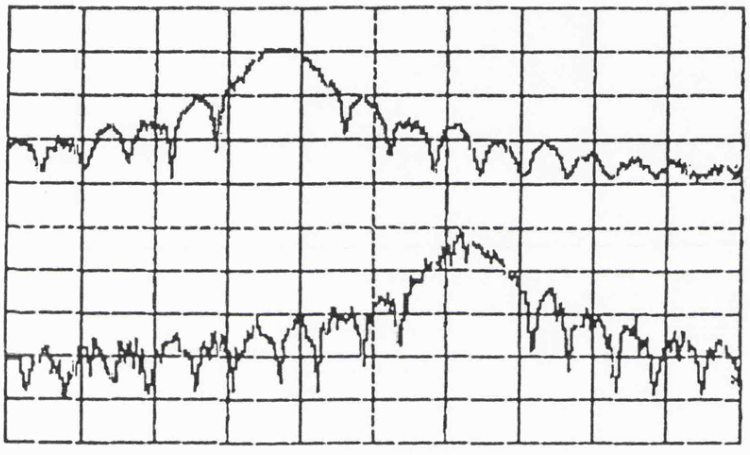

Centre Frequency: 10.7025MHz ,Horizontal: 2KHz/Div. ,
Vertical: 20dB/Div.

(a) Inchannel and Adjacent Channel Signals Spectrums.

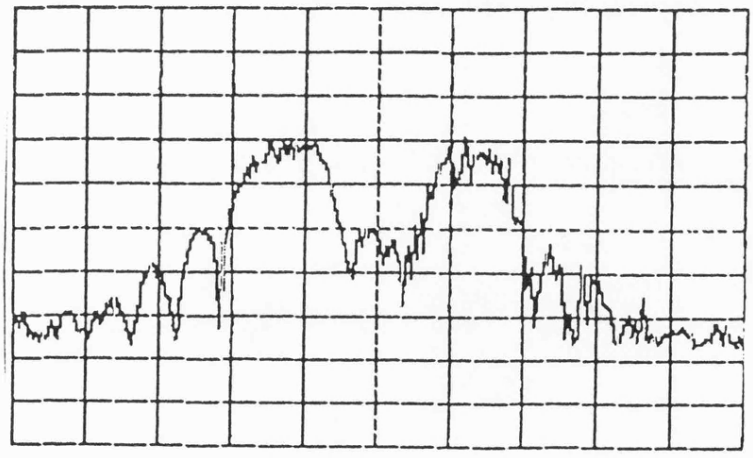

Centre Frequency & Horizontal as in (a) ,Vertical: 10dB/Div.

(b) Spectrum at the Receiver Input.

Figure 5.17 Adjacent Channel Interference.

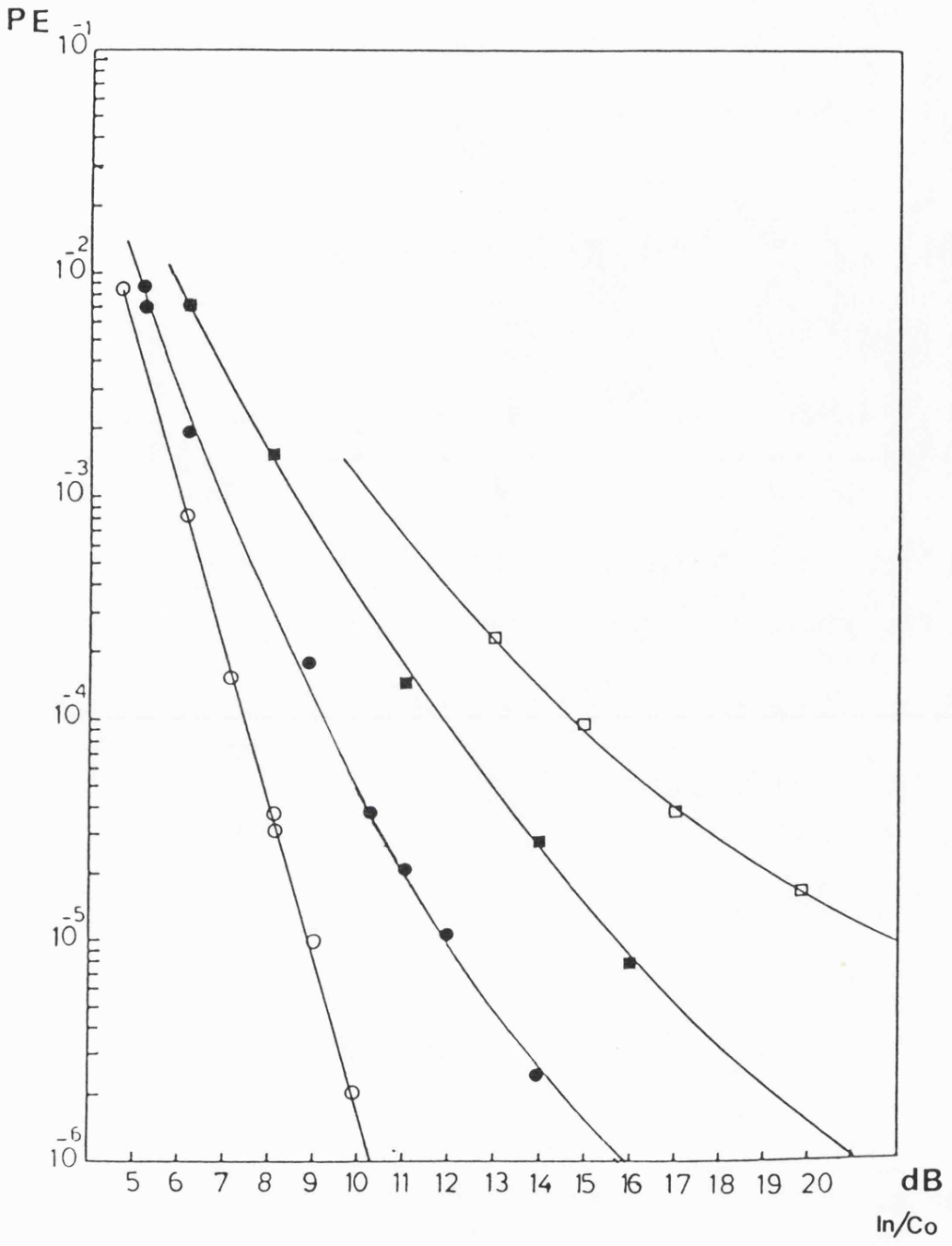

○ E_b/N_o=14.7dB, ● E_b/N_o=12.7dB, ■ E_b/N_o=11.7dB, □ E_b/N_o=10.7dB.

Figure 5.18(a) Effect of Cochannel Interference on Coherent Demodulator Performance (ω_n=10 rad/sec.).

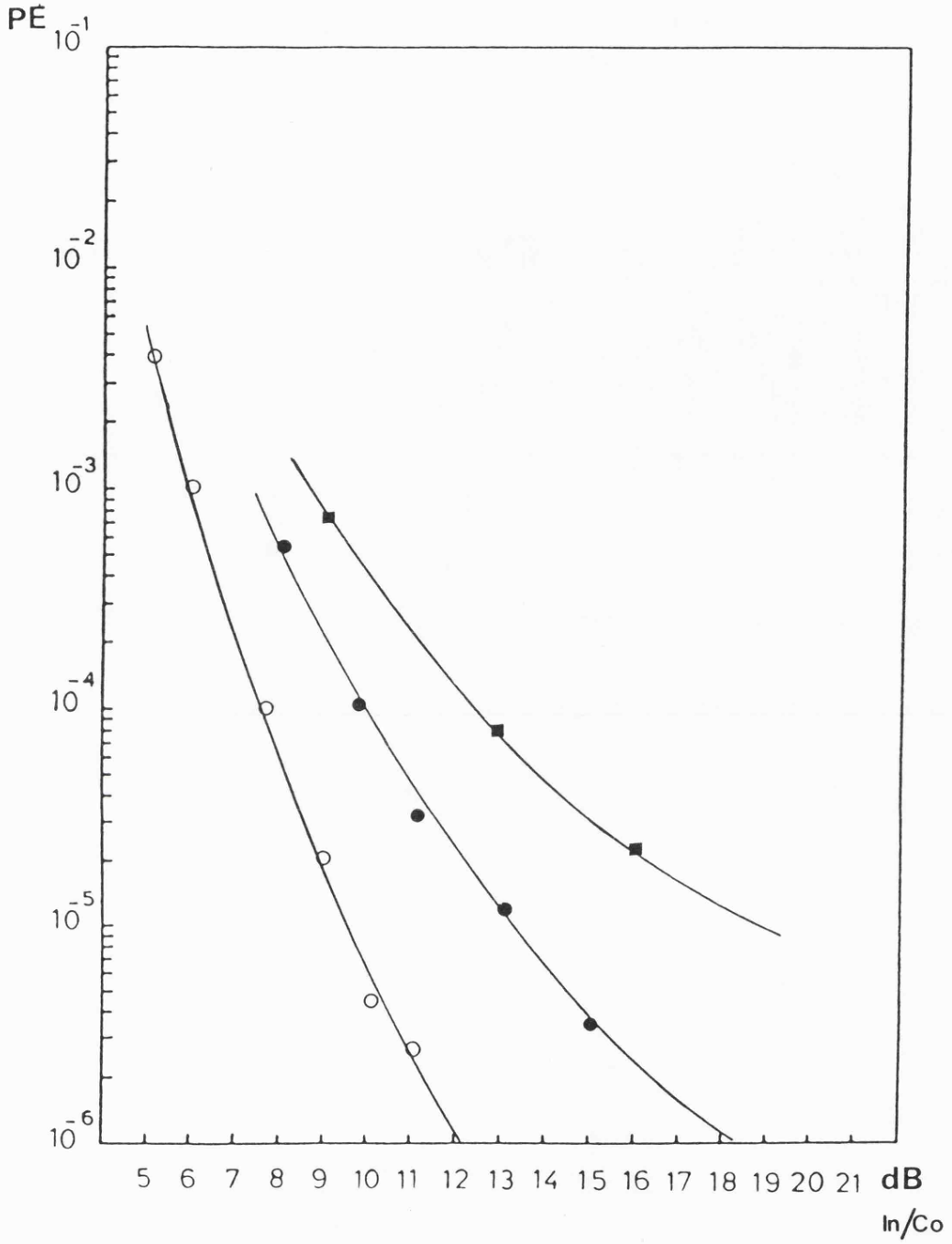

○ E_b/N_o=16dB, ● E_b/N_o=14dB, ■ E_b/N_o=13dB .

Figure 5.18(b) Effect of Cochannel Interference on coherent Demodulator(ω_n=100)Performance.

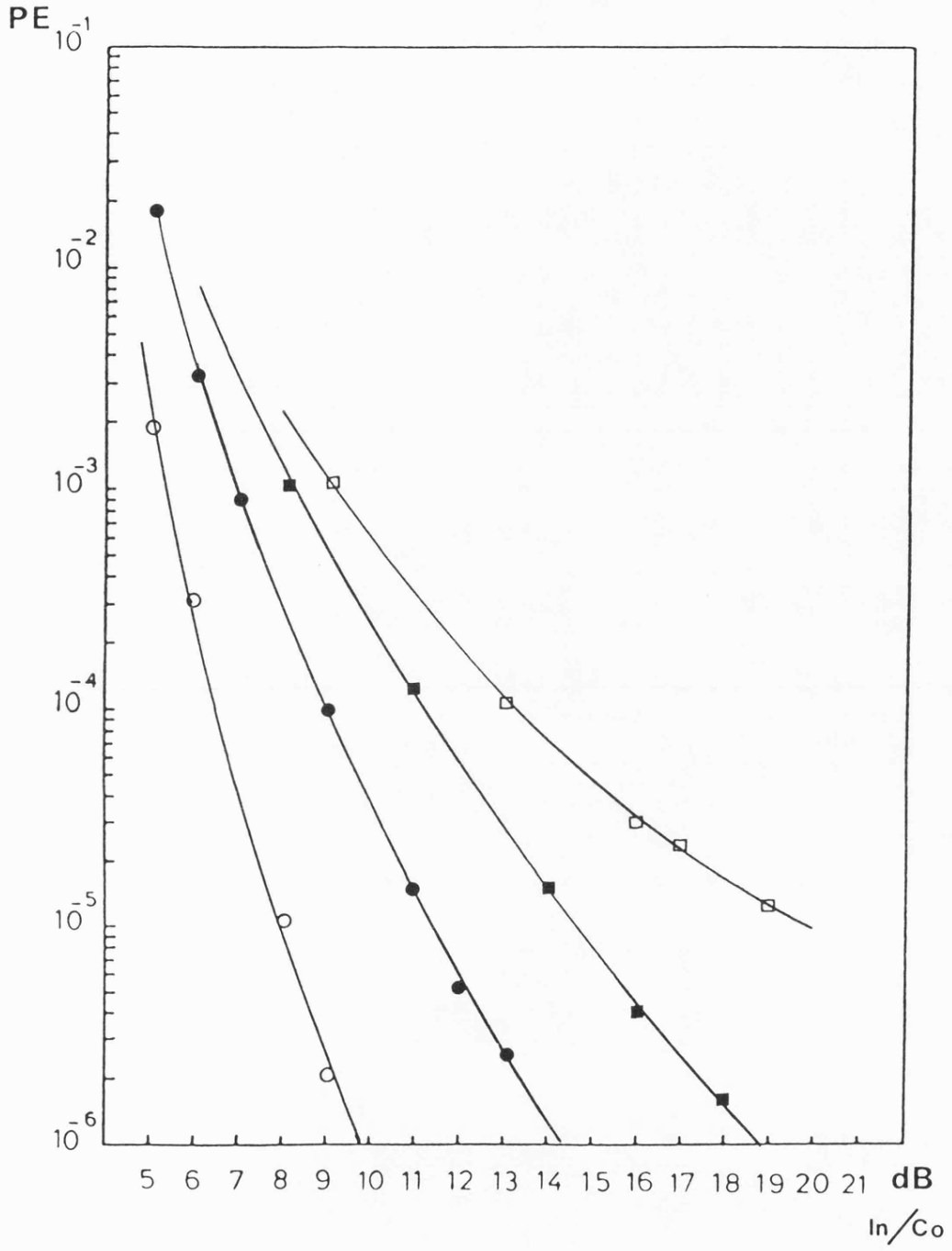

○ E_b/N_o=19dB, ● E_b/N_o=17dB, ■ E_b/N_o=16dB, □ E_b/N_o=15dB .

Figure 5.18(c) Effect of cochannel Interference on Noncoherent Demodulator Performance.

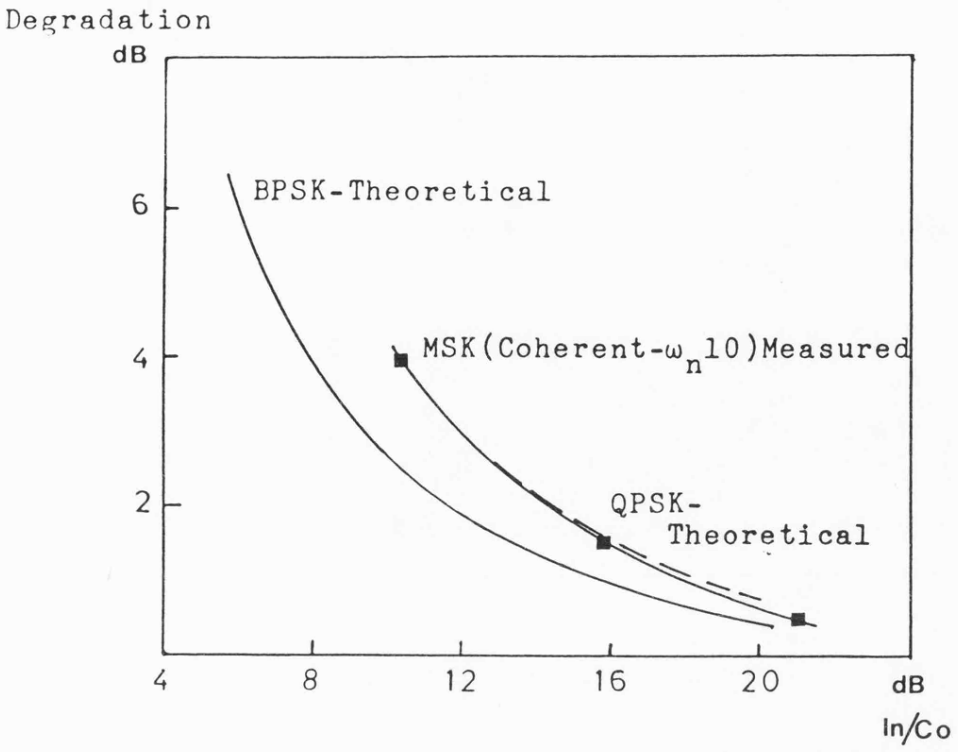

Figure 5.19(a) Performance Degradation Due to Cochannel Interference - PE=10^{-6}.

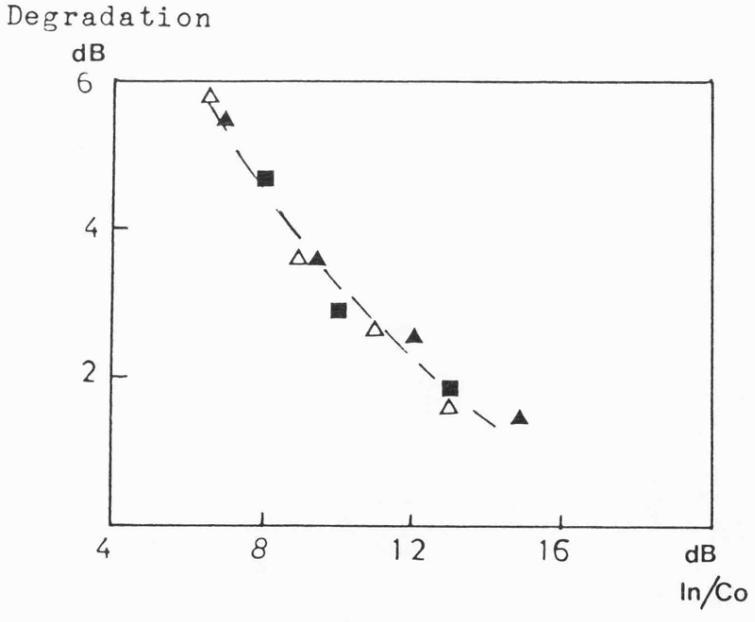

Coherent:■ω_n=10 ,▲ω_n=100 rad/Sec.

Noncoherent: △

Figure 5.19(b) Performance Degradation due to Cochannel Interference - PE=10^{-4}

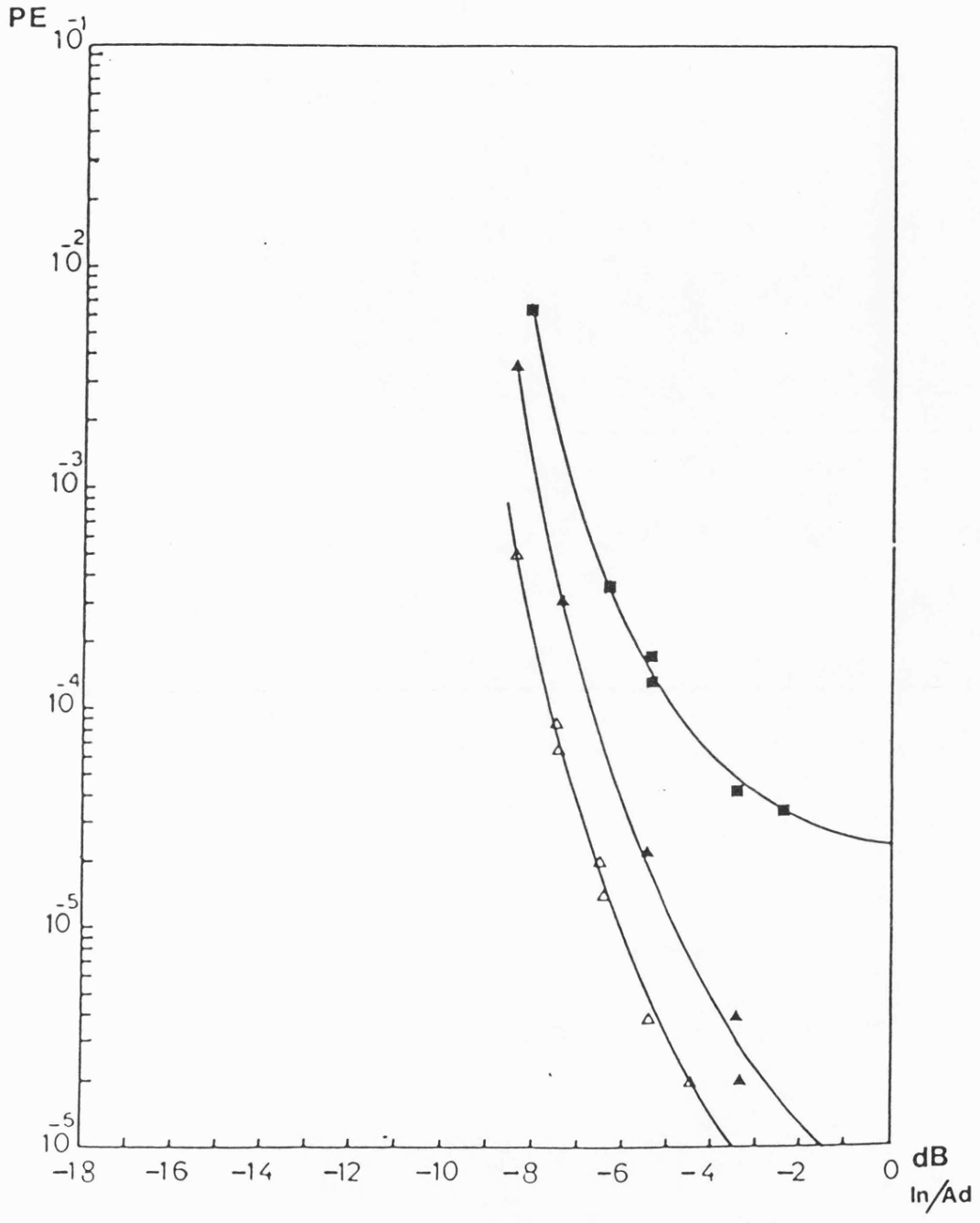

△ E_b/N_o = 12dB , ▲ E_b/N_o = 11dB , ■ E_b/N_o = 10dB .

Figure 5.20(a) Effect of Adjacent Channel Interference on Coherent Demodulator Performance (ω_n=10)- First IF filter Case.

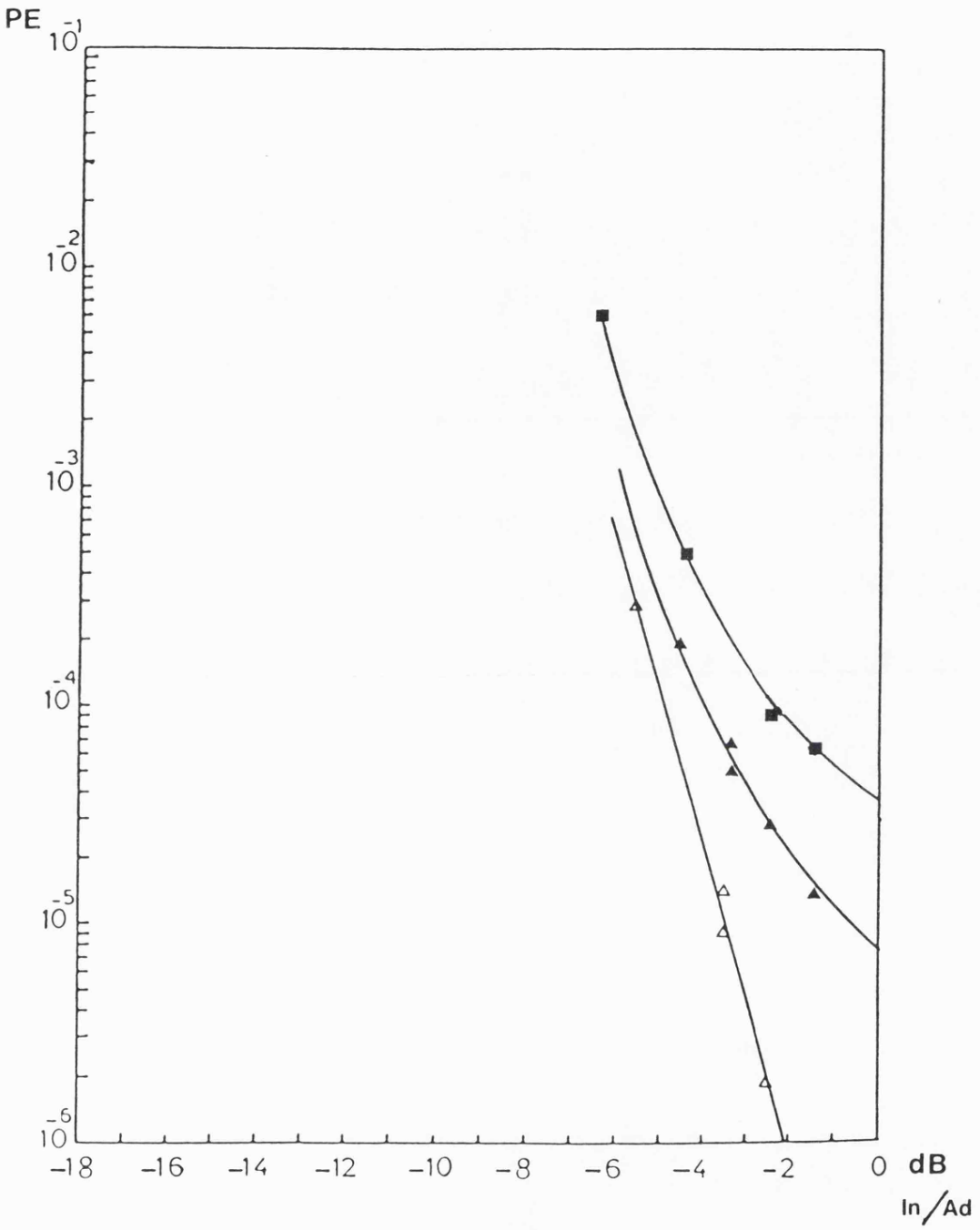

△ E_b/N_o = 16dB , ▲ E_b/N_o = 15dB , ■ E_b/N_o = 14dB .

Figure 5.20(b) Effect of Adjacent Channel Interference on Noncoherent Demodulator Performance-First IF Filter Case.

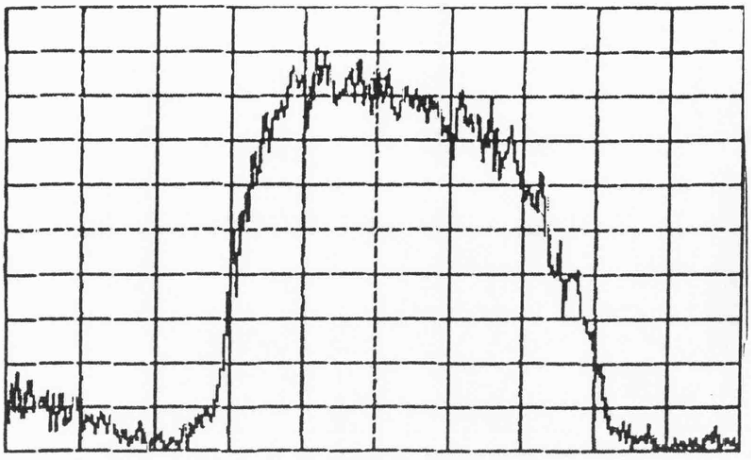

(a) First Filter.

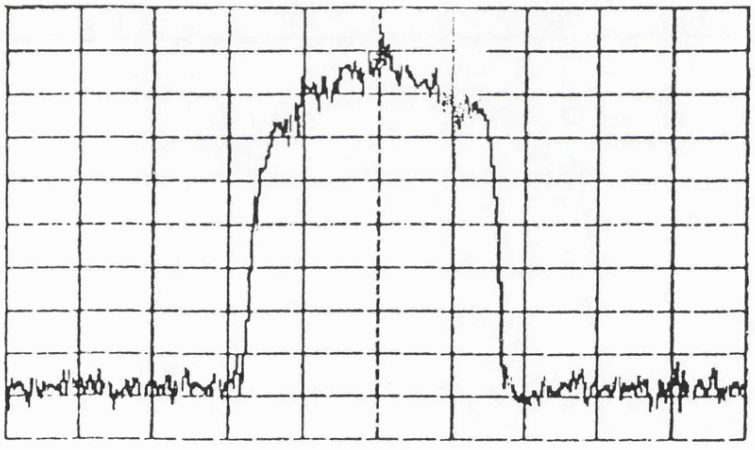

(b) Second Filter.

Centre Frequency: 455KHz , Horizontal: 2KHz/Div. ,
Vertical : 5dB/Div.

Figure 5.21 First and Second IF Fiters Noise Spectrum.

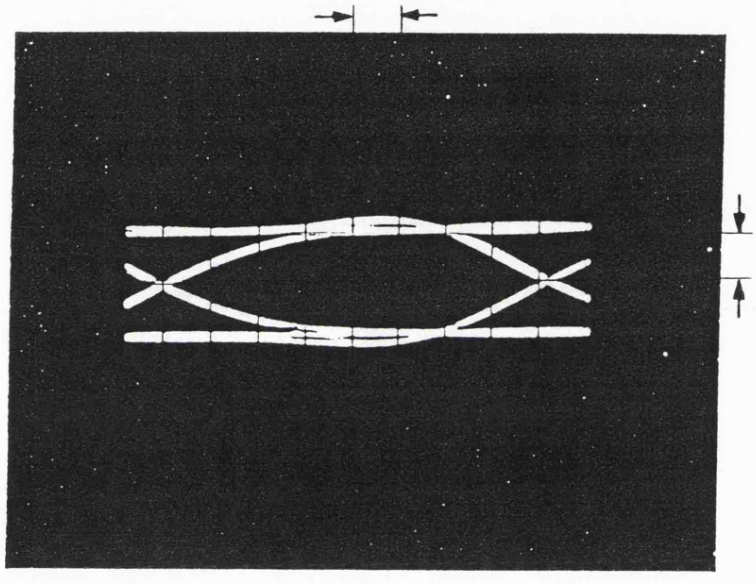

Horizontal : 0.05mSec/Div.

Vertical : 0.5V/Div.

Figure 5.22 Noncoherent Demodulator Eye Pattern — Second IF Filter.

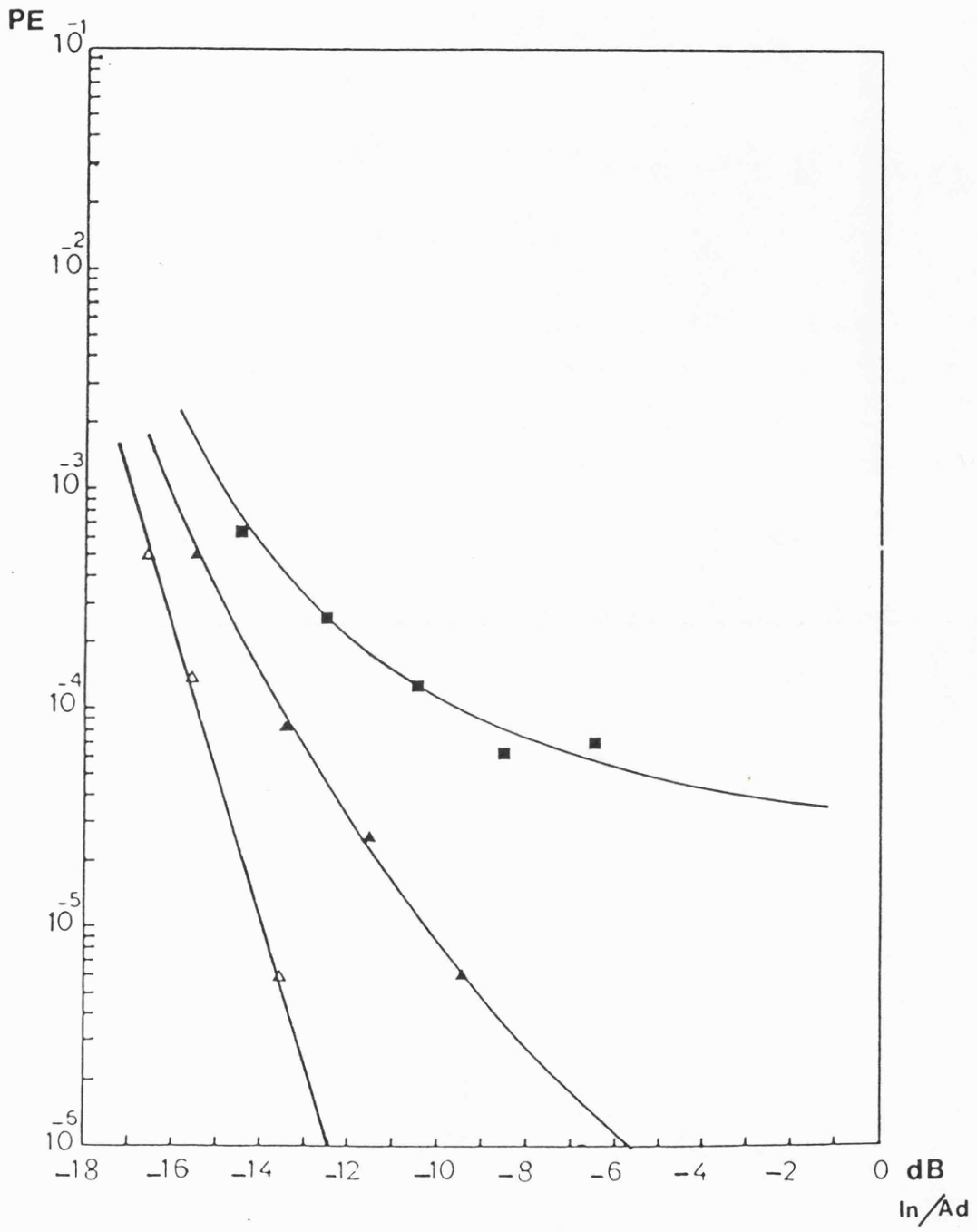

△ E_b/N_o = 13dB , ▲ E_b/N_o = 12dB , ■ E_b/N_o = 11dB .

Figure 5.23(a) Effect of Adjacent Channel Interference on Coherent Demodulator Performance (ω_n =10)- Second IF Filter Case.

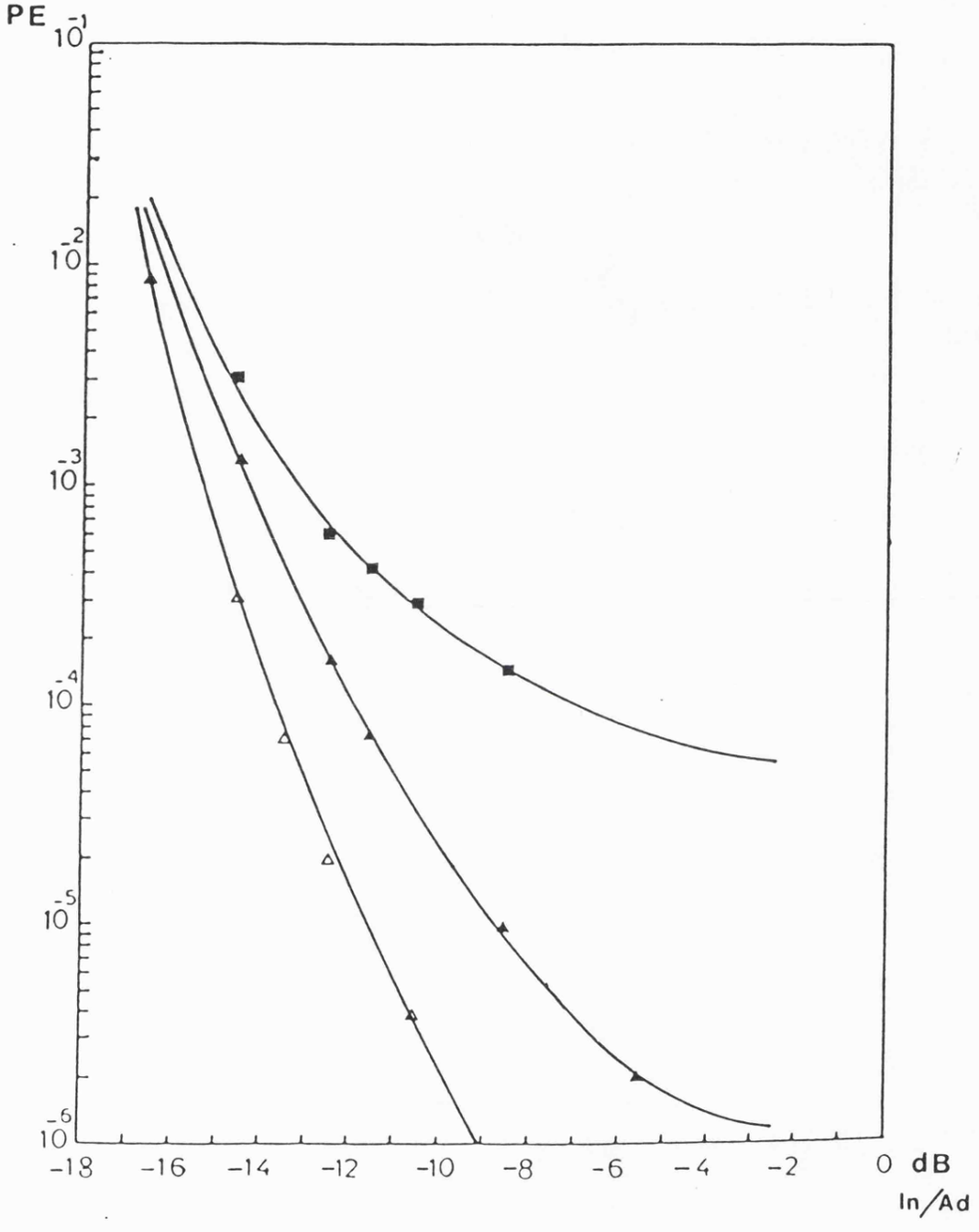

$\triangle E_b/N_o$ = 15.5dB , $\blacktriangle E_b/N_o$ = 14.5dB , $\blacksquare E_b/N_o$ = 12.5dB .

Figure 5.23(b) Effect of Adjacent Channel Interference on Coherent Demodulator (ω_n=100) Performance-Second IF Filter Case.

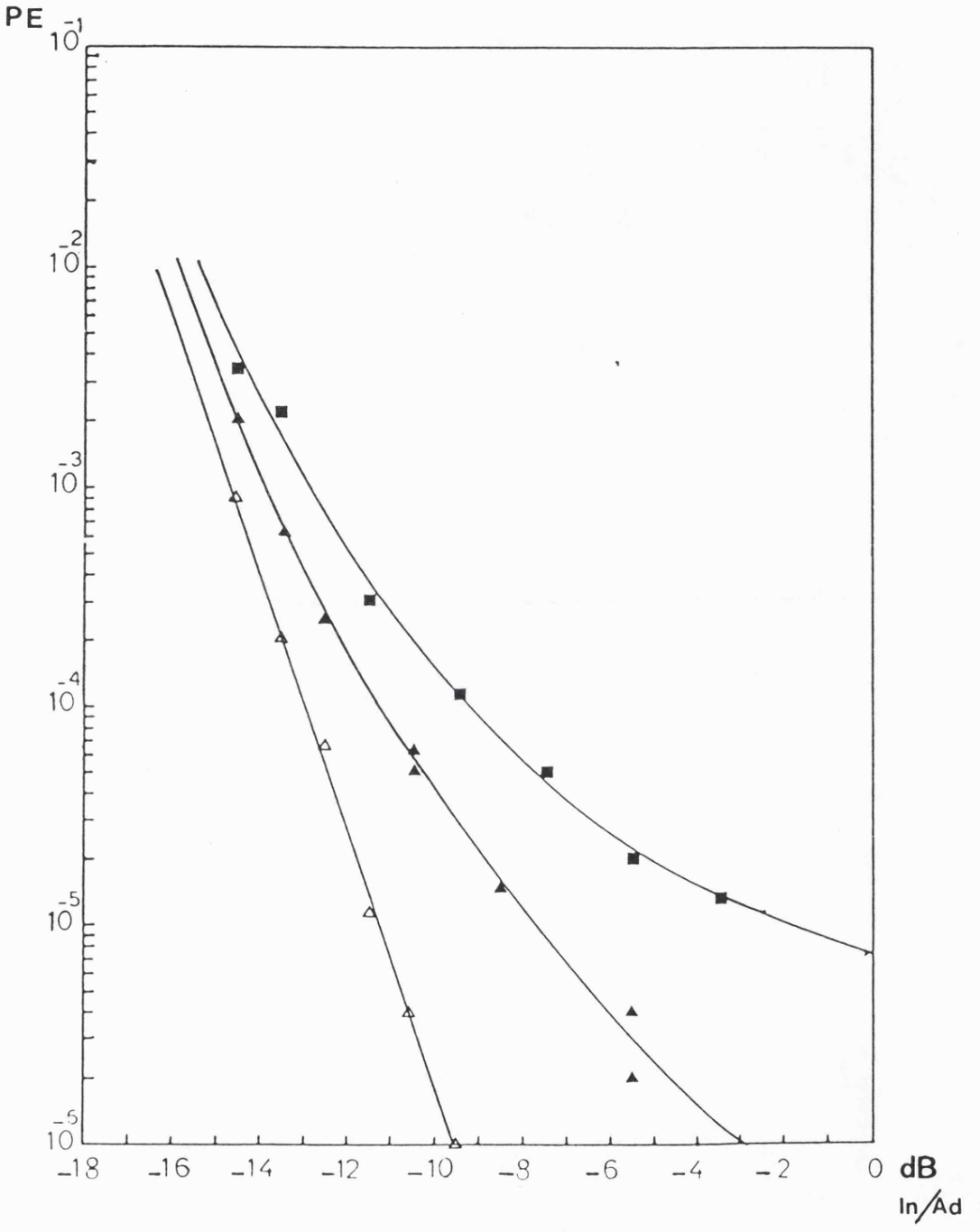

$\Delta E_b/N_o$ = 18.5dB , ▲ E_b/N_o = 16.5dB , ■ E_b/N_o = 15.5dB .

Figure 5.23(c) Effect of Adjacent Channel Interference on Noncoherent Demodulator Performance- Second IF Filter Case.

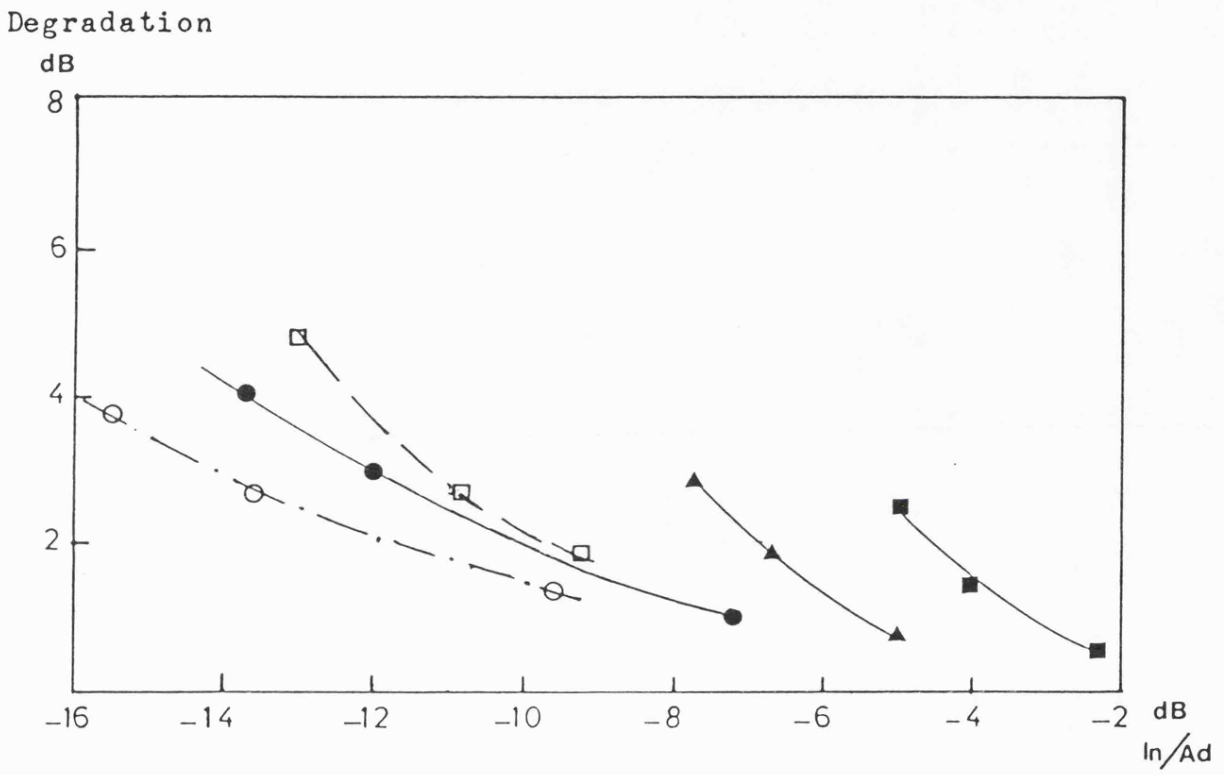

First IF Filter Case: ▲ Coherent (ω_n=10), ■ Noncoherent.

Second IF Filter Case: ○ Coherent (ω_n=10), ● Coherent (ω_n=100), □ Noncoherent.

Figure 5.24 Performance Degradation due to Adjacent Channel Interference - PE=10^{-4}.

CHAPTER 6

CONCLUSIONS AND RECOMMENDATIONS FOR FURTHER WORK

6.1 Conclusions

The superiority of the MSK modulatioin over all other conventional narrow band digital modulation schemes for land mobile radio digital transmission applications has been demonstrated through studying their theoretical performances in typical mobile channel conditions.

A stable and flexible modulator structure whose output frequency spectrum agrees with the theoretical spectrum of the MSK signal has been built and tested. By using the polar loop technique, it has been shown that the bandlimited MSK signal can be amplified with a power efficiency equivalent to that of a class C amplifier while maintaining linearity.

A coherent and a noncoherent MSK demodulator were implemented. The coherent demodulator performance shows 0.8dB implementation loss (ω_n = 10), which can be described as reasonable giving the complicated overall demodulator structure that includes analogue as well as digital signal processing circuits.

The reference signals recovery phase locked loops were designed with flexibility and stability taken into consideration. They allow the coherent demodulator to function over a wide range of data rates with simple digital programming of four binary dividers, for each bit

rate chosen. This flexibility is achieved while maintaining the loop stability offered by the use of voltage controlled crystal oscillators.

The measured performance of the analogue FM quadrature discriminator detector used for noncoherent demodulation of the MSK signal has shown very close agreement with the theoretical performance of other types of noncoherent MSK demodulators.

By analysing the extensive measurements carried on both demodulators in typical land mobile radio simulated channel conditions, it was shown that the use of the noncoherent demodulator is favoured for this type of application. This is not only due to its better performance in fading conditions, especially with respect to random FM noise, but also and most importantly because of its very simple structure. Furthermore, the noncoherent demodulator can double as an analogue FM detector.

The use of the coherent demodulator cannot be justified unless partial response or pre-modulation filtered MSK signals are used. These will be used only if spectrum efficiency is sought coupled with the use of non-linear class C amplifiers for power efficiency. A simpler approach to achieve both objectives has been suggested. The use of post-modulation filtering of the MSK signal offers the spectrum efficiency, while the use of the polar loop transmitter accomplishes linear power amplification with the efficiency of a class C power amplifier.

The polar loop transmitter adds an analogue IF signal processing

circuit to the system, which has no effect on the MSK signal properties. However, this is a simple addition compared to the analogue and digital circuitry needed in the modulator for precise pre-modulation filtering or partial response signalling to eliminate the radiated MSK signal spectrum side-lobes, while maintaining the constant envelope signal. Furthermore, if these are used to control the MSK signal radiated spectrum instead of postmodulation filtering, a coherent demodulation becomes essential for an acceptable error rate versus signal to noise ratio performance. Thus leading to a complicated demodulator structure. By proper design of the post-modulation filter delay characteristics, spectrum efficiency can be achieved while still using a noncoherent demodulator.

A clock recovery digital circuit which provides both demodulators with the timing signals necessary for data recovery operations and any subsequent decoding process has been analysed and constructed. The local reference clock is generated by a 12MHz crystal oscillator and the circuit is composed totally of digital components, thus offering extremely stable operation. The circuit implementation can be easily altered to reduce the nummber of TTL digital integrated circuits used and replace most of them by CMOS circuits to achieve smaller power consumption. The circuit provided the demodulators with ideal timing signals when they were tested, at 2.4kbit/sec, in both static and fading conditions. The minimum and the maximum fading rates tested were 0.15Hz and 100Hz respectively. Furthermore, it was demonstrated that it can maintain receiver clock timing integrity during deep fades of up to 20 second duration, given crystal oscillators stability of ±10 parts per million. Longer fades can be survived if more stable oscillators are used in the

transmitter and the receiver.

A fast initial clock acquisition circuit was also implemented and the basics for its operation were given. The same circuit was shown to be equally useful to speed reacquisition after a deep fade. However, the need for it did not arise for the values of fading rates tested.

The recovery circuit can be programmed to operate over higher bit rates than 2.4kbit/sec, which are likely to be used in today's channel spacing.

6.2 Recommendations for Further Work

Due to signal fading, digital modulation systems used in land-mobile radio channels exhibit poor error performance. This occurs because the error rate increases sharply to 0.5 during deep fade intervals. Furthermore, random FM noise will cause an irreducible error rate which represents a lower ceiling, in most situations, on the system performance that cannot be reduced by increasing the received signal to noise ratio. Therefore, a scheme to reduce the effect of these impairments should be investigated.

It is well known that diversity techniques can be used to minimise the effect of both signal level fading and random FM noise and in some techniques to eliminate the latter. One of the simplest of these techniques which effectively reduces both impairment effects is space/switching diversity.

When this is used with a single receiver, ie. the switching

action takes place at the diversity branch antenna output, phase and amplitude discontinuities will occur at switching instants. The amplitude discontinuities will be removed by the receiver limiter stages. The phase discontinuities will have an effect similar to that of the random FM noise on digital modulation systems, ie. will cause an irreducible error rate.

However, because of the simple noncoherent MSK receiver structure, two (or more, depending on the number of diversity branches) independent receivers can be used with the switching taking place at the demodulator output, ie. at the baseband. The post-demodulation switching approach will eliminate the switching transient noise. The block diagram of a possible two branch post-demodulation diversity scheme for the noncoherent MSK demodulator is shown in Fig 6.1.

As can be seen from this figure, the data and clock recovery circuits are common for both demodulators. The fast clock acquisition circuit described in Chapter 4 can be used for rapid compensation of the delay between the data transition edges of both demodulatros which will appear in the baseband signals mainly due to asymmetry in the receiver circuits of the two diversity branches. Alternatively, the baseband signal of one of the receivers can be delayed with respect to the other to compensate for the difference in time delay between them.

The most important part for a successful switching diversity reception is the signal level sensor, which controls the switching between the different branches. A digital signal level sensor, based

on the operational principle of the signal state detector described in Chapter 4, can be built. When used for this application, each of the detector counters will be counting the transition edges of one of the diversity receiver's baseband signal. When one of the counters reaches the pre-programmed counting limit, the signal level sensor will switch the other branch. The optimum settings of the counting limit will have to be investigated.

After implementing a diversity scheme, most of the remaining errors will be due to ignition interference. A greater degree of suppression of one's own vehicle ignition system will be required in data transmission than in the case of analogue transmission. The residual errors, caused by ignition interference from other nearby vehicles, can be overcome either by using an automatic repeat request strategy or forward error correction coding. The choice of an error correction code should take into account the burst property of errors caused by ignition interference.

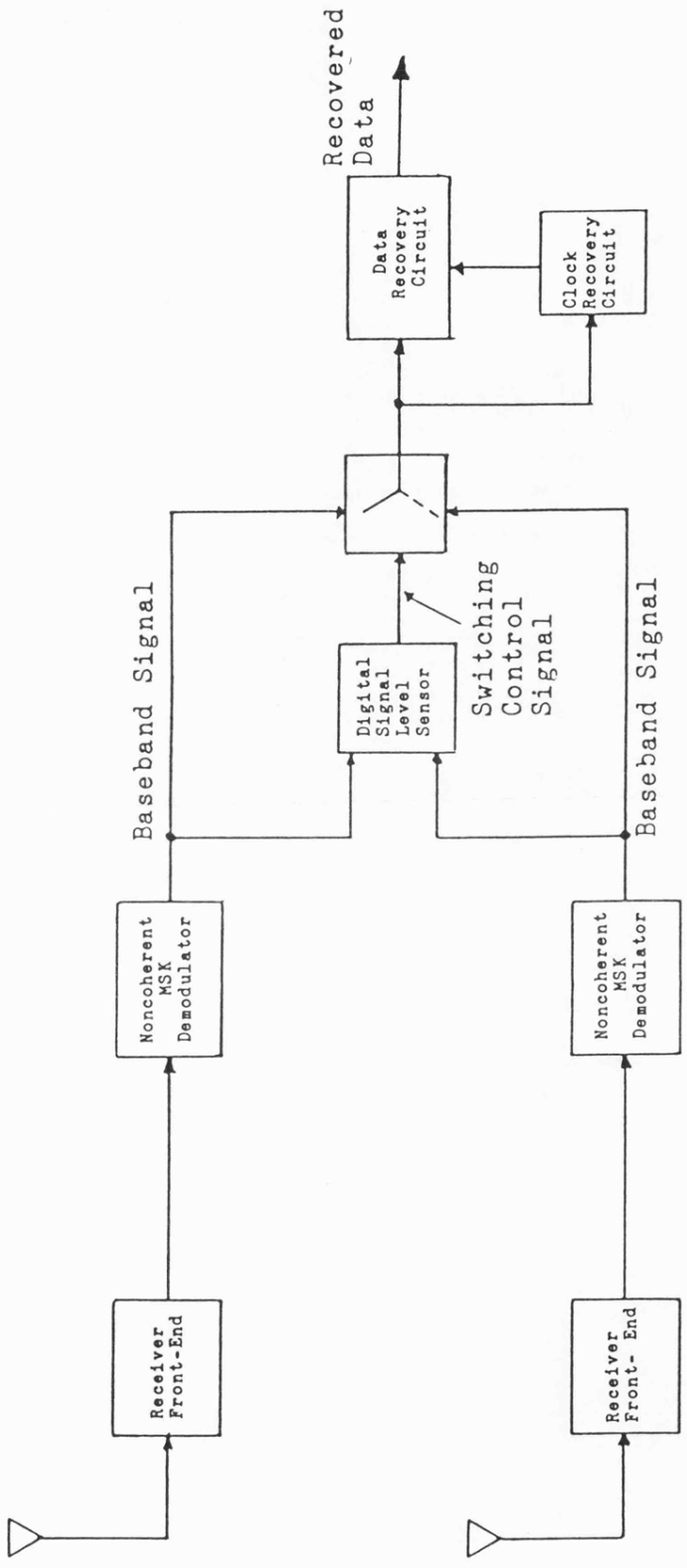

Figure 6.1 Block Diagram of a Switching Diversity System for the Noncoherent MSK Demodulator.